Innovative multifunctional materials with low environmental impact for energy saving, comfort and health of indoor environment

Ph.D. Dissertation of:

Chiara Giosuè

Supervisor:

Prof. Francesca Tittarelli

Co-supervisor:

Prof. Maria Letizia Ruello

Coordinator:

Prof. Ferruccio Mandorli

XV Cycles - New series

Acknowledgements

Abstract

Recent European laws and directives are stricter in terms of energy efficiency of buildings. Constructions are currently built up more sealed and air changing is not enough. This condition leads to a greater risk of unhealthy indoor environments. Due to the changing in lifestyle, people are nowadays spending indoor mostly of their time, so, indoor air quality (IAQ) is becoming a critical issue.

Mortars, plasters and finishes can have an active role to improve IAQ. This study focused on innovative and multifunctional mortars to be used as finishes, able to improve IAQ, without wasting energy. The action of different binders (cement, photocatalytic cement, natural hydraulic lime with and without photocatalytic agents) was studied as well as the effects of adsorbent materials used as unconventional aggregates/fillers. The effect of using biomass waste materials was also investigated, to the aims of sustainability.
In particular, multifunctional finishes can adsorb airborne pollutants in micro-nano-scale where they will be removed ensuring enough efficiency during time.

The results show that the innovative multifunctional mortars for finishes, besides fulfilling the ordinary requirements, are able to improve passively IAQ, for the health and comfort of occupants, in terms of permeability, moisture buffering ability and depolluting activity.

L'esigenza di un'elevata efficienza energetica degli edifici porta ad avere strutture isolate con limitati ricambi d'aria. Di conseguenza ci può essere un peggioramento della qualità dell'aria interna con aumento delle concentrazioni degli inquinanti aereo-dispersi e conseguenti ambienti confinati caratterizzati da una scarsa qualità dell'aria. Si spende molto tempo in ambienti confinati come uffici, residenze, scuole e altre strutture pubbliche che devono necessariamente avere un microclima sano e confortevole. Ristagni di umidità e concentrazioni elevate di inquinanti aereodispersi possono avere severe e gravi conseguenze sullo stato di salute degli occupanti degli edifici come la ben nota Sindrome da Edificio Malato (Sick Building Syndrom, SBS).

Da qui nasce l'esigenza di sviluppare tecnologie che passivamente riescano a migliorate la qualità dell'aria indoor senza andare a inficiare sul conteggio energetico dell'edificio stesso. Lo scopo della ricerca è quello di sviluppare malte e/o finiture multifunzionali innovative che, senza ulteriori dispendi energetici, riescano a garantire un elevato comfort e la salubrità degli ambienti indoor. L'obiettivo sarà raggiunto impiegando nelle miscele preparate con diversi leganti (cemento, cemento fotocatalitico, calce idraulica naturale con e senza agente fotocatalitico)

aggregati/filler non convenzionali con elevate capacità adsorbenti anche tramite l'utilizzo di sottoprodotti industriali.

Le finiture multifunzionali potranno così adsorbire gli inquinanti aereodispersi in un reattore a micro-nano scala dove verranno rimossi, mantenendo nel tempo un'elevata efficienza.

Dai risultati ottenuti si è dimostrato come le malte innovative multifunzionali, oltre a soddisfare i requisiti ordinari, sono in grado di migliorare passivamente la qualità dell'aria di ambienti confinati. In particolare le finiture garantiscono elevata traspirabilità, sono buoni tamponi igroscopici e hanno un'elevata capacità disinquinante.

Contents

Chapter 1

1. Introduction

1.1.   Indoor Air Quality

Sustainability of buildings is becoming day by day a remarkable issue. Recent European laws and directives are stricter in terms of energy efficiency of buildings. The building sector aims to reduce emissions: in fact, constructions contribute for 40% on global carbon dioxide emissions [1]. Changes in building design devised to improve energy efficiency have meant that modern homes and offices are frequently more airtight than older structures [2]. In fact, constructions are currently being built more sealed and sometimes there is not enough guaranteed air changing [3]. Several studies show that concentrations of pollutants are higher outside than inside of buildings [4]. This situation leads to Indoor Air Quality (IAQ).
IAQ has received a lot of attention in the latest years. People are spending 90% [5] of their time in indoor environments, much more than years ago. These environments correspond to e.g. buildings offices, school, public transports. Researches, policy makers and experts have discussed about the role of IAQ in several documents and they stressed the determinant role of IAQ on population health [6]. The risk of unhealthy indoor environment due to high concentrations of pollutants is great.
Pollutants are classified into three broad categories: physical, chemical and biological. Some examples are Volatile Organic Compounds (VOCs), the most present of which are formaldehyde, toluene, benzene; carbon monoxide; nitrogen dioxide, ozone, particulate matter (PM), tobacco smoke, asbestos, other anhydrides (XO). The physical agents are: radon natural and artificial electromagnetic fields and noise. Biological agents are: molds, bacteria, fungi, pollen [7].
The effects can be short term effects, or long terms effects such as the well-known Sick Building Syndrome (SBS). SBS is recognized by the USA National Institute for Occupational Safety and Health (NIOSH) and the major cause is the poor quality of ventilation.
Another important aspect is moderating the indoor variations in Relative Humidity (RH) in buildings because indoor humidity affects warm respiratory comfort, skin humidity and perceived IAQ [8] Not adequate levels of RH have negative effects on well-being of occupants [9].

RH can become a threshold factor for durability of different building materials increasing maintenance costs as well as promoting biological attack surface [6]. Fungi

and microorganism are also unhealthy for people and occupants since they may produce contaminants, such as spores, allergens, toxins and other metabolites that can contribute to the degradation of IAQ [10] with consequent allergies, irritations and skin diseases.

1.1.1. Conventional strategies for Indoor Air Quality

There are conventionally three broad strategies to reduce levels of indoor air pollution: source control, dilution by ventilation and active engineered control systems (in Heating, Ventilation, and Air-Conditioning, HVAC) or as stand-alone air purifiers [11]. The method of source control limits harmful emission by locking the source. This method bases its effectiveness on the limitation, for example, of furniture or forbidding smoking in indoor environments. Source control is the best way to reduce indoor pollution but sources usually cannot be avoided because pollutants come from occupant activities. The method of ventilation is based on the local extraction of pollutants emitted by the occupant activities.
Odor and pollutants, emitted by unavoidable sources, are removed and displaced by ventilation. To improve this method gas adsorption and chemical gas filters are used together with dilution and ventilation.
Active system control like air conditioning provides an adequate mechanical ventilation. Generally active systems like air cleaners are more effective than passive systems for the control of IAQ but ventilation has substantial energy loss.

1.1.2. New perspective for Indoor Air Quality: passive systems

Reducing energy consumption and make healthier indoor environment is a socio-economical problem.
As [12] confirmed in a previous study, conventional indoor air cleaning methods are usually ineffective since they merely replace the contaminated air with new polluted air (ventilation systems) or change the pollutant to another phase without neutralizing it (air purifiers).
Buildings materials (e.g. mortars, internal plasters and finishes) can positively interact with indoor environment, as reactive building materials can help active systems to be effective using less amount of energy [13]. It has been demonstrated that indoor materials can act as buffers for VOCs, and it has been highlighted that polar compounds were more strongly adsorbed by highly porous materials [14].
Depolluting process in passive building materials can be promoted by two different processes: adsorption and Photocatalytic Oxidation (PCO).
Adsorption is a process where fluid phase components (adsorbates), which can be gaseous or liquid, are transferred on the solid surface (adsorbent). This is a passive removal system of substance. Forces of attraction are established among the compounds of fluid phase: the adsorbate covers the surface of the adsorbent with a molecular layer.
The methods used to capture are: differences in polarity (force of electrostatic nature), difference in molecular weight (components with higher molecular weight will have a higher boiling temperature, so it will deposit preferentially on the surface of the solid)

difference in size (geometry of the particle size is the base for a mechanism, the solid has the function of molecular sieve).

A fundamental requirement for the adsorption process is the high specific surface of the solid adsorbent because the adsorption process is focused on the surface of the solid (the process needs a high contact area soil-fluid). Very porous particles are needed to achieve the process (surface area of $300 - 3000$ m^2/g). A wide surface area of adsorptive materials is required for cleaner air to obtain high removable efficiency of pollutants [11].

PCO can also represent an optimum option to provide a healthier indoor environment. The application of nanotechnology in the civil engineering related industry can play an important role in the quality of building materials [15]. One of the most famous nano-catalysist that can be used is TiO_2: nowadays there is an increasing interest in using this catalysist in cementitious materials [16], [17]. PCO is a superficial phenomenon [18] well researched for the decomposition of pollutants in less harmfully compounds. PCO degradation of pollutants implies different steps, indicated to previous authors [19], [20]. The reaction mechanism needs UVA light wave-length (320 - 400 nm) to be activated, so it is possible the generation of hole/pair. This step is then followed by the adsorption phase of the pollutants onto the TiO_2.

Fundamental requirement for indoor materials is the high transpirability, to avoid the storage of humidity and the ability to be a hygroscopic buffer able to absorb and desorb moisture [21], [22]. A promising strategy in this sense is related to the use of hygroscopic materials to dampen indoor humidity variations [22]. Daily changes in RH can be modulated by the indoor porous materials. Water vapor is absorbed during exposure at high levels of RH and then released during the desorption phase. This capacity can be expressed in terms of Moisture Buffering Value (MBV) [23].

Against the growth of molds, TiO_2 is tested. If activated, TiO_2 gives a high photocatalytic activity, and increases not only the efficiency of NO removal but also a total inactivation of molds [24]. Furthermore, the general high alkalinity of cement-based mortars could inhibit itself the biological attack [25].

1.2. Research objectives and strategies

1.2.1. Research objectives

The current work is aimed to develop innovative multifunctional mortars for finishes able to passively improve IAQ, for the health and comfort of occupants, in terms of permeability, moisture buffering value, depolluting activity and molds growth, besides fulfilling the ordinary requirements.

For this purpose, in new mortars, inorganic binders are used with and without photocatalytic agents. Moreover, conventional sand has been replaced by volume with unconventional aggregates, characterized by high adsorption properties and currently used not in the building sector but in chromatography or filters for water/air depuration processes [26].

If a photocatalytic agent as titanium-dioxide is present, the addition of the unconventional aggregates, thanks to their high specific surface, give larger contacting areas to TiO_2 possibly improving the depollution activity of the material [27]. In this way, saturation of adsorbents materials could also be avoided for the maintenance of the same efficiency during the time [28].

Mortars are designed, prepared and tested not only for these innovative properties but also, obviously, according to the current standard for mortars.

1.2.2. Research plans and sub objectives

Research starts with the use of a commercially available photocatalytic binder [29] compared to white cement. In this case, the use of an hydrophobic admixture is also tested in order to evaluate the influence on the properties of the mortar [30], [31]. Unconventional aggregates are able to give depolluting properties to mortars for indoor applications [26]: for example, literature reports that the additions of low quantitative of active carbon on photocatalytic cementitious matrix enhances the decomposition of NOx, improving the adsorptive phase of the process [32]. In this thesis, the feasibility of the total replacement of conventional aggregates with unconventional ones is evaluated.

It is well known that hydraulic lime is more sustainable than cement [33], subsequently, cement has been replaced with hydraulic lime [34]. Hydraulic lime based mortars can have higher depolluting properties than cement based mortars due to higher presence of pores: PCO capacity is very influenced on the microstructure, particularly in terms of macro/micro pores [35]. Moreover, high quantity of cementitious products could hide the catalyst [36].

To improve sustainability of these building materials [37], the use of biomass as unconventional aggregates has been considered. "Green" building materials with depollution property toward ozone has been used successfully [4]. The use of biomass materials can reduce both the carbon impact of construction and indoor Volatile Organic Compounds (VOCs) by adsorption [38].

Finally, a 'hybrid' aggregate based on unconventional adsorbent aggregate and biomass waste has been tested to optimize the depollution and mechanical performances of the final product. A doped TiO_2 agent has been also added and activated under UV and visible radiation [39].

Under visible radiation, the effectiveness of the used doped TiO_2 agent was not high as expected [40]. Therefore, another doped TiO_2 agent has been tested in this condition in lightweight mortars manufactured with expanded waste glass at the University of Eindhoven under the supervision of prof.dr.ir. H.J.H. Brouwers and dr. Q. Yu, with succesful results.

Table 1 shows an overview of the materials used and the relative evaluated properties in order to summarize the experimental program of this thesis. Fresh state properties, mechanical characterization, pore size distribution and capillary water absorption are provided for all materials.

Table 1 Overview of materials and properties investigated in the thesis

Chapter	Binder	Aggregates	Others	Properties investigated
Chapter 3	White Cement CEM II Photocatalytic Cement CEM II	Calcareous Sand Zeolite Silica Gel Active Carbon	Hydrophobic admixture	Drying shrinkage Water vapor permeability Moisture Buffering Capacity Adsorption and photocatalysis of VOC, Photocatalysis of NO
Chapter 4	Hydraulic Lime HB 3.0	Calcareous Sand Zeolite Silica Gel Active Carbon	Hydrophobic admixture Photocatalytic agent TiO_2	Water vapor permeability Moisture Buffering Capacity Inhibition of molds growth Adsorption and photocatalysis of VOC
Chapter 5	Hydraulic Lime HB 3.0	Calcareous Sand Spruce sawdust shavings as it is and roasted Bottom/Fly Ash from biomass		Water vapor permeability Moisture Buffering Capacity Adsorption of VOC LCA
Chapter 6	Hydraulic Lime HB 3.0	Calcareous Sand Commercial Kerakoll Commercial CIM Silica Gel Bottom/Fly Ash from biomass as it is and calcinated	Photocatalytic agent TiO_2	Drying shrinkage Water vapor permeability Moisture Buffering Capacity Adsorption and photocatalysis of VOC, Colorimetric differences
Chapter 7	Grey Cement CEM I Natural Hydraulic Lime NHL 3.5 Coal Fly Ash	Expanded silicates Expanded glass	Photocatalytic agent TiO_2	Drying shrinkage Thermal properties Photocatalysis of NOx

Chapter 2

2. Characterization of materials and definition of methods

2.1. Introduction

A variety of materials are used in this research. All the materials used in the experimentation are studied and characterized with the specific methods described in this chapter.

The binders are inorganic binders. Cement, photocatalytic cement, hydraulic binder such as hydraulic lime and natural hydraulic lime are used.

Aggregates can be divided in two main categories: conventional and unconventional. A calcareous sand is used as conventional aggregate.

The unconventional aggregates are divided in mineral materials, such as zeolite, active carbon, silica gel and organic materials, such as spruce sawdust shavings as it is and roasted. An alternative use of ashes coming from biomass, both fly ash and bottom ash, have also been studied. Lightweight aggregates based on expanded silicates are used to develop lightweight mortars without adsorbent properties.

In addition to mortars, the influence of different types of nano-TiO_2 and a hydrophobic admixture have been considered.

In this chapter, also different methodologies, used to test the mortars, are listed and described. Characterization is done in terms of fresh state and hardened state properties. For the hardened state properties, mechanical, morphological and microstructural properties, related to durability, have been investigated.

Also, the effect of mortars on the comfort and health of indoor environment has been investigated in terms of thermo-hygrometric (permeability, moisture buffering ability, thermal conductivity) and depollution properties (adsorbent properties, photocatalytic properties, inhibition of mold growth). Finally, also the aesthetical properties and the Life Cycle Analysis (LCA) have been roughly evaluated.

2.2. Materials

2.2.1. Methodology for materials characterization

2.2.1.1. Density

Specific density
The specific density of materials, also referred as real density, is defined as its mass divided by the volume:

$$\rho_{spe} \frac{m}{V_{true}} \; [\text{kg/m}^3]$$

Where:
ρ_{spe}: specific density of the material, in kg/m^3;
m: mass of the material, in kg;
V_{true}: the true volume occupied by the material, excluding the porosity in m^3.
In this study this property is evaluated with a gas pycnometer (Figure 1) AccuPyc II 1340 Gas Pycnometer.
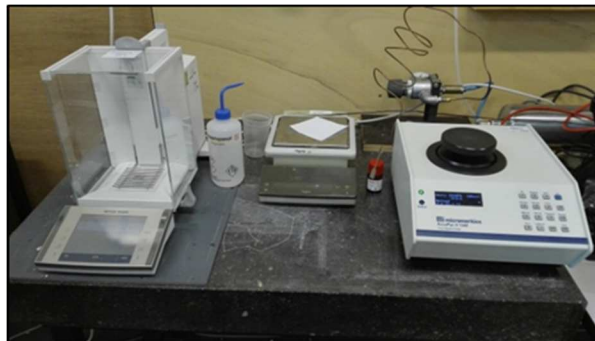
Figure 1 AccuPyc II 1340 Gas Pycnometer

The technique uses the gas displacement method (helium is used as inert gas and displacement medium) to measure the volume accurately. In order to minimize the uncertain values, each measurement is repeated 5 times and the average value reported. After the instrument calibration, the analysis is performed. First the analyzed specimens are dried at 105 °C in an oven until constant mass. Constant mass is reached when, after 24 hours in oven, the measured weight value is different than less than 0.1% compared to the previous one. Then specimens are weighted and inserted inside the cell for the measure. The sample is sealed and the gas pressure is applied in order to guarantee the flux. Helium molecules rapidly fill pores as small as one angstrom in diameter.

Particle density
The density of aggregates is necessary to evaluate the best mortar mix. If density is not declared in sheets, it is experimentally evaluated.

A few amounts of aggregates (in saturated surface dry condition, ssd) are weighted into graduated cylinder.

Water is added into a graduated cylinder until known volume. The cylinder with the aggregate and water is then weighted. The density of the water is known ($1000 \ kg/m^3$) so thanks to the difference between the two weights it is possible to calculate the volume of the aggregate.

The density is defined as weight per unit volume (kg/m^3). It occurs at least three values to work out an average.

2.2.1.2. Grain size analysis

The grain size is evaluated with two different methodologies.

For high diameter, the particle size distribution curve is obtained by sieving. Sieves with decreasing opening size are placed from the top to the bottom. By weighing the material on the sieves and the total amount the pass percentage and the retained percentage are evaluated.

For low diameter ($d \leq 0.063 \ \mu m$) this technique can not be used, so the powders are analyzed by Laser Light Scattering (LLS) Mastersizer 2000 (Figure 2).

Figure 2 Mastersizer 2000 Malvern Instrument

The characterization of size distribution is performed with LLS technique that measure the angular variation in intensity of scattered light as a laser beam passes through dispersed particles. The wet-mode analysis is used in this thesis, with water and propanol for cement, natural hydraulic lime and fly ash.

2.2.1.3. Chemical characterization: TGA and XRF

In Thermal Gravimetric Analysis (TGA) the sample is heated at defined steps while a scale is controlling the weight loss. TGA is performed until T = 1000 °C. Heating rate is 2 °C per mins.

X-ray fluorescence (XRF) is used to quantify the composition of materials in terms of oxides percentage, quantifying the emission of fluorescent X-rays from a material subjected to high energy X rays or gamma rays.

2.2.2. Binders

2.2.2.1. Cement

Cement is one of the mostly used binder all over the word. This massive use implies higher emission in terms of CO_2: it is evaluated that the cement industry is a major producer of CO_2, accounting for 5 - 7% of man-made CO_2 emissions [33].
Grey cement used in this work belongs to CEM I 42.5 N class. It is provided by ENCI. Cement is the most used in related previous studies reported in the literature [17], [41] and [42].
The density of CEM I 42.5 N is 3136 kg/m^3 and it is directly evaluated with gas pycnometer. The oxides percentage, determined with XRF analysis, is reported in Table 2. In this case, also the particle size distribution, necessary for the mix design, is valuated. Results are shown in Figure 6.
For the experimental program, also white cement CEM II B/LL 42.5 R Roccabianca and Photocatalytic withe cement CEM II B/LL 42.5 R TX Aria with photocatalytic active principle TX Active® (both provided by Italcementi) are used and compared. (Figure 3) Those commercial products have density = 3050 kg/m^3 and the Blain finess = 410 m^2/kg.

Figure 3 Different cements used in the experimental program: a) grey cement, b) white cement and c) photocatalytic white cement.

2.2.2.2. Hydraulic lime

Natural Hydraulic lime is obtained from calcination of calcareous marl (with about 6 - 22% of clay) at T = 850-1000 °C. This temperature is lower than the temperature necessary to produce cement with consequently lower carbon dioxide emissions. Hydraulic Lime is usually obtained diluting cement with a calcareous filler.
Figure 4 shows the different types of hydraulic binders used. The most remarkable differences between cement based mortar and hydraulic lime mortar are: lower mechanical resistance, lower elastic modulus and higher transpirability.
The Hydraulic binder used in this thesis belongs to LIC 3.0 according to UNI EN 15368:2010. This hydraulic lime is considered with a density of 2650 kg/m^3. The commercial product is called Plastocem, produced by Italcementi.
The Natural Hydraulic Lime (NHL) is provided by KEIM. This product belongs to NHL 3.5 according to UNI EN 459-1:2010. The density is measured by pycnometer and it is 2537 kg/m^3. The particle size distribution of the powered is shown in Figure 6.

Characterization of materials and definition of methods
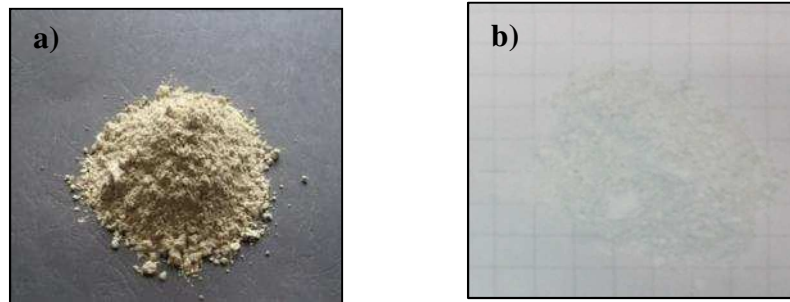
Figure 4 Different hydraulic binders used in the experimental program: a) Hydraulic Lime and b) Natural Hydraulic Lime.

TGA analysis is performed on a sample of NHL. Results are shown in Figure 5.
Water evaporates as vapor at about T = 100 - 150 °C.
At 450 °C about 5% of mass is lost due to $Ca(OH)_2$ [43]. The reaction at this temperature is:

$$Ca(OH)_2 \rightarrow CaO + H_2O$$
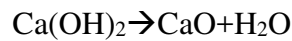
knowing the percentage (5%) of mass loss, the percentage of total content of $Ca(OH)_2$ in NHL (21%) is calculated.
At 650 °C, about 25% of mass is lost.
The mass loss around 700 °C is due to decarbonation of $CaCO_3$ [43] according to the reaction:

$$CaCO_3 \rightarrow CaO + CO_2$$

Knowing the percentage (25%) of total content of $CaCO_3$ in NHL (57%) is calculated.
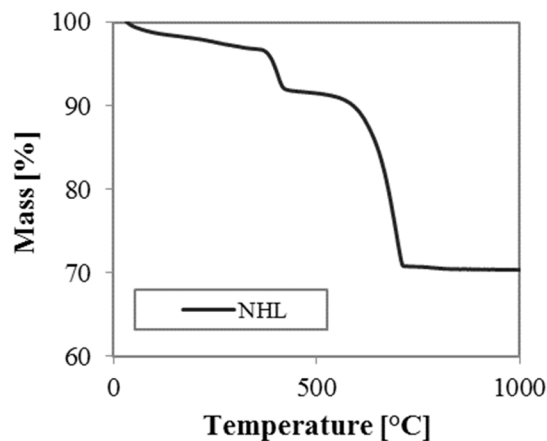
Figure 5 TGA of NHL

2.2.3. Pozzolanic additions, admixtures and additives

2.2.3.1. Pozzolanic additions

Another method to increase the sustainability of cementitious materials is the partial replacement of cement with waste materials such as fly ash (FA) from coal combustion. The results obtained from the chemical and physical characterization of the adopted fly ash are provided in Table 2 and Figure 6. Fly ash (supplied by Vliegasunie B.V., the Netherlands) belongs to Class F fly ash according to ASTM C 618 [44].

Table 2 Chemical composition (wt.%) expresses as oxide percentage from XRF analysis of cement CEM I 42.5 N (CEM), Fly Ash (FA), hydraulic binder as hydraulic lime (HL4) natural hydraulic lime (NHL). FA has some traces (value about 0.01%) of: CuO, Ga$_2$O3, As2O$_3$, Rb$_2$O, PbO.

	CEM I 42.5 N	HL	NHL	FA
SiO$_2$	29.67	8.40	7.35	51.71
Al$_2$O$_3$	3.74	0.10	1.49	27.11
Fe$_2$O$_3$	1.80	0.60	-	8.12
CaO	59.25	65.70	87.48	5.76
MgO	1.15	2.6	1.16	1.19
K$_2$O	0.79	0.3	0.53	1.8
TiO$_2$	0.09	<0.10	0.11	1.73
SO$_3$	3.25	<0.2	1.01	1.14
P$_2$O$_5$	-	-	-	0.87
SrO	-	-	-	0.24
MnO	-	-	-	0.08
V$_2$O$_5$	-	-	-	0.07
In$_2$O$_3$	-	-	-	0.05
Cr$_2$O$_3$	-	-	-	0.03
ZnO	-	-		0.02
NiO	-	-	-	0.02
Na$_2$O	0.26	<0.1	-	-
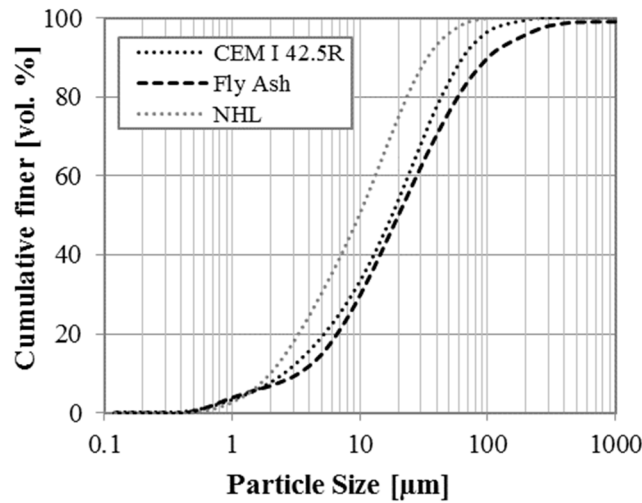
Figure 6 Particle Size Distribution (PSD) curves of cement CEM I 42.5R, fly ash and Natural Hydraulic Lime (NHL).

2.2.3.2. Hydrophobic admixture

Mortars belong to porous materials subjected to capillary water rising. In fact, an ordinary mortar, made with cement or lime, calcareous or siliceous sand and water has a hydrophilic surface. A water droplet, in this case, wets the solid surface by spreading itself and by absorption on the surface. The value of the pressure is according to the Washburn' equation [45]:

$$\Delta P = \frac{2\gamma \cos\theta}{r} \text{ [Pa]}$$

Where:
γ is the surface tension of mercury;
θ is the contact angle;
r is the radius of the pores.
Capillary forces allow water to enter inside concrete and mortar porosities. The contact angle is less than 90 °C and the liquid fills the porosity spontaneously. Some organic materials applied on mortar/concrete surface change the water contact angle up to 90 °C, lowering the molecular attraction between water and mortar/concrete pore walls. Alkyl-alkoxy-silane based materials [46] are an example.
In the experimentation, a hydrophobic admixture based on a 45% water solution of butyl-ethoxy-silane provided by Chem Spec. S.r.l. is added in some mixtures at the maximum dosage suggested by the data sheet, 6.3 g of solution in 1 l mix.

2.2.3.3. Photocatalytic agents: titanium dioxide

The application of nanotechnology can play an important role in the quality of building materials [15]. Different commercially available titanium dioxides (TiO_2) are tested and compared in this thesis. The photocatalytic products are: P-25 Aeroxide® by

Evonik and two different products by KRONOS International, I.n.c., activated by visible light (according to the technical datasheet).

Figure 7 Photocatalytic powers used in this experimental program a) P25 AEROXIDE by Evonik and b) KRONOClean 7000 by KRONOS c) KRONOClean 7404 by KRONOS

P-25 is probably the most used photocatalytic agents UVA sensible in commerce. The properties are taken by the data sheet. This TiO_2 is a mixture of anatase-rutile-amorphous phases, 78 – 14 - 8% in weight, respectively. Particles have nano-size of about 20 - 50 nm. The specific surface, measured by BET, is 35 - 65 m^2/g. The pH value in 4% dispersion is 3.5 - 4.5. Density is evaluated as 3.1 g/cm^3.

KRONOClean® is a TiO_2-photocatalysis that degrades pollutants with visible light and with UV radiation, as reported in the data sheet. TiO_2 content is higher than 97.5%, with a prevalence of anatase phase. Crystallite size is approximately 15 nm. The specific surface area measured by BET is declared higher than 225 m^2/g. pH values is 4-9, density is 3.9 g/cm^3.

KRONOS produces also a TiO_2 photocatalyst in slurry form to be added in water during the preparation of mortars. The slurry is the commercial product KRONOClean 7404, a carbon-dopes titanium dispersed in water (40% of TiO_2 and 60% of water) with a pH of 7 - 8 and a density at 20 °C of about 1.4 g/cm^3.

2.2.4. Aggregates

2.2.4.1. Calcareous sand

Conventional aggregate is calcareous sand. Figure 8 shows the aspects of this aggregate. Conventional aggregates do not take part in hardening process.

Figure 8 Calcareous sand

In this experimentation, the commercial product CA 400 provided by Cava gola della Rossa is used. Purity is 98%. Aggregates are added during the cast at saturated surface dry (ssd) condition when the moisture fills all the void of the aggregate but the surface is dry. In this condition, the aggregate does not absorb or release water in the mix, not changing the water to binder ratio (w/b). The water necessary to reach this condition is 5% in weight. Density in ssd condition is 2.65 g/cm^3. Grain size distribution curve is reported in on Figure 9.
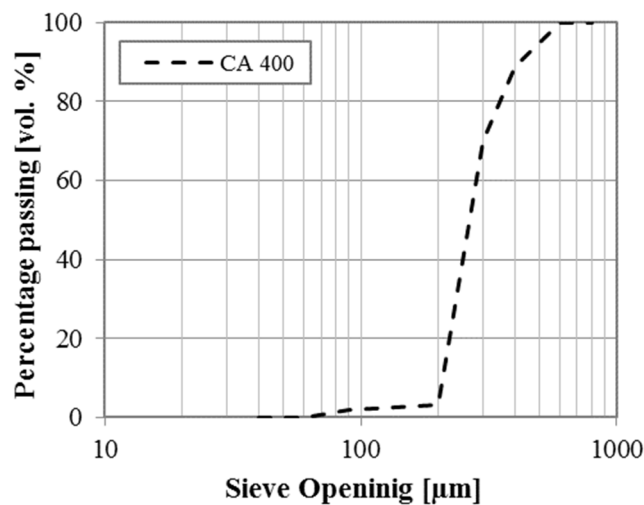
Figure 9 Grain size distribution curve of calcareous sand

2.2.4.2. Zeolite

On 1956 the Swedish mineralogist Axtel Fredrick Cronstedt discovered natural zeolite. These minerals are volcanic rocks, which can be also synthesized. The elementary building units of zeolites are SiO_4 and AlO_4 tetrahedral. Common oxygen atom links the adjacent tetrahedral. The intrinsic structure of zeolite permits to have a framework with channels, channel intersections and/or cages with dimensions from 0.2 to 1 nm. Water molecules and small cations compensating the negative framework charge are inside these voids [47]. The minimum formula $MeAl_mSi_nO_{2(m+n)}$ z H_2O corresponds to the class of tectosilicates. From a chemical point of view zeolites are silico-aluminates

hydrates of alkaline metals and/or alkaline-earth metals which structurally belong to the class of tectosilicates.

The use of hydrophobic zeolite is known in literature for the dual function adsorbent/catalyst medium [48]: this mineral is usually employed in fluid filters and purifiers as molecular sieving. Zeolite is also used in lime based mortar to improve the pozzolanicity of the mix [49]. Previous study successfully used zeolite not only to improve mechanical properties but also to give to the mortar the real capacity of adsorb airborne pollutants [26].

For the purpose of this thesis zeolite is evaluated as an optimum unconventional aggregate. The used zeolite is a natural clinoptilolite zeolite, commercially available, provided by Samore S.r.l..

Physical characteristics are provided by the technical data sheet. Maximum diameter is 250 µm. Low maximum diameter and high specific surface area of the zeolite (evaluated by literature data of about 600 m^2/g [26]) imply about 20% in weight of water to reach ssd condition. Density in this condition is evaluated as 1.6 g/cm^3.

Figure 10 Zeolite

2.2.4.3. Silica gel

Colloidal silica is a compound made by variable units of SiO_2. It has a high specific surface and high porosity. Silica gel is a non-toxic adsorbent material usually employed to uptake high quantities of moisture from the environments.

For this experimentation, a commercial product, Inodorina, distributed by PetVillage S.r.l., is used. The product is in forms of granules of about 10 mm maximum diameter. For the scope of this thesis it is grinded and sieved in order to obtain aggregate with maximum diameter of 300 µm. Ssd condition is reached when about 86% of water is added (in weight) to silica gel. In this condition density is 1.31 g/cm^3.

Figure 11 Silica gel

2.2.4.4. Activated carbon

Activated carbon is one of the most popular adsorbent materials used in filter and air/water purifying process. Activated carbon is microcrystalline, non-graphitic form of carbon that has been processed in order to develop the internal porosity [50].
BMD S.p.A. provides the activated carbon used in this experimentation. The commercial name of the product is 205E. This product is in form of cylindrical granules with maximum shape of 4mm. According to the data sheet density is 0.53g/cm^3. The specific surface area is 900 m^2/g. Otherwise active carbon is a hydrophobic material, the practical experience suggested to add 30% of water during the cast to reach the same workability of other mortars.
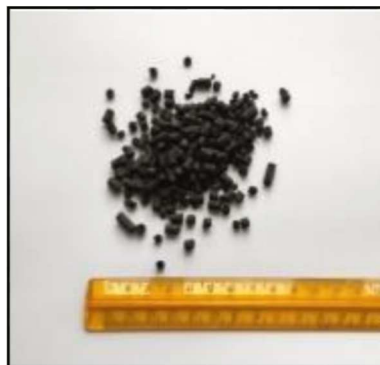
Figure 12 Pellets of activated carbon

2.2.4.5. Biomass ashes

Ashes are a mixture of mineral and organic elements, un-burnt components, produced during the combustion processes. In this case two different types of biomass ashes are used. Type A comes from the production of energy in power plants located in Italy. Type B comes from plants burning corn cobs in U.S.A. Both types of ashes are in two forms: bottom ash and fly ash.
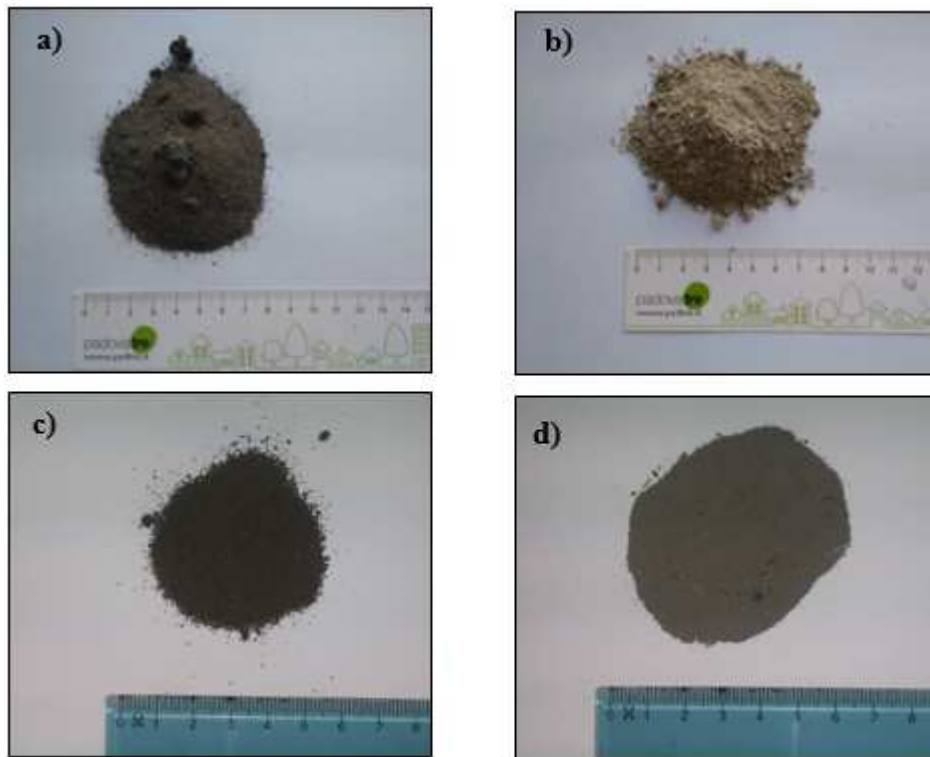
Figure 13 Biomass ashes: a) Bottom ash A, b) Fly ash A, c) Bottom ash B, d) Fly ash B.

The use of biomass ashes is presently under study because their recycling in the production of cement based materials could have a beneficial impact on environment [51]. Biomass, such as wood, is considered as carbon neutral, because it binds the same amount of CO_2 when growing as it is released in combustion Moreover, the resulting concrete-mortars products have good mechanical properties, long durability and low elution release of hazardous elements [53].

The elements typically present in the ash are silica, calcium, potassium, phosphorus, manganese, iron, zinc, sodium and boron, in the form of oxides. Dangerous metals (Pb, Cd and Zn), relatively more volatile, accumulate in the fly ash; the less volatile metals (Co, Ni, Cr and V), accumulate generally in the bottom ashes. However, studies demonstrated that the use of ashes in mortars does not influence negatively the ecotoxicity of materials [54]. Furthermore, the dangerous substances are fixed by the binder and can not be dispersed in indoor environments.

Grain size distribution curves are obtained for bottom ash (Figure 14) by mechanical sieving. Before the application, both bottom ashes are sieved at maximum diameter of 500 µm.

Characterization of materials and definition of methods
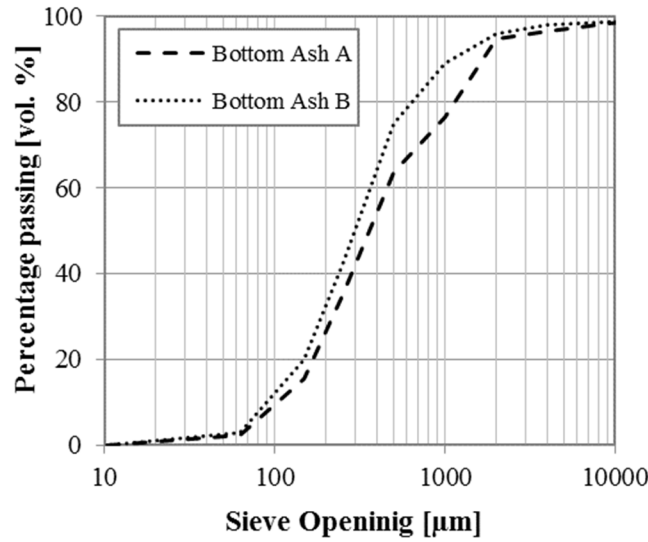
Figure 14 Grain size distribution curve of bottom ash A and bottom ash B

Fly ashes have smaller maximum diameter than bottom ash, d_{max} is about 150-210 µm. The water absorption to reach the ssd condition is 20% for bottom ash and 49% for fly ash. Density, evaluated by laboratory tests at ssd condition, is 1.96 g/cm³ for bottom ash and 1.41 g/cm³ for fly ash. Due to the uncertain origin of type B biomass ashes, TG/DTA analysis are carried out. Results are shown in Figure 15 and Figure 16.
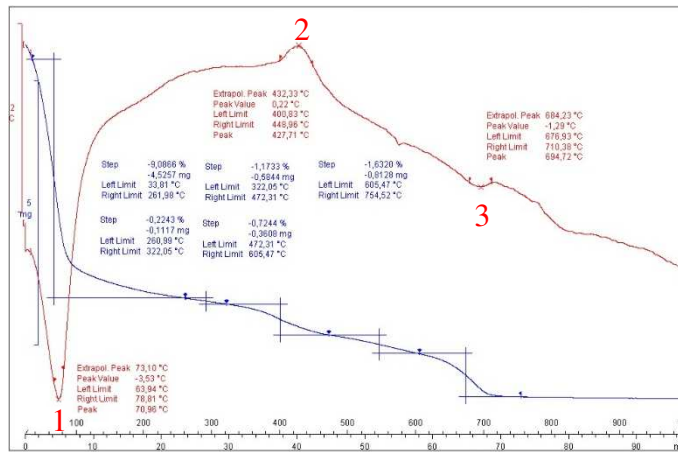
Figure 15 TG/DTA of bottom ashes, type B
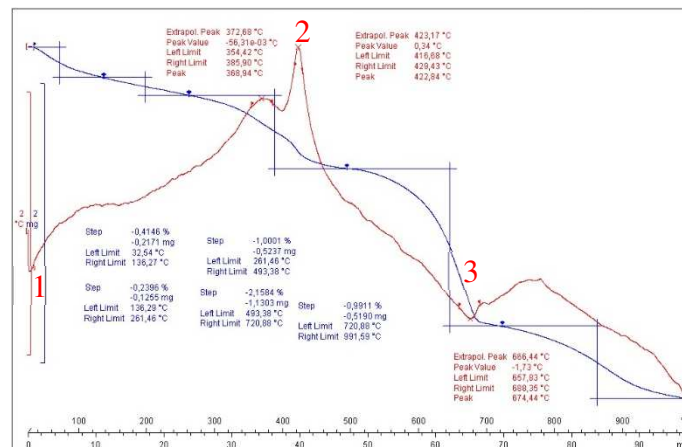
Figure 16 TG/DTA of fly ashes, type B

Three are the main steps found with the analysis, numbered from 1 to 3 in the graphs. Step 1 (endothermic reaction) is related the loss of water up to 70-80 °C. Step 2 is an exothermic reaction at 400 °C due to combustion of residual un-burnt organic material. Step 3 is an endothermic reaction at 700 °C to the decomposition of the carbonate.

2.2.4.6.   Bio-based wood waste

To investigate the possibility of using forest waste materials as unconventional aggregates, spruce sawdust shavings are also considered in this thesis. Two different types of spruce sawdust shavings are considered: one as it is and the other previously roasted by torrefaction. Torrefaction process is conducted at Agricultural, Food and Environmental Sciences Department of Università Politecnica delle Marche under the supervision of Prof. Giuseppe Toscano. Figure 17 shows the aspect of these materials. The torrefaction process is a thermal treatment of biomass in an atmosphere without oxygen at T = 300 °C and atmospheric pressure. A roasted material does not have moisture and the calorific value of the material is increased. Furthermore, there is a reduction in the O/C ratio, a reduction of moisture uptake capacity and a reduction of organic compounds, as example lignin [55].

Characterization of materials and definition of methods
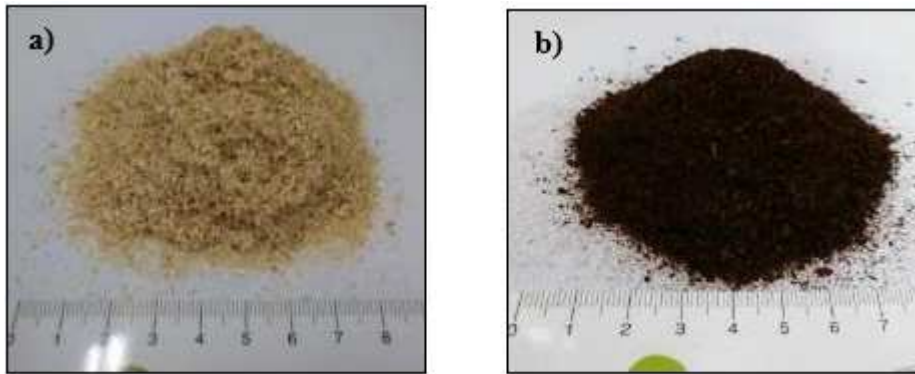
Figure 17 Bio-based wood waste: a) spruce sawdust shavings as it is b) roasted spruce sawdust shavings.
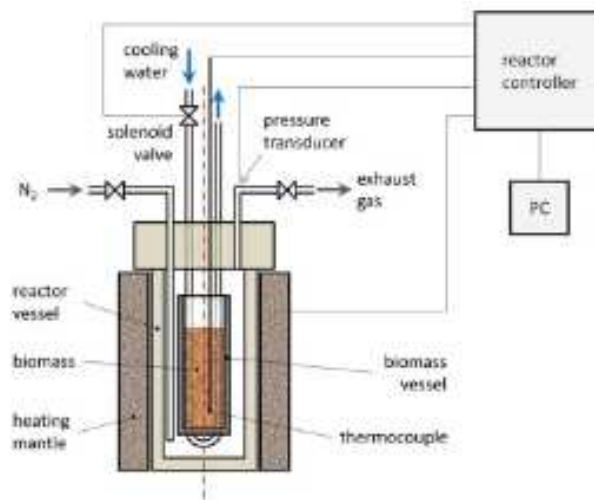
Figure 18 Reactor used for the torrefaction test [55]

Pure spruce sawdust shavings are previously stabilized at 45 °C. Density and water absorption are evaluated for both materials. The density of spruce sawdust shavings as it is, is 0.64 g/cm³. The density of roasted spruce sawdust shavings, obtained by torrefaction process, is 0.17 g/cm³.
Figure 19 shows the grain size distribution curves. These materials have very high water absorption capacity: for spruce sawdust shavings as it is, water absorption is about 300%, for roasted spruce sawdust shavings is about 240%.
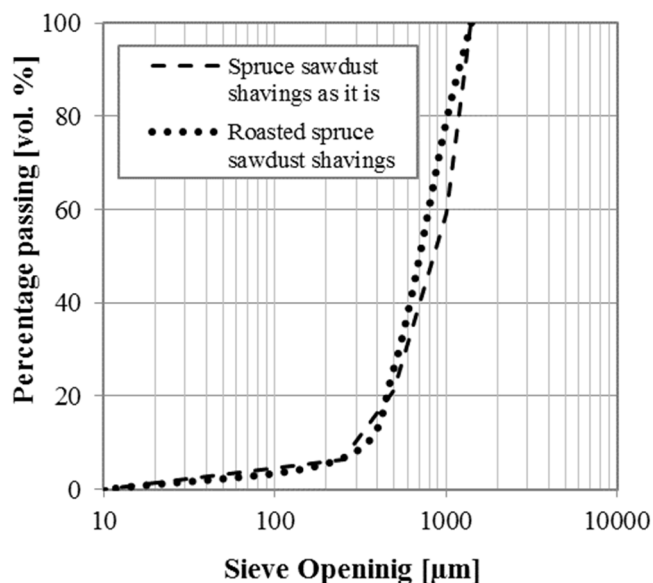
Figure 19 Grain size distribution curves of spruce sawdust shavings, as it is and roasted

2.2.4.7.   Lightweight aggregates

During the research, two lightweight aggregates commercially available are used. The first is a natural expanded silicate called Rotocel®, which have volcanic origins. The second comes from thermal treatment of waste glass, not possible to melt down to obtain new glass, and is called Liaver®.
All the necessary information is taken from the data sheet and reported in Table 3. These two products are provided in bags with different grain size.

Table 3 Bulk and particle densies of different lightweight aggregates

Lightweight aggregates	code	Bulk density kg/m³	Particle density kg/m³
ROTOCEL® 90-300	ES A	360	700
ROTOCEL® 0.25-0.5	ES B	320	700
ROTOCEL® 0.5-1	ES C	310	600
LIAVER® 0.1-0.3	EG A	450	800
LIAVER® 0.25-0.5	EG B	300	540
LIAVER® 0.5-1	EG C	250	450

Rotocel® has the ES code and Liaver® has the EG code. The relative grain size distributions are shown in Figure 20. For both types of lightweight aggregate, a letter from A (bigger size) to C (smaller size) is assigned depending on diameter.
Liaver® has round and more regular spheres than Rotocel®, which has natural origins and irregular granules shape.
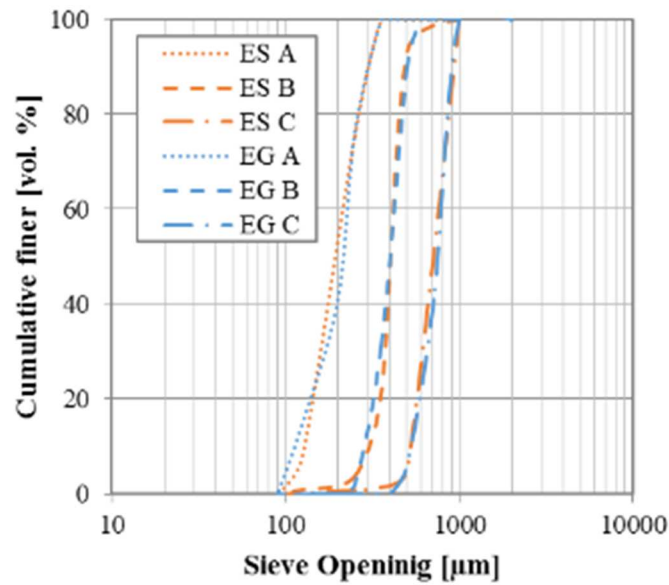
Figure 20 Grain size distribution curves of lightweight aggregates
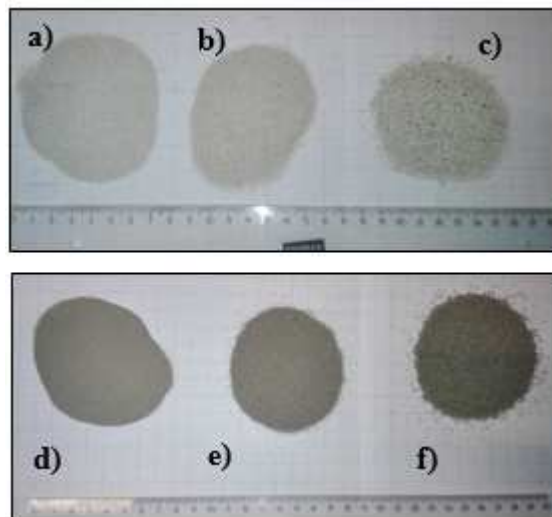
Figure 21 Lightweight aggregates: a) Rotocel® 90-300, b) Rotocel® 0.25-0.5, c) Rotocel® 0.5-1, d) Liaver® 0.1-0.3, e) Liaver® 0.25-0.5, f) Liaver® 0.5-1.

2.2.5. Commercial products for comparison: pre-mixed mortars

Two pre-mixed mortars are declared able to improve IAQ. Data and technical sheets well describe these two products. These products are commercialized by Kerakoll and Marcellina Calce and called Biocalce and CIM BIO - Cover M, respectively

The first product consists of pure natural lime NHL 3.5, that contains natural raw materials and recycles minerals with particle size range between 0-2.5 mm and mixing water amounts of about 5.1 l for 1 bag 25 kg of product.

The second product consists of natural hydraulic lime NHL 3.5, TX Active (the same active principle of photocatalytic cement produced by Italcementi) and calcareous and

siliceous aggregates with grain size range from 0.6 to 1.2 mm and mixing water amounts of about 21%.

These commercial pre-mixed products are used to compare their properties with those of the innovative mortars prepared during the experimentation.
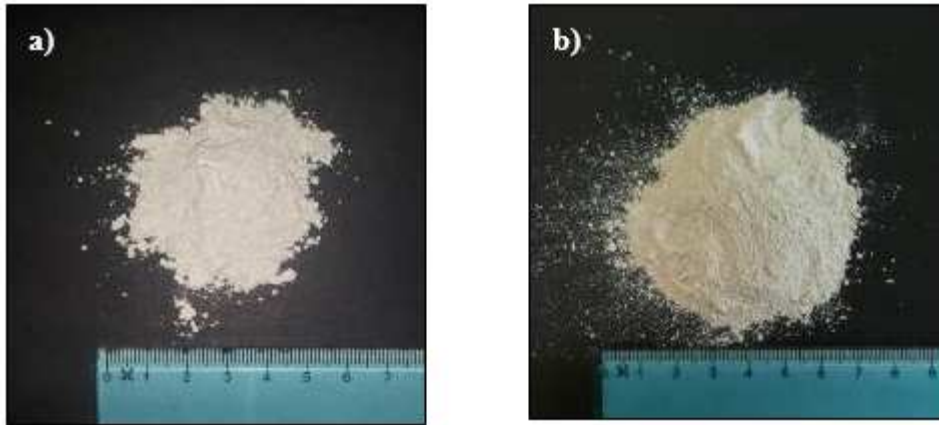
Figure 22 Pre-mixed mortars a) Kerakoll and b) Marcellina

2.3. Methods

In this research the characterization of mortars is made in terms of conventional properties and additional ones related to indoor air comfort and health.

2.3.1. Fresh state properties

The determination of consistence of fresh mortar by flow table is done according to the Italian standard UNI EN 1015-3:2007 [56].

The apparatus consists in the following main parts: stand, rigid plate and disc, horizontal shaft and lifting cam, lifting spindle.

Fresh mortar is inserted in a truncated conical mould with the dimension of 60 ± 0.5 mm in height and 100 ± 0.5 mm internal diameter at the bottom and 100 ± 0.5 mm internal diameter at the top. 2 mm is the minimum thickness. The moulds should be in the center of the disc of flow table. Mortar is introduced in two layers; each layer has been compacted and skimmed off the excess mortar with a palette knife.
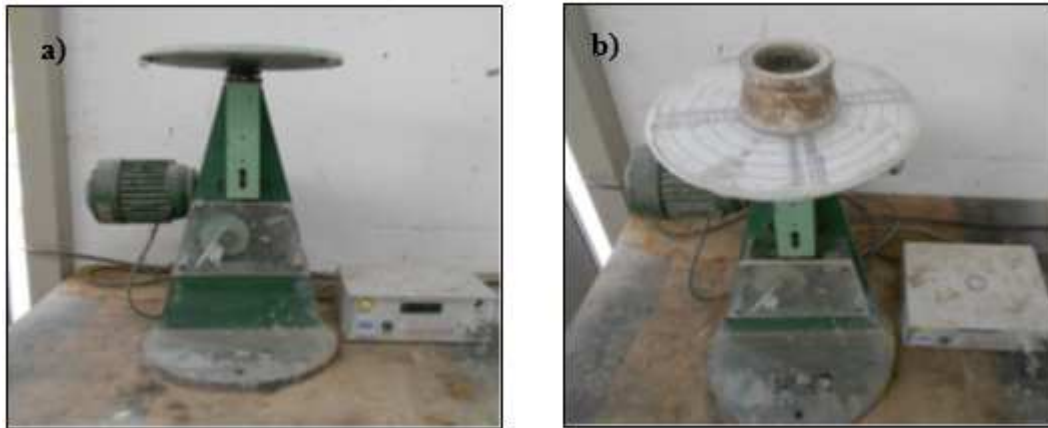
Figure 23 a) Flow table apparatus, with b) truncated conical mould

After 15 second the mould is risen vertically and the mortar spreads out, on the disc by jolting the flow table 15 times at a constant frequency (one per second). After 15 times, the diameter of mortar is measured. Through this measure the consistence of the mortar is defined [57]:

- stiff mortars: diameter till 140 mm;
- plastic mortars: diameter from 140 to 200 mm;
- soft mortars: diameter higher than 200 mm.

The results are expressed with the suggested equation, which defines the consistence of fresh mortar:

$$C = \frac{d_m - d}{d} 100 \ [\%]$$

Where:
C is the consistence of the fresh mortar, in percentage;
d_m is the measured diameter, in mm;
d is the internal diameter of the bottom of truncates conical mould, in mm.

2.3.2. Mechanical properties and microstructure of hardened mortars

2.3.2.1. Flexural and compressive strength

The strength corresponds to the maximum stress that a material, in the form of a given geometrical shape (specimen), can bear before breaking. Depending on the type of stress (flexural or compressive) the related measured mechanical property is flexural strength or compressive strength [58].

Tests to define flexural and compressive strength are performed according to the Italian standard UNI EN 1015-11:2007 [59]. Specimens are prism with 40x40x160 mm. Specimens are casted and cured for 7 days at 20 ± 2 °C and RH 95 ± 3%. For the following 21 days specimens are kept at the same temperature but exposed to a RH = 65 ± 3%.

Figure 24 Electro-hydraulic servo universal testing machine

The machine for flexural strength (Figure 24) (hydraulic press 'Galdabini') has two steel supporting rollers and a third steel roller of the same length and diameter located centrally between the support rollers. It shall be parallel equidistant and normal to the direction of prism under the test.

Machine for compressive strength is the same for flexural strength with different support plate. The machine has an upper platen able to align freely as contact with the specimen is made. There are two bearing plates.

Before casting, moulds are cleaned and lubricated at the internal faces by a thin layer of mineral oil preventing adhesion of mortar. At the age of 28 days, three specimens are tested. The load is applied without shock at a uniform rate (10 N/s for flexural strength and 200 N/s for compressive strength).
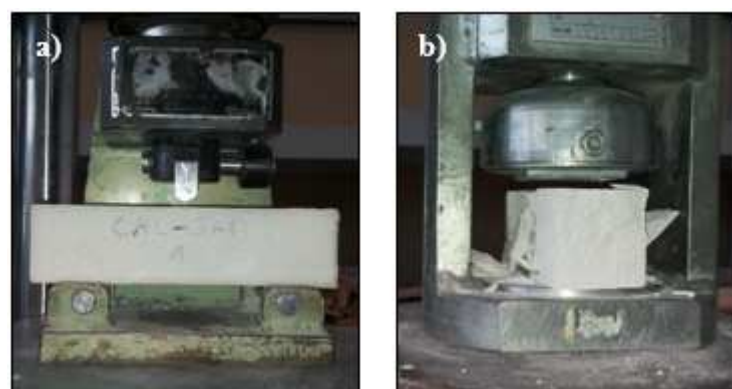
Figure 25 Specimens during a) flexural strength test and b) compression strength test

The maximum load is recorded and flexural strength R_f, in MPa, is calculated by:

$$R_f = 1.5 \frac{F \cdot l}{b \cdot d^2} \text{ [MPa]}$$

Where:

F is the result from test in kN;

l is the distance between the steel support, in mm;

b, d are the internal mould dimensions., in mm.

Compressive strength, R_c, in MPa, is calculated as the maximum load carried by the specimen divided by its cross-sectional area.

$$R_c = \frac{F}{b \cdot d} \text{ [MPa]}$$

Where:

F is the result from test in kN;

b, d are the dimensions of specimens, in mm.

After 28 days of curing, also the density of hardened mortars is calculated.

Knowing the hardened density, the specific strength of mortars is evaluated as:

$$R_{CS} = \frac{R_c}{\rho} \text{ [MPa/(kg/m}^3\text{)]}$$

Where:

R_{sc} is the specific strength of the mortar, in MPa/(kg/m^3);

R_c is the compressive strength, in MPa;

ρ is the hardened density, in kg/m^3.

Specific strength, also known as the strength-to-weight ratio, is most commonly used for comparing materials [60].

2.3.2.2. Morphology and microstructure of mortars

It is important to investigate the pore size distribution of the mortar to relate the microstructure to the macro-properties.

In cementitious materials porosity can be divided in [61]:

- gel pores: nano-pores inside the hydration products, with pore diameter of about 0.5-10 nm;
- capillary pores: micro-pores between the hydration products, with pore diameter between 10 nm and 1 µm, strongly dependent on hydration degree and w/b;
- macro pores: pores due to entrained air with spherical micro-bubbles, with pore diameters higher than 10 µm;
- porosity into the aggregate: in this experimentation is very important to take into account this porosity that influences a lot the properties of mortars. In this case the aggregates can have nano porosity (e.g. zeolite, silica gel or activated carbon) or macro pores (e.g. bottom ashes or lightweight aggregates).

Pore size distribution is mostly studied used with Mercury Intrusion Porosimetry (MIP). In this case, a Thermo Fisher, Pascal series 240 equipment is used. Mercury is a liquid which do not wet the surfaces of the specimens. It needs a pressure to be intruded inside the pores, the higher is the pressure, the lower is the pore radius. The principle is based on the Washburn' equation [45]:

$$\Delta P = \frac{2\gamma \cos\theta}{r} \ [\text{Pa}]$$

Where:

γ is the surface tension of the mercury, in Pa;

θ is the contact angle;

r the radius of the pores.

By the evaluation of the pressure applied and the volume of mercury intruded it is possible to know the pore distribution.

Authors [62] indicate the combined use of mercury and nitrogen as a possible development to study the porosity of materials. With Brunauer-Emmett-Teller (BET), Micrometics Tristar II, it is possible to investigate nano-pores. BET measurement is based on the physical adsorption of nitrogen on the specimen surface. This technique can measure both specific surface and nano-pores volume and distribution.

Measurements are performed on specimens after 28 days of curing. Hydration of mortars is stopped by the total immersion of specimen fragments in ethanol. Then samples are dried. For MIP analysis, fragments sampled for each mortar mix are about $1 \ \text{cm}^3$ in volume. For BET measurement, 3-4 fragments are sampled for each mortar mix to obtain at least are about $1 \ \text{cm}^3$ in volume.
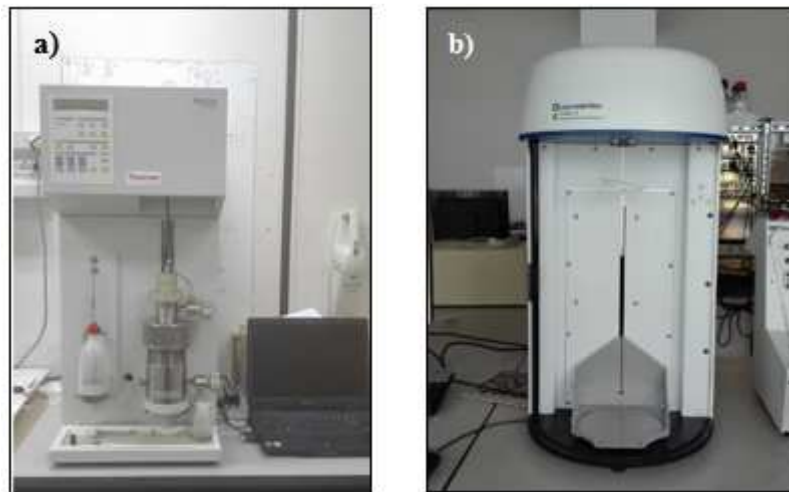
Figure 26 a) Porosimeter b) BET

Morphology of specimens is investigated with Scanning Electron Microscope (SEM) equipped with EDX probe. An image of the specimen is obtained scanning a sample area with a focused beam of electron. A surface exposed to high energy electron beams releases backscattered electrons, secondary and Auger, X-ray fluorescence and other photons. The images in SEM analysis method are produced with the signal of secondary and backscattered electrons. An image of the specimen is constructed by exploiting the direct relationship between intensity of backscattered electrons and the specimen surface.

Magnification provided by SEM is:

$$M = \frac{W}{w} \text{ [-]}$$

Where:
W is the size of display;
w is the size of once scanning.
Data are collected and measured by energy dispersion system. The samples to be analyzed, should be conductive in order to allow the passage of electrons and avoid problem of charge accumulation. With this aim, they are previously covered with a graphite layer.

2.3.2.3. Drying free shrinkage measurement

If mortars are applied in an environment with RH less than 95% they are subjected to a change in length, expressed as millimeter on meter (mm/m) referred as shrinkage. Shrinkage is measured in laboratory according to UNI 6687:1973 [63]. Specimens are prisms of 40x40x160 mm, casted and cured at 20 ± 2 °C and RH $95 \pm 3\%$ for 24 hours. Specimens are de-moulded after 24 hours and then exposed at the T = 20 ± 2 °C and RH $50 \pm 5\%$ in a climatic chamber. Free shrinkage is monitored at least for 30 days from the cast. During the cast, inside the specimens, on axial direction, metallic references are inserted, that permit to have fixed points to measure. Measurements are made for difference between the length of the specimens and the length of a reference stainless steel bar with constant length of 160 ± 1 mm. Measurements are made with a micrometer.
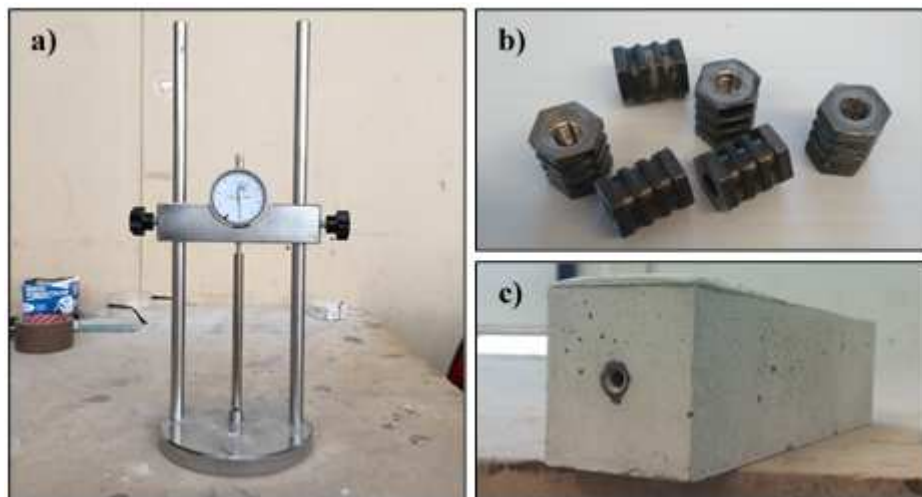
Figure 27 Equipment and specimens for free shrinkage measurement: a) micrometer and stainless steel reference bar, b) metallic references before and c) after the cast.

For each specimen 2 or 3 measurements are taken and then the averaged obtained value is calculated. The difference in length is calculated as:

$$\Delta_{1t} = L_{st} - L_{rt} \text{ [mm]}$$

Where:

Δ_{1t} is the average difference in length at time t, in mm;

L_{st} is the length of the specimen at time t, in mm;

L_{rt} is the length of the reference bar at time t, in mm.

The measure is taken different times during the exposure to a RH less than 95 ± 3%. The length contraction from the first day (0 day of exposure to RH less than 95 ± 3%) to day "t" is expressed as:

$$\Delta = \Delta_{1t} - \Delta_{10} \; [\text{mm}]$$

Where:

Δ is the longitudinal contraction of the specimen, in mm;

Δ_{1t} is the average difference in length at time t, in mm;

Δ_{10} is the average difference in length at time 0, first day at RH 95 ± 3%, in mm.

The drying shrinkage is expressed as:

$$\varepsilon = \frac{\Delta}{L} \; [\text{mm/m}]$$

Where:

ε is the strain due to free drying shrinkage, in mm/m;

Δ is the longitudinal contraction of the specimen, in mm;

L is the initial length of the specimen, in m.

The percentage of weight loss corresponds to evaporation of free water and is calculated by:

$$w_i = \frac{m_i - m_0}{m_0} 100 \; [\%]$$

Where:

w_i is the percentage of weight loss;

m_i is the weight at i-day, in g;

m_0 is the weight 24 hours after the cast, in g.

Both free shrinkage and percentage of weight loss are evaluated and plotted with time. Free shrinkage for mortars depends on three main factors: the dimension of pores, the quanty of total porosity and elastic modulus (Ec) of mortars.

Shrinkage of mortars is related to the dimension of mortar pores: the lower the pore radius the higher the induced stress [61] following Laplace equation:

$$\sigma_{cap} = \frac{2\gamma}{r} \; [\text{Pa}]$$

Where:

σ_{cap} is the tensile stress, in Pa;

γ is the liquid surface tension, in N/m;

r is the pore radius, in m.

Shrinkage of mortars is related to the total volume of pores: the higher the volume of pores, the higher the possibility of water vapor to evaporate.

Shrinkage is also depending on elastic modulus (Ec) of mortar, the higher E is, the lower is the shrinkage. Elastic modulus can be evaluated by the empirical relation suggestion by ACI Committee (ACI 318-95) and used by other authors [64]:

$$E_c = 4.73 \cdot f_c^{0.5} \text{ [MPa]}$$

Where:
Ec is the elastic modulus (MPa);
fc is the compressive strength of conglomerates (MPa).

2.3.3. Durability of mortars

The capillary water rising affects all mortars in contact with the ground, in environments with high humidity or exposed to atmospheric phenomena. It is related to the durability of the material itself: water could transport aggressive agents or can deteriorate the finishes.

Capillary water absorption is affected by the distribution of the pore network, since the lower diameter of pores is, the higher is the level reached by the rising water, due to Washburn equation [45]. In addition, obviously, the higher the connected porosity is, the higher is the water that can fill the pores.

Two different methodology are used in order to study the capillary water rising: one indicates the procedure to evaluate the water absorption coefficient due to capillary action, the other indicates the procedure to measure in time the water absorption.

2.3.3.1. Water absorption coefficient due to capillary action of hardened mortar

The determination of water absorption coefficient due to capillary action of hardened mortar is calculated with UNI EN 1015-18:2004 [65].

The test specimens shall be prism 160x40x40 mm broken into two halves. Specimens are placed in a box, kept at a distance from the bottom via suitable supports, immersed in water at a depth of 5 to 10 mm for the duration of the test. The level of water is kept constant during the test. The box is then covered to prevent water evaporation.
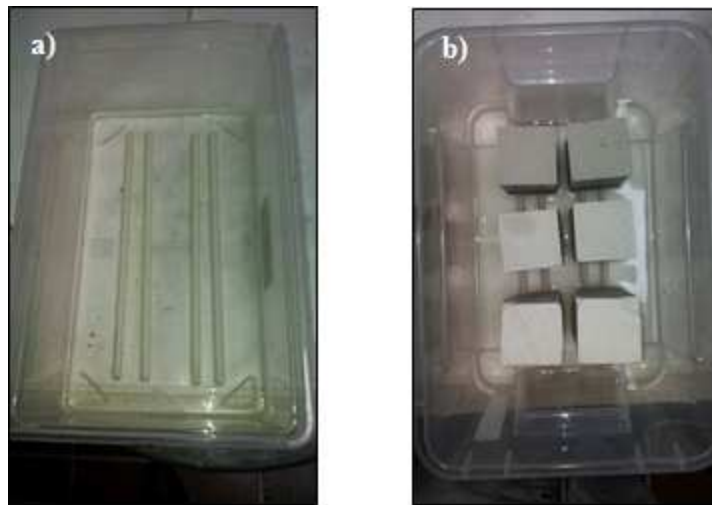
Figure 28 Test box a) before the insertion of the specimens and b) after

Specimens are removed from the box after 10 min, the surface is quickly dried to remove the excess of water and weighted and immediately putted them back into the box. The procedure is repeated after 90 min.

The determination of water absorption coefficient due to capillary action of hardened mortar is obtained by:

$$C = 0{,}1 * (M_2 - M_1) \frac{kg}{m^2 * \sqrt{min}}$$

Where:

C is the capillary water absorption coefficient ($kg/(m^2 min^{0.5})$);

M_1 is the weight at 10 minutes, in g;

M_2 is the weight at 90 minutes, in g.

2.3.3.2.   Water absorption: development during time

In order to explore better the behavior of mortar in terms of water absorption by capillary action the specimens are tested according to the standard UNI EN 15801:2010 [66]. The standard determines the amount and rate at which a specimen absorbs water by capillarity through the test surface when it is in contact with filter paper saturated with water. The test specimens shall be prism 160x40x40 mm broken into two halves. The area in contact with filter paper is 16 cm^2.

Figure 29 Specimens placed in boxes where a filter paper layer of 10 mm soaked with deionized water is inserted

The capillary water absorption is monitored in time by weighing the specimens periodically (m_i at t_i). The amount of water absorbed by the specimen per unit area Q_i (kg/m^2) at time t_i (s$^{0.5}$) is calculated as follows:

$$Q_i = \frac{m_i - m_0}{A} \ [\text{kg/m}^2]$$

Where:
m_i is the mass of the specimen at time t_i, in kg;
m_0 is the mass of the dry specimen, in kg;
A is the area of the specimen in contact with water, in m^2.

2.3.4. Interaction between finishes and indoor environment: hygro-thermal behavior

Porous structure of the mortar influences properties such as permeability and moisture buffering ability.
Construction materials should permit a good transpirability for multiple reasonssuch as the human health and the dispelling humidity of the environments. A high permeability to water vapor facilitates the drying process of rendering mortars and masonry assemblage, as well as allowing the passage of water vapor produced inside a building. Ideally, a low permeability to water, a low capillary absorption coefficient and high permeability to water vapor would be the most favorable characteristics that can be expected from a high durability mortar [67]. But this capacity should be high not only in static condition (indoor environment with the same value of RH), but also in dynamic conditions when RH changes. Indoor environments are subjected to quick changing in RH and building materials should be able to be a buffer for the moisture. This ability is expressed as moisture buffering capacity.

2.3.4.1. Water vapor permeability

Water vapor permeability measurements are carried out according to the UNI EN 1015-19:2007 [68]. Data are then processed according to UNI EN ISO 12572:2007

[69]. Specimens of mortar (d = 12.5 cm; h = 3 cm) are placed on the top of a sample-holder with inside a saturated solution of KNO_3 (RH of 93 ± 3%). The specimens are sealed with a non-breathable film on the side surface in order to guarantee the unidirectional flow of the water vapor due to the difference of RH inside and outside the chamber. In fact, the different partial pressure between the vapor pressure and the climatic chamber that occurs through the permeable specimens causes a vapor transport. The containers are placed in a climatic chamber at 20 ± 2 °C and 50 ± 5% RH.

After the preparation of the specimens the test starts. The mass of the specimens is monitored day by day until stationary condition is reached. It means that the difference in mass over time should be the same and, in a graph mass-time, the mass values should be on a straight line.

Figure 30 Specimens on the sample-holder inside the climatic chamber.

The aim of this test is to evaluate the water vapor diffusion resistance factor, μ. At first the velocity of mass variation is evaluated as:

$$\Delta m_{12} = \frac{m_1 - m_2}{t_1 - t_2} \text{ [kg/s]}$$

Where:
Δm_{12} is the mass difference during a specific time for a specimen, in kg/s;
m_1 is the mass of system (specimens, sample holder, saturated solution, non-breathable film) at time t_1, in kg;
m_2 is the mass of system at time t_2, in kg.
The regression line between time and mass is plotted. The flux G (kg/s) is calculated by the slope of the last linear part of the curve. Then the flow rate of water vapor (g) is:

$$g = \frac{G}{A} \text{ [kg/m}^2\text{s]}$$

Where:
A is the exposed area of the specimens, evaluated as the average between the bottom and the upper surfaces of the specimen, exposed to two different RHs, in m^2.
The ratio between g and the difference in pressure between two layer of specimens is water vapor permanence (W_p):

Characterization of materials and definition of methods

$$W_p = \frac{g}{\Delta_{pv}} \ [\text{kg/(m}^2\text{sPa)}]$$

Where:

$$\Delta_{pv} = p_{sat} \cdot (UR_1) - p_{sat} \cdot (UR_2)$$

Where:
$p_{sat}(UR_1)$ is the water pressure inside the sample holder, in Pa;
$p_{sat}(UR_2)$ is the water pressure inside the chamber, in Pa.
Those values are evaluated with:

$$p_{sat} = \exp[65.81 - \frac{7066.27}{T+273.15} - 5.976 \cdot \ln(T + 273.15)] \ [\text{Pa}]$$

Where:
T is the temperature, in °C.
Water vapor permeability is evaluated with:

$$\delta_p = W_p \cdot h \ [\text{kg/(msPa)}]$$

Where:
h is the height of the specimens, evaluated through the average measured in 5 different high, in m.
Water vapor diffusion resistance factor, µ-value is:

$$\mu = \frac{\delta_a}{\delta_p} \ [\text{-}]$$

Where:
δ_a is the permeability evaluated according to the Schirmer formula:

$$\delta_a = 0.0000231 \cdot \left(\frac{p_0}{p \cdot R \cdot T}\right) \cdot \left(\frac{T}{273K}\right)^{1.81} \ [\text{kg/(msPa)}]$$

Where:
p: is the barometric standard pressure, equal to 1013.25 hPa;
p is barometric pressure p, in this case evaluated according to the barometric standard pressure, 1013.25 hPa;
T is the temperature, 293.15 °K;
R is the individual Gas Constants for air and water vapor, 462 in Nm/(kg K).

For the interpretation of data is reported the Kats and Thompson relation [70], permeability of mortars is proportional to the cube value of average radius of pore network. This fact well explains the behavior of current mortars, since the lower the pore radius, the lower the transpirability [60].

2.3.4.2. Moisture Buffering Capacity

The Moisture Buffering Capacity (MBC) is defined as the capacity of a material to absorb and release moisture from/to the environment where it is placed [71]. The Moisture Buffering Value (MBV) indicates the amount of water vapor that is transported on the open surface, during a certain period and at a certain RH. In the current thesis, MBV is assessed by a simplified version of the NORDTEST method [72].

In order to simulate the behavior of materials exposed to indoor air and the relative influence on the regulation of RH, specimens are cyclically exposed to different RH for fixed periods.

Cylindrical specimens (d = 10, h = 3 cm) are manufactured and cured according to UNI EN 1015-11:2007. Before testing, specimens are pre-conditioned in a climate chamber at T = 20 ± 2 °C and RH = 50 ± 3% until constant weight is reached.

Cycles consist in 8 hours at high level of RH = 75 ± 3% and 16 hours at low level of RH 33 ± 3%. The salts are magnesium chloride, $MgCl_2$, RH 33 ± 3%, and sodium chloride, NaCl, for RH = 75 ± 3%. These two conditions are reached in two sealed boxes where a saturated salt solution is placed on the bottom. These boxes are placed inside a climatic chamber to maintain the temperature constant at T = 20 ± 2 °C.
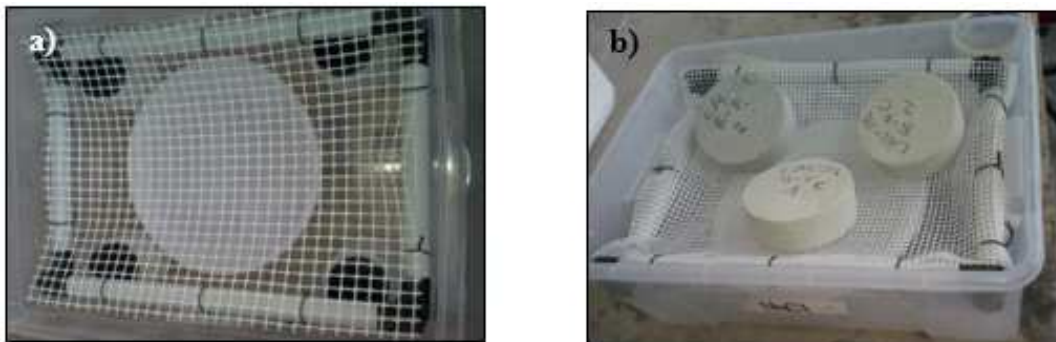
Figure 31 Sealed boxes with different RH a) without and b) with specimens inside

The duration of the entire cycle is 24 h. By the differences in mass at the end of the period the quantity of water vapor uptaken and released on the environment is evaluated.

Differences in mass during adsorption phase are evaluated as:

$$m_a = m_8 - m_0 \text{ [g]}$$

m_a is the mass change during adsorption phase, in g;
m_8 is the mass measured after 8 hours at RH 75 ± 3%, in g;
m_0 is the mass measured before the test, in g.

Differences in mass during desorption phase are evaluated as:

$$m_d = m_{24} - m_8 \text{ [g]}$$

Where:

m_d is the mass change during desorption phase, in g;

m_{24} is the mass measured after 16 hours at RH 33 ± 3%, in g;

m_8 is the mass measured after 8 hours at RH 75 ± 3%, in g.

Difference are then normalized with respect to the exposed surface:

$$\Delta_a = \frac{m_a}{S} \ [g/m^2]$$

$$\Delta_d = \frac{m_d}{S} \ [g/m^2]$$

Where:

Δ_a is the variation in mass with respect unit of surface during the absorption phase, in g/m^2;

Δ_d is the variation in mass with respect unit of surface during the absorption phase, in g/m^2;

m_a is the mass change during adsorption phase, in g;

m_d is the mass change during desorption phase, in g;

S is the exposed area of the specimens, in m^2.

The mass-change per surface unit is then plotted against time. These results are evaluated for each specimen and the average value is calculated. The average between adsorption and desorption phases is also calculated in order to evaluate Practical MBV. MBV is defined as the amount of moisture content that passes through the unit open surface of the material when the material is exposed to variation in RH of the surrounding air [73]:

$$MBV = \frac{\Delta m}{S \cdot (RH_{high} - RH_{low})} \ [g/(m^2 \% RH)]$$

Where:

MBV is the practical moisture buffering value, in $g/(m^2 \% RH)$];

Δm is the moisture uptake/release during the period, as the average between adsorption and desorption phase $m_a - |m_d|/2$ (g);

S is the surface of exposed specimens;

RH_{high} is high RH, 75 ± 3%;

RH_{low}: is low RH, 33 ± 3%.

MBV is evaluated on the average of the values obtained in the last 3 cycles with constant variations.

2.3.4.3. Thermal conductivity

Specimens are 10x10x10 cm cured at least 21 days (7 days at 95 ± 3% RH and 21 ± 2 °C and then following 14 days at 60 ± 3% RH and 21 ± 2 °C). Then, specimens are dried in a ventilated oven at 75 ± 3 °C until constant mass is reached and cooled down

at room temperature. Thermal conductivity and the specific heat capacity of the specimens is measured with the thermal conductivity equipment ISOMET 2014.

Figure 32 Thermal conductivity equipment, ISOMET 2014

The used probe can measure thermal conductivities in the range between 0.04 W/mK and 0.3 W/mK. The measurements are performed in two different conditions of specimens: dry condition and in a humidity controlled chamber at $60 \pm 5\%$ RH until constant mass is reached, in order to evaluate the influence of the humidity of the environment.

2.3.5. Health of occupants: resistance to biological attacks and depollution properties

2.3.5.1. Molds growth

The study of mold growth on mortar is performed according to UNI EN 15457:2014 [74]. This standard is for painting so it has been adapted for mortars.
At first the cast of the specimens needs to be performed in sterile condition. To guarantee sterile conditions all ingredients are weighted and mixed in dry condition. Powders are put in an oven at 150 °C to sterilize them. The powers are mixed with distilled and sterilized water under a chemical laboratory fume hood. The cast is performed on filter papers (surface exposed 6.5 x 6.5 cm); an example of specimens is shown in Figure 33. Two filter papers without mix are prepared to have blank samples. The specimens are inserted in petri boxes to maintain sterility outside the hood.

Characterization of materials and definition of methods
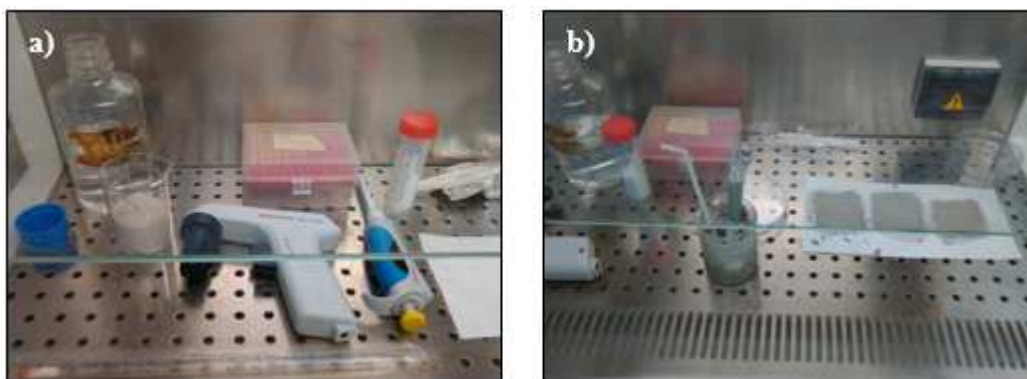
Figure 33 a) Tools for cast sterilizing, b) manufactured specimens

After 2 months of curing the pH of mortars is controlled. 1 g of material is collected on a glass slide; a drop of water (about 1 ml) is added and the pH of the solution is measured. The obtained value is approximate, it serves to ensure that the sample has already carbonated, losing its initial basicity.

Aspergillus niger is the mold chosen to study the inhibition of the growth. The inoculation is performed with the strain of Aspergillus niger (F18) taken from the Urbino University culture collection and propagated on Potato Dextrose Agar (Oxoid). After cultivation. Conidia are harvested for 7 days at T = 28 ± 0.5 °C stirring the culture with a sterile 0.85% NaCl (Sigma–Aldrich St. Louis, MO, USA) solution containing 0.05% Tween 80 (Sigma–Aldrich St. Louis, MO, USA) for 5 min. The conidia suspension is gently probed with a pipette tip and filtered to separate conidia from hyphal fragments. The transmittances of the conidia suspensions are adjusted using a BOECO Germany S-30 Spectrophotometer to provide a final test inoculum of about 106 conidia/ml (ODλ530 0.1). To allow conidia to adhere to the mortar surface 10 µl of Potato Dextrose Agar were added to 10 µl of conidia solution and placed in the middle of mortar specimens described above. Only conidia are chosen to perform the inoculum to reproduce better the dynamics of colonization commonly found in nature. Following inoculation, the specimens are arranged in Petri dishes incubated for 4 weeks at 25 ± 2 °C and RH = 80 ± 5%. The period of inoculation is evaluated sufficient from previous studies [75]. At the end of the test, the mold growth is evaluated by means of several quantitative parameters.
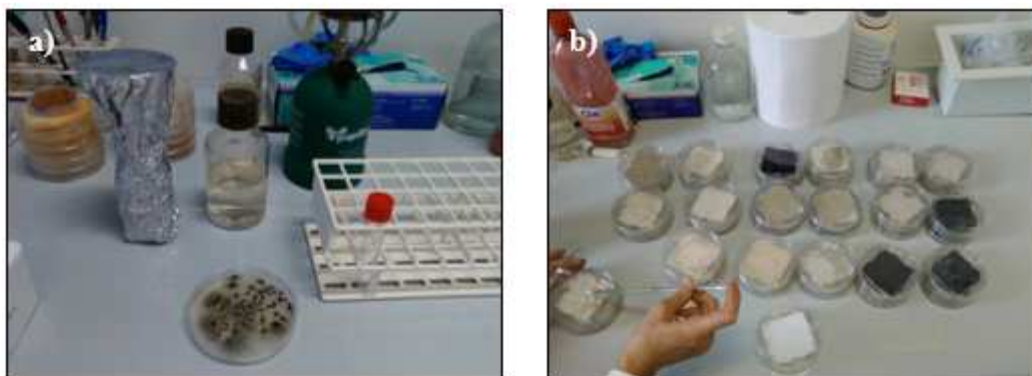
Figure 34 a) Aspergillum niger, b) inoculum of aspergillum niger

Each week, photos of specimens are taken. The images are elaborated with two different software, ImageJ and GIMP2. Pixels, corresponding to the percent of area colonized with molds, are counted. Images are divided in 3 different zones: zone 1: completely colonized; zone 2: boundary zone, where the molds are growing and zone 3: not colonized. The sum of pixels in zone 1 and 2 gives the amount of area colonized.

2.3.5.2. Removal of Volatile Organic Compounds

Chromatography is an analytical method for the quantitative determination of the solutes in a mixture.

In this thesis, a gas chromatography is used in order to study the depolluting rate of mortar samples that operate in two different ways: pure adsorption and adsorption and photocatalytic oxidation if irradiated by light or UV radiation.

Gas Chromatography (GC) is a separation technique in which the components of the vaporized specimen are separated thank to the interaction between a mobile phase and a stationary phase inside the chromatographic column (in this case the column is a capillary column).

The mobile phase does not interact with the analytes (the molecules to be separated) but it is just a carrier. A known volume of the specimen is introduced into the injector by a micro-syringe. The adopted GC configuration is: injector split 1:15, carrier control by flow, capillary column length 25 m, thickness 0.52 um, φ 0.32 mm, crosslinked Methyl Siloxane, isotherm 40 °C, FID Detector.

Figure 35 Gas chromatography apparatus

The output from gas chromatography analysis is a graph with peaks, whose areas correspond to the measure of the analytes concentration (mg/m^3).

In this study methylethylketone, MEK ($CH_3COC_2H_5$) is chosen as tracer for its chemical stability and because MEK is a typical model tracer for the odors.

The analytical sample is air that comes from a sealed box where the concentration of MEK is known and air mixing is guaranteed.

Two boxes are used. A silicate-glass box of 16.65 l and a silicate-glass box of 1 l. Specimens are placed inside the box and the surrounding air is sampled and analyzed. If photocatalytic properties shall be measured, a black cover is placed on the wall of the box and different lamps are placed inside the box. A 12 V fan is placed on the bottom of the box. The fan makes air circulation, operates continuously by mixing the air in the box (Figure 36).
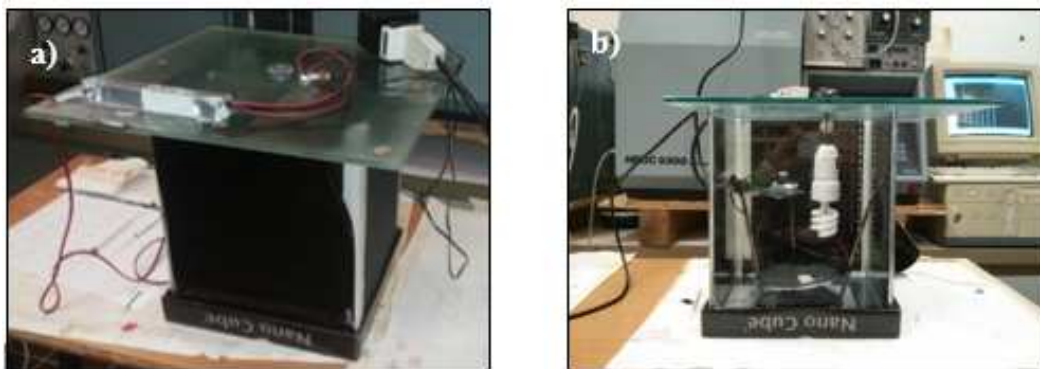
Figure 36 a) Sealed box used (16.65 l) for the study of depolluting properties. b) light source placed inside the box

It is possible to know the concentration of MEK inside the box with a calibration line that relates the peak area of the chromatograms to known volumetric load of MEK. Usually, the calibration line is performed at different MEK load, specified in each chapter.

When the specimen is placed inside the chamber, its efficiency of MEK removal is evaluated by monitoring in time the concentration of MEK (air is sampled with

intervals of 8 ± 2 minutes). The initial load of MEK is considered the theoretical maximum concentration inside the box (C_0, at the time t = 0).

In order to allow an objective comparison between different tests, these considerations must be made:

- eliminate not significant data. The data is not significant when the outputs values of the tests (value of peak areas) are affected by problems caused by, for example, an obstruction of the microsyringe for injections;
- start the data elaboration after at least 10 mins form the load of MEK inside the box so MEK can completely vaporize;

normalize the concentration load compared to the initial theoretical concentration C_i/C_0;

- evaluate the trend lines as logarithmic functions. The lines have to represent the best adsorption data trend.

2.3.5.3. Removal efficiency of nitrogen oxides: plug-flow test

Photocatalytic activity is quantified according two different standards: UNI 11247:2010 and ISO 22197-1:2007, ISO 22197-2:2011, ISO 22197-3:2011. The principle is the same, the main differences are on the chamber for the analysis. At first the reaction mechanism needs irradiation to be activated, so the generation of hole/pair is possible. This step is then followed by the adsorption phase of the pollutants onto the TiO_2. The following steps are explained in literature [20]:

$$h^+ + H_2O \rightarrow OH^\cdot + H^+$$

$$e^+ + O_2 \rightarrow O_2^-$$
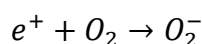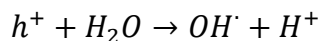
The adsorbed pollutants can be oxidized by these radicals:

$$NO + OH^\cdot \rightarrow HNO_2$$

$$HNO_2 + OH^\cdot \rightarrow NO_2 + H_2O$$

$$NO_2 + OH^\cdot \rightarrow NO_3^- + H^+$$
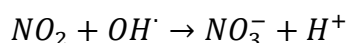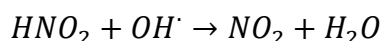
The generated superoxide can be also attacked the following routes:

$$O_2^- + H^+ \rightarrow HO_2$$

$$NO + HO_2 \rightarrow NO_3^- + H^+$$
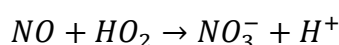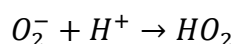
The continuous flow test is performed according to the operational scheme provided by Italian standard UNI 11247:2010. Following the procedure already reported in literature [16], the specimen (a cylinder with 9 cm diameter and 3 cm high, with a total

exposed surface of about 65 cm^2) is placed inside a borosilicate glass chamber of 3.58 l on a tripod in order to irradiate the surface with UVA radiation provided by an UVA metal-halogen quartz lamp with mercury vapor, peak at 360 nm and adsorbed power of 400 W. The distance of the surface of the sample from the lamp guarantees a specimen irradiance of about 20 W/m^2. The inlet gas is a mixture of synthetic air and NO$_x$. The chamber is linked to an analyzer Monitor Labs, Nitrogen Oxides Analyzer model 8841. The inlet concentration guarantee is of 550 ppb of NO$_x$ and the abatement coefficient is evaluated according to:

$$A_c = 100 \times \frac{(C_B - C_L)}{C_B} \times \frac{I_N}{I} \times \frac{S_N}{S} \ [\%]$$

Where:
A_C is the percentage of pollutant abated, in this case NO, in %;
C_B is the concentration of NO out from the reactor at dark condition, in ppb;
C_L is the concentration of NO out from the reactor at UVA condition, in ppb;
I is the irradiance detected during the test, in W/m^2;
I_N is the nominal irradiance (20 W/m^2);
S is the surface of the specimen, in cm^2;
S_N is the nominal surface of the specimen (64cm^2).

The experimental plug-in set up used to perform the test according to ISO 22197-1:2007 is reported in Figure 37. The used pollutant is NOx, mixed with synthetic air. Concentration of pollutant and flow rate are chosen in order to have more reliable conditions.
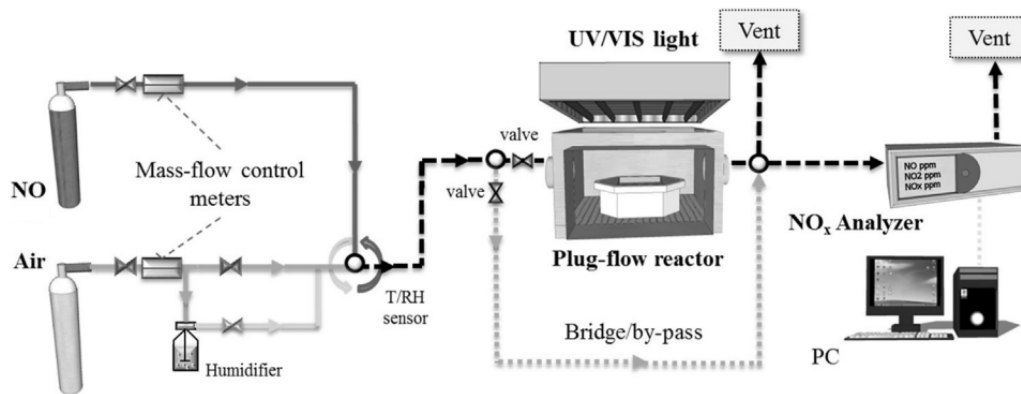
Figure 37 Scheme of the plug-in experimental set-up [20]

The test is performed under two different radiation sources: UVA ($\lambda = 300 - 400$ nm) and daylight. Radiation sources are provided with six fluorescent tubes (Philips). For both cases the intensity of the radiation is checked before each test adjusted to about 10 W/m^2. There are 6 mm from the boro-silicate surface of the reactor and the sample inside it. Specimen has 200x100 mm surface exposed. For each measurement, experimental conditions are controlled in order to better evaluate results. Temperature and humidity are kept constant at 22 ± 2 °C and $50 \pm 3\%$ RH for all the measurement.

The concentration of pollutants (NO, NO_x, NO_2) is measured by an online NO_x analyzer ANPA-370 (Horiba) continuous monitoring. The following formula is used in order to determine the degradation of total NO_x (NO+NO_2):

$$NO_x degradation = \frac{[c_{NO_x}]_{in} - [c_{NO_x}]_{out}}{[c_{NO_x}]_{in}} \times 100 \ [\%]$$

Where:
NO_xdegradation is the percentage of NO_x decomposed;
$[C_{NOx}]_{in}$ is the initial concentration, in ppm;
$[C_{NOx}]_{out}$ is the outlet concentration, in ppm.
Both values are the average between 5 mins measurement.

2.3.6. Aesthetic appearance of mortars

Mortars for indoor application should be able to be applied without painting. So, if color pigments are added, they should find a substrate as clear as possible. The differences in color are evaluated by scanning of 40x40x160 mm specimens. After the acquisition of the images, different points on the surface are selected with an images elaboration software such as Photoshop. RGB coordinates are evaluated in 5 different points and the average values are calculated.

2.3.7. Life Cycle Assessment

The life cycle assessment (LCA) is carried out to quantify the environmental impact of the mortar [51], [76]. It quantifies all relevant emissions and resources consumed and the related environmental, health impacts and resource depletion issues that are associated with any goods or services [77].
The GaBi 6 Professional software integrated with the EcoInvent 2.2 database is used for LCA. The energetic account is provided with a database. The functional unit is 1 m^3 of mortar, and the system boundaries consider the mortar preparation, the materials used and the avoided landfill. The impact category climate change was selected, evaluated with the Baseline model of 100 years of the IPCC, with the indicator of global warming potential (GWP100) expressed in terms of CO_2-Equiv.

Chapter 3

3. Mortars based on white and photocatalytic cement with unconventional aggregates

3.1. Introduction

In this study TiO$_2$-enriched cementitious mortars [28] are tested in mixes with unconventional aggregates, with the purpose of enhance IAQ. These products are cement-based binders with self-cleaning and/or depolluting properties [78].

A silane-based hydrophobic admixture is added in the matrix in order to evaluate the influence on durability and IAQ properties.

The transport of the pollutants over the "activated" catalytic surface is the first necessary step for heterogeneous photocatalysis. Maintaining a high adsorption capacity of material is possible by using an adsorbent material. In this way mortars not only fulfill the traditional requirements but also, having higher water vapor permeability, the ability to regulate indoor moisture, and depollution properties can enhance the IAQ and realize healthy environment.

In particular, sixteen different types of mortars have been manufactured with traditional commercial sand, as reference aggregate, and with three different adsorbent aggregates both with a photocatalytic and white cement, with and without hydrophobic admixture, in order to investigate the combined effect on the properties. Mortars have been compared in terms of mechanical strength, morphology and microstructure, capillary water absorption, shrinkage, permeability, moisture buffering ability and de-pollution properties.

3.2. Materials

White cement CEM II A/LL 42,5 R Roccabianca, Italcementi (C) and 'TX ARIA', Italcementi (PC) are used as traditional and photocatalytic binders, respectively. These products are cement based binder, described in § 2.2.2.1.

As unconventional aggregates, lightweight commercial materials, generally used as adsorbent for heavy metals, dyes and oil removal from aqueous solutions, and/or acting as heterogeneous catalysts, adsorbents and molecular sieves in gas separation processes, are adopted. In particular, calcareous sand is used as reference-conventional aggregate and the unconventional adsorbent aggregates are zeolite (A1), silica gel (A2)

and activated carbon (A3), described in §2.2.4.1, 2.2.4.2, 2.2.4.3, 2.2.4.4. Silane based hydrophobic admixtures (h) used is described in § 2.2.3.2.

3.2.1. Mix design

Conventional mortars are manufactured with cement (white and photocatalytic) and commercial sand, with and without hydrophobic admixture added in quantities indicates in data sheet. Mortars have a w/b of 0.5 by weight and an aggregate to binder ratio (a/b) of 3.5 by volume. From the traditional mortars, 100% sand volume is replaced by different unconventional aggregates. Table 4 reports the combinations, the codes and the colors used to recognize the different mortars.

Table 4 Mortars prepared: summary of different combinations

Binder	Aggregate	Admixture	Code ID	Code Color
White Cement	Calcareous sand	-	C-S	
White Cement	Calcareous sand	Silane-based	C-S h	
Photocatalytic Cement	Calcareous sand	-	PC-S	
Photocatalytic Cement	Calcareous sand	Silane-based	PC-S h	
White Cement	Zeolite	-	C-A1	
White Cement	Zeolite	Silane-based	C-A1 h	
Photocatalytic Cement	Zeolite	-	PC-A1	
Photocatalytic Cement	Zeolite	Silane-based	PC-A1 h	
White Cement	Silica Gel	-	C-A2	
White Cement	Silica Gel	Silane-based	C-A2 h	
Photocatalytic Cement	Silica Gel	-	PC-A2	
Photocatalytic Cement	Silica Gel	Silane-based	PC-A2 h	
White Cement	Active Carbon	-	C-A3	
White Cement	Active Carbon	Silane-based	C-A3 h	
Photocatalytic Cement	Active Carbon	-	PC-A3	
Photocatalytic Cement	Active Carbon	Silane-based	PC-A3 h	

The appropriate volume required for casting is evaluated according to the different tests that are performed. Aggregates are added in ssd conditions. Hydrophobic

admixture is added in a water dispersion: the additional water is then removed from the water amount. Mix designs are shown in Table 5.

Table 5 Mix proportions (kg/m³) of mortars

Mix	Water	White cement	Photo-catalytic cement	Sand S	Zeolite A1	Silica Gel A2	Active Carbon A3	Hydro-Phobic Adm.
C-S	256	512	-	1535	-	-	-	-
C-S h	253	512	-	1535	-	-	-	6
PC-S	256	-	512	1535	-	-	-	-
PC-S h	253	-	512	1535	-	-	-	6
C-A1	256	512	-	-	927	-	-	-
C-A1 h	253	512	-	-	927	-	-	6
PC-A1	256	-	512	-	927	-	-	-
PC-A1 h	253	-	512	-	927	-	-	6
C-A2	256	512	-	-	-	759	-	-
C-A2 h	253	512	-	-	-	759	-	6
PC-A2	256	-	512	-	-	759	-	-
PC-A2 h	253	-	512	-	-	759	-	6
C-A3	256	512	-	-	-	-	683	-
C-A3 h	253	512	-	-	-	-	683	6
PC-A3	256	-	512	-	-	-	683	-
PC-A3 h	253	-	512	-	-	-	683	6

Mortars are casted in different moulds in order to obtain the specimens suitable for the determination of each property. During the cast mortars are vibrated manually to eliminate the excess of air. Vibration is carried out manually in order to avoid the segregation of lightweight aggregates from cement paste.

3.3. Methods

Mortars are characterized in terms of fresh state properties. Workability is measured with flow tables, according to the current standards (§ 2.3.1).
After 28 days of curing, flexural and compressive strength are tested. Also, the specific strength is evaluated (§ 2.3.2.1).
After 28 days of curing, morphologies are investigated by Scanning Electron Microscope (SEM) and pore size distribution is evaluated by Mercury Intrusion Porosimetry (MIP) (§ 2.3.2.2).
Free shrinkage and weight loss due to the water evaporation of mortars are monitored for about 50 days (§ 2.3.2.3).
Water is the medium where ions can be transported and can compromise the durability of building material. Water transport in mortars is evaluated with two different methodologies (§ 2.3.3.1 and § 2.3.3.2).

Transpirability of mortars for renders is a fundamental property, evaluated according to § 2.3.4.1.

The moisture buffering capacity of mortars is evaluated over dynamic variation of RH with a simplified procedure of the NORDTEST method (§ 2.3.4.2).

De-pollution properties of different mortars are evaluated by two different experimental tests: in batch (§ 2.3.5.2), to explore adsorbent/photocatalytic properties, and in continuous flow test (§ 2.3.5.3).

3.4. Results and discussions

3.4.1. Workability

Table 6 shows workability of mortars in terms of slump flow and consistency value.

Table 6 Workability of different mortars: picture of mortar at fresh state after slump flow test, slump flow values and consistency.

Mix	C-S	C-S-h
Slump (mm)	120	115
Consistency (%)	20	15
Mix	PC-S	PC-S h
Slump (mm)	120	115
Consistency (%)	20	15
Mix	C-A1	C-A1 h

Mortars based on white and photocatalytic cement with unconventional aggregates

Slump (mm)	108	107
Consistency (%)	8	7
Mix	**PC-A1**	**PC-A1 h**

Slump (mm)	106	106
Consistency (%)	6	6
Mix	**C-A2**	**C-A2 h**

Slump (mm)	128	122
Consistency (%)	28	22
Mix	**PC-A2**	**PC-A2 h**

Slump (mm)	124	128
Consistency (%)	24	28
Mix	**C-A3**	**PC-A3 h**

Slump (mm)	110	110
Consistency (%)	10	10
Mix	**PC-A3**	**PC-A3 h**

Slump (mm)	110	111
Consistency (%)	10	11

All mortars have the same consistency. The slump value is lower than 140 mm for all the mixes and, according to UNI EN 1015-6 [57], mortars are defined stiff.
The aggregates are added in ssd condition.

3.4.2. Mechanical strength

Figure 38 shows the results in terms of maximum flexural strength. The use of different binder or the use of admixture does not imply differences in flexural strength results. The main differences are shown with different aggregates.
Mortars with conventional aggregate, with both cement and with or without hydrophobic admixture, show the highest flexural resistance.
Activated carbon (A3) mortars have 30% mechanical strength of sand-based mortars. Both zeolite (A1) and silica gel (A2) based mortars have the lowest flexural mechanical resistance, 20% of mechanical strength of that measured in sand-based mortars.
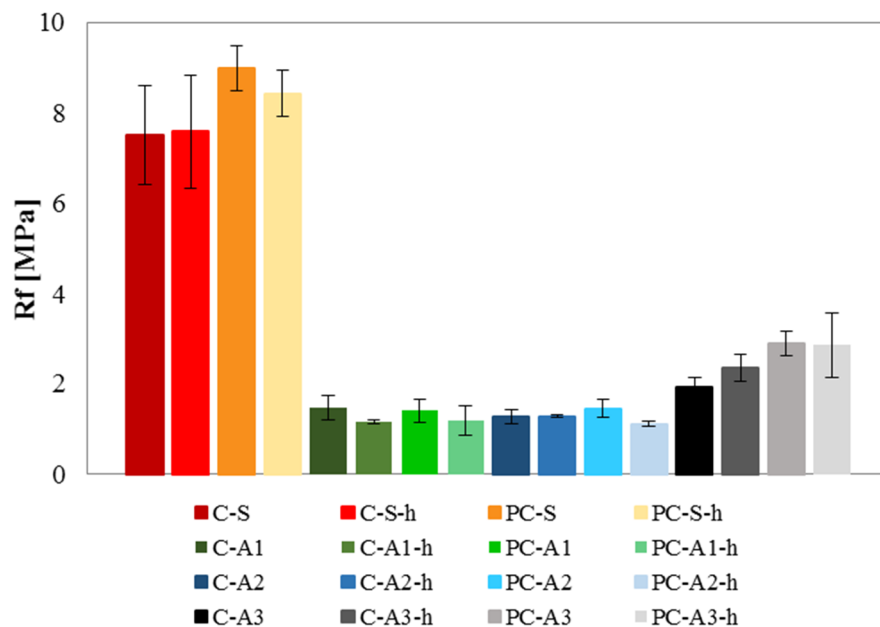
Figure 38 Flexural strength of cement-based mortars

Mortars based on white and photocatalytic cement with unconventional aggregates

Compressive strength is evaluated at 28 days and results are reported in Figure 39. It is evident that, in general the use of different binder or the use of the hydrophobic admixture do not imply differences in compressive strength results. This result is on contradiction with previous results reported in the literature that show a decrease in mechanical resistance [79]. Differences of 5% in results can be due to the experimental procedure: the manual vibration of specimens can sometimes let air bubbles inside the matrix. The main differences are shown with different aggregates.

Also in this case, mortars prepared with silica gel (A2) show the lower value in terms of mechanical strength: maximum load that can be sustained is 80% less than the value of sand-based mortars.

In case of active carbon (A3) based mortars, mechanical strength is 70% less than the value of sand-based mortars.

Best results are recorded in zeolite (A1) based mortars with values slightly higher (5%) than those of reference mortar.
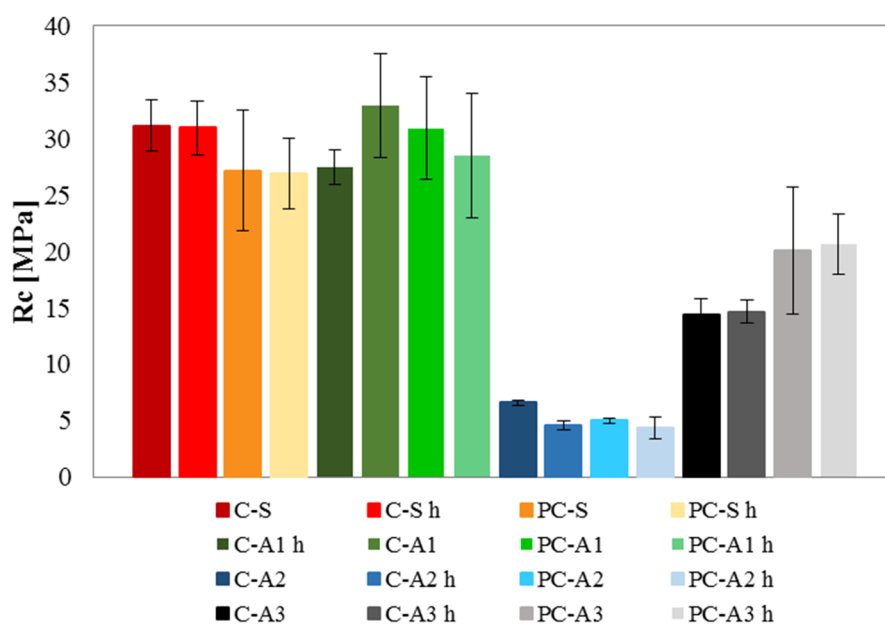
Figure 39 Compressive strength of cement-based mortars

According to the current standard UNI EN 998-1:2010 [80], the maximum value of density for indoor mortar to be classified as lightweight is 1300 kg/m^3. Figure 40 shows the results of density.

Thanks to the total replacement of calcareous sand with unconventional aggregates as silica gel (A2), it is possible to obtain lightweight finishes. This property is highly appreciated for non-structural materials: there are benefits in terms of less final gravity weight of the structure, sound adsorption, and costs of the buildings [81].

All mortars belong (according to [80]) to CS IV category a part from silica gel based mortars, C-A2, C-A2 h, PC-A2 and PC-A2 h, that belong to CSII.

50
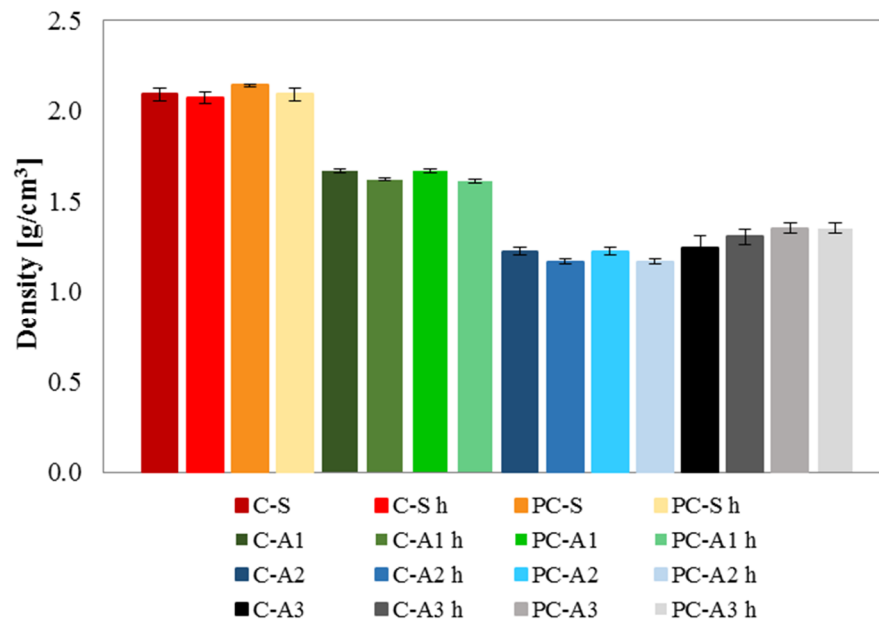
Figure 40 Hardened density (ρ) of cement-based mortars

Table 7 summarizes the average values of flexural, compressive strength, density and compression specific strength.

With regard to specific resistance Rcs, besides the low densities, unconventional mortars have higher value of Rcs.

Zeolite (A1) based finishes reach the highest value.

Reference mortar with sand has the same value of active carbon (A3) based mortars.

Silica gel (A2) based mortars have four times less specific resistance of sand based mortar.

Also in this case, there are no relevant differences in using different binders or the hydrophobic admixture.

Table 7 Mechanical tests results: flexural strength (Rf), compressive strength (Rc) hardened density (ρ), and compression specific strength (Rcs) of cement-based mortars.

Mix	Rf [MPa]	Rc [MPa]	ρ [g/cm^3]	R_{cs} Pa/(kg/m^3)
C-S	7.5	31.2	2.09	14.93
C-S h	9.0	31.2	2.14	14.58
PC-S	7.6	31.0	2.07	14.98
PC-S h	8.4	26.9	2.09	12.87
C-A1	1.5	32.9	1.67	19.70
C-A1 h	1.2	27.5	1.62	16.98
PC-A1	1.4	30.9	1.67	18.50
PC-A1 h	1.2	28.5	1.61	17.70
C-A2	1.3	6.6	1.22	5.41
C-A2 h	1.3	4.6	1.17	3.93
PC-A2	1.5	5.0	1.22	4.10

PC-A2 h	1.1	4.4	1.17	3.76
C-A3	1.9	14.4	1.24	11.61
C-A3 h	2.4	14.7	1.30	11.31
PC-A3	2.9	20.1	1.35	14.89
PC-A3 h	2.9	20.7	1.35	15.33

3.4.3. Microstructure of mortars: morphology and pore size distribution analysis

The mechanical results are explained by morphological observations obtained by SEM images. Only specimens with white cement and without hydrophobic admixture are compared.

In Figure 41 the good adhesion between sand and cementitious paste is evident, explaining the good mechanical behavior of the mortar. Figure 42 shows EDAX probe findings. The aggregate is calcareous sand and in fact the main component is Ca. When binder is investigated, Ca is accompanied to Si, S and Al, elements present in the cement paste.
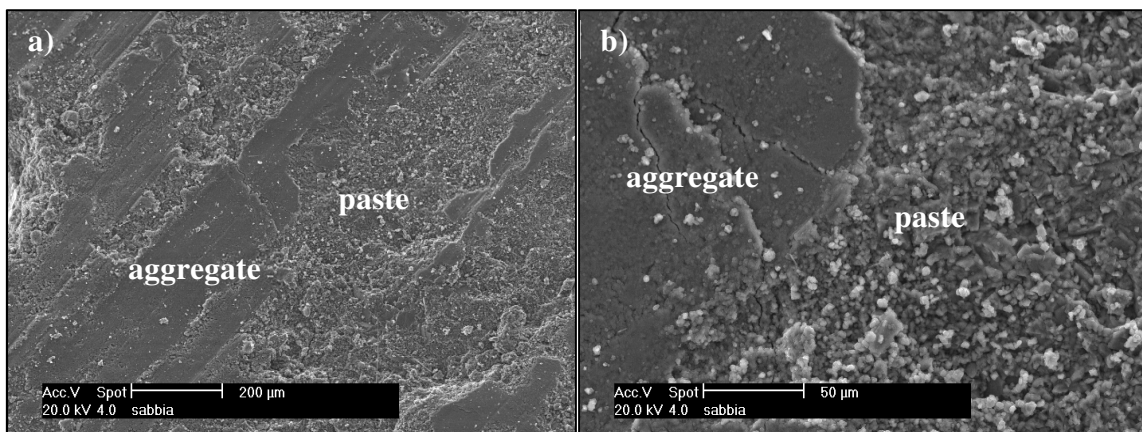
Figure 41 SEM images of C-S specimen
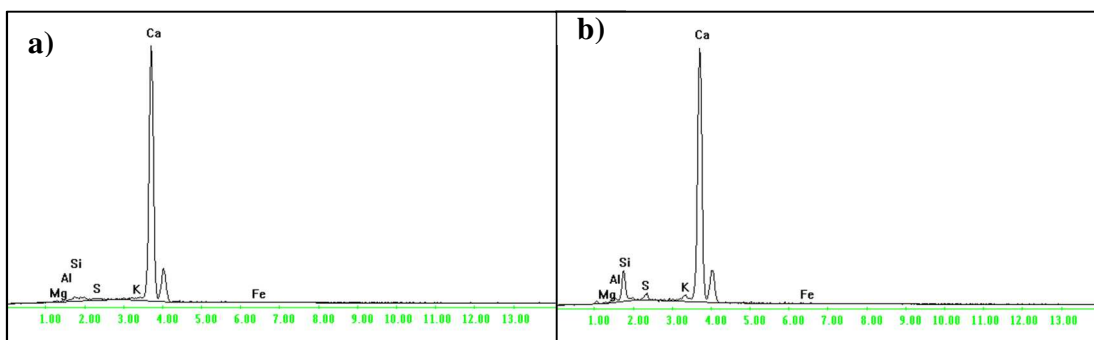
Figure 42 EDAX performed on C-S on a) aggregate, b) cement paste

In Figure 43 the optimum adhesion between zeolite and cementitious paste is evident, justifying the best mechanical behavior of this mortar in terms of compressive strength.

Zeolite (A1) as aggregate improves the mechanical behavior thanks to the well know pozzolanic activity [82], [49]. Figure 44 shows EDAX probe finding: zeolite is a Si Al rich material so the percentage of this elements increase significantly compared to sand based mortars.
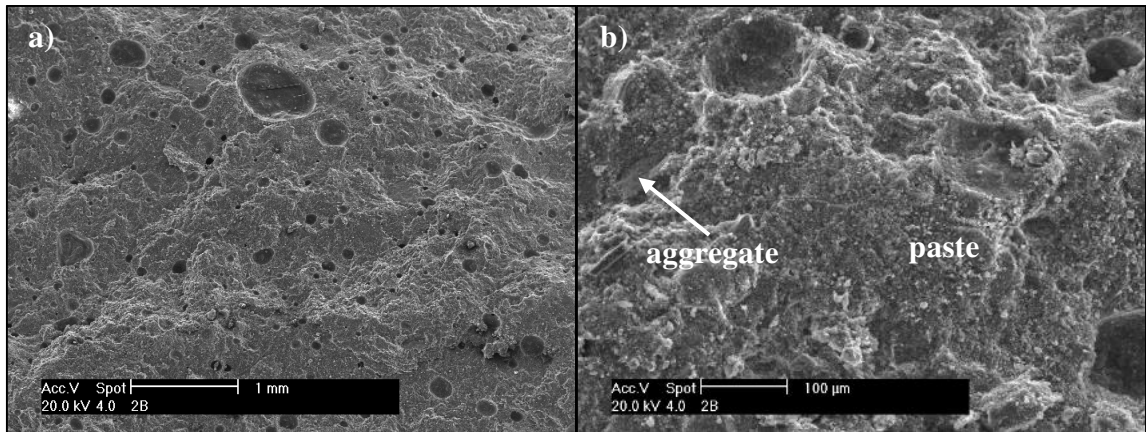
Figure 43 SEM images of C-A1 specimen
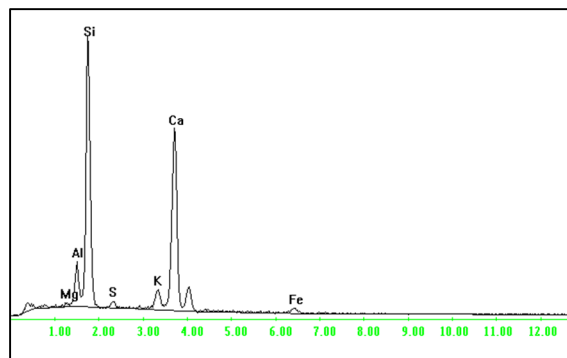
Figure 44 EDAX performed on C-A1 (particles of aggregate)

Figure 45 shows silica gel (A2) based mortar that has the worst mechanical behavior due to the bad adherence between cement and aggregate. It is possible to recognize clearly the Interfacial Transition Zone (ITZ) that is not cohesive with the matrix. Also in this case, EDAX analysis is performed on the aggregate, that is pure SiO_2. Figure 45 shows that Si and Ca are the most prevalent elements.

Figure 45 SEM images of C-A2 specimen
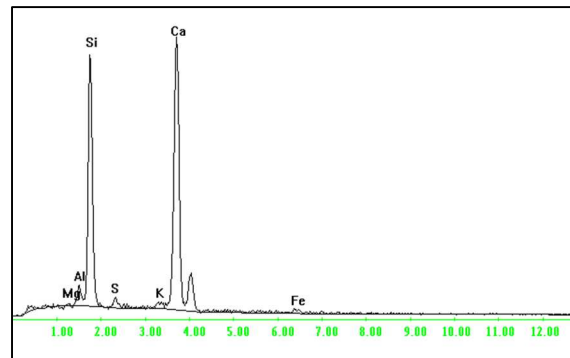
Figure 46 EDAX performed on C-A2 (particles of aggregate)

Figure 47 shows that in activated carbon (A3) based mortar the binder-aggregate ITZ is better than that of the specimens made with silica gel (A2). This explain why the mechanical strength, especially in compression, is significantly higher compared to that of silica gel (A2) mortars, but still worse than the mechanical strength of sand (S) or zeolite (A1) based mortar.
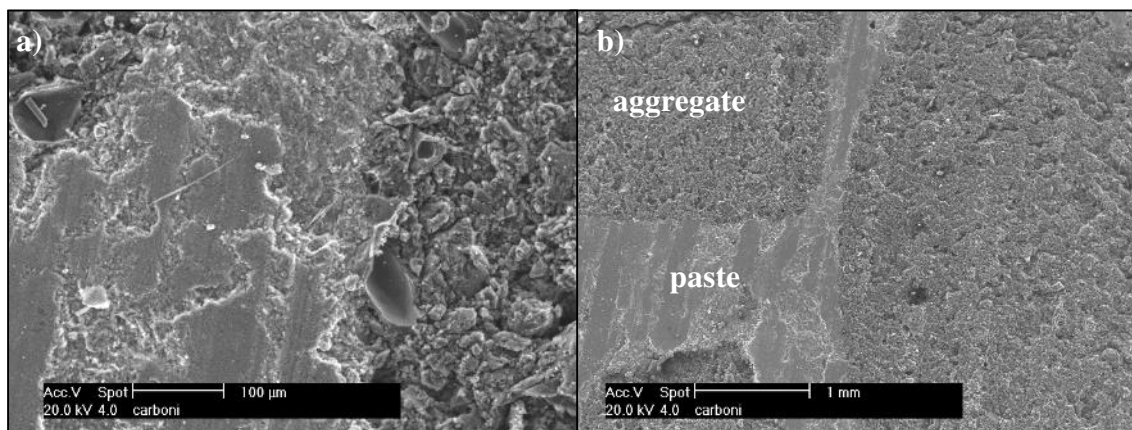
Figure 47 SEM images of C-A3 specimen

From the mechanical results, the introduction of the hydrophobic admixture in this case study does not change the mechanical strength of materials. To validate this sentence, Figure 48 compares the result of MIP analysis in terms of relative pore volume obtained for sand based mortars.

Part a) shows the C-S, C-S h, PC-S and PC-S h mortar results. All curves have a bi-modal distribution, with 2 main peaks: the first is around pore diameters of 0.43 µm, the second around pore diameters of 0.0131 µm. The threshold diameter is 1.54 µm for C-S, 1.54 µm for C-S h, 1.98 µm for PC-S and 1.98 µm PC-S h mortars.

The addition of hydrophobic admixture does not generate differences in terms of pore size distribution: the threshold pore diameter and the total porosity are the same (more evident in Figure 50 and Figure 51). Main differences in pore size distributions are introduced with the use of unconventional aggregates.

In case of zeolite (A2) based mortars, there is a tri-modal distribution of porosity. Peaks are at 0.43 µm, 0.08 µm and 0.01 µm respectively.

Silica gel (A2) and active carbon (A3) based mortars show bi-modal distribution of pores. Peaks are at 0.93 µm and 0.21 µm for silica gel and 3.27 µm and 0.1 µm for activated carbon based mortars (the great differences between the curves are related to the high porosity).

If photocatalytic binder is used there are highest quantity of pores distributed for smaller diameter. Also in previous study [34] the introduction of 5% in weight of TiO_2 in mortars caused a shift of the pores from higher to smaller diameter.
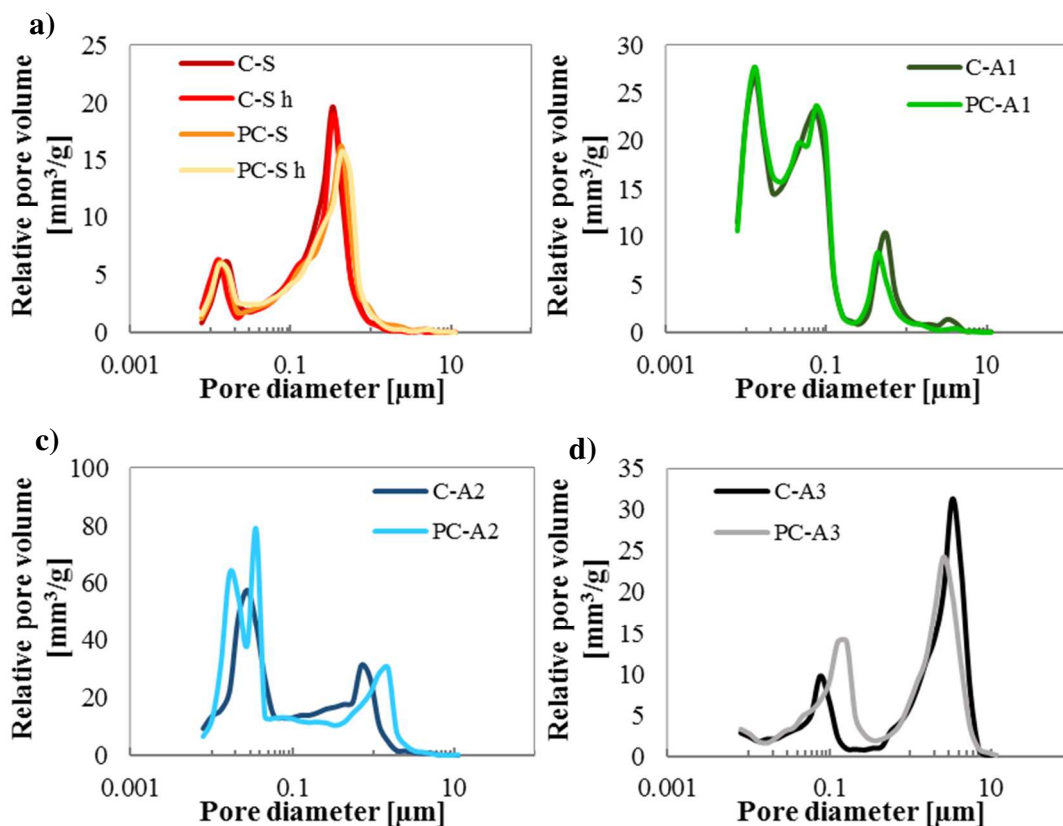
Figure 48 Relative pore volume distribution of different mortar: a) with conventional aggregates (S), b) with zeolite (A1) -based mortar without hydrophobic admixture, c) with silica gel (A2) -based

mortar without hydrophobic admixture and d) activated carbon (A3) - based mortar without hydrophobic admixture,
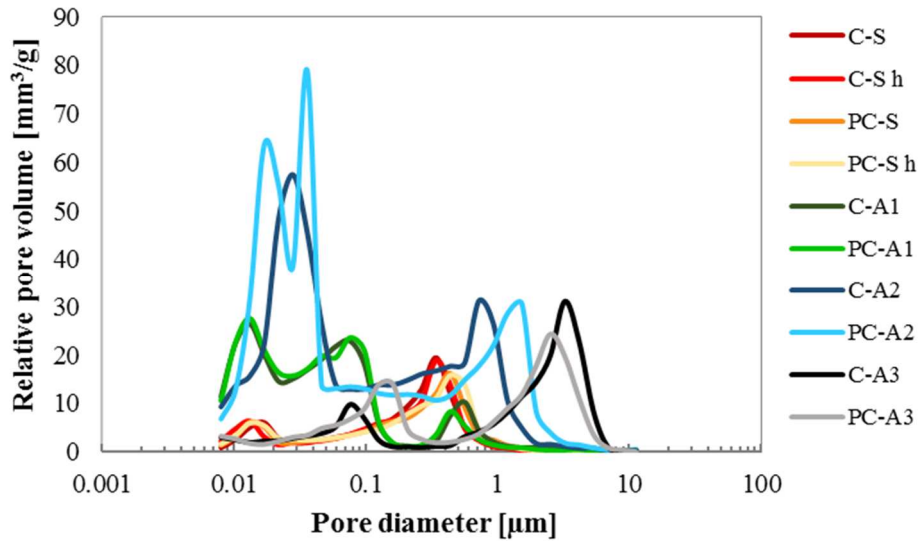
Figure 49 Relative pore volume distribution of different mortars: comparison between all results.

Total porosity can be evaluated both in the cumulative pore volume graph (Figure 50) and in the percentage of volume of pores graph (Figure 51).
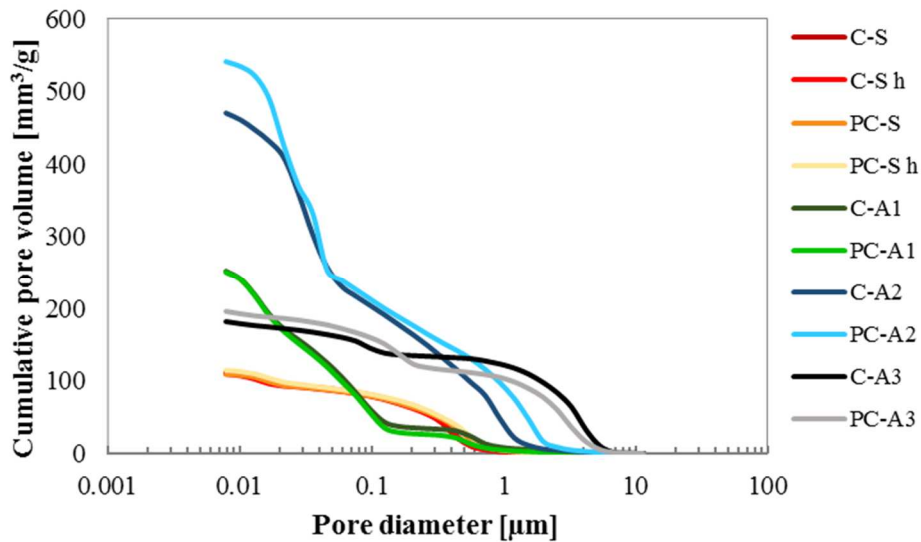
Figure 50 Cumulative pore volume distribution of different mortars: comparison between all results.

Conventional aggregate (S)-based mortars are specimens with the lowest percentage of void (about 22%).
Activated Carbon based (A3) mortars have a 15% more total porosity (Vp is about 26%).

Despite zeolite (A1) based mortars show the best mechanical behavior in terms of compressive strength, the total pore volume of these mortars is about 36%, 60% higher than sand-based mortars.

Mortars with the highest value of total porosity are silica gel (A2) based mortars with about 50% of pore volume, more than 2 times higher than that measured in sand based mortars.
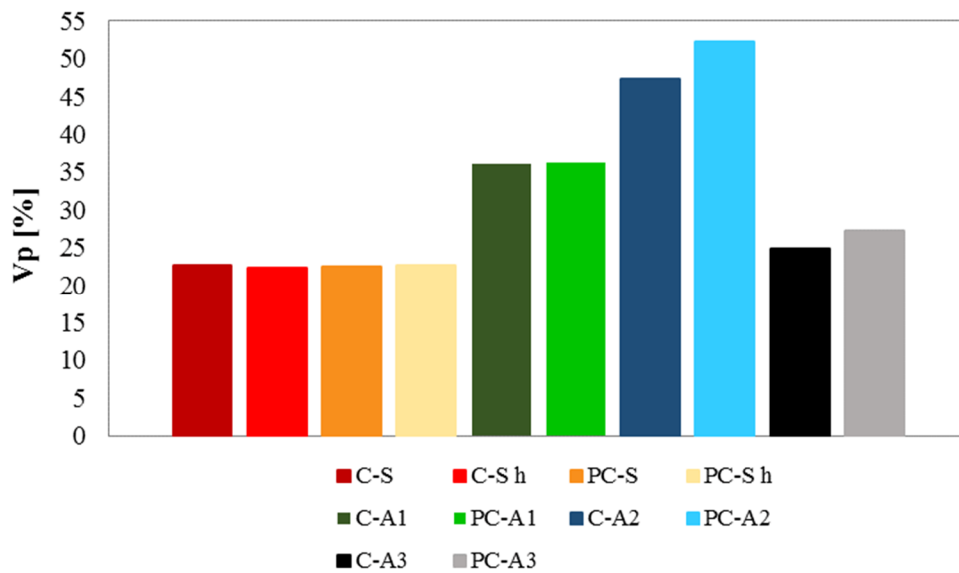
Figure 51 Total porosity of different mortars

3.4.4. Drying shrinkage and water loss measurement

Drying shrinkage is measured for 40 and 60 days. Different times are chosen because some specimens still show significant differences in length after 40 days.

Mortars based on white and photocatalytic cement with unconventional aggregates
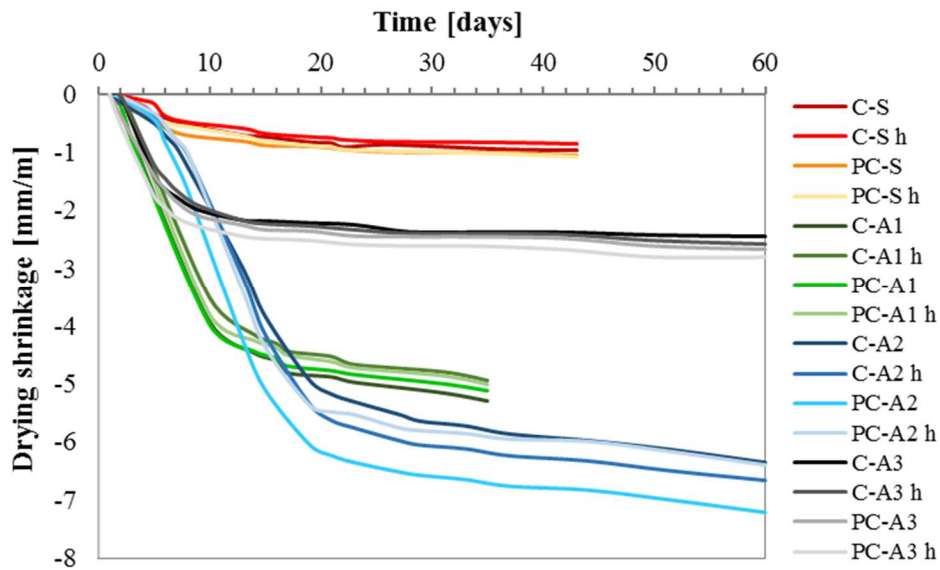
Figure 52 Monitoring of drying shrinkage of mortars at RH = 50% and T =20 °C
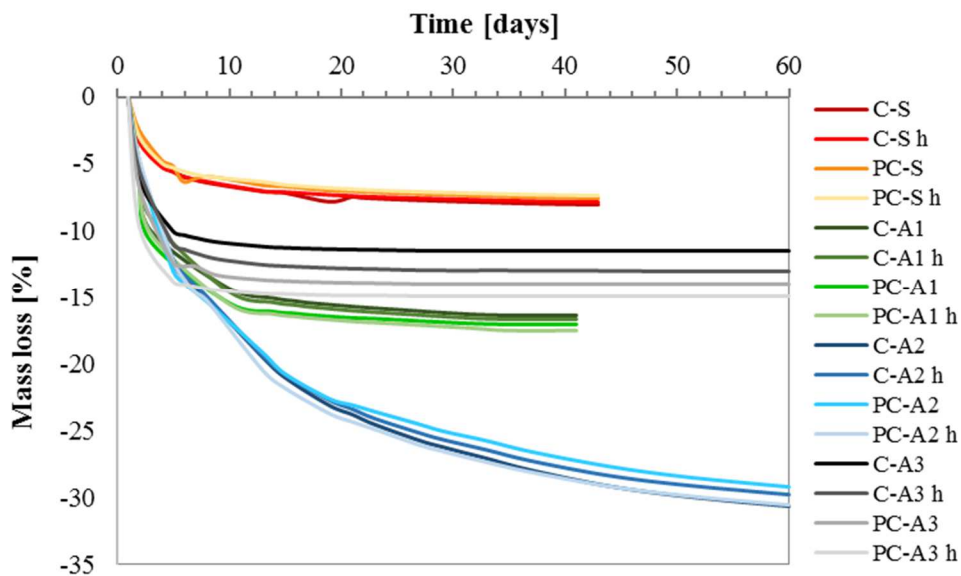
Figure 53 Monitoring of mass evaporation during drying shrinkage of mortars at RH = 50% and T =20 °C

The results are shown in Figure 52 and Figure 53. Values are obtained by the monitoring the length of specimens placed in a climatic chamber at UR = 50% RH and T =20 °C. The comparison of the results after 40 days of measurement is reported in Figure 54.

Sand based mortars have the lowest value of shrinkage and water loss. After one week of measurements, the specimens do not show significant length variation. The replacement of sand with unconventional aggregate in mortars implies high value of shrinkage and water loss also after 25 days from the first measurement (if silica gel A2 is used).

58

The replacement of sand with unconventional aggregates as active carbon (A3) implies 2.5 times higher value of shrinkage related to a higher weight loss than conventional mortar.

When zeolite (A1) and silica gel (A2) are used, mortars have values of shrinkage 5 and 7 times higher than reference respectively. Relative trends are confirmed also by the weight loss due to water evaporation into the environment. Figure 55 reports the linear correlation found between shrinkage values and water loss.
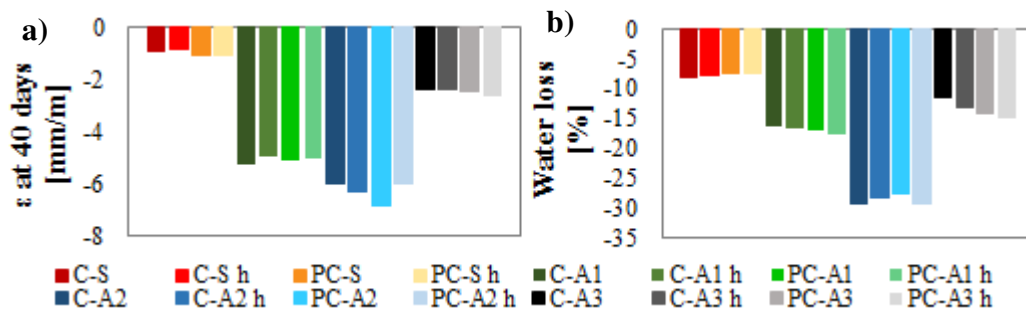
Figure 54 Drying shrinkage measurements at 40 days a) differences in length and water loss.
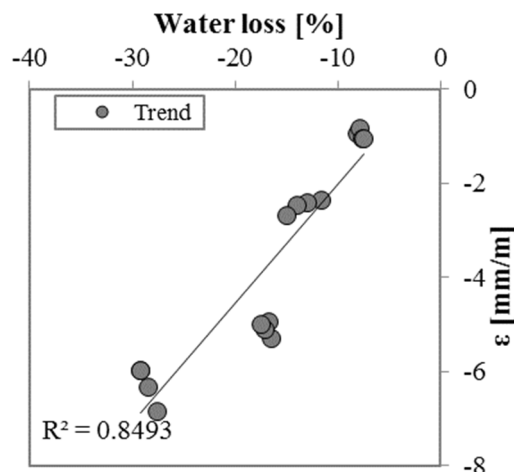
Figure 55 Linear correlation between shrinkage values and water loss of the mortars

Shrinkage of mortars depends on pore distribution [61], volume of pores and elastic modulus of mortars (§ 3.4.4).

In this case, zeolite (A1) and silica gel (A2) based mortars have the higher quantity of pores at lower diameter, as reported in the cumulative pore distribution curve, (Figure 50).

Despite activated carbon (A3) based mortars have higher quantity of higher diameters pores compared to reference mortar, mortars prepared with this aggregate shows a higher value of shrinkage compared to reference one. This is due to the higher amount of total open porosity Vp, which permits a higher water evaporation and therefore higher value of shrinkage.

Mortars with the highest value of Ec are sand based mortars and these mortars result having the lowest shrinkage values.

Figure 56 shows correlations between shrinkage value and total porosity and between shrinkage and Ec. In zeolite based mortars the relation between ε and Ec has not the same trend than that detected on other mortars (red dots on the Figure 56 b), due to high elastic modulus obtained from the relation between the mechanical compressive strength.
There are no relevant changes induced by the use of different binder or the addition of a hydrophobic admixture.
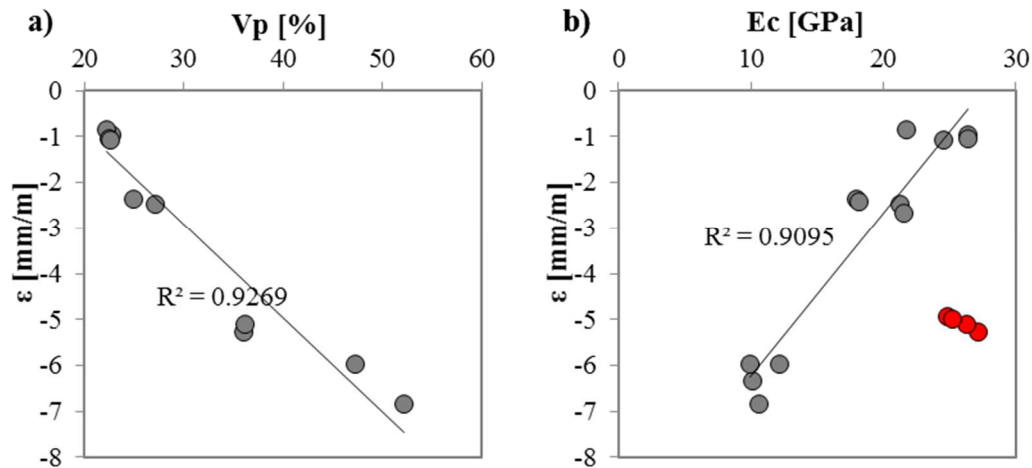
Figure 56 Correlations between shrinkage value at 40 days and a) total volume of porosity and b) elastic modulus

3.4.5. Capillary water absorption of mortars

Before testing, mortars are dried in ventilated oven, at T = 40 °C inside. The temperature is chosen in order to not affect the polymeric bounds and efficiency of hydrophobic admixture.
The efficiency of hydrophobic admixture is previously tested on specimens by a visual test: placing little drops of water on the surface of the specimens (Figure 57).
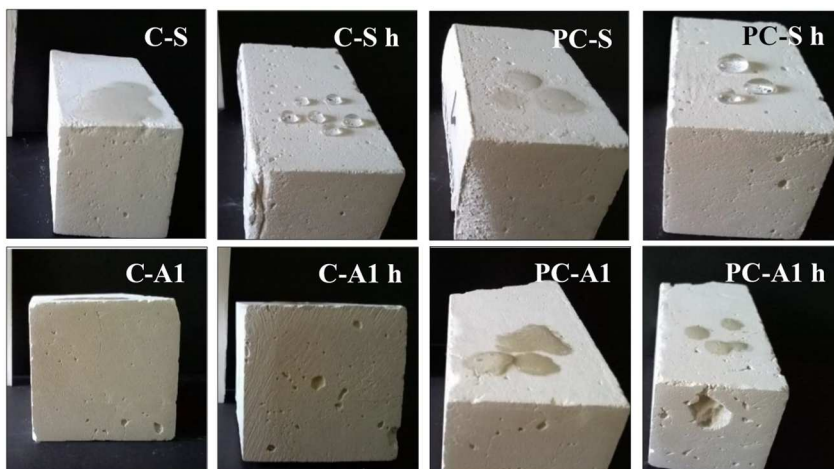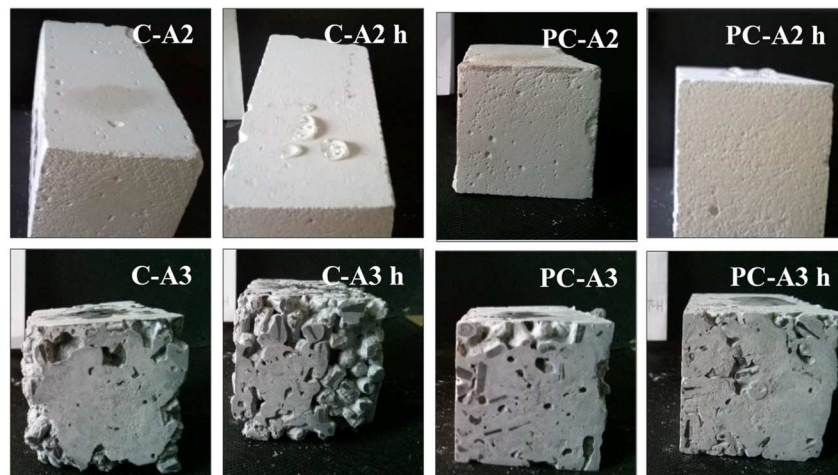
Figure 57 Water-drop test of cementitious mortar.

The test is necessary in order to evaluate if the mortar is hydrophobic or not.

In sand (S) and silica gel (A2) based mortars the quantity of hydrophobic admixture added is enough to prevent the capillary water absorption under atmospheric pressure.

In zeolite (A1) and (A3) activated carbon hydrophobic admixture is not able to oppose the water inlet. This can be due to the high specific surface of the aggregates that should need more hydrophobic admixture than the suggested quantity.

With this preliminary test is easier to explain also the results obtained by capillary water absorption test.

Capillary water absorption coefficient of mortars is evaluated according to the Italian standard UNI EN 1015-18:2004 [65]. Figure 58 shows the results.

In case of sand (S) based mortars the use of hydrophobic admixture influences the water uptake, that becomes 8 times lower than that of mortars without admixture.

In this case, with different binder, the presence of photocatalytic agent influences mortars properties: a slight increase of about 5% in water absorption of cement is detected. Usually hydrophilicity is given to the mortar by the addition of TiO_2 in the matrix as reported in literature [83] or [84]. This property is probably given by the illumination of the laboratory (the light is on visible light range) that permits to activate TiO_2 agent. In presence of hydrophobic admixture, the value is very low so this property is not appreciable.

In case of zeolite (A1) based mortars the use of hydrophobic admixture influences the water uptake, that becomes 3 times lower compared to that of mortars without admixture and 27% more than that of sand based mortars without the hydrophobic admixture. Photocatalytic cementitious mortars have C values 15% higher than that of photocatalytic cement mortars.

Silica gel (A2) and active carbon (A3) have C value higher 3 and 2 times, respectively, than sand based mortars.

In case of silica gel (A3) based mortars, the use of hydrophobic admixture decreases C value 3 times less than that of the same mortar without the admixture. The use of photo-catalytic binder increases C in PC-A2 of about 35% compared to C-A2 values. The highest value of C is due to the highest pore volume of the matrix (§ 2.3.3).

Mortars based on white and photocatalytic cement with unconventional aggregates

In case of activated carbon (A3), a decrease of 50% in C is recorded when hydrophobic admixture is used: this can be due to the high nano-porosity of activated carbon, which implies higher specific surface and less efficiency of the hydrophobic admixture (as shown in Figure 57). Also in this case the use of photocatalytic binder implies an increase of C for about 5%.

All mortars are classified as W2, according to UNI EN 998-1:2010 [80], apart from sand and zeolite based mortars with the hydrophobic admixture, that are W0.

However, between binders, aggregates, and use of hydrophobic admixture, the admixture and the aggregates are the characteristics than influence the most the capillary water absorption coefficient [45].
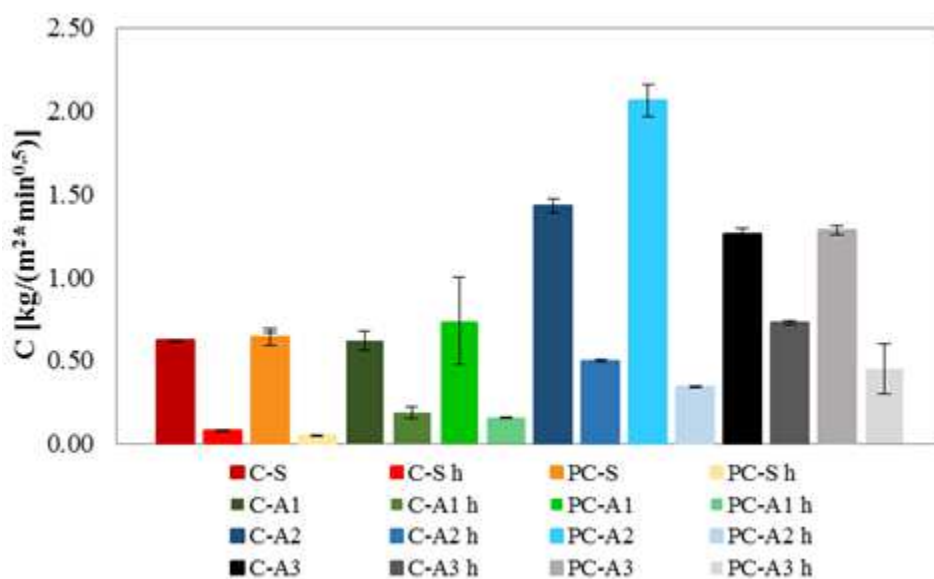
Figure 58 Capillary water absorption coefficient of different mortars according to UNI EN 1015-18.

UNI EN 15801:2010 [66] test is performed and Figure 58 shows the obtained results. Also, in this test, with sand-based mortar, in case of using the hydrophobic admixture a decrease in total amount of water adsorbed is detected. The use of hydrophobic admixture implies a decrease of the absorption of water of about 2.5 times.

Mortars with zeolite (A1) adsorb nearly 50% more than sand-based mortar, with both binders and with and without admixture.

Mortars with silica gel (A2) show the highest value of absorption of water. In this case, without hydrophobic admixture, silica gel based mortars absorb two times higher quantity of water than that with the hydrophobic admixture.

Active carbon based mortars (A3) absorb 15% more than reference mortar. There is 70% lower absorption in case of mortars with the hydrophobic admixture. However, active carbon based mortars show different behaviors than that observed during UNI EN 1015-18:2004 [65]. It is probably due to a certain hydrophobicity of the aggregate, more evident in water saturated filter paper test (UNI EN 15801[66]) than in semi-immersion condition in free water test (UNI EN 1015-18 [65]).

Active carbon mortars absorb lower amount of water compared to cement-sand based mortars because the pore network distribution has higher pores diameters (peak around

4 µm). Sand and zeolite based mortars adsorb a quantity of water similar to that of sand based mortars.

Mortars with higher quantity of pores (such as silica gel mortar) absorb the highest quantity of water. This can be also related to the very high amount of water that the silica gel absorbs: in fact, it needs 86% of water to be saturated (as reported in § 2.2.4.3).

If hydrophobic admixture is not influencing the hydrophobicity of mortars it is possible to state that, mortars with higher quantity of pores (such as silica gel porosity), absorb higher quantity of water.

Active carbon mortars absorb lower or comparable (depending on the test method) amount of water compared to cement-sand based mortars because the pore network distribution is more characterized by higher pores diameters (peak around 4 µm).

Zeolite based mortars adsorb similar quantity of water than reference mortars.
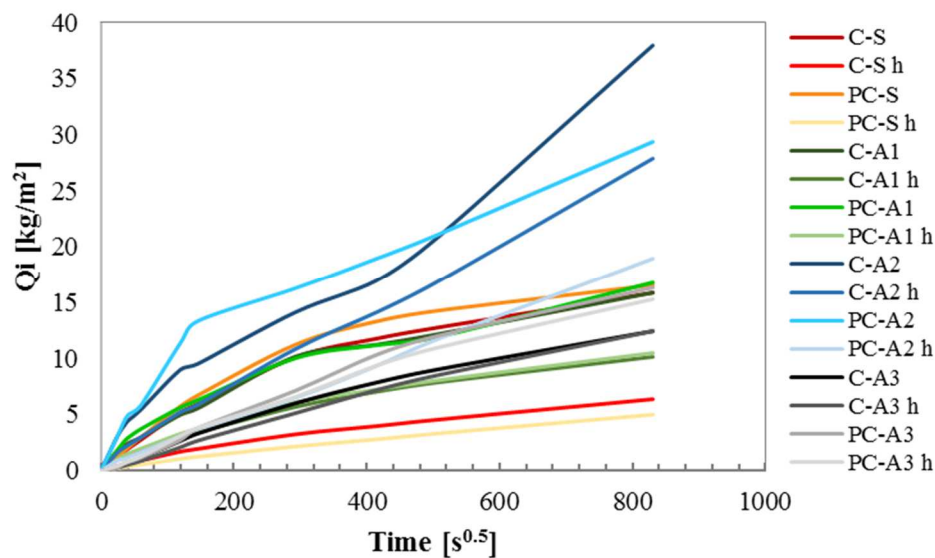
Figure 59 Capillary water absorption in time of cementitious mortars

3.4.6. Water vapor permeability

Water vapor permeability results, expressed in terms of µ factor, are shown in Figure 60. Lower value of µ factor indicates higher value of permeability.

For all mortars the use of photocatalytic cement or white cement and the hydrophobic admixture does not seem to change the results.

Sand based mortars have the highest value of µ which means the lowest water vapor permeability.

Zeolite (A1) based mortars shows a 20% less µ value.

Silica gel (A2) and active carbon (A3) have a very low µ value, approximately 70% lower than sand based mortars.

All mortars have permeability to water vapor proportional to the porosity percentage, according to Kats and Thompson relation [70], the more volume of pores there is, the

less is the hygroscopic resistance factor. This value is very low, meaning very permeable structures, comparable to that of hemp-lime mortars with $\mu \sim 10$ [85].

So, differences in results is mainly due to the porosity induced by different aggregates.
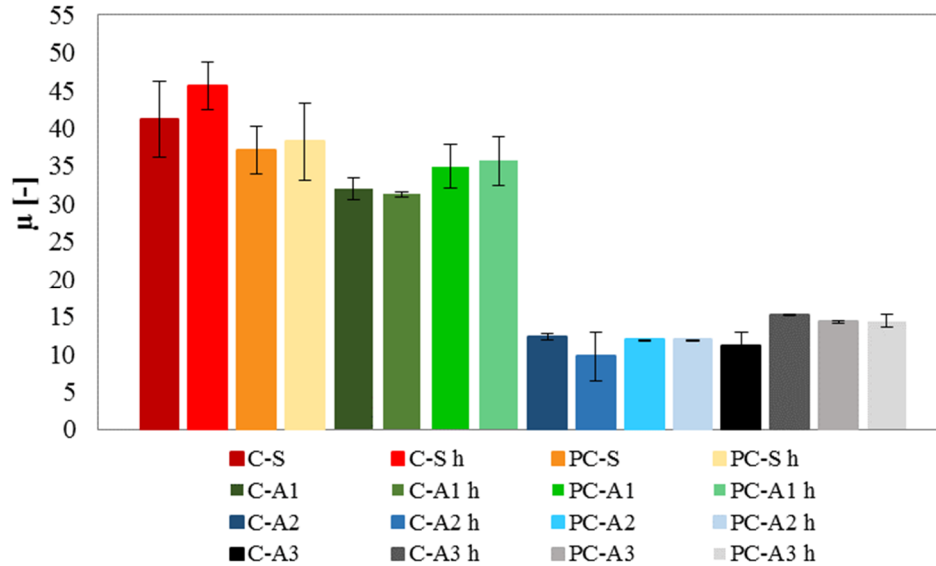
Figure 60 Water vapor resistance factor μ of cement-based mortars

3.4.7. Moisture Buffering Capacity

The interaction between mortars and the humidity of indoor environment is also studied through measuring the changing in moisture content of specimens exposed at different RH. Figure 61 shows the change in water content (Δm) normalized on the exposed surface of the specimens.

At first it is important to note that the use of different binders or a hydrophobic admixture does not affect this behavior. The use of different aggregates mainly influences the results.
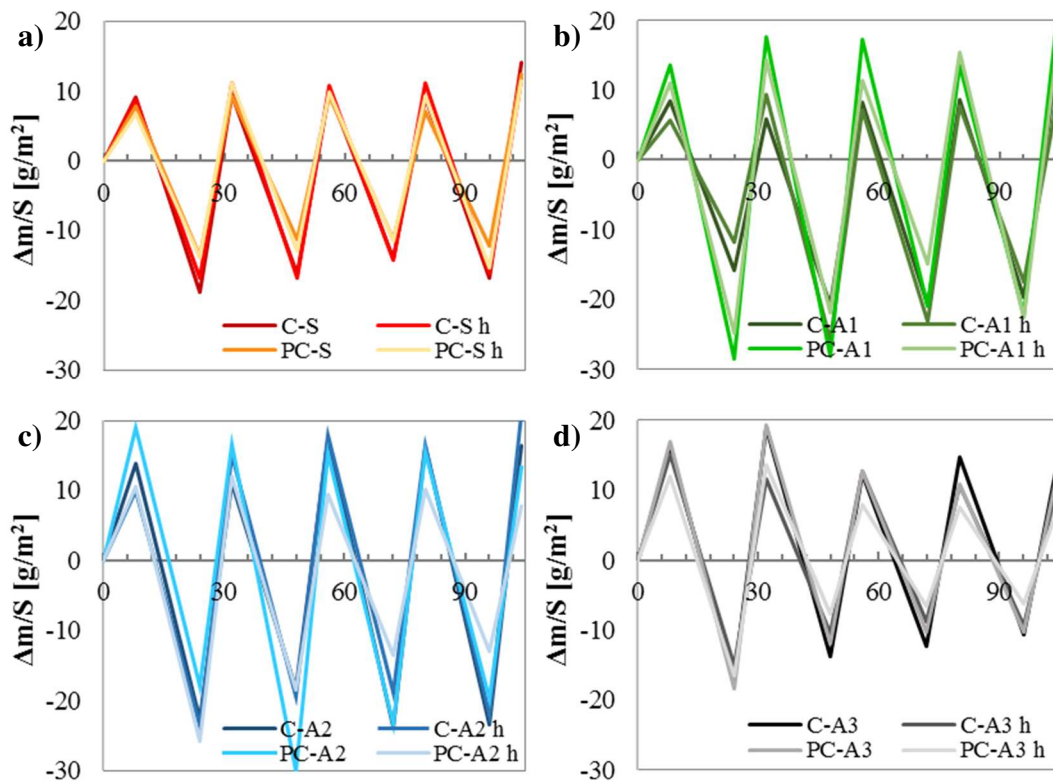
Figure 61 Changing of mass due to absorption/desorption phases, normalized on the specimens surface, for: a) sand, b) zeolite, c) silica gel and d) active carbon based mortars

Sand based mortars have the smallest exchange of water vapor.

Zeolite (A1) based mortars adsorbs and desorbs two times more water vapor then sand based mortars.

Silica gel (A2) based mortars have the same behavior of zeolite based one.

Active carbon (A3) based mortars have a slightly (20%) higher capacity of absorbing/desorbing water vapor than sand based mortar.

Results expressed in terms of MBV are shown in Figure 62. The average is made on the last three cycles. The values are consistent with those found in literature [23] for cementitious materials.

Mortars based on white and photocatalytic cement with unconventional aggregates
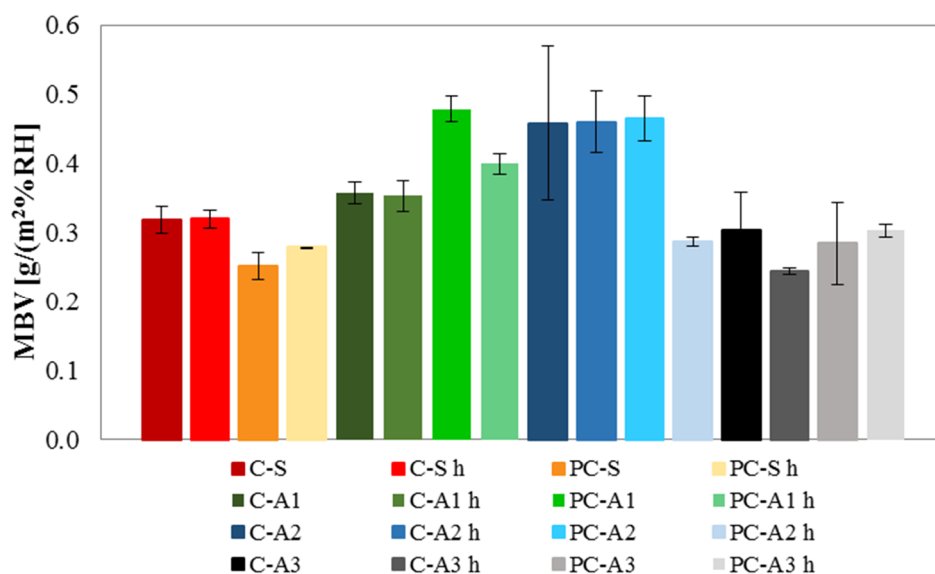
Figure 62 Moisture buffering value of cementitious mortars

Again, the differences in results are related to the pore size network of the mortars. In Figure 63 the correlation between MBV value and percentage of porosity is reported. In this case the best trend line is logarithmic function.

In case of zeolite based mortars the behavior is related more to the pore size distribution than to the total percentage of porosity. The lower is the quantity of pores with small diameter (nano pores of 0.01 µm), the higher is the possibility of water vapor to be trapped at high RH condition and be released in low environmental RH conditions.

Moreover, higher the quantity of the pores, higher the ability of the material to uptake/relies water vapor: in fact, silica gel based mortars have the highest percentage of porosity and show the best behavior in terms of MBV. In this case, the available mortar surface with large pore volume can provide enough space for adsorbate to be trapped in [86].

This situation could give hysteresis phenomena where the water vapor is absorbed during high humidity exposition but not completely released during the desorption phase. However, here this problem is not detected.
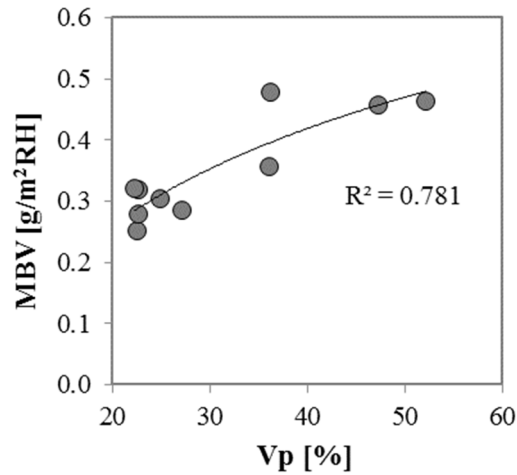
Figure 63 Correlation between porosity and MBV value

3.4.8. Depollution properties

3.4.8.1. VOC as tracer

Gas Chromatography (described in § 2.3.5.2) is the technique used to analyze depolluting properties of mortars in batch condition. This test is conducted in 2 different conditions: dark condition and under UVA radiation. An UVA radiation of 10 W/m^2 on the surface of the specimens is guarantee. Specimens are cylinders 3.2 cm in diameter and 4 cm high.

The first step is to carry out the calibration curve. A known quantity of MEK is injected inside the 16.65 l box, areas of the areas of the chromatographic peaks are detected and related with concentration in a graph. The concentrations of the tracer are given in Table 8.

Table 8 Concentration of MEK, values for calibration curve elaboration

Volume of MEK	Weight of MEK	Concentration of MEK
μl	g	mg/m^3
5	0.004	240
10	0.008	480
25	0.020	1201
50	0.040	2402
75	0.060	3603

Two different curves are elaborated: under dark condition (dark) and under UVA radiation (UV). Figure 64 shows the detected data. The found equation is necessary to convert the detected area in MEK concentration inside the box.

Before the test, the specimen is placed inside the box and the box is sealed. For each specimen, the residual concentration of MEK inside the box is monitored during the time.

a)

b)
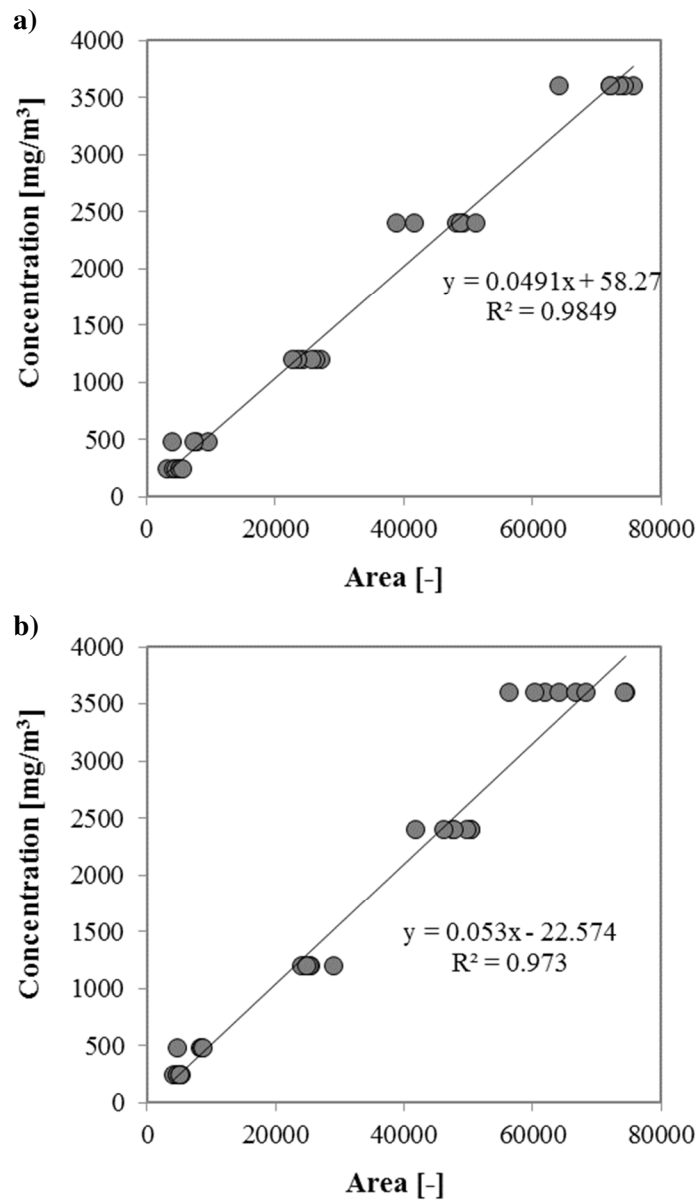
Figure 64 Calibration curves MEK Concentration vs GC area a) dark condition and b) UV light condition

The following figures (Figure 65, Figure 66, Figure 67 and Figure 68) summarize the obtained results They show the residual percentage of MEK inside the box in time. Percentage is evaluated as C_i/C_0 where C_i is the MEK concentration detected inside the box and C_0 is the MEK theoretical initial concentration. In this case the theoretical initial concentration is 2402 mg/m^3 (the MEK load is 50 µl).
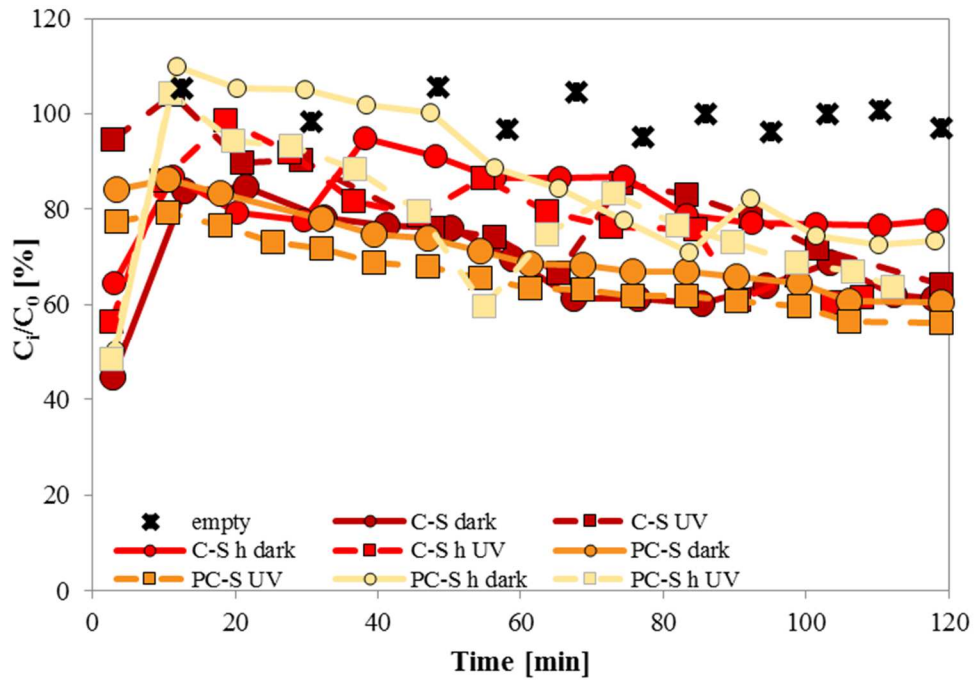
Figure 65 Sand based mortars depolluting tests with MEK
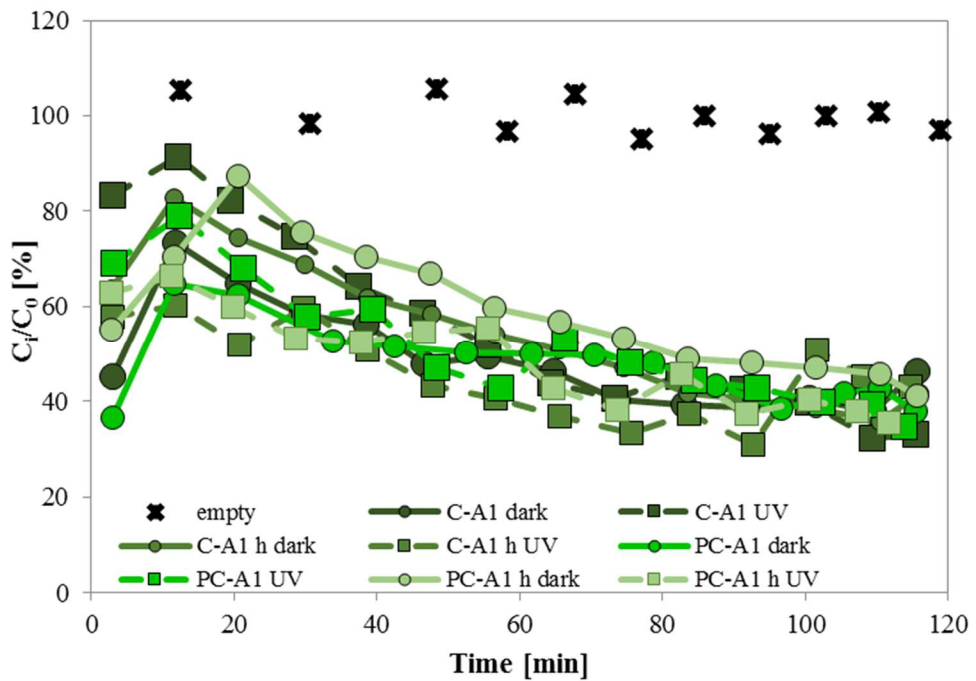
Figure 66 Zeolite based mortars depolluting tests with MEK
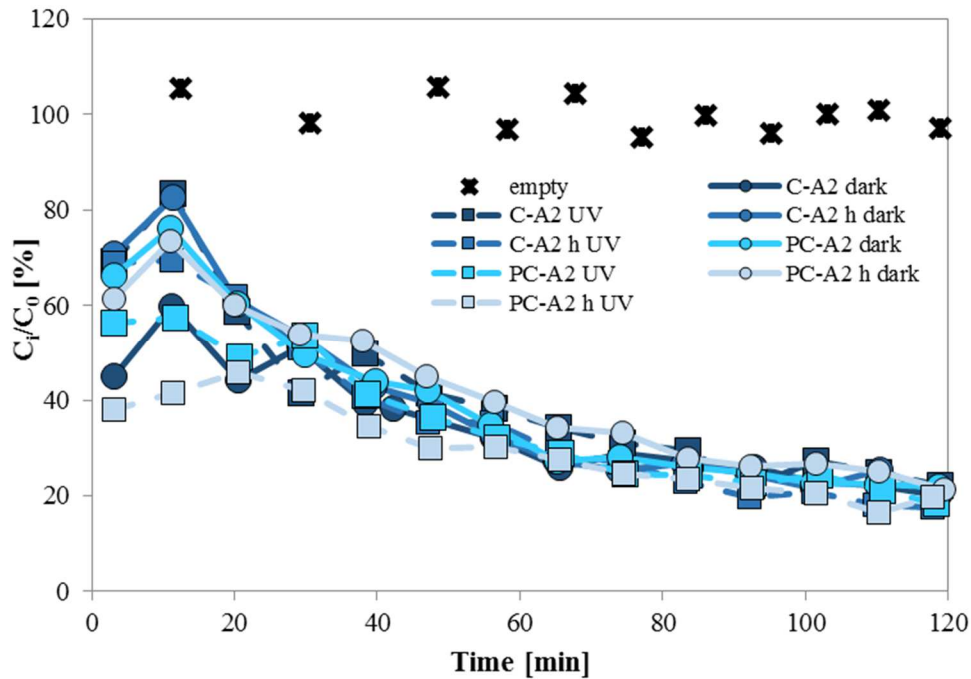
Figure 67: Silica gel based mortars depolluting tests with MEK
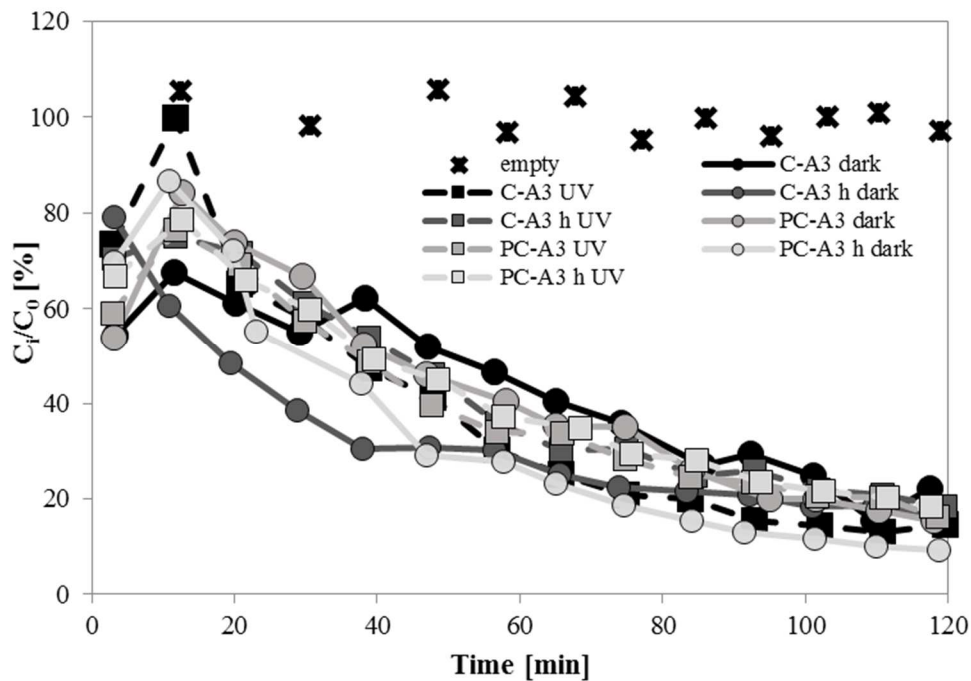
Figure 68 Active carbon based mortars depolluting tests with MEK

From results of sand based mortars it is clear that C-S mortar has the same trend with and without UVA radiation, with 66% left percentage of MEK inside the box. In presence of the photocatalytic binder, under UVA radiation there is an increase in removal efficiency of about 5%. The use of a hydrophobic admixture generally does not influence the depolluting properties of mortars. As regards the combination PC-S

h, with and without UV, the adsorption difference, in favor of the test condition under light, is 15%.

Zeolite based mortars (A3) have up to 30% higher depolluting capacity compared to cement based mortars. The residual concentration is about 40% after 120 mins of test. There is a slight difference in case of the same binder and different radiation conditions and at the same radiation and different binder. Also, the hydrophobic admixture does not influence depolluting properties.

In case of silica gel (A2) based mortars, if compared to sand – based mortars, there is a significant increase in removal efficiency, up to 80%. The residual concentration is 20% after 120 min of test. There is a slight difference in case of the same binder with and without different radiation conditions and at the same radiation and different binders. Also, the hydrophobic admixture does not influence depolluting properties. The adsorption process of the aggregate predominates on the photocatalytic action of the binder under UVA radiation.

Active carbon (A3) based mortars show about 100% higher depolluting capacity than sand based mortars. If white cement is used, there are no differences in dark or UVA conditions. In this case, the adsorption process of the aggregate predominates also on the photocatalytic action of the binder under UVA radiation. There are no relevant differences in using a hydrophobic admixture.

In order to better compare the results Figure 69 shows trend line and Figure 70 the residual percentage inside the box, after 120 mins of test.

In general, it is possible to conclude that:

- hydrophobic admixture does not influence depolluting properties;
- different binders do not influence the adsorption phase of mortars;
- the use of photocatalytic binder implies higher efficiency in MEK removal in conventional based aggregates;
- the main difference in the adsorptive phase is due to the presence of unconventional aggregates: reference mortars absorb about 40% of initial concentration after 2 hours of test, zeolite based mortars show an enhancement in adsorption of about 30% compared to the reference one. The adsorption process is highly improved by the use of silica gel and active carbon aggregates: in these cases, the removal efficiency by adsorption process is about two times higher than the reference mortar.
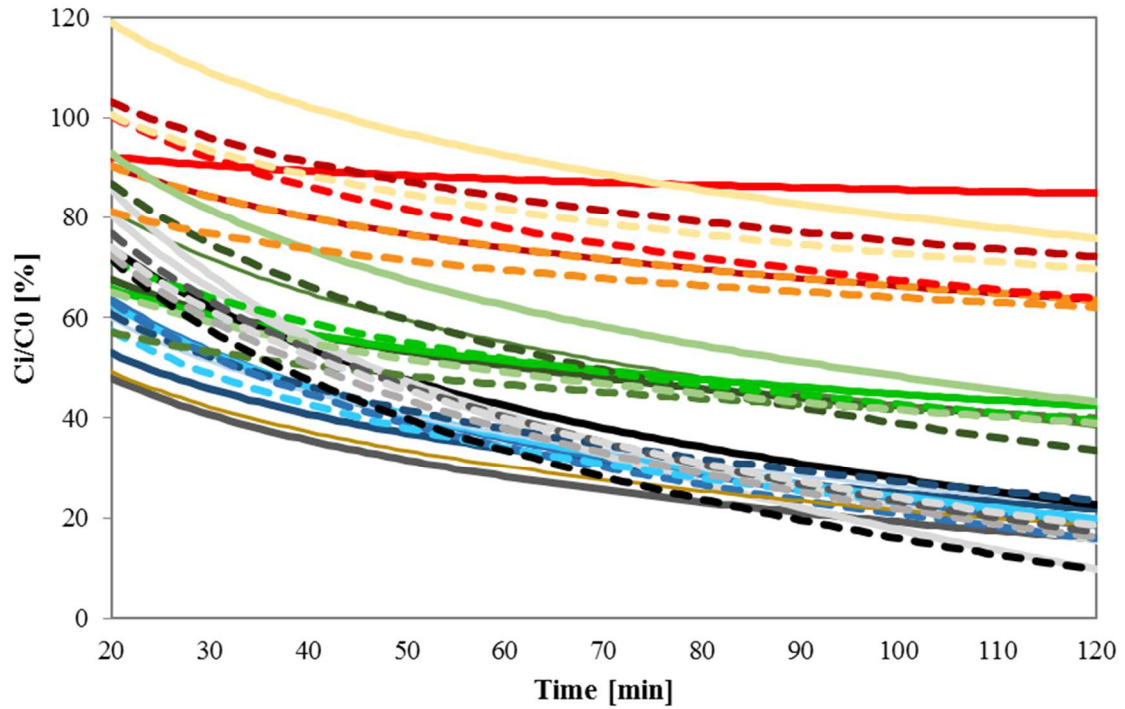
Figure 69 Trend line of MEK removal, legend is in Figure 70
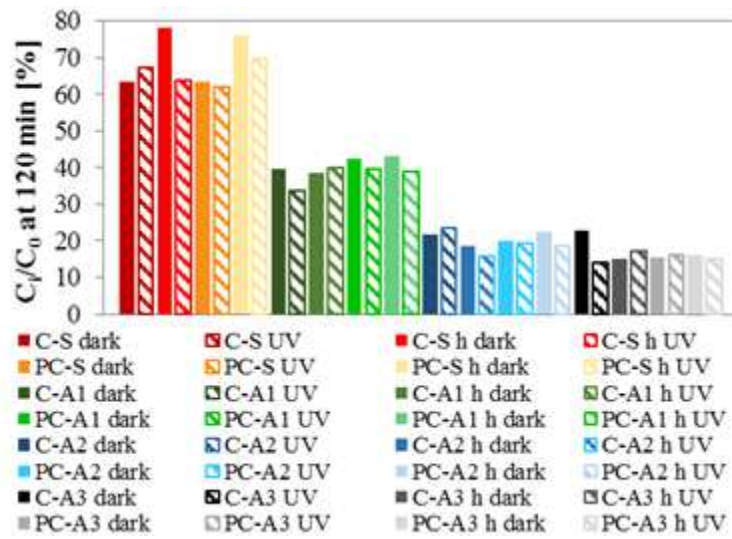
Figure 70 Residual concentration inside the test box after 120 mins

3.4.8.2. NO as tracer

From the results obtained during the depolluting activity in § 3.4.8.1 it is decided to perform this test only on specimens without the hydrophobic admixture.

The photocatalytic efficiency of mortars is tested in terms of NO abatement under UVA radiation and results are shown in Figure 71.

There is a decomposition of NO only in presence of a photocatalytic binder. The slight abatement of NO detected when white cement is used is probably due to the presence of little amount of titanium dioxide usually present in this cement.

Despite the best performance is reached with sand based mortar with a 25% of efficiency, silica gel (A1) based mortar has about 90% of efficiency compared to the reference one and active carbon (A3) based one about 70%. The worst interaction between the photocatalytic binder and unconventional aggregate is detected in zeolite (A1) based mortars where the detected efficiency is about 40% compared to that measured in reference mortars. This behavior is probably due to the nature of zeolite. Zeolite enhances the hydration products [87], due to its pozzolanic activity. This ensure that there is an increasing of some properties such as compressive strength but, at the same time, can cover the active sites of titanium dioxide [88] with a consequentially reduction in NO abatement.
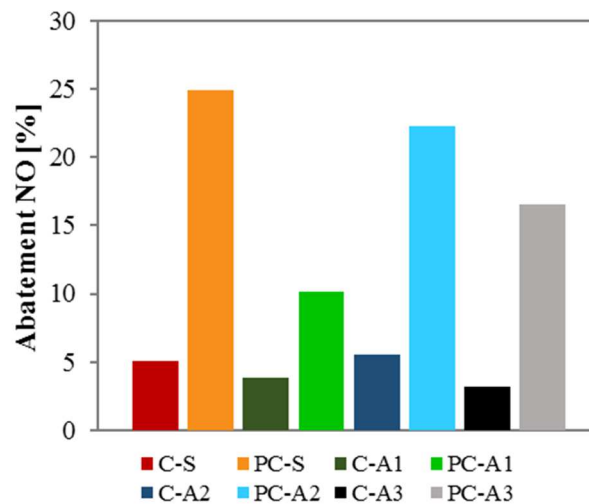
Figure 71 Photocatalytic efficiency under UVA radiation of different mortars

3.5.   Conclusions

In conclusions, the results of this experimentation can be summarized as:
- Mortars have the same stiff workability.
- Mortars with sand and zeolite have the highest compressive strength. Mortars with silica gel have the lowest mechanical compressive strength, 80% less than reference mortars (5.2 MPa). Active carbon mortars resist till 17.5 MPa, 40% less than reference mortars. However, all the values of mechanical properties are still acceptable.
- Mortars with silica gel and active carbon are classified as lightweight mortars, with value of density of about 1.2 and 1.3 g/m^3. Sand based mortars have density of 2.1 and zeolite based 1.6 g/m^3. According to UNI EN 991-1, silica gel based mortars are classified as CS III mortars. All the others mortars belong to CS VI.
- Mortars with conventional aggregate have the lowest porosity, followed by activated carbon mortars (with highest pores diameters) and then zeolite based

mortars (with smallest pores diameters). Silica gel based mortars have the highest total amount of volume of pores.

- Mortars with conventional aggregates has lower value of shrinkage. Silica gel based mortars have value of shrinkage 6 times higher.
- Mortars with silica gel have in average 170% higher capacity of water absorption compared to reference mortars. Hydrophobic admixture reduces the water absorption capacity of about 60-80%.
- Mortars with silica gel and active carbon have the highest permeability to water vapor, 70% higher than sand based mortars.
- Mortars with silica gel have the highest moisture buffering value. Zeolite and silica gel based mortars adsorb and desorb two times more water vapor then sand based mortars. Active carbon based mortars have only a 20% higher capacity of adsorbing/desorbing water vapor compared to sand based mortar.
- Mortars with silica gel and activate carbon have 80% remove efficiency of MEK. Zeolite based mortars removes about 60% MEK after 2 hours test.

The adsorption process is prevalent on the photocatalytic one. Photocatalytic efficiency of reference mortar is confirmed by 25% NO abatment. Also in batch test, photocatalysis under UVA irradiation is appreciable on sand based mortar where the decomposition of MEK is up to 15% higher than in dark conditions.

Chapter 4

4. Mortars based on hydraulic lime with unconventional aggregates

4.1. Introduction

High adsorbent materials are used as aggregates to prepare unconventional mortars able to improve IAQ. Hydraulic lime is used as binder. The volume of cement is replaced with hydraulic lime, a binder more sustainable [89] than cement in terms of footprints and more suitable for restoration purpose [90].

A silane-based hydrophobic admixture is added in the matrix in order to evaluate the influence on durability and IAQ related properties.

The possibility to obtain mortars with photocatalytic activity, is investigated by the addition of 5% of titanium dioxide [34], in order to guarantee the decomposition of airborne pollutants.

In particular, sixteen different types of mortars have been manufactured with traditional commercial sand, as reference aggregate, or three different adsorbent aggregates in hydraulic lime as binder, with and without hydrophobic admixture, with and without TiO_2 in order to investigate the combined effect of adsorption and photocatalysis.

Mortars have been compared in terms of mechanical strength, morphology and microstructure, capillary water absorption, shrinkage, permeability, moisture buffering ability, de-pollution properties and inhibition of growth of molds. Test for inhibition of growth of molds is performed thanks to the collaboration with Department of Life and Environmental Sciences, Università Politecnica delle Marche, under the supervision of prof. Francesca Biavasco and prof. Barbara Citterio.

4.2. Materials

The binder is hydraulic lime Plastocem, provided by Italcementi (HL), described in § 2.2.2.2.

The unconventional materials used as aggregates are the same in § 3.2.

In particular, calcareous sand is used as a reference-conventional aggregates and the unconventional adsorbent aggregates are zeolite (A1), silica gel (A2) and activated carbon (A3), described in §2.2.4.1, 2.2.4.2, 2.2.4.3, 2.2.4.4.

Silane based hydrophobic admixtures (h) used is described in § 2.2.3.2.

Titanium dioxide (TiO_2) is P 25 AEROXIDE provided by Evonik (§ 2.2.3.3).

4.2.1. Mix design

Conventional mortars are manufactured with hydraulic lime and commercial sand, with and without TiO_2 and with and without hydrophobic admixture added at the same quantities as suggested for cementitious mortars. Mortars have the same w/b ratio by volume of previous mixes (§3.2.1). w/b is 0.58 by weight due to the lower weight of hydraulic lime compared to cement. The a/b ratio is 3.5 by volume. 5% of volume of binder is substituted with titanium dioxide in order to give photocatalytic properties to mortar.

From the traditional mortars, 100% sand volume is replaced by different unconventional aggregates. Table 8 reports combinations, color and codes used to recognize mortar.

Table 9 Mortars prepared. Summary of different combinations

Binder	Aggregate	Admixture	Photocatalytic agent	Code ID	Code Color
Hydraulic lime	Calcareous sand	-	-	HL-S	
Hydraulic lime	Calcareous sand	Silane-based	-	HL-S h	
Hydraulic lime	Calcareous sand	-	Titanium dioxide P25	HL-S TiO2	
Hydraulic lime	Calcareous sand	Silane-based	Titanium dioxide P25	HL-S TiO2 h	
Hydraulic lime	Zeolite	-	-	HL-A1	
Hydraulic lime	Zeolite	Silane-based	-	HL-A1 h	
Hydraulic lime	Zeolite	-	Titanium dioxide P25	HL-A1 TiO2	
Hydraulic lime	Zeolite	Silane-based	Titanium dioxide P25	HL-A1 TiO2 h	
Hydraulic lime	Silica gel	-	-	HL-A2	
Hydraulic lime	Silica gel	Silane-based	-	HL-A2 h	
Hydraulic lime	Silica gel	-	Titanium dioxide P25	HL-A2 TiO2	
Hydraulic lime	Silica gel	Silane-based	Titanium dioxide P25	HL-A2 TiO2 h	
Hydraulic lime	Active carbon	-	-	HL-A3	

Hydraulic lime	Active carbon	Silane-based	-	HL-A3 h	
Hydraulic lime	Active carbon	-	Titanium dioxide P25	HL-A3 TiO2	
Hydraulic lime	Active carbon	Silane-based	Titanium dioxide P25	HL-A3 TiO2 h	

The appropriate volume required for casting is evaluated according to the different tests that are performed. Aggregates are added in ssd conditions. The hydrophobic admixture is added in a water dispersion: the additional water is then removed from the water amount. Titanium dioxide is previously mixed with the binder in order to guarantee homogenization during the mixing phase. Mix designs are shown in Table 10.

Table 10 Mix proportions (kg/m³) of mortars

Mix	Water	Hydr-aulic Lime	Sand S	Zeolite A1	Silica Gel A2	Active Carbon A3	Hydro-Phobic Adm.	TiO₂
HL-S	255	440	1535	-	-	-	-	-
HL-S h	252	440	1535	-	-	-	6	-
HL-S TiO2	255	414	1535	-	-	-	-	26
HL-S TiO2 h	252	414	1535	-	-	-	6	26
HL-A1	255	440	-	927	-	-	-	-
HL-A1 h	252	440	-	927	-	-	6	-
HL-A1 TiO2	255	414	-	927	-	-	-	26
HL-A1 TiO2 h	252	414	-	927	-	-	6	26
HL-A2	255	440	-	-	759	-	-	-
HL-A2 h	252	440	-	-	759	-	6	-
HL-A2 TiO2	255	414	-	-	759	-	-	26
HL-A2 TiO2 h	252	414	-	-	759	-	6	26
HL-A3	255	440	-	-	-	683	-	-
HL-A3 h	252	440	-	-	-	683	6	-
HL-A3 TiO2	255	414	-	-	-	683	-	26
HL-A3 TiO2 h	252	414	-	-	-	683	6	26

Mortars are casted in different moulds in order to obtain the specimens suitable for the determination of each property. During the cast mortars are vibrated manually to eliminate the excess of air. It is decided to use the manual method because the mechanical vibration can induce a segregation of the lightweight aggregate with the lime paste.

4.3. Methods

Mortars are characterized in terms of fresh state properties. Workability is measured with a flow table, according to the current standards (§ 2.3.1).

After 28 days of curing, flexural and compressive strength are tested. Also, the specific strength is evaluated (§ 2.3.2.1).

After 28 days of curing, morphologies are investigated by Scanning Electron Microscope (SEM) and pore size distribution is evaluated by Mercury Intrusion Porosimetry (MIP), as described in § 2.3.2.2.

Water is the medium where ions can be transported and can compromise the durability of building material. Water transport in mortars is evaluated with two different methodologies (§ 2.3.3.1 and § 2.3.3.2).

Transpirability of mortars for renders is a fundamental property, evaluated according to § 2.3.4.1.

The moisture buffering capacity of mortars is evaluated over dynamic variation of RH with a simplified procedure of the NORDTEST method (§ 2.3.4.2).

The ability of different mortars to enhance IAQ is evaluated in terms of inhibition of mold growth (§ 2.3.5.1) and de-pollution property (§ 2.3.5.2).

4.4. Results and discussions

4.4.1. Workability

Table 11 shows workability of mortars in terms of slump flow and consistency values.

Table 11 Workability of different mortars: picture of mortar at fresh state after slump flow test, slump flow values and consistency.

Mix	HL-S	HL-S h
Slump (mm)	127	123
Consistency (%)	27	23
Mix	HL-S TiO2	HL-S TiO2 h
Slump (mm)	118	122
Consistency (%)	18	22

Mix	**HL-A1**	**HL-A1 h**
Slump (mm)	110	112
Consistency (%)	10	12
Mix	**HL-A1 TiO2**	**HL-A1 TiO2 h**
Slump (mm)	110	110
Consistency (%)	10	10
Mix	**HL-A2**	**HL-A2 h**
Slump (mm)	123	120
Consistency (%)	23	20
Mix	**HL-A2 TiO2**	**HL-A2 TiO2 h**
Slump (mm)	118	123
Consistency (%)	18	23
Mix	**HL-A3**	**HL-A3 h**

Slump (mm)	105	110
Consistency (%)	5	10
Mix	**HL-A3 TiO2**	**HL-A3 TiO2 h**
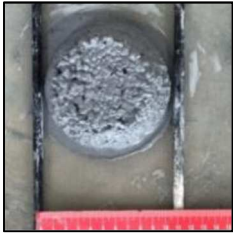
Slump (mm)	111	108
Consistency (%)	11	8

All mortars have the same consistency. The slump value is lower than 140 mm for all the mixes and, according to UNI EN 1015-6 [57], mortars are defined stiff. The aggregates are added in ssd condition.

4.4.2. Mechanical strength

Figure 72 shows the results in terms of maximum flexural strength.
Mortars with the conventional aggregate have the best performance in terms of flexural strength. The addition of TiO_2 does not change the behavior. The main differences are shown with different aggregates.
Activated carbon (A3) mortars have 30% lower mechanical strength value than sand-based mortars.
Zeolite (A1) based mortars have 35% lower mechanical resistance than reference.
Silica gel (A2) based mortars have the lowest flexural mechanical resistance, 20% mechanical strength of sand-based mortars.
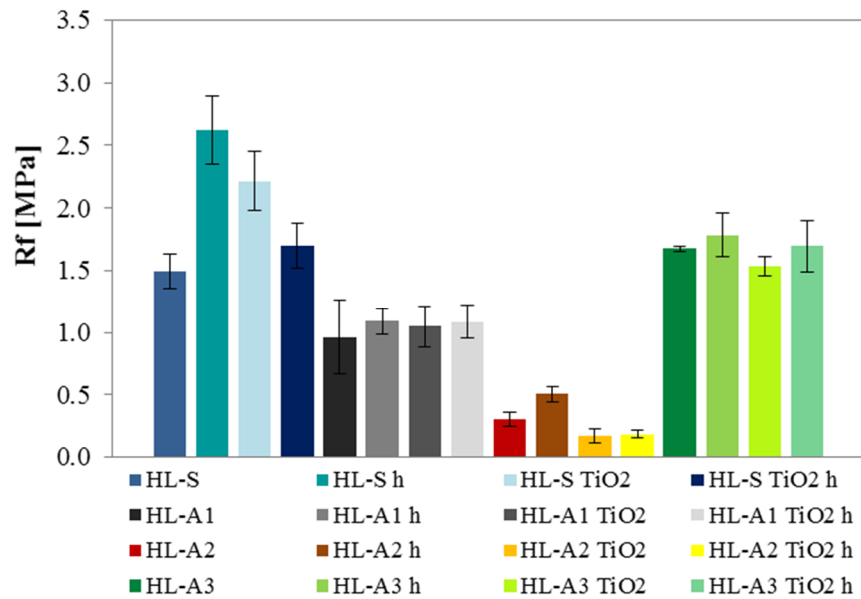
Figure 72 Flexural strength of hydraulic lime-based mortars

Compressive strength is evaluated at 28 days and results are reported in Figure 73. The introduction of TiO_2 or the use of admixture in mortars, does not imply differences in compressive strength results. As previously detected, § 3.4.2, these results do not confirm literature evidences [79]. Evidences in literature show that TiO_2 could decrease [29], if it decreases the amount of binder, or increase [83], due to pore refilling and accelerating effect on hydration, mechanical strength of mortars.

In this case mortars prepared with silica gel (A2) also show the lowest value in terms of mechanical strength: maximum load is 90% less than sand-based mortars.

In case of zeolite based mortars, values are slightly higher (about 5%) than the reference mortar.

The best results are recorded in active carbon (A3) based mortars, mechanical strength is 35% higher than the value of reference based mortar.
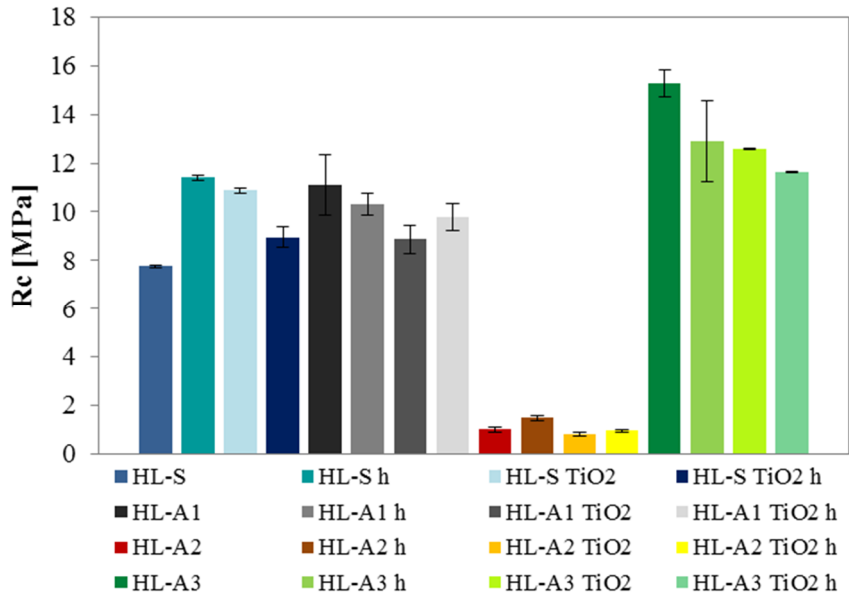
Figure 73 Compressive strength of hydraulic lime based mortars

According to the current standard UNI EN 998-1:2010 [80], the maximum value of density for indoor mortar to be classified as lightweight is 1300 kg/m^3. Figure 74 shows the results of density values for the different mortars.

Thanks to the total replacement of calcareous sand with silica gel (A2) and active carbon (A3), it is possible to obtain a lightweight finish. As previously mentioned, this property is highly appreciated for non-structural materials [81], [91].

All mortars according to [80] belong to CS IV category a part from silica gel based mortars, that belong to CS I.
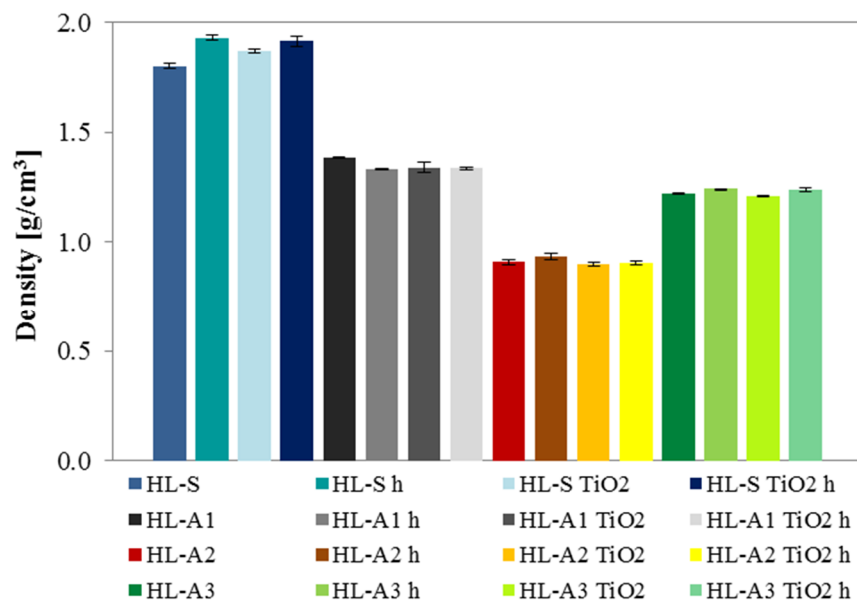
Figure 74 Hardened density (ρ) of hydraulic lime based mortars

Table 12 summarizes the average values of flexural and compressive strength, density and compression specific strength.

With regard to specific resistance Rcs, it is evident how, besides the low densities, the unconventional mortars have higher value of Rcs than reference one, apart from silica gel mortar.

Zeolite (A1) based finishes reach the highest value. The use of zeolite (A1) improves the mechanical resistance of mortars of about 42%.

Silica gel (A2) based mortars have 80% less value than reference mortars.

Active carbon (A3) based mortars have double mechanical resistance than conventional based mortars.

Also in this case, there are not relevant differences in using TiO_2 and hydrophobic admixture.

Table 12 Mechanical tests results: flexural strength (Rf), compressive strength (Rc) hardened density (ρ), and specific strength (Rsc) of hydraulic lime-based mortars.

Mix	Rf [MPa]	Rc [MPa]	ρ [g/cm³]	R_{cs} Pa/(kg/m³)
HL-S	1.49	7.76	1.80	4.31
HL-S-h	2.62	11.40	1.93	5.90
HL-S TiO2	2.21	10.87	1.87	5.81
HL-S TiO2 h	1.70	8.96	1.92	4.68
HL-A1	0.96	11.10	1.39	8.00
HL-A1 h	1.09	10.29	1.33	7.74
HL-A1 TiO2	1.05	8.87	1.34	6.62
HL-A1 TiO2 h	1.08	9.77	1.34	7.31
HL-A2	0.30	1.00	0.91	1.10

HL-A2-h	0.50	1.47	0.94	1.57
HL-A2 TiO2	0.17	0.80	0.90	0.89
HL-A2 TiO2 h	0.18	0.94	0.91	1.04
HL-A3	1.68	15.28	1.22	12.49
HL-A3-h	1.79	12.90	1.24	10.37
HL-A3 TiO2	1.54	12.57	1.21	10.39
HL-A3 TiO2 h	1.70	11.65	1.24	9.40

4.4.3. Microstructure of mortars: morphology and pore size distribution analysis

The mechanical results are explained by morphological observations obtained by SEM. The comparison is made only with specimens with different aggregates.
Figure 75 shows the good adhesion between sand and hydraulic lime paste, explaining the good mechanical behavior of the mortar. Figure 76 shows EDAX probe findings. The aggregate is calcareous sand and in fact the component is Ca. When the binder is investigated, Ca is accompanied to Si, S and Al, element present in the hydraulic-lime paste.
Even if TiO_2 nanoparticles are added, it is not possible to observe it (Figure 77). The evidences of the TiO_2 presence are given by EDAX analysis, shown in Figure 78.
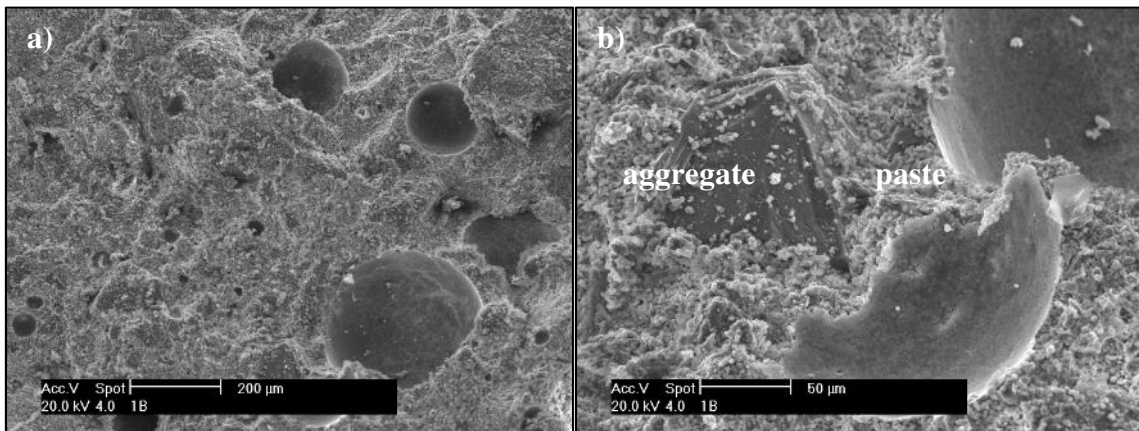
Figure 75 SEM images of HL-S specimen
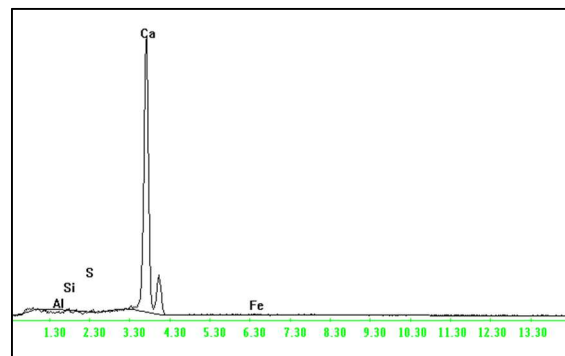
Figure 76 EDAX performed on HL-S (particles of aggregate)
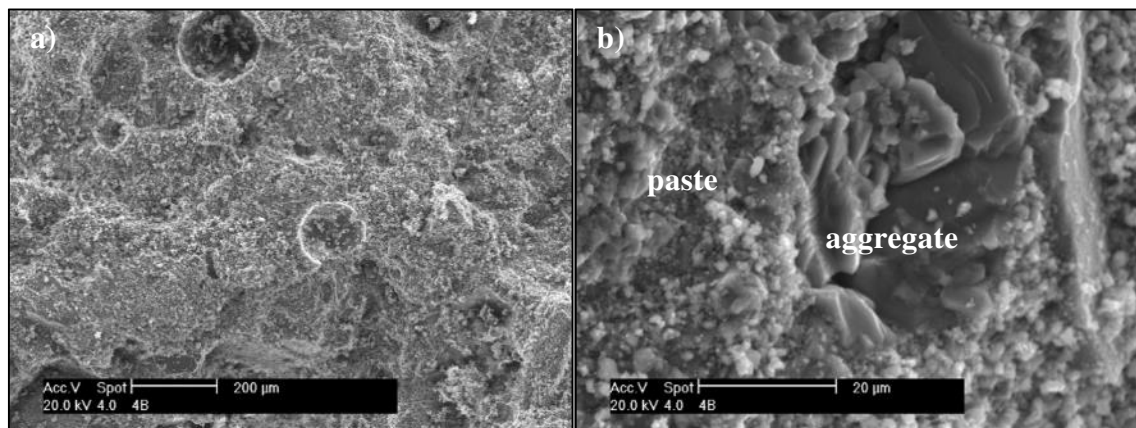
Figure 77 SEM images of HL-S TiO2
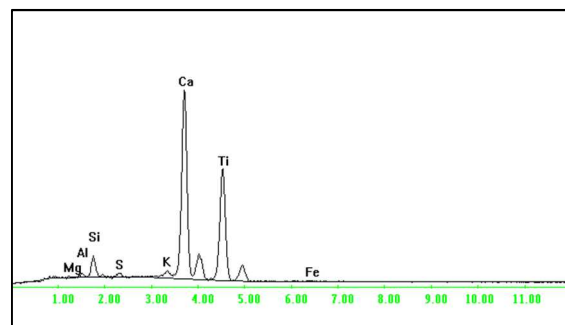
Figure 78 EDAX performed on HL-S TiO2 on Figure 77 a)Figure 77 SEM images of HL-S TiO2

With zeolite (A1) the mechanical resistance is enhanced by zeolite pozzolanic activity that forms additional hydration products, shown in Figure 79 [82], [49]. EDAX probe shows the most relevant elements of this mortars: Ca, due to the binder and Si and Al due to the aggregate.
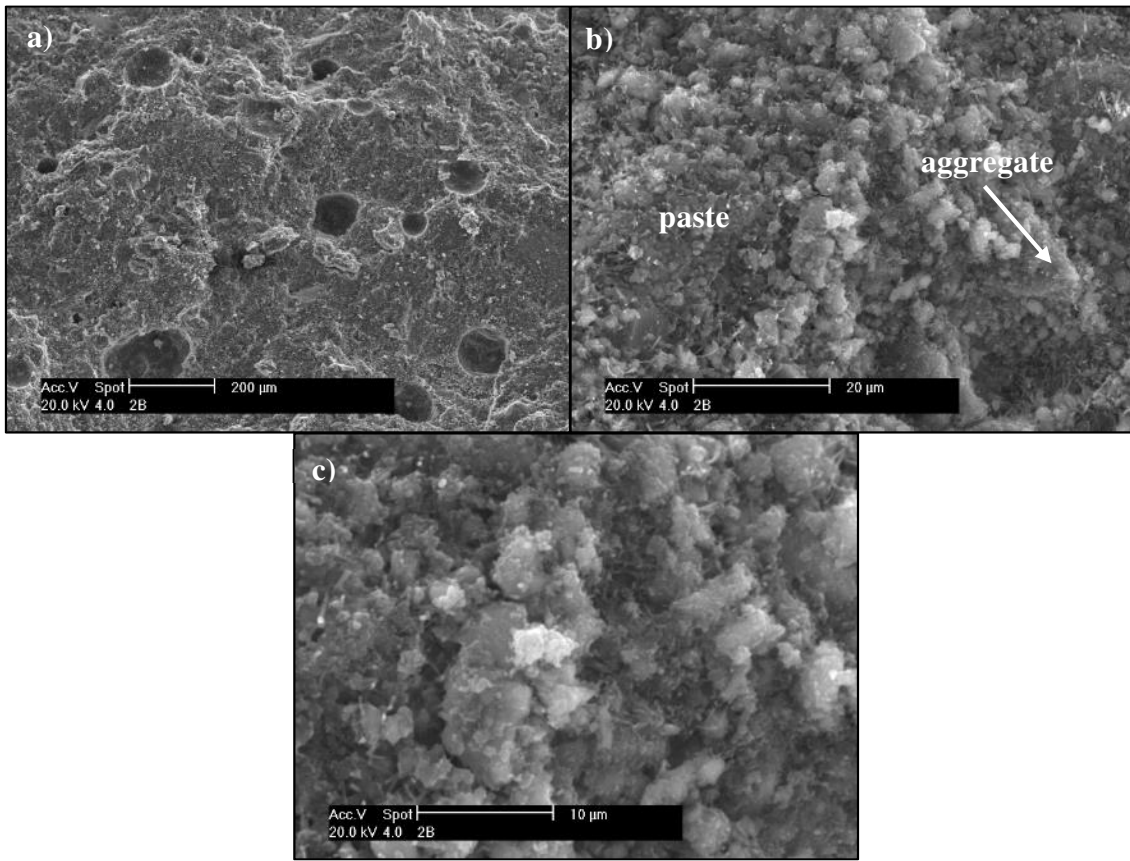
Figure 79 SEM images of HL-A1 specimen a) and b) aggregate and paste c) additional hydration products
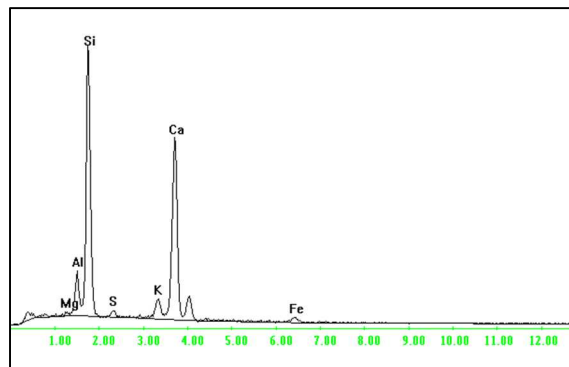
Figure 80 EDAX performed on HL-A1 (particles of aggregate)

In Figure 81 the interfacial transition zone of silica gel and hydraulic lime is shown. Silica gel based mortars have the worst mechanical behavior, due to the poor adherence between aggregate and hydraulic lime. Also in this case, EDAX analysis is performed on the aggregate, and shows that is pure SiO_2. Figure 82 reports that Si and Ca (due to the paste) are the most prevalent elements.
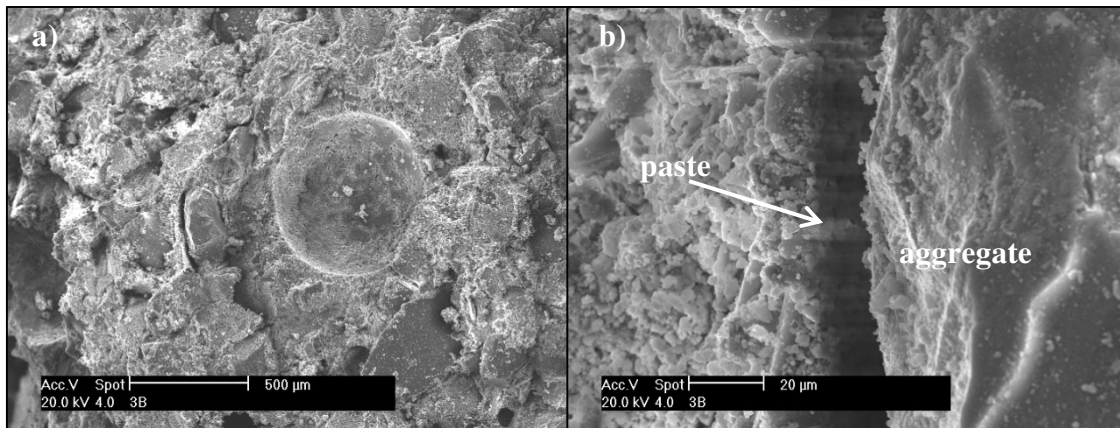
Figure 81 SEM images of HL-A2 specimen
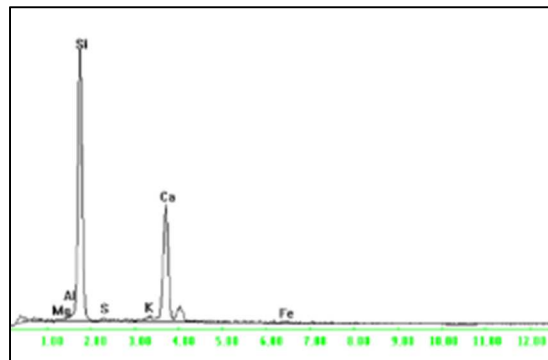
Figure 82 EDAX performed on HL-A2 (particles of aggregate)

Figure 83 shows how in activated carbon (A3) based mortar the binder-aggregate ITZ is better than that of the specimens with silica gel (A2). In this case the mechanical resistance, comparable to sand based mortars, of the mortars can be explained by the shape of the aggregate.
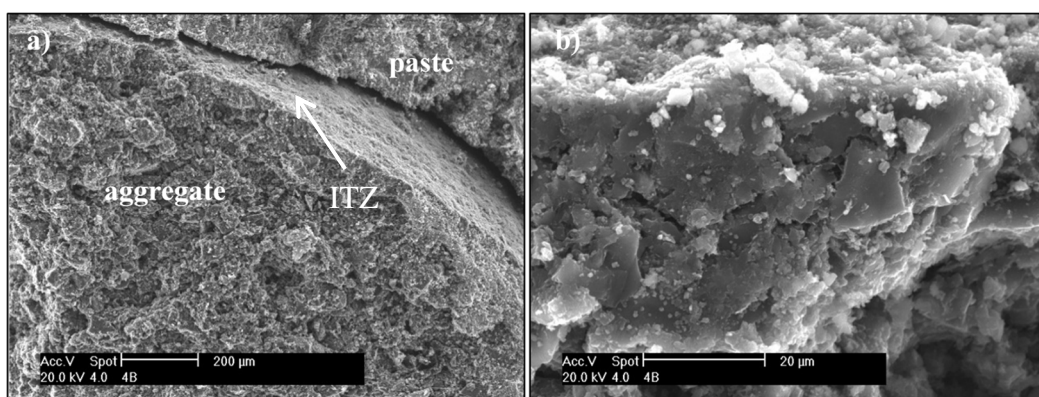
Figure 83 SEM images of HL-A3 specimen a) interface between aggregate and paste, b) zoom on the aggregate

From the results shown in Figure 84, the pore size distributions of HL-S and HL-S TiO2 h is unimodal. Peaks correspond to a pore diameter of 1.199 µm and 0.7259 µm.

The threshold pore diameter is 2.545 µm, the same for both mortars. The use of hydraulic lime introduces into the matrix a porosity with higher threshold pores diameter compared to cement mortar, as already discussed (§ 3.4.3). In case of hydraulic lime mortars, main differences in pore size distributions are introduced with the use of different unconventional aggregates.

In case of zeolite (A2) and active carbon (A3) based mortars, the pore distribution is bi-modal. Peaks are at 0.1254 µm and 0.0216 µm for zeolite mortars and 2.545 µm and 0.1254 µm for active carbon mortars. Threshold diameters are 1.199 µm for zeolite mortars and 6.942 µm for active carbon mortars.

Silica gel based mortar has a too low mechanical resistance to perform this test: the induced pressure on the mercury is not filling the pores but is breaking the materials itself. In literature is well explained that sometimes using this technique there is a threshold issue for mortar and concrete [92].
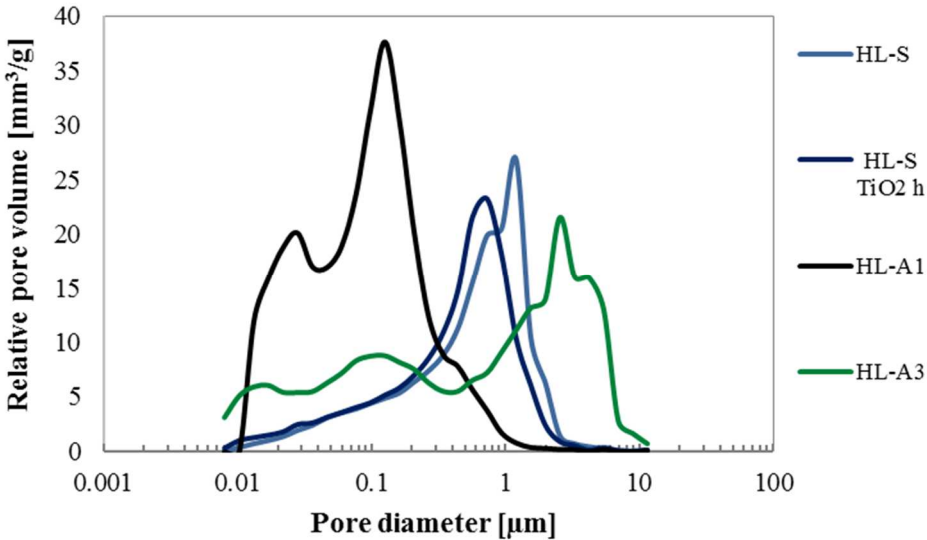
Figure 84 Relative pore volume distribution of different hydraulic lime based mortars

Total porosity can be evaluated both in the cumulative pore volume (Figure 85) and in the percentage of volume of pores (Figure 86).

Conventional aggregate (S) based mortars have the lowest percentage of void (about 30%).

Active carbon based mortars have about 35% of the total percentage of porosity, about 15% more than sand based mortars.

Zeolite based mortar has a total volume porosity 30% more than sand based mortars.
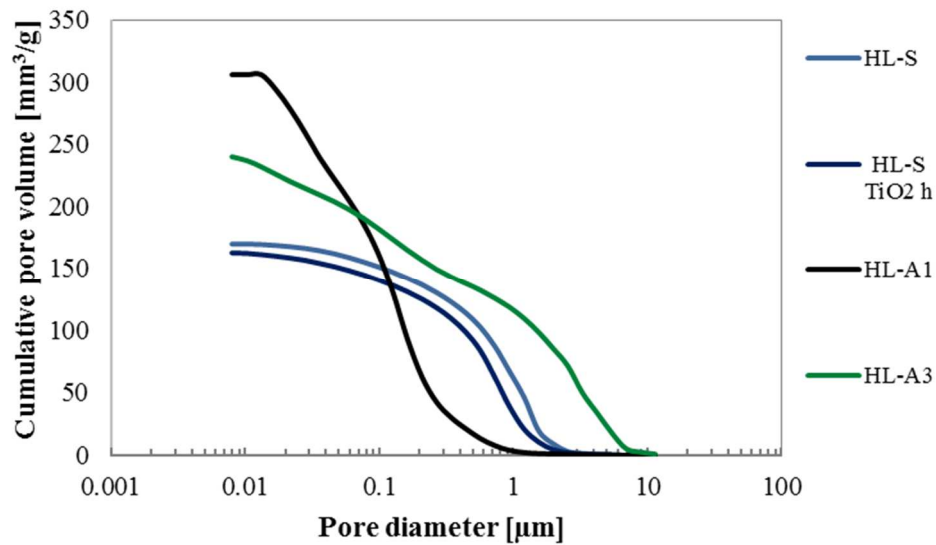
Figure 85 Cumulative pore volume distribution of different mortars: comparison between all results.
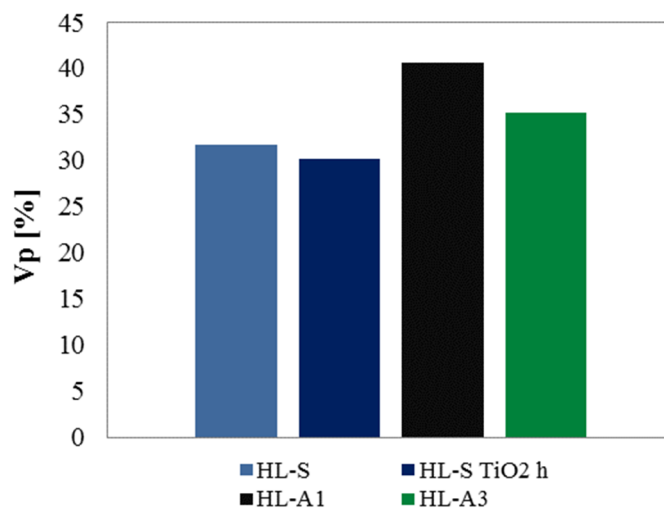
Figure 86 Total porosity of different mortar

4.4.4. Capillary water absorption of mortars

Before testing, mortars are dried completely in a ventilated oven at T = 40 °C. The temperature is chosen in order to not affect the polymeric bounds and the efficiency of hydrophobic admixture.

The efficiency of the hydrophobic admixture is previously tested on specimens with a visual test: placing little drops of water on the surface of the specimens.

Mortars based on hydraulic lime with unconventional aggregates
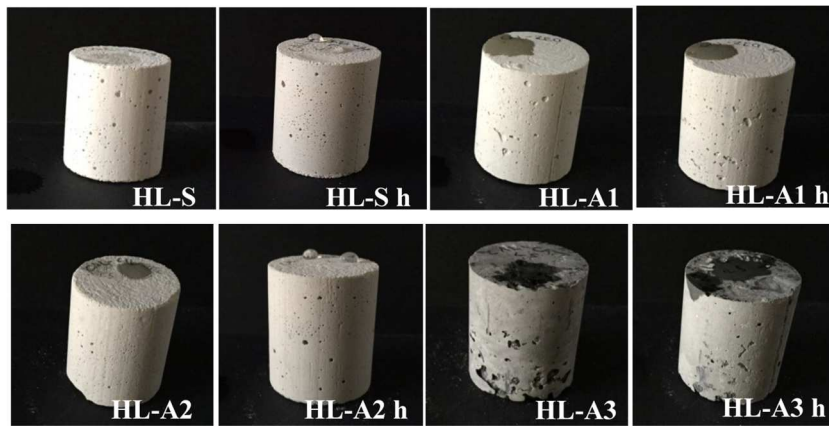
Figure 87 Water-drop test on hydraulic lime based mortars

The test is necessary in order to evaluate if mortars are hydrophobic or not.

The results from hydraulic lime based mortars are the same already discussed in § 3.4.5: zeolite (A1) and activated carbon (A3) based mortars with the hydrophobic admixture are not able to oppose to the water inlet due to the high specific surface of the aggregates.

The test is performed on specimens without TiO_2 because the influence of this addition is not relevant (TiO_2 is not activated by UV light).

The results obtained with the drop-test permit to explain better the results obtained by capillary water absorption tests.

Capillary water absorption coefficient of mortars is evaluated according to the Italian standard UNI EN 1015-18 [65]. Figure 88 shows the results.

In case of sand (S) based mortars, the use of hydrophobic admixture influence the water uptake, which becomes around 40% in terms of C value of specimens without the admixture. The introduction of TiO_2 does not enhance the capillary water absorption as previously detected in § 3.4.5 or in [83] and [36]. This can be due to a decrease in binder content since TiO_2 is replacing 5% of binder volume. Hydraulic lime adsorbs higher quantity of water than cement [26], so a decrease in binder paste can imply a decrease in capillary water absorption coefficient. In presence of hydrophobic admixture, the C value is so low that differences due to TiO_2 addition are not detectable.

In case of zeolite (A1) based mortars, the use of hydrophobic admixture influences the water uptake, which becomes 30% less than mortar without admixture. In hydraulic lime based mortars, if the aggregate is zeolite, the behavior is the same of conventional aggregate mortars, with and without TiO_2 (where C in mortar with TiO_2 is 30% less than one without).

In case of zeolite (A1) based mortars, the use of hydrophobic admixture reduces the water uptake of about 70%. The water uptake is similar to that of conventional aggregate mortars, with and without TiO_2 (where in mortar with TiO_2, C is 30% less than without).

Active carbon (A3) based mortar are not influenced by the addition of hydrophobic admixture and TiO_2 nanoparticles. The values of C in these mortars are 15% lower than sand-based mortars.

The values of silica gel (A2) mortars are the highest. They are double compared to the values of sand based mortars. This is due probably to the high total porosity (deduced by the mechanical test results and/or SEM images). The use of the hydrophobic admixture implies a reduction of about 95% of the C value compared to the value of the same mortars without.

All mortars without hydrophobic admixture and all A3 mortars are classified as W0 mortars, according to UNI EN 998-1:2010 [80]. A1 based mortars with hydrophobic admixture are in W1 class. The other mortars with hydrophobic admixture belongs to W2 class.
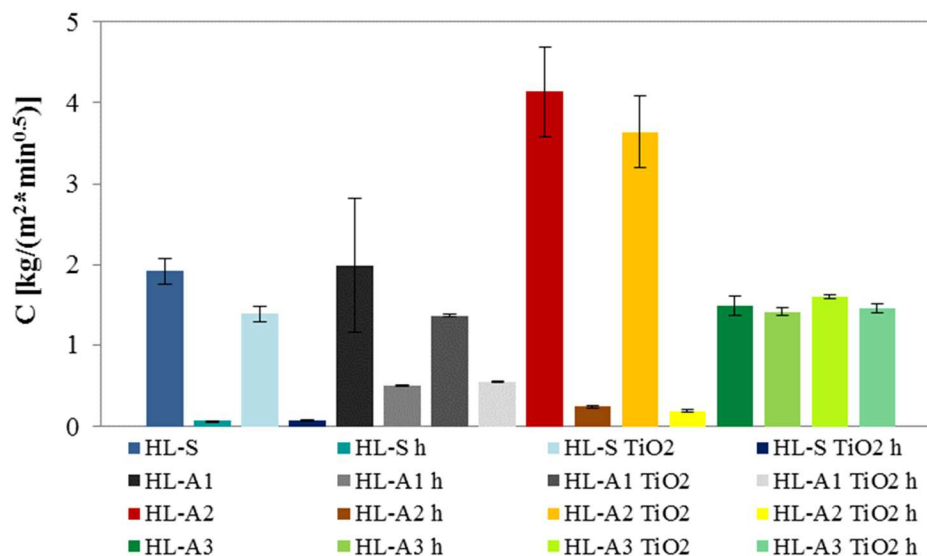
Figure 88 Capillary water absorption coefficient of different mortars according to UNI EN 1015-18.

Results of UNI EN 15801 [66] test are shown in Figure 89.

In this test, in case of using the hydrophobic admixture with sand-based mortar, there is also a decrease in total amount of water adsorbed that becomes 4 times lower.

Zeolite (A1) based mortars, without the admixture, adsorb a total amount of water 60% higher than sand based mortars.

Despite silica gel (A2) based mortars have the highest water absorption (80% higher compared to sand-based mortar), these mortars have the best interaction between the mortar and the hydrophobic admixture.

Results for active carbon (A3) based mortars are influenced by the high specific surface of the aggregate. The absorption is 40% higher than sand based mortars.

Mortars with higher quantity of pore volume (such as silica gel) absorb higher quantity of water. Active carbon mortars absorb lower or confrontable amount of water than lime-sand based mortars because the pore network distribution is more characterized by high pores diameters (peak around 6 µm).

Sand and zeolite based mortars adsorbs similar quantity of water.
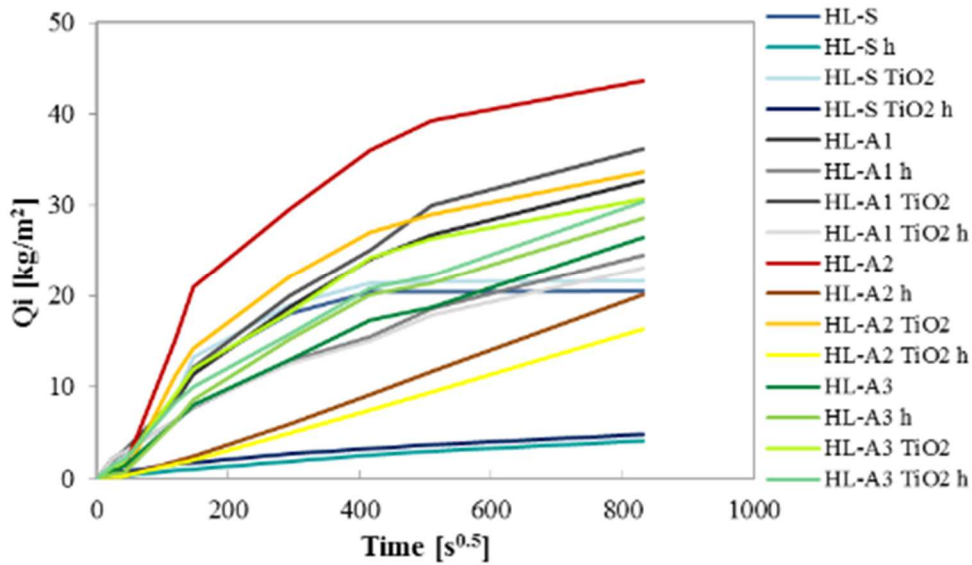
Figure 89 Capillary water absorption in time of hydraulic lime based mortars

4.4.5. Water vapor permeability

Permeability to water vapor expressed in terms of μ factor is shown in Figure 90. Lower value of μ factor indicates higher value of permeability. Different behaviors are due to different aggregates used.

Sand (S) based mortars have the highest μ value, due to the lower accessible porosity detected.

Zeolite (A1) based mortars shows μ value 25% less the sand based mortars. Also in these cases the introduction of TiO_2 or the use of hydrophobic admixture do not introduce relevant changing.

Silica gel (A2) and active carbon (A3) have a very low value of μ, approximately 60% lower than sand based mortars. Also in these cases the introduction of TiO_2 or the use of hydrophobic admixture do not introduce relevant changing.

For the analyzed mortars, mostly for A2 and A3 based, this value is very low, that means very permeable structures: permeable and hygroscopic structures can significantly reduce peak RH values and daily changes in RH improving the IAQ perception [93].

All mortars have permeability to water vapor proportional to the porosity percentage, lower the hygroscopic resistance factor, higher the percentage of pores. This behavior can explain results from silica gel mortars.

Low value of active carbon based mortars are well explained thanks to Kats and Thompson relation [70]: lower the pore radius, lower the transpirability [60].
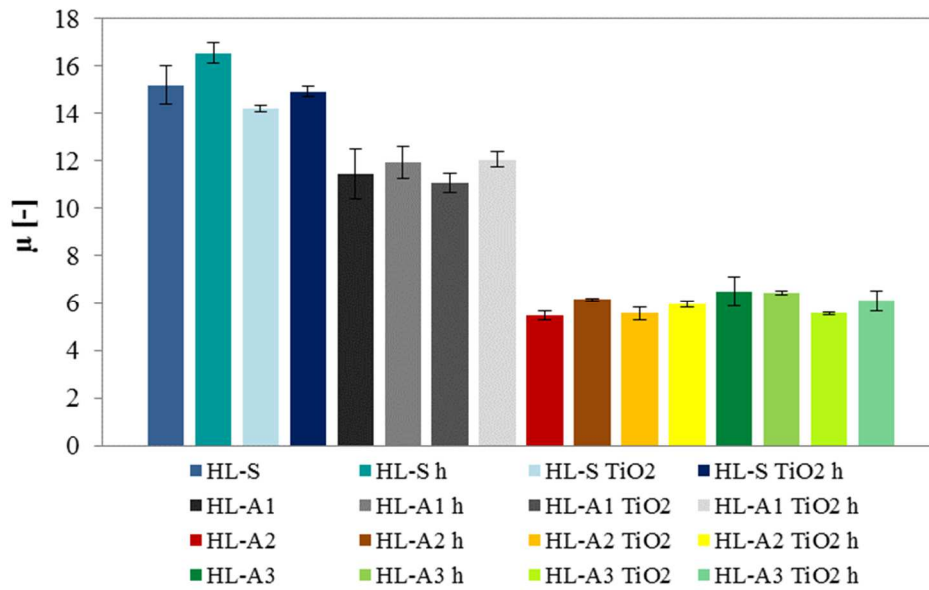
Figure 90 Water vapor resistance factor μ of different mortars

4.4.6. Moisture Buffering Capacity

The interaction between mortars with the humidity of indoor environments is also studied through the evaluation of changing in moisture content of specimens under cyclic conditions. Figure 91 shows the change in water vapor content (Δm) normalized on the exposed surface of the specimens.

At first it is important to note that there are not influences on the MBC of mortars with hydraulic lime and TiO_2 or with and without hydrophobic admixture. The use of different aggregates manly influence the results.
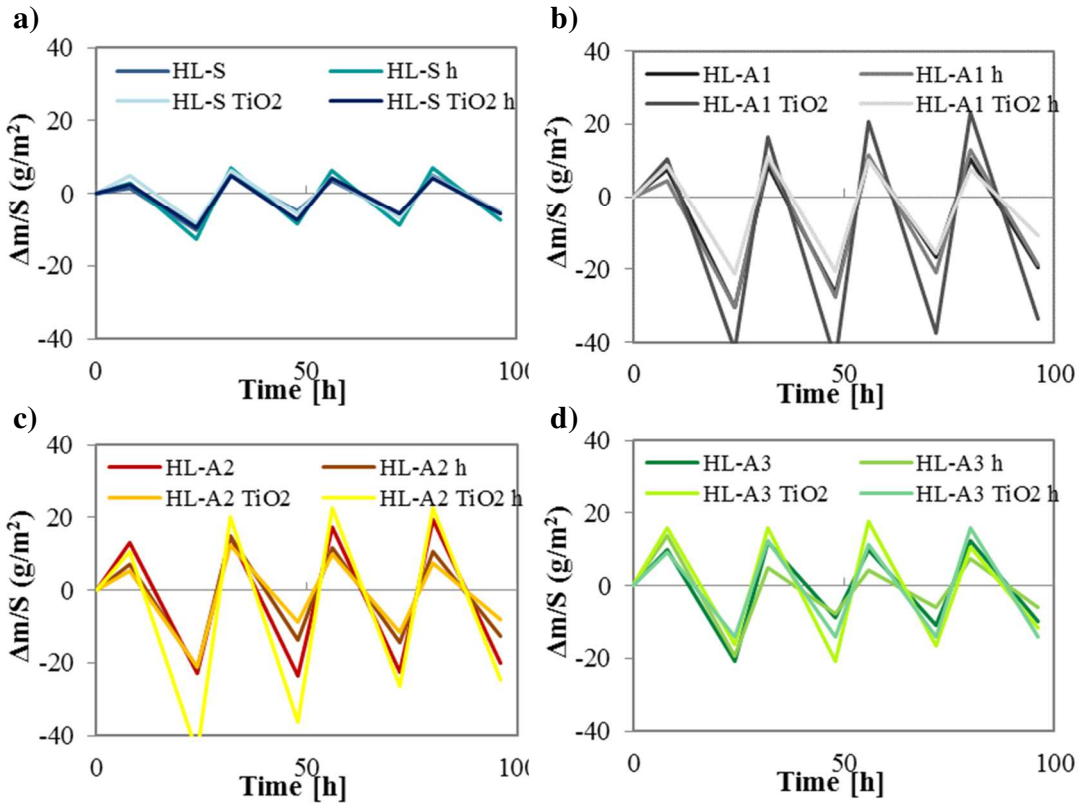
Figure 91 Changing of mass due to absorption/desorption phases, normalized on the specimens surface, for: a) sand, b) zeolite, c) silica gel and d) active carbon based mortars

Sand based mortar specimens show the smallest ability to exchange water vapor with the environment. Data confirm that differences due to the introduction of TiO_2 or the hydrophobic admixture are not detectable.

Zeolite (A1) based mortars adsorb and desorb three times more water vapor then sand based mortars.

Silica gel (A2) based mortars have water changes 2.5 times higher than sand based mortars.

Active carbon (A3) based mortars have about 80% higher capacity of adsorbs/desorbs water vapor than sand based mortar.

Results are expressed in terms of MBV and shown in Figure 92.
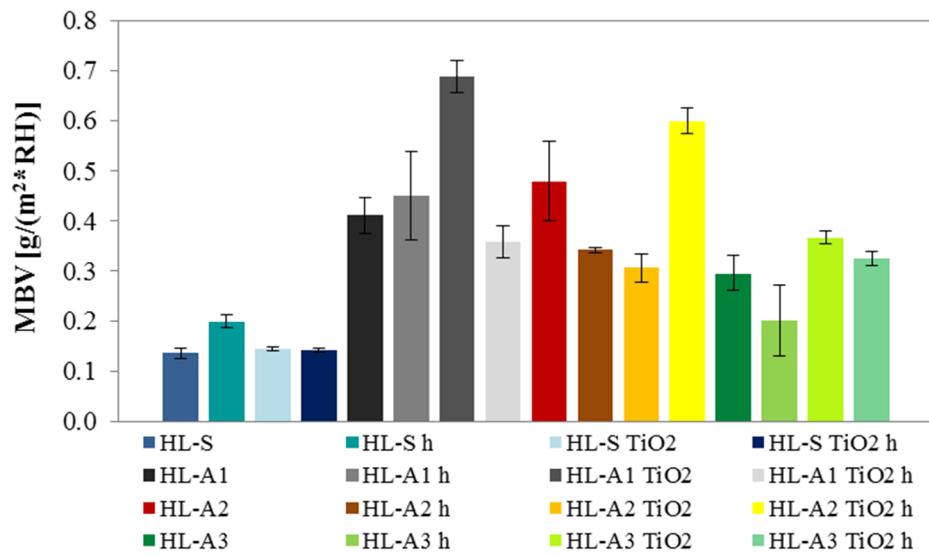
Figure 92 Moisture buffering value of hydraulic lime based mortars

The differences in results are related to the pore size network of mortars. In this case the best correlation of MBV and the percentage of porosity is linear Figure 93. Higher the quantity of pores, higher the ability of the material to uptake/release water vapor.
In case of zeolite based mortars the results are more related to the total surface exposed: higher the total volume of pores, higher the surface available on mortar with large pore volume as previously discussed [86], § 3.4.7.
Silica gel based mortars have probably the highest percentage of porosity and show the best behavior in terms of MBV.
This situation can be a problem related to hysteresis phenomena, since the water vapor is absorbed during high humidity exposition but not completely released during the desorption phase. During the test this behavior is slightly detected.
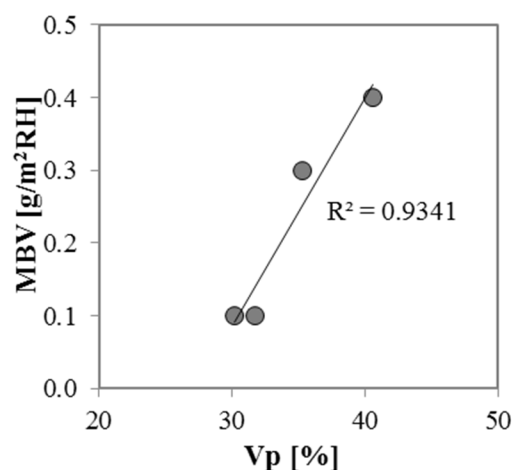
Figure 93 Correlation between MBV values and porosity

4.4.7. Inhibition of molds growth on mortars

The inhibition of molds growth is evaluated in order to compare the behavior of different mortars exposed to biological colonization.

Before the test, pH is evaluated as described in § 2.3.5.1. Table 13 shows the results of pH measurements. pH of mortars is currently on a range compatible to the Aspergillus growth, samples have already carbonated losing their initial basicity.

Table 13 Measure of pH of hydraulic lime based mortars

Mix	HL-S	HL-A1	HL-A2	HL-A3
pH	8.5	8.5	8.5	8

The middle of the sample is inoculated using 100 µl of conidia suspension (2.59 x 105 conidia/ml).

To assess the conidia vitality, 100 µl of conidial suspension is inoculated on two sheets of sterile filter paper of the same size of the mortar specimens and incubated in Petri dishes. These two particular samples act as the blank specimens because the filter paper does not show any inhibitory effect on the conidia germination.

Test is assessed for 28 days. Specimens are tested as it is, without TiO_2 activation under UVA radiation, in order to isolate and evaluate the effective inhibition capacity of mortars.

Once per week, pictures are taken to monitor the growth of the molds. The images of days 21 and 28 are processed on a software able to quantify the different pixels (differences in color) to know the percentage of colonized area. The colonized area is evaluated as a percentage of total pixels of the specimen images. Pictures of each specimen are rotated and cut with a photo editing program (Figure 94), selecting about the same number of pixels for all images, taking care to exclude the pixels of the sample holder frame.
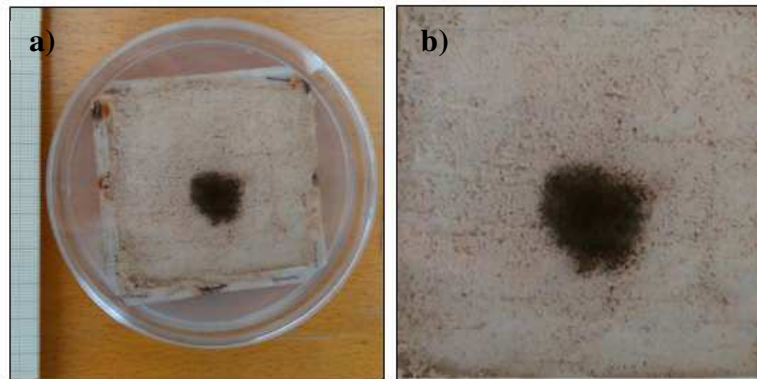
Figure 94 Example of first data elaboration: a) photo acquired at 28 days and b) elaboration of the photo with software

Images are divided in three zones: zone 1 zone 2 and zone 3:

- **Zone 1**: a central zone colonized by the molds, color tending to black, where the hyphae have already differentiated conidia;
- **Zone 2**: an intense growth zone, where are the younger hyphae, characterized by a lighter color than the first;
- **Zone 3**: not colonized zone.

The number of pixels related to each zone is evaluated with Gimp2. The elaboration for active carbon, due to the dark color of the specimens, is more difficult than the others, so it is necessary to evaluate the colonization by visual observations. Then, collected data are validated with a stereomicroscope provided with a high-resolution camera for images acquisitions.
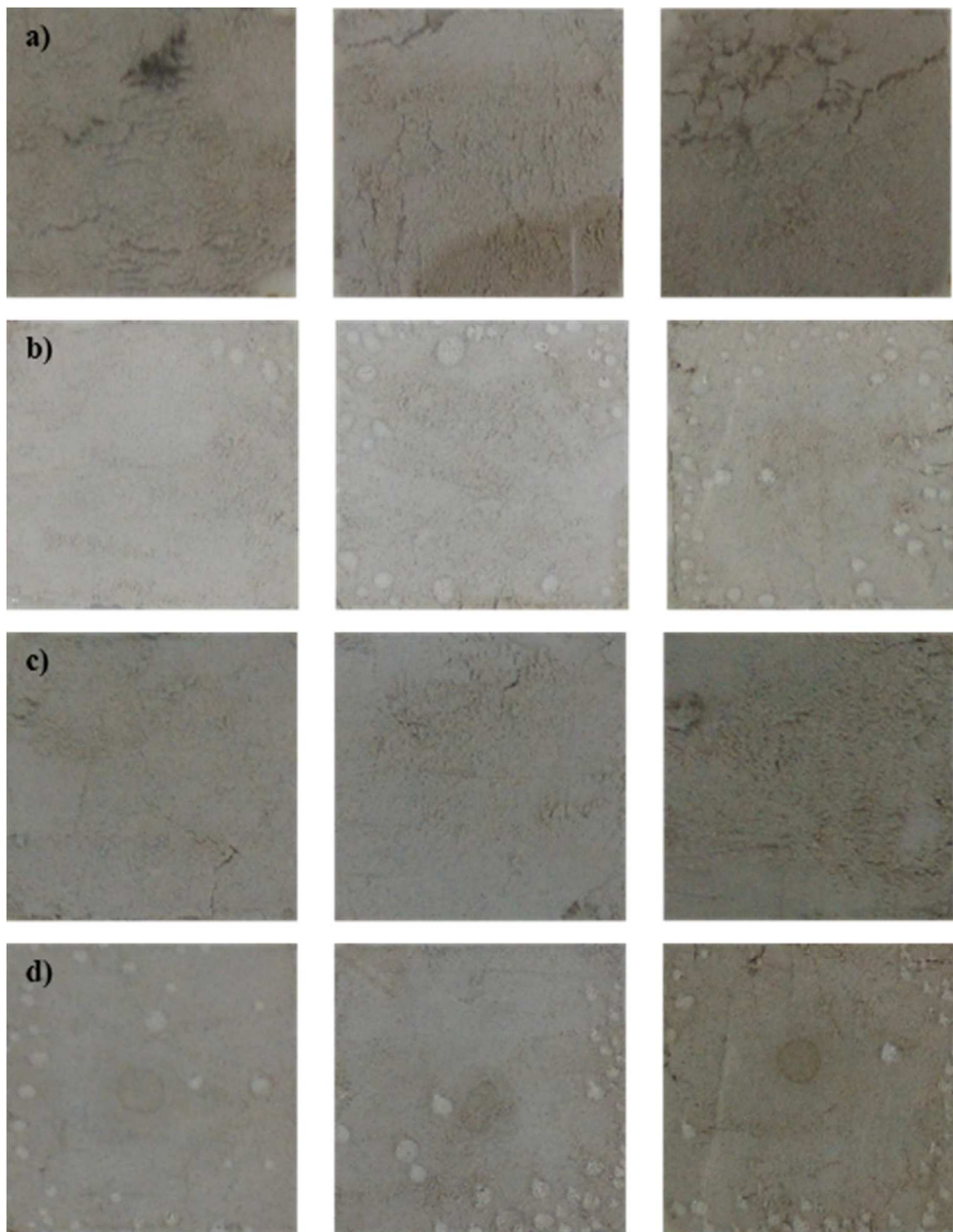
Figure 95 Pictures at 7days: a) HL-S b) HL-S h c) HL – S TiO2 c) HL – S TiO2 h
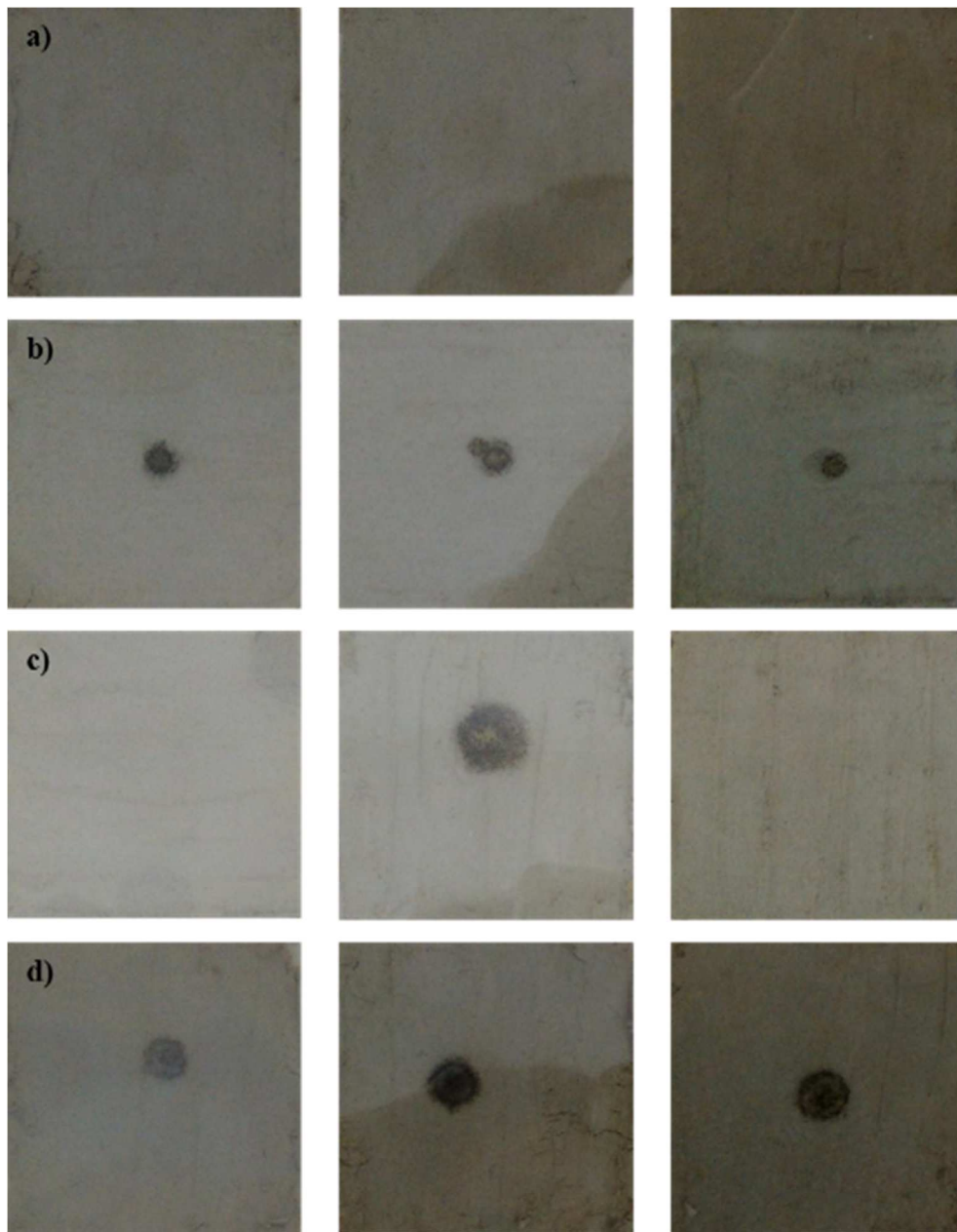
Figure 96 Pictures at 7days: a) HL-A1 b) HL-A1 h c) HL – A1 TiO2 c) HL – A1 TiO2 h

Figure 97 Pictures at 7days: a) HL-A2 b) HL-A2 h c) HL – A2 TiO2 c) HL – A2 TiO2 h
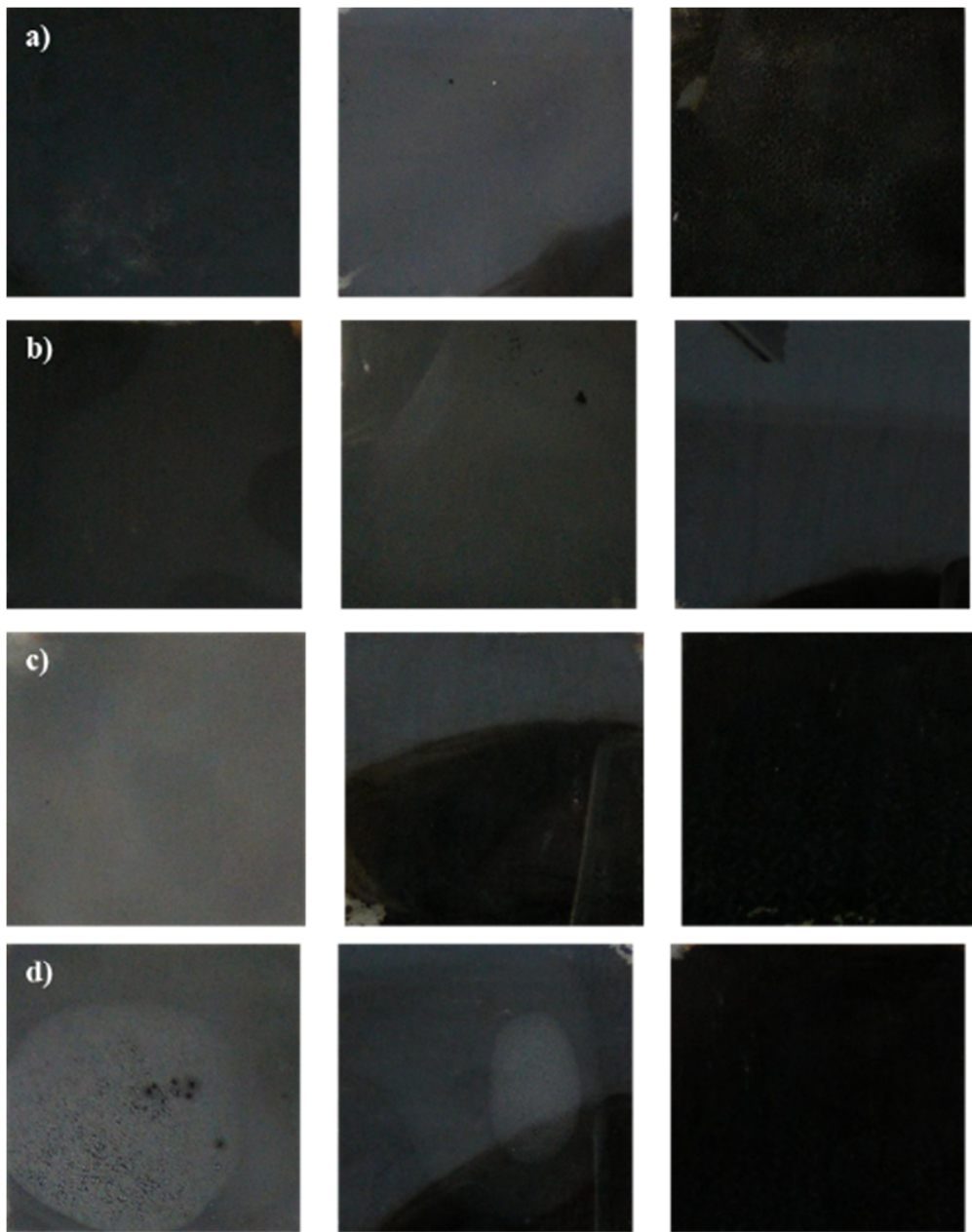
Figure 98 Pictures at 7days: a) HL-A3 b) HL-A3 h c) HL – A3 TiO2 c) HL – A3 TiO2 h
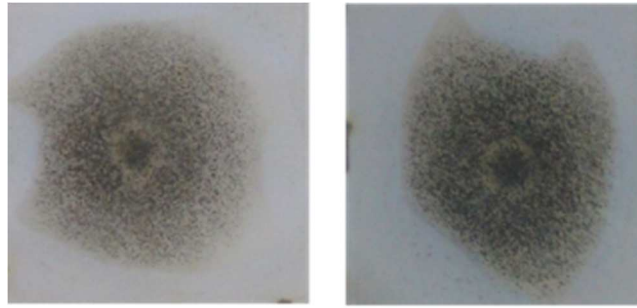
Figure 99 Pictures at 7 days: blank specimens
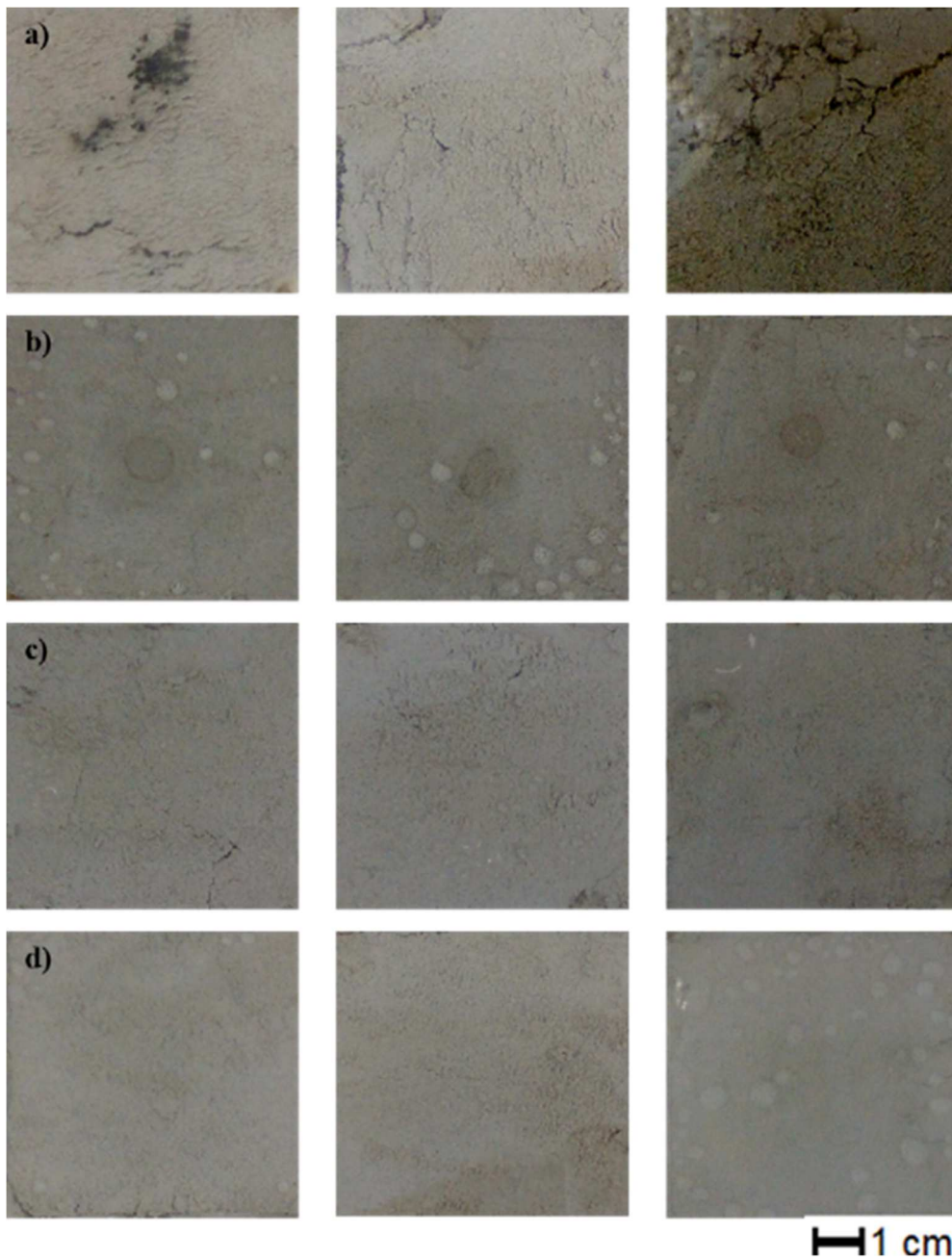
Figure 100 Pictures at 14 days: a) HL-S b) HL-S h c) HL – S TiO2 c) HL – S TiO2 h
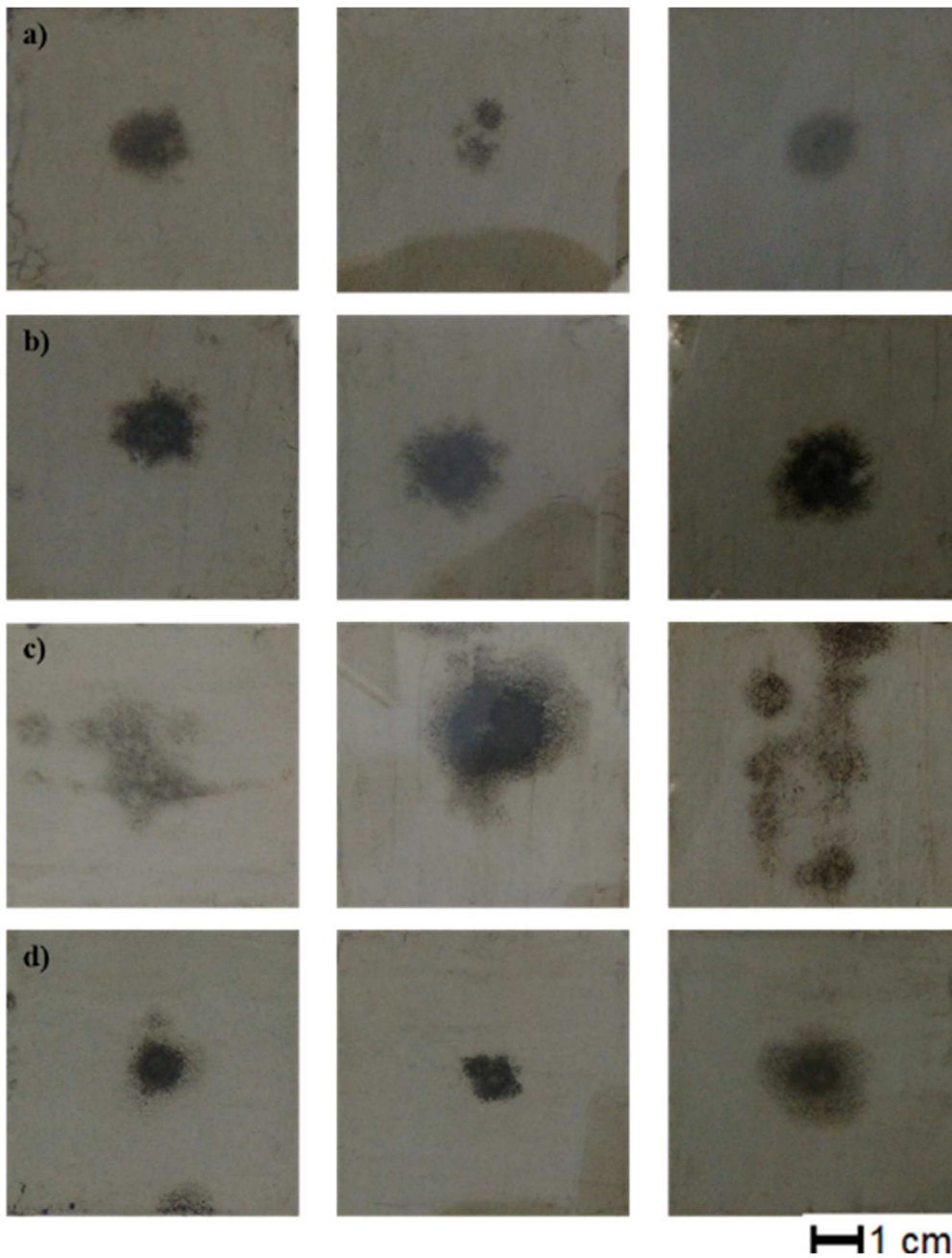
Figure 101 Pictures at 14 days: a) HL-A1 b) HL-A1 h c) HL – A1 TiO2 c) HL – A1 TiO2 h
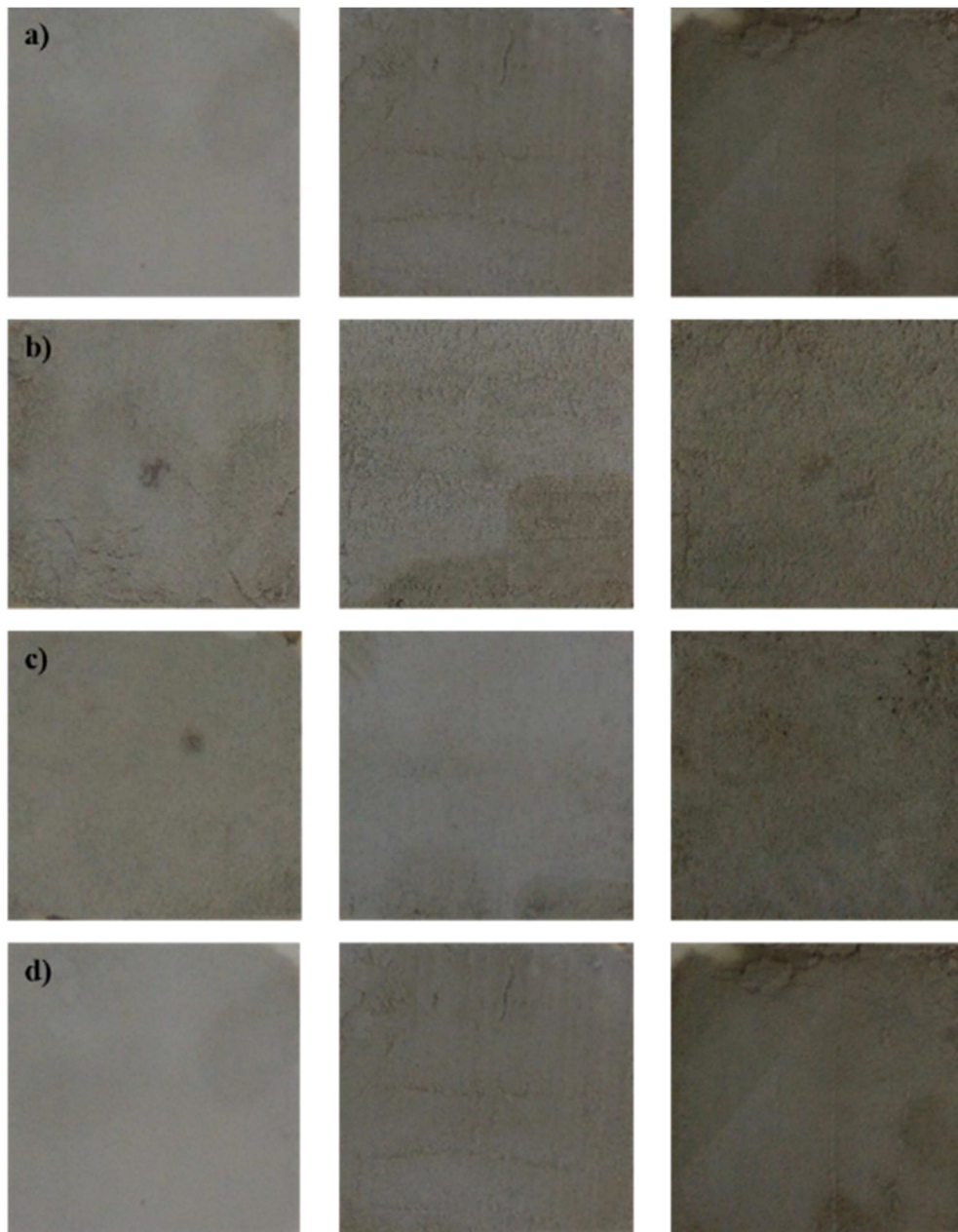
Figure 102 Pictures at 14 days: a) HL-A2 b) HL-A2 h c) HL – A2 TiO2 c) HL – A2 TiO2 h
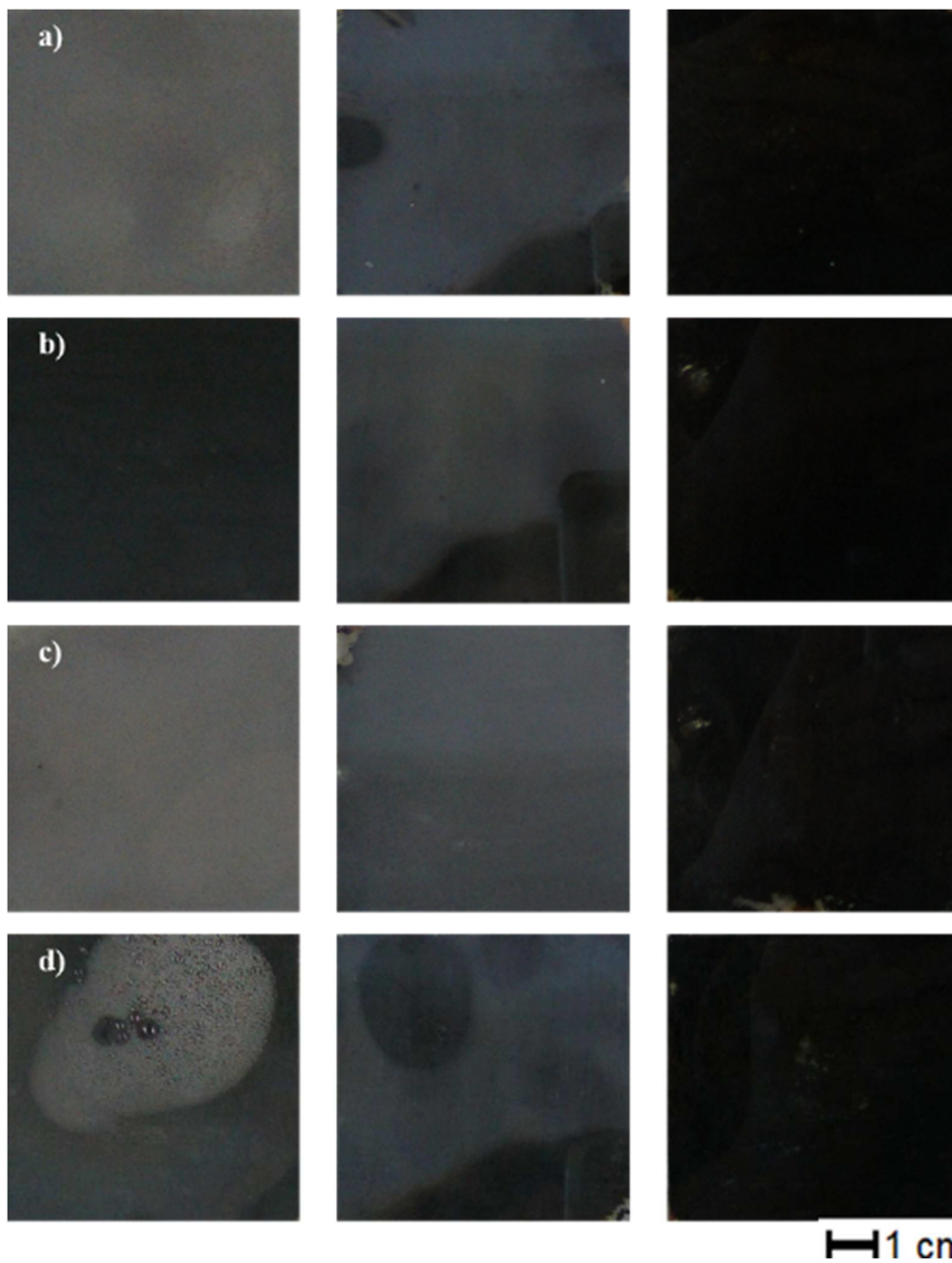
Figure 103 Pictures at 14 days: a) HL-A3 b) HL-A3 h c) HL – A3 TiO2 c) HL – A3 TiO2 h
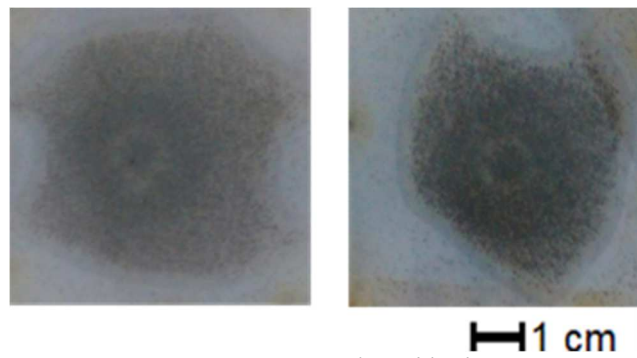
Figure 104 Pictures at14 days: blank specimens

The following images (from Figure 105 to Figure 120) report the results at 21 days of observation: the data indicates are data from the software evaluation, without data interpretation.

Although the colonization of the specimens with activated carbon is visible, on the pictures the image with the hue of very similar colors makes it difficult to effectively divide the regions of interest.
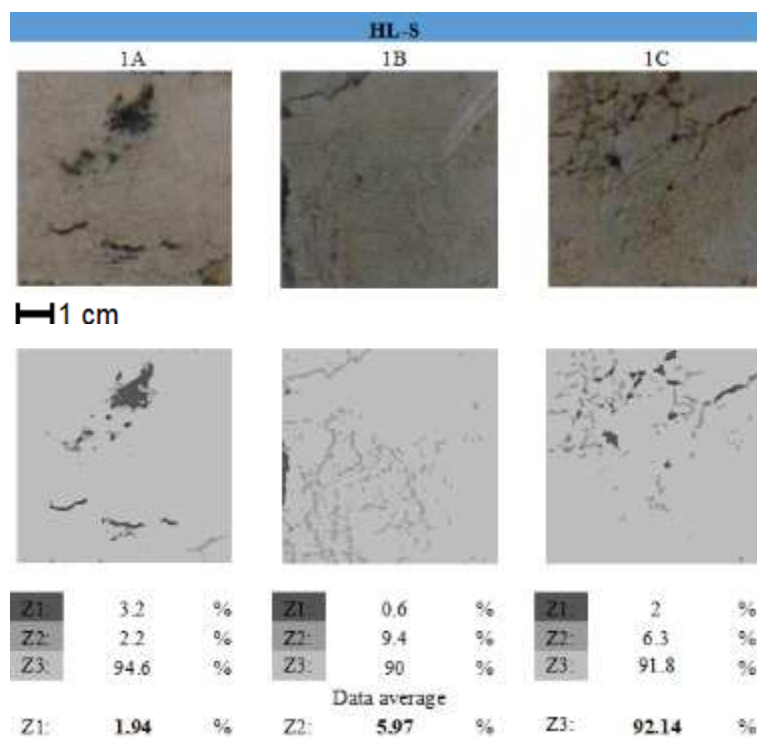
Figure 105 Pictures at 21 days: HL-S photo (three specimens) and elaboration of images

		HL-S-H				
	3A		3B		3C	
Z1:	1.4	%	Z1:	3.1	%	Z1:	3	%
Z2:	6.6	%	Z2:	2.9	%	Z2:	4.4	%
Z3:	92	%	Z3:	94	%	Z3:	92.5	%

Data average

| Z1: | 2.5 | % | Z2: | 4.64 | % | Z3: | 92.84 | % |
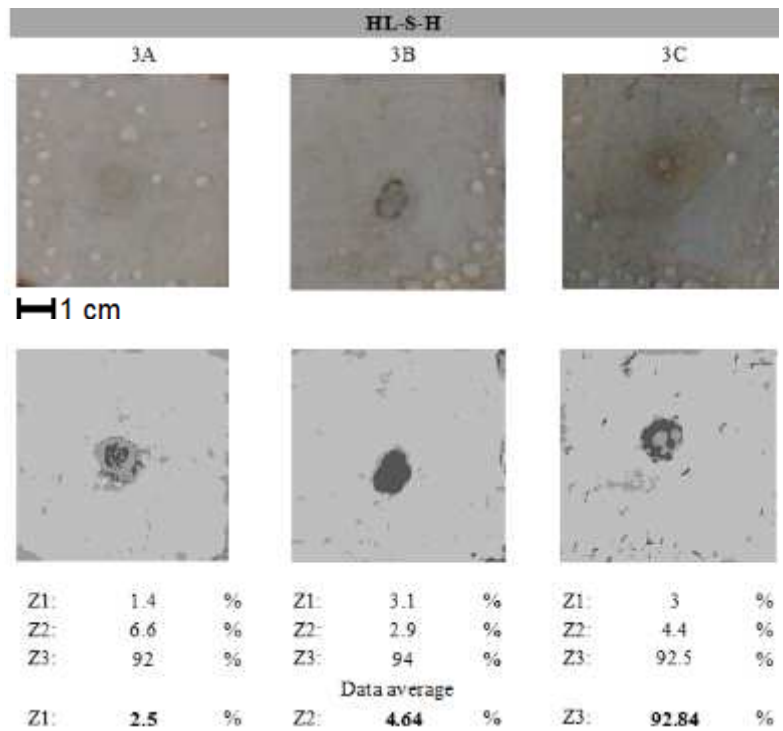
Figure 106 Pictures at 21 days: HL-S h photos (three specimens) and elaboration of images

		HL-S-TiO2				
	4A		4B		4C	
Z1:	0.9	%	Z1:	1.7	%	Z1:	2.5	%
Z2:	7.7	%	Z2:	7.9	%	Z2:	17.2	%
Z3:	91.3	%	Z3:	90.4	%	Z3:	80.3	%

Data average

| Z1: | 1.7 | % | Z2: | 10.94 | % | Z3: | 87.34 | % |
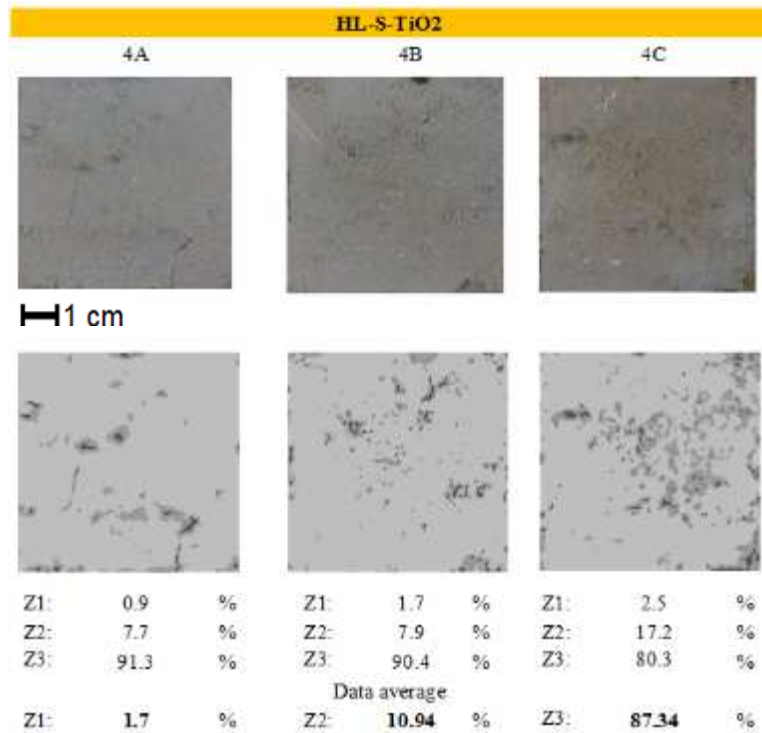
Figure 107 Pictures at 21 days: HL-S TiO2 photos (three specimens) and elaboration of images
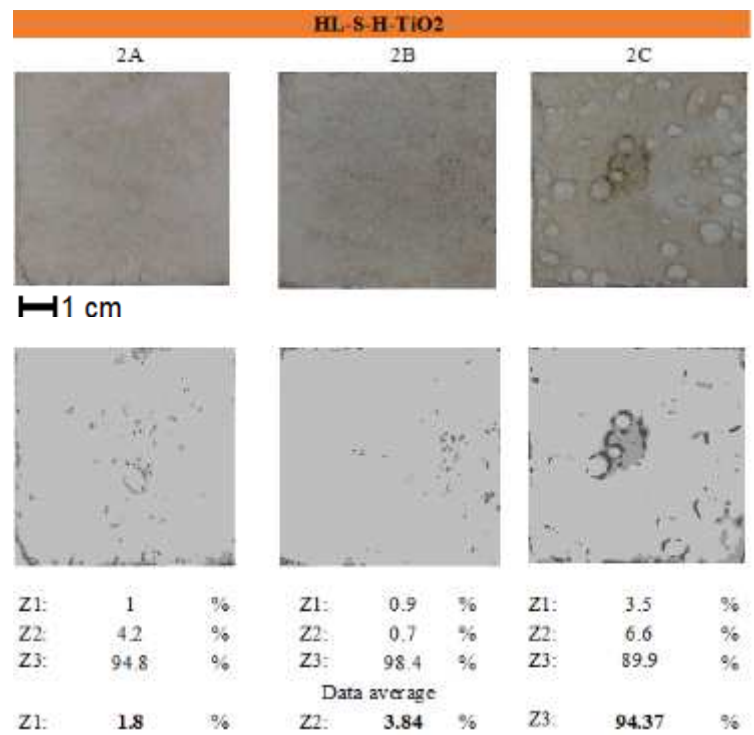
Figure 108 Pictures at 21 days: HL-S TiO2 h photos (three specimens) and elaboration of images
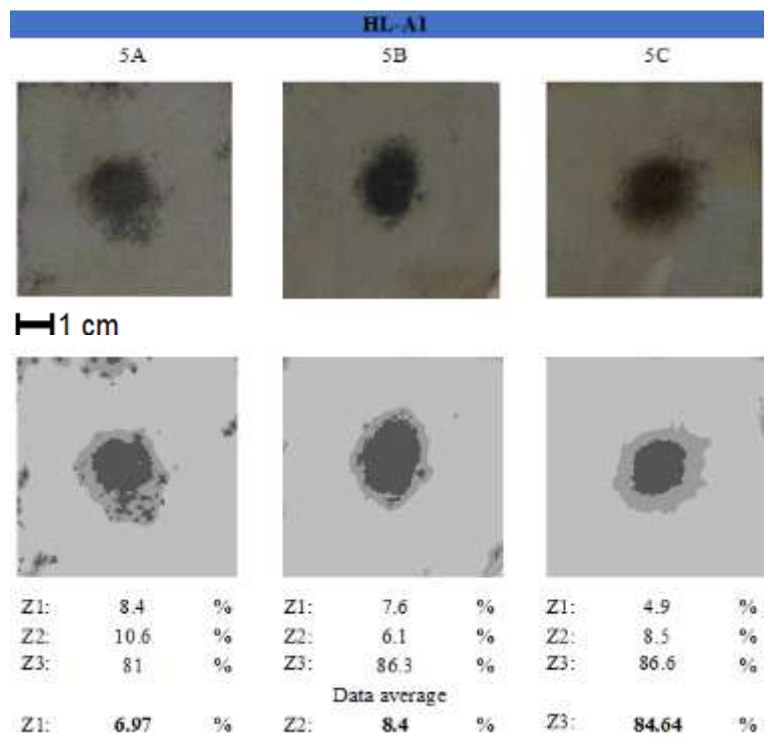
Figure 109 Pictures at 21 days: HL-A1 photos (three specimens) and elaboration of images
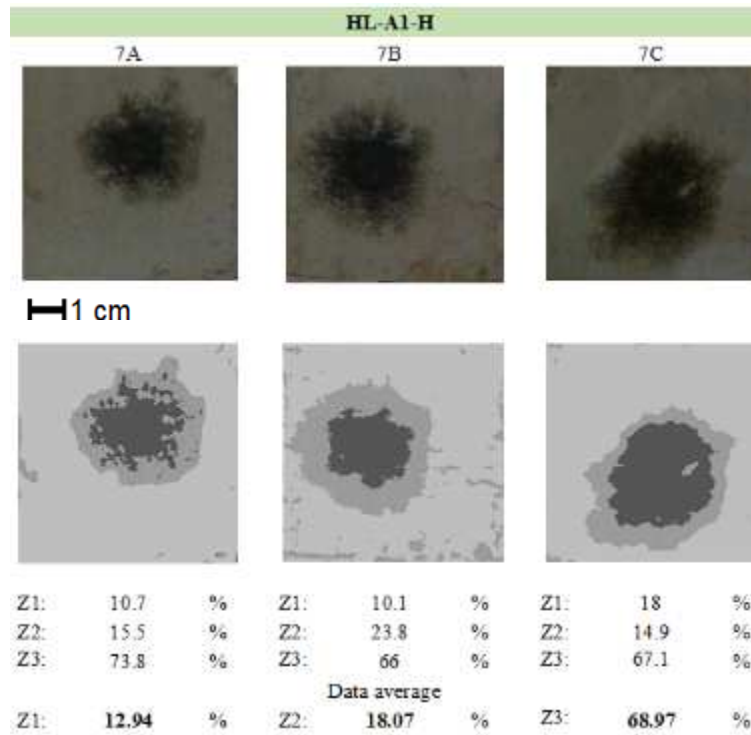
Figure 110 Pictures at 21 days: HL-A1 h photos (three specimens) and elaboration of images
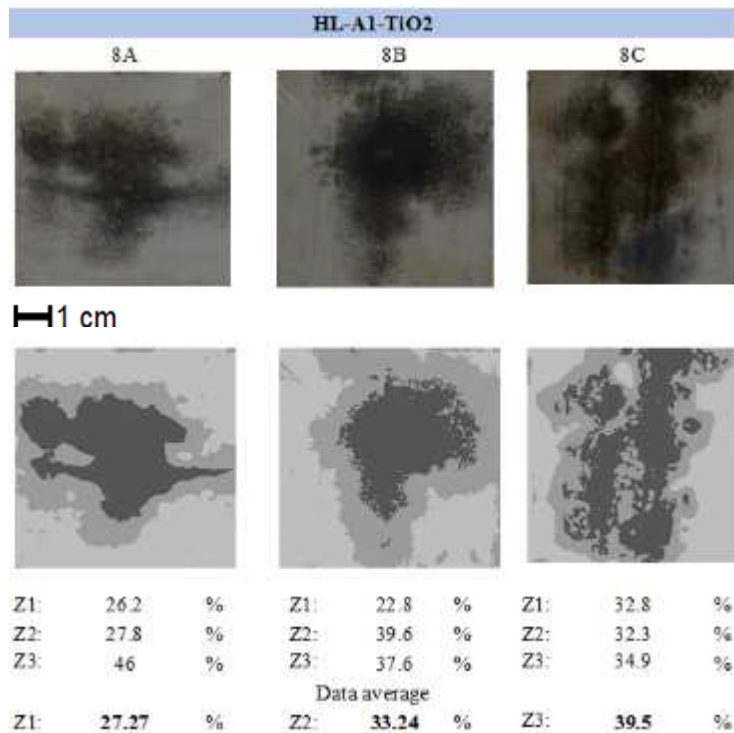
Figure 111 Pictures at 21 days: HL-A1 TiO2 photos (three specimens) and elaboration of images
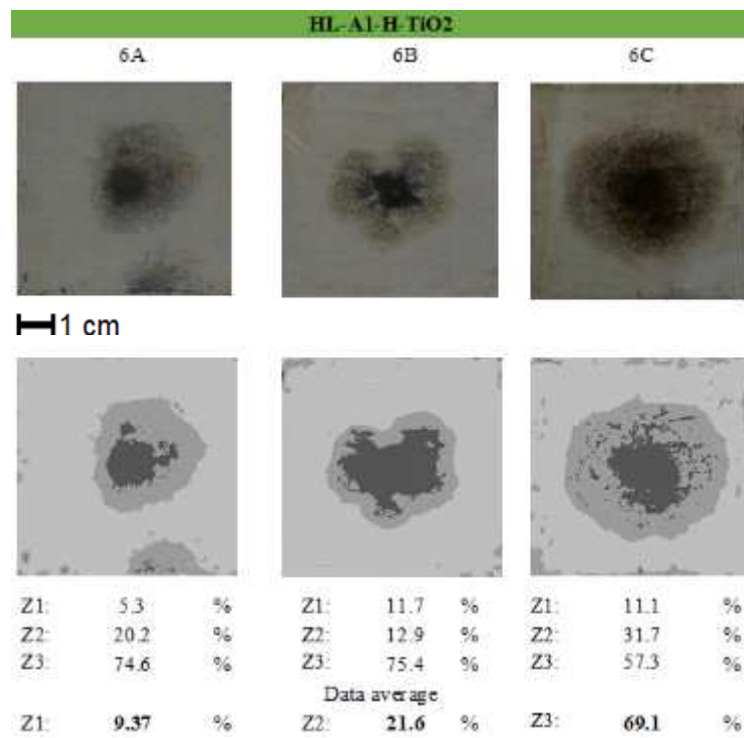
Figure 112 Pictures at 21 days: HL-A1 TiO2 h photos (three specimens) and elaboration of images
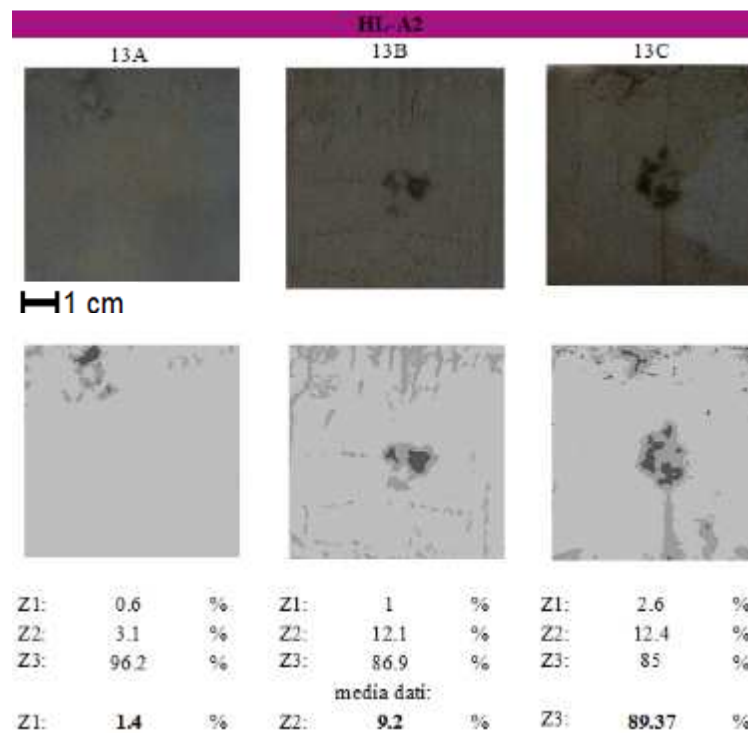
Figure 113 Pictures at 21 days: HL-A2 photos (three specimens) and elaboration of images
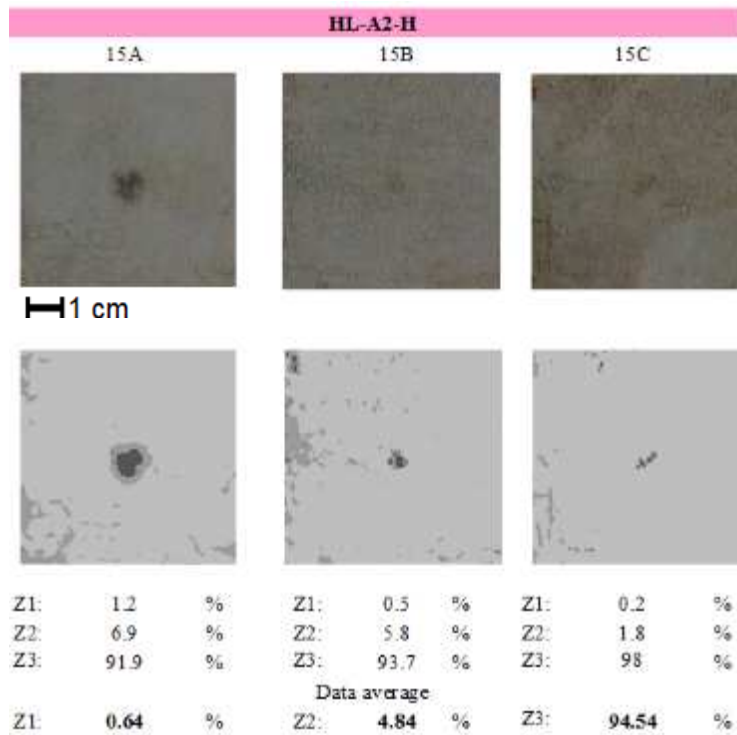
Figure 114 Pictures at 21 days: HL-A2 h photos (three specimens) and elaboration of images
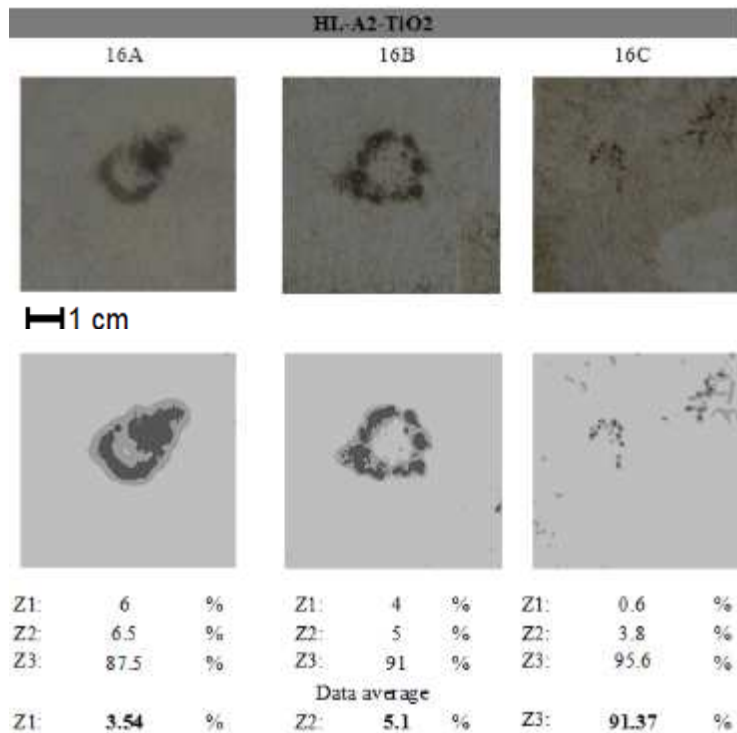
Figure 115 Pictures at 21 days: HL-A2 TiO2 photos (three specimens) and elaboration of images
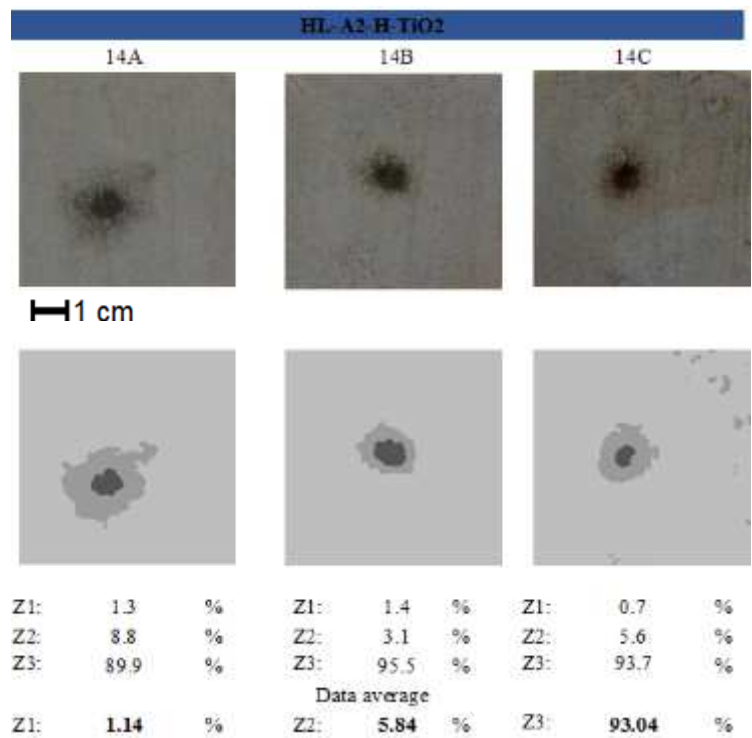
Figure 116 Pictures at 21 days: HL-A2 TiO2 h photos (three specimens) and elaboration of images
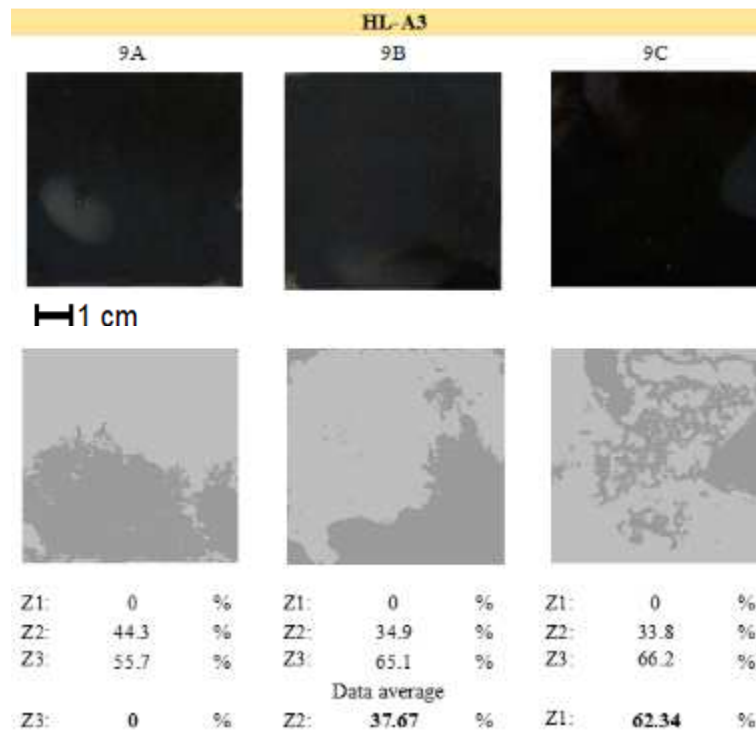
Figure 117 Pictures at 21 days: HL-A3 photos (three specimens) and elaboration of images
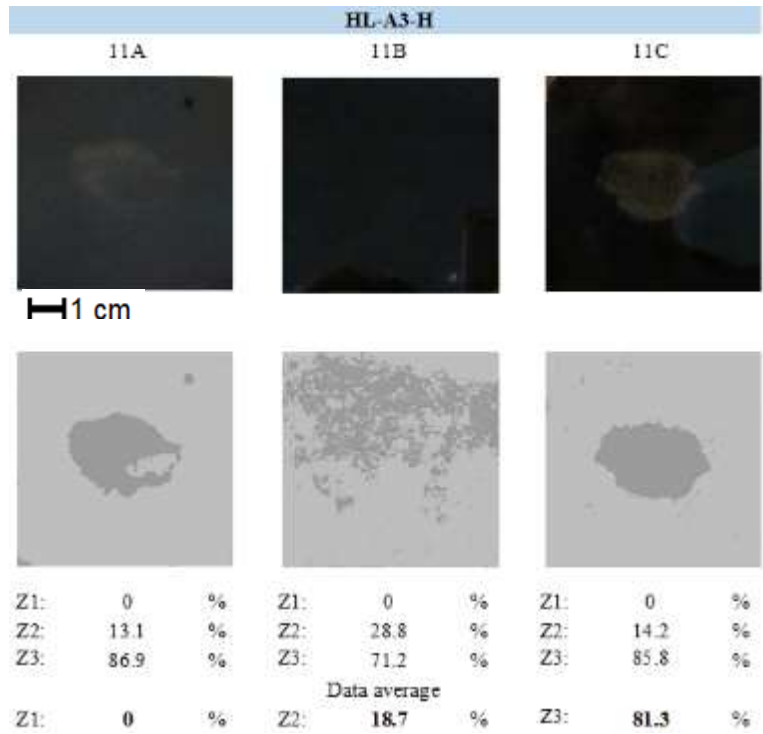
Figure 118 Pictures at 21 days: HL-A3 h photos (three specimens) and elaboration of images
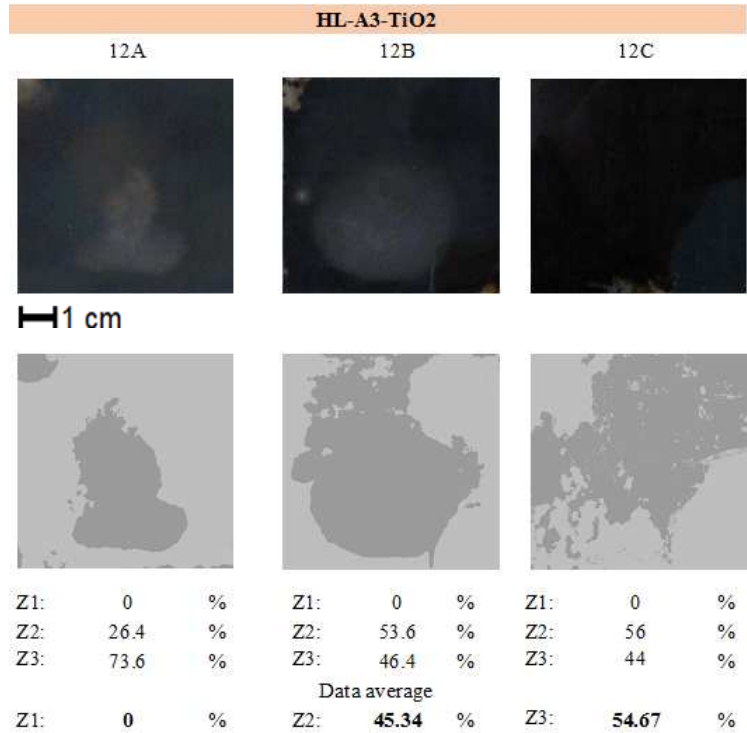
Figure 119 Pictures at 21 days: HL-A3 TiO2 photos (three specimens) and elaboration of images
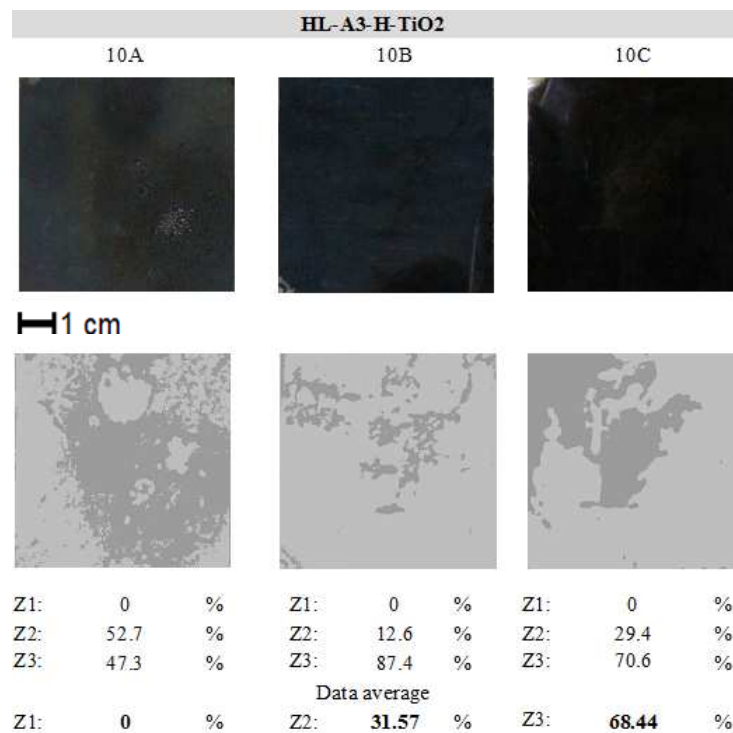
Figure 120 Pictures at 21 days: HL-A3 TiO2 h photos (three specimens) and elaboration of images
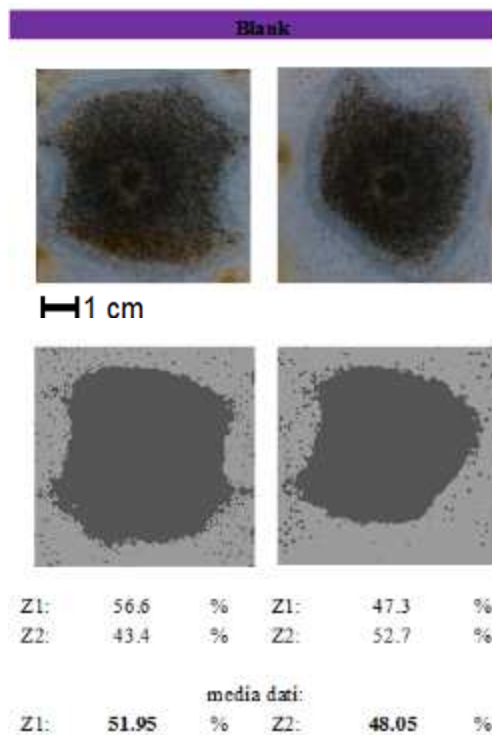
Figure 121 Pictures at 21 days: blank (two replicas) and elaboration of images

Following pictures (from Figure 122 to Figure 138) show the results at 28 days of observation. Also in this case the active carbon (A3) based mortars is colonized but,

due to the dark color of the specimens is not possible quantify the pixels that corresponds to the colonized area.
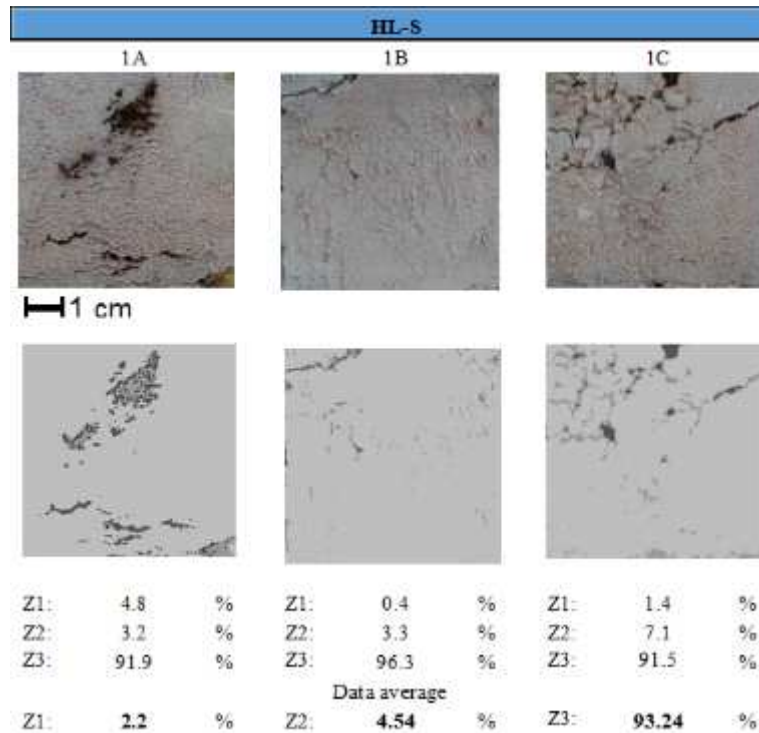
Figure 122 Pictures at 28 days: HL-S photo (three specimens) and elaboration of images
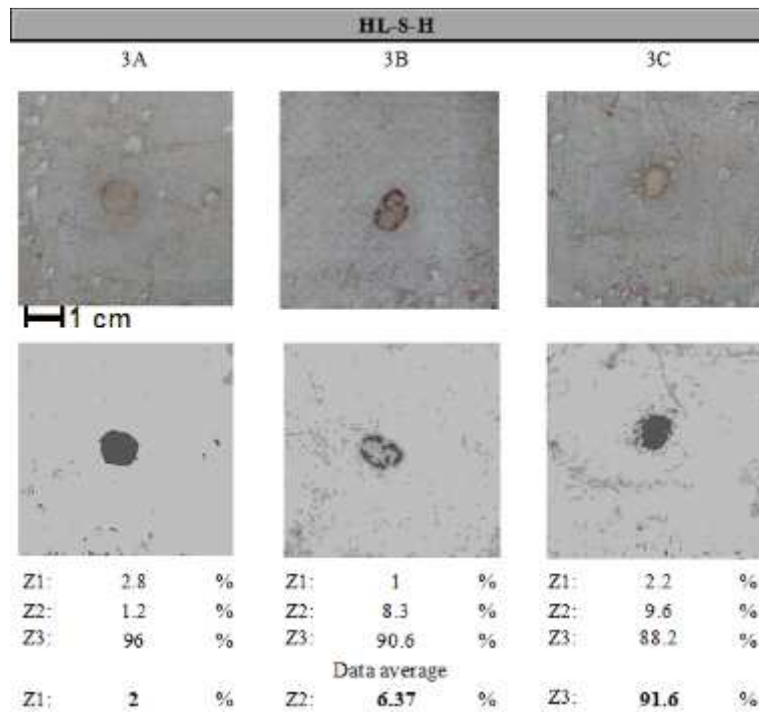
Figure 123 Pictures at 28 days: HL-S h photos (three specimens) and elaboration of images

HL-S-TiO2					
4A		4B		4C	
Z1:	1.5 %	Z1:	1.1 %	Z1:	0.1 %
Z2:	3.3 %	Z2:	9.7 %	Z2:	10.4 %
Z3:	95.2 %	Z3:	89.2 %	Z3:	89.5 %

Data average

Z1:	0.9 %	Z2:	7.8 %	Z3:	91.3 %
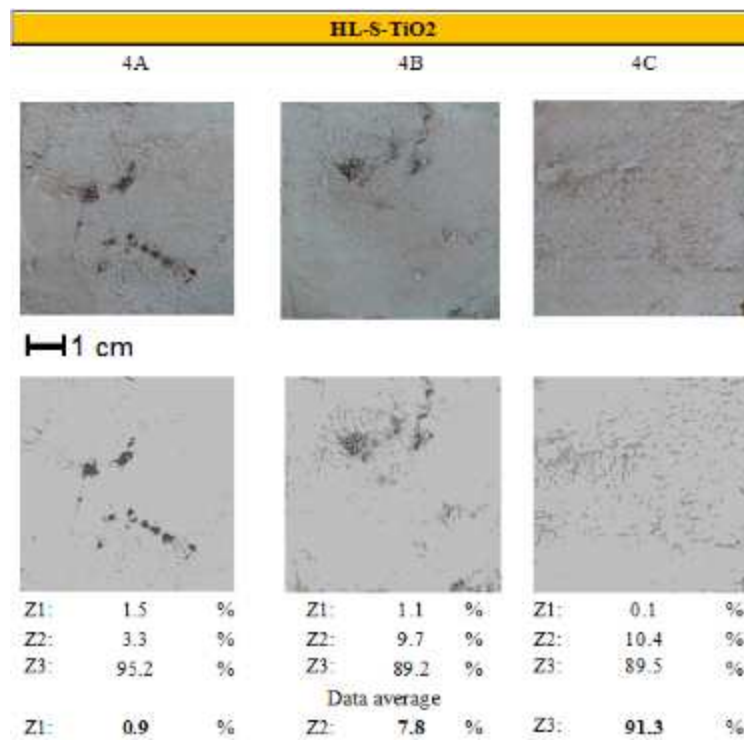
Figure 124 Pictures at 28 days: HL-S TiO2 photos (three specimens) and elaboration of images

HL-S-H-TiO2					
2A		2B		2C	
Z1:	1 %	Z1:	0.1 %	Z1:	1.8 %
Z2:	4.3 %	Z2:	10.7 %	Z2:	11.4 %
Z3:	94.7 %	Z3:	89.2 %	Z3:	86.9 %

Data average

Z1:	0.97 %	Z2:	8.8 %	Z3:	90.27 %
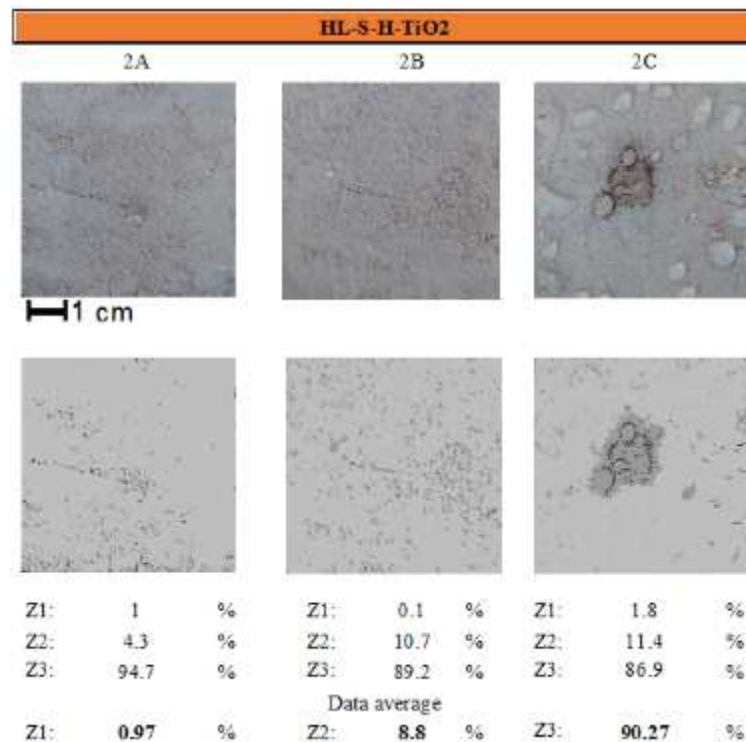
Figure 125 Pictures at 28 days: HL-S TiO2 h photos (three specimens) and elaboration of images
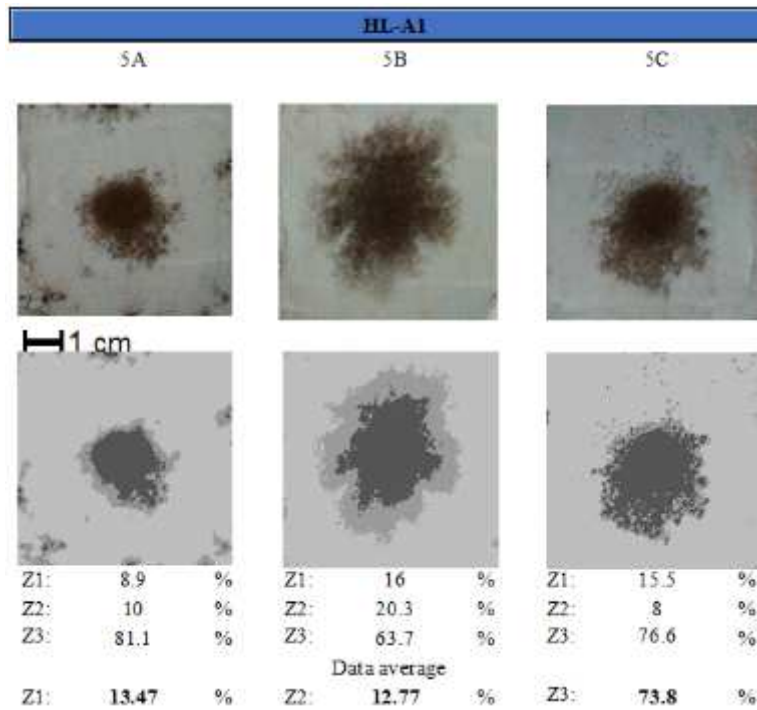
Figure 126 Pictures at 28 days: HL-A1 photos (three specimens) and elaboration of images
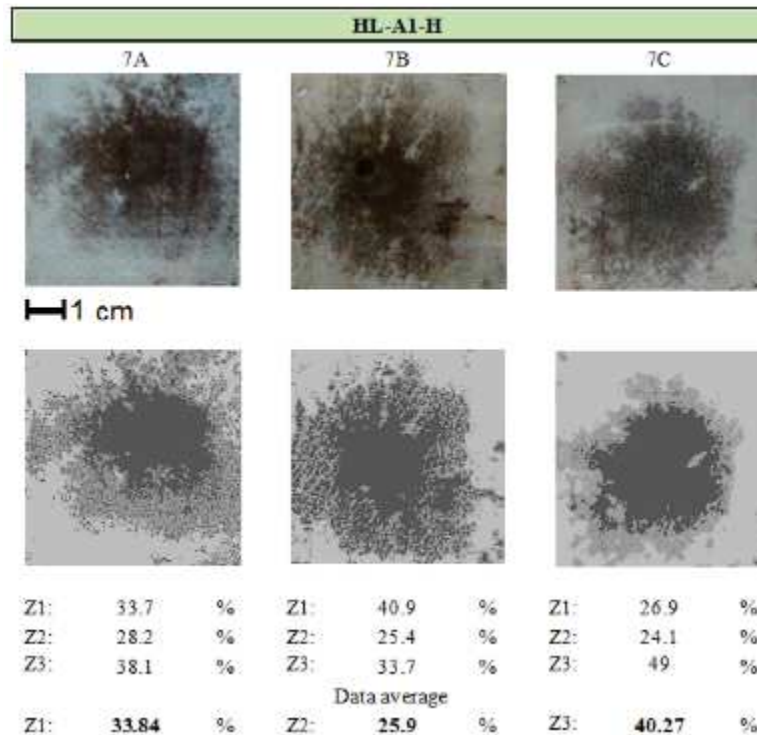
Figure 127 Pictures at 28 days: HL-A1 h photos (three specimens) and elaboration of images
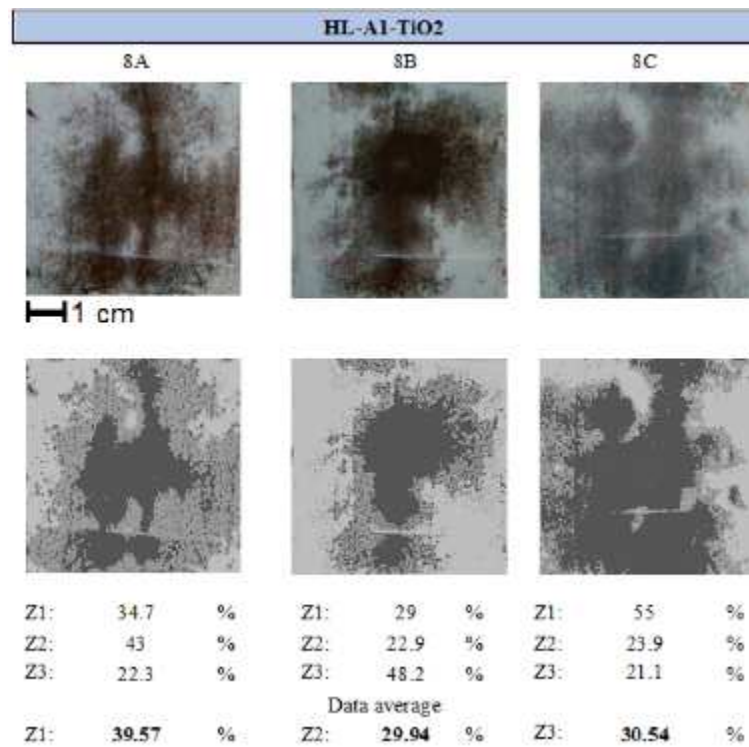
Figure 128 Pictures at 28 days: HL-A1 TiO2 photos (three specimens) and elaboration of images
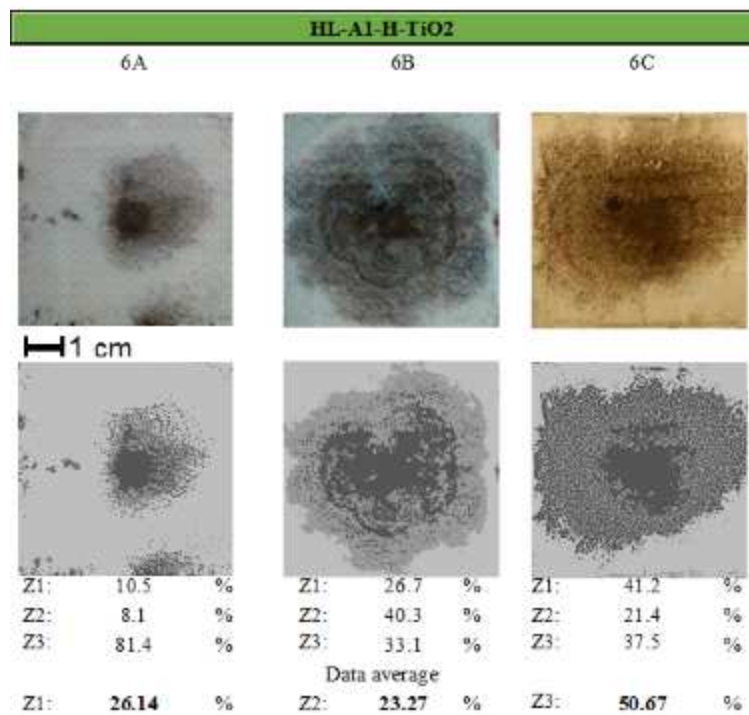
Figure 129 Pictures at 28 days: HL-A1 TiO2 h photos (three specimens) and elaboration of images
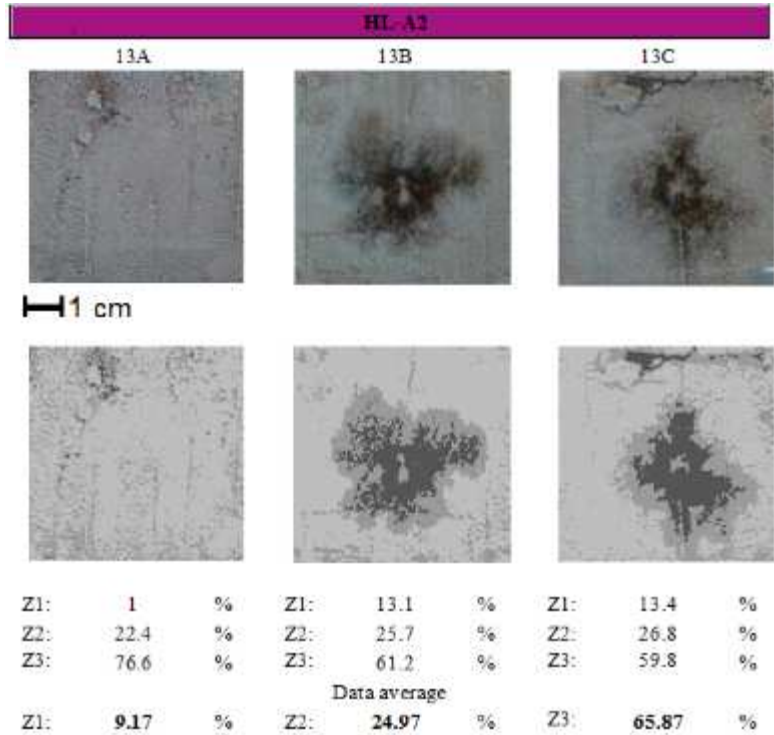
Figure 130 Pictures at 28 days: HL-A2 photos (three specimens) and elaboration of images
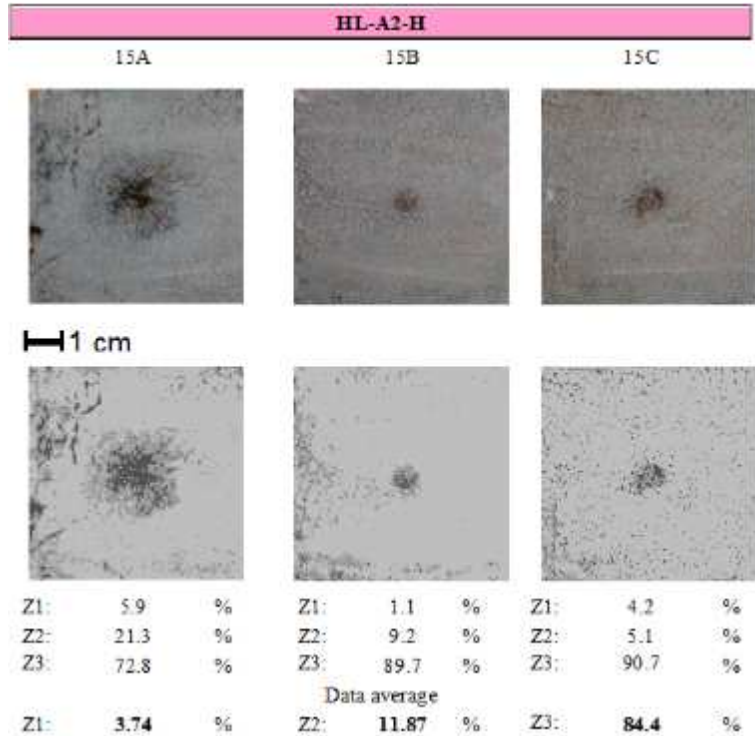
Figure 131 Pictures at 28 days: HL-A2 h photos (three specimens) and elaboration of images
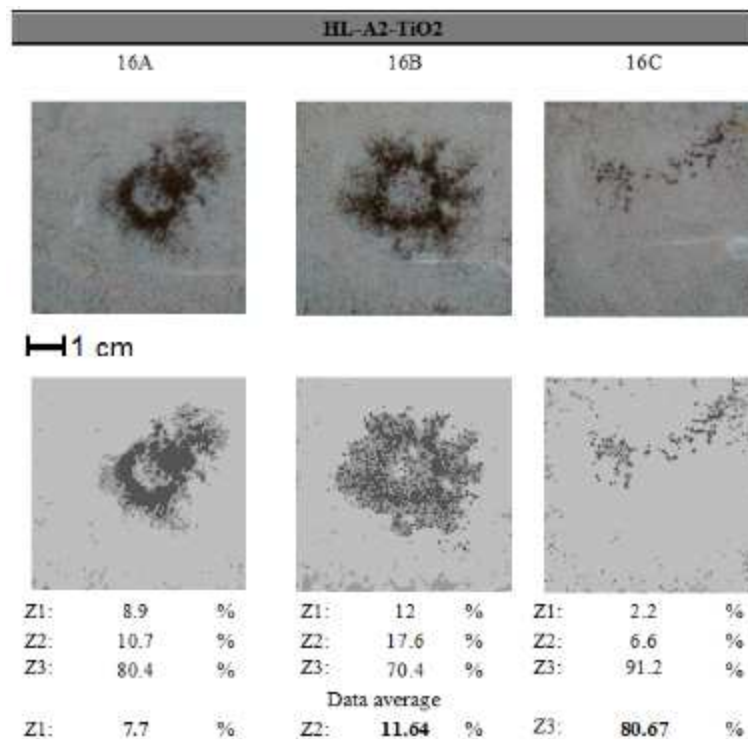
Figure 132 Pictures at 28 days: HL-A2 TiO2 photos (three specimens) and elaboration of images
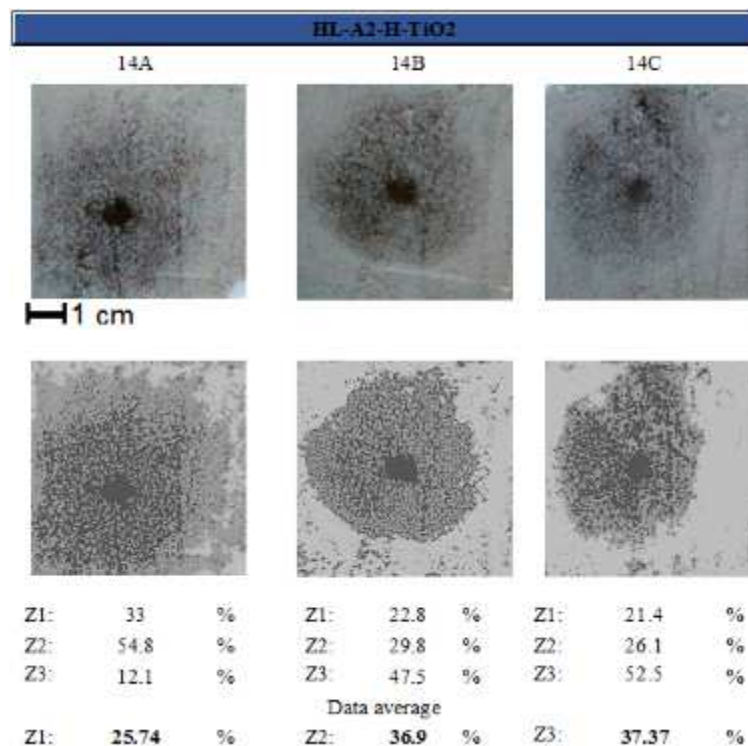
Figure 133 Pictures at 28 days: HL-A2 TiO2 h photos (three specimens) and elaboration of images
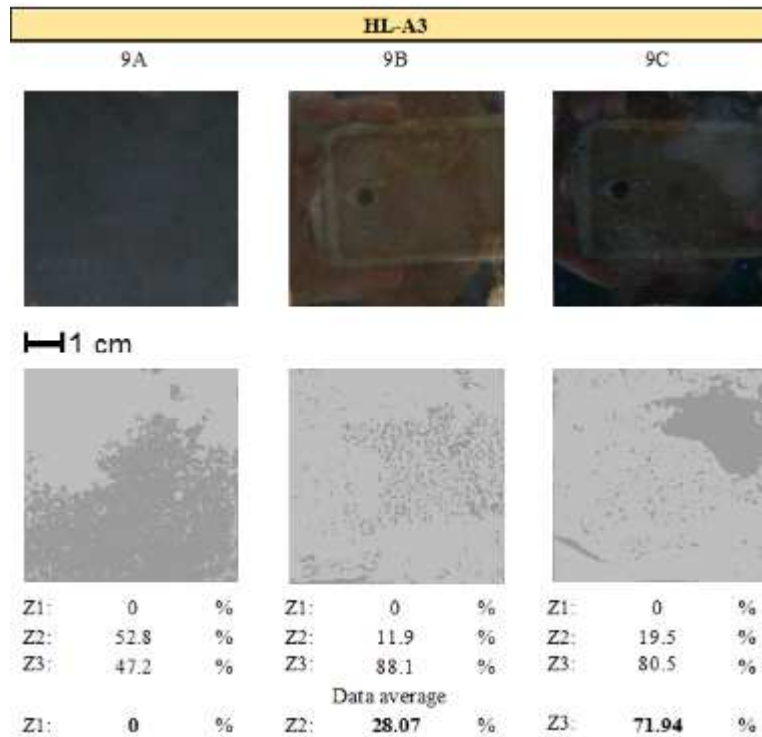
Figure 134 Pictures at 28 days: HL-A3 photos (three specimens) and elaboration of images
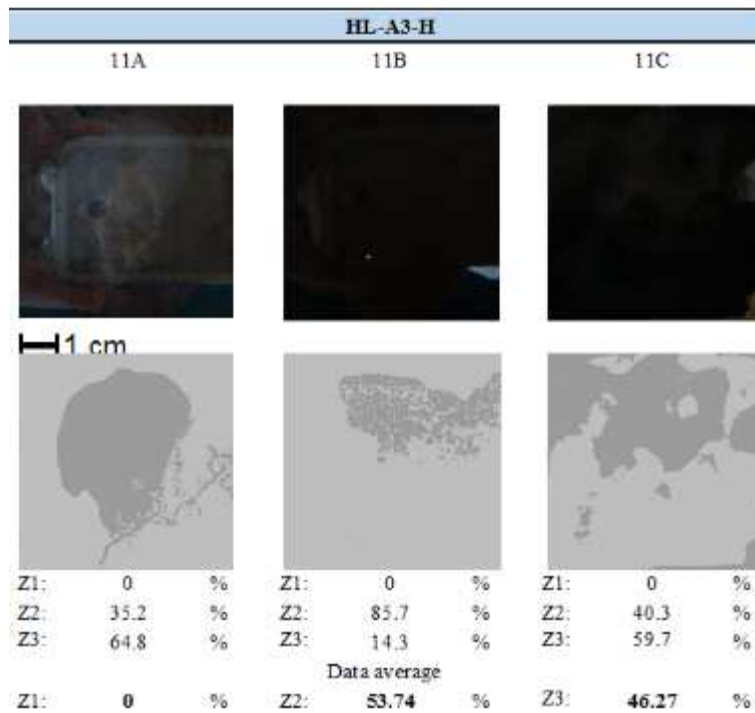
Figure 135 Pictures at 28 days: HL-A3 h photos (three specimens) and elaboration of images
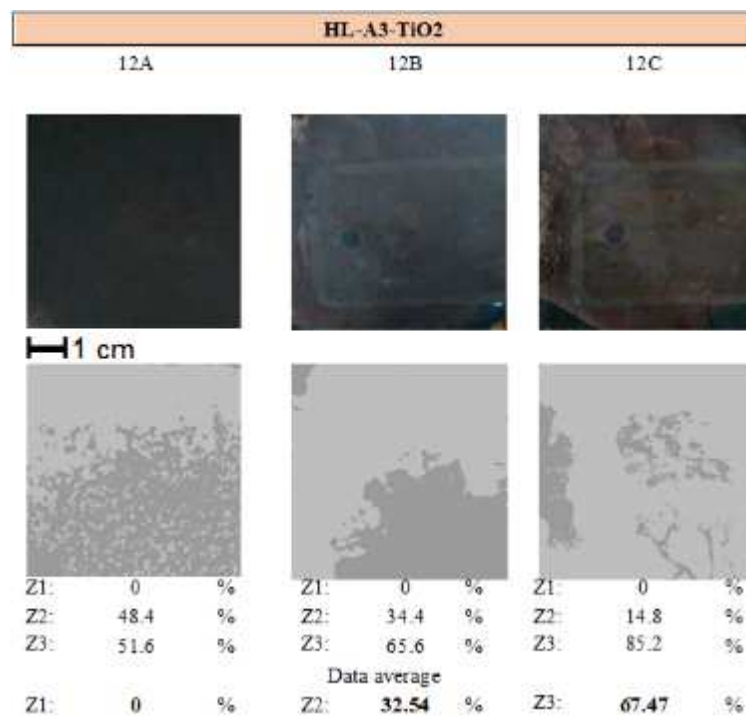
Figure 136 Pictures at 28 days: HL-A3 TiO2 photos (three specimens) and elaboration of images
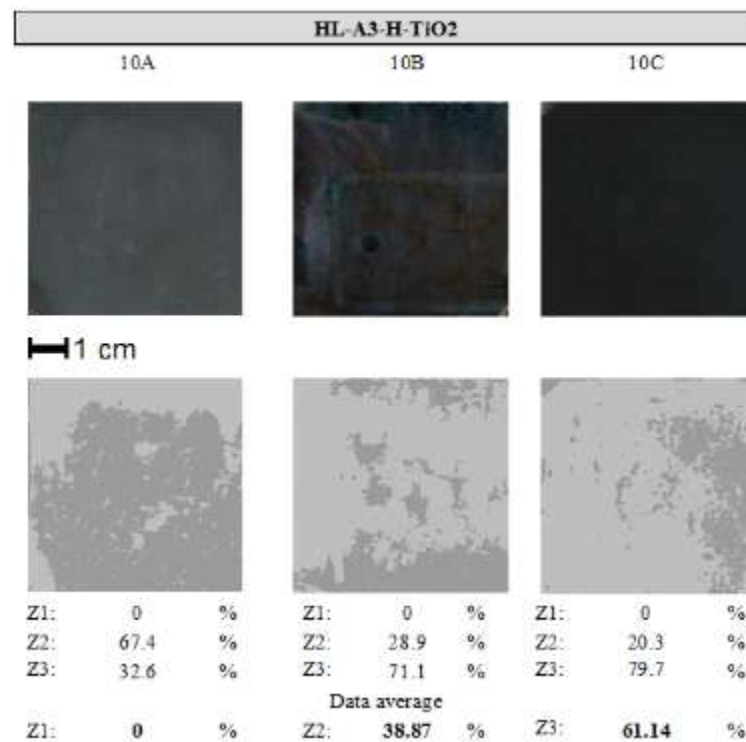
Figure 137 Pictures at 81 days: HL-A3 TiO2 h photos (three specimens) and elaboration of images
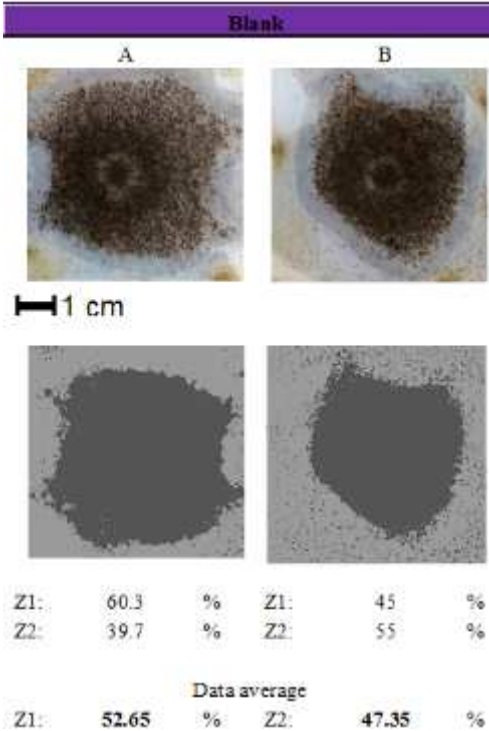
Figure 138 Pictures at 28 days: blank (two replicas) and elaboration of images

Figure 139 shows the stereomicroscope images carried out in order to validate the results obtained by visual observation at 28 days of molds growth.
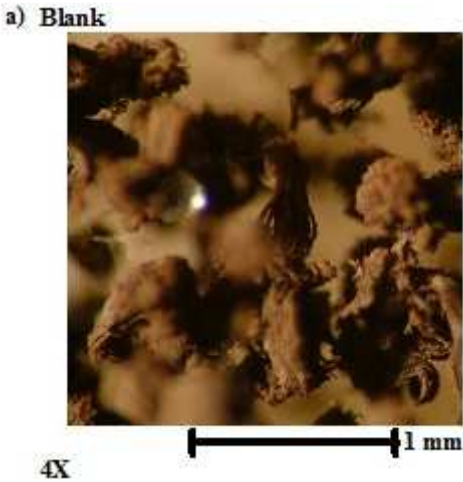
b) HL-S

1X
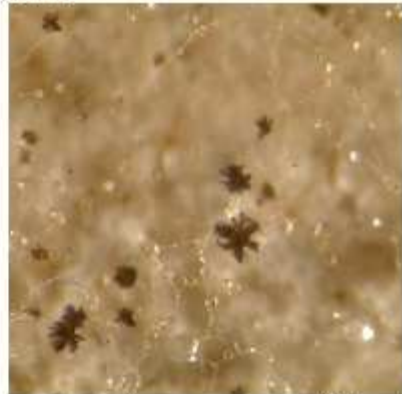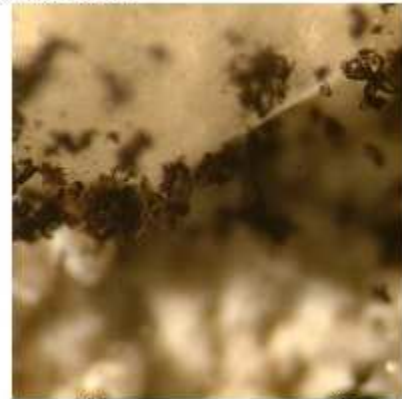
c) HL-S h

4X

d) HL-S TiO2 h

5X

e) HL-S TiO2 h

5X

f) HL- Al

4X
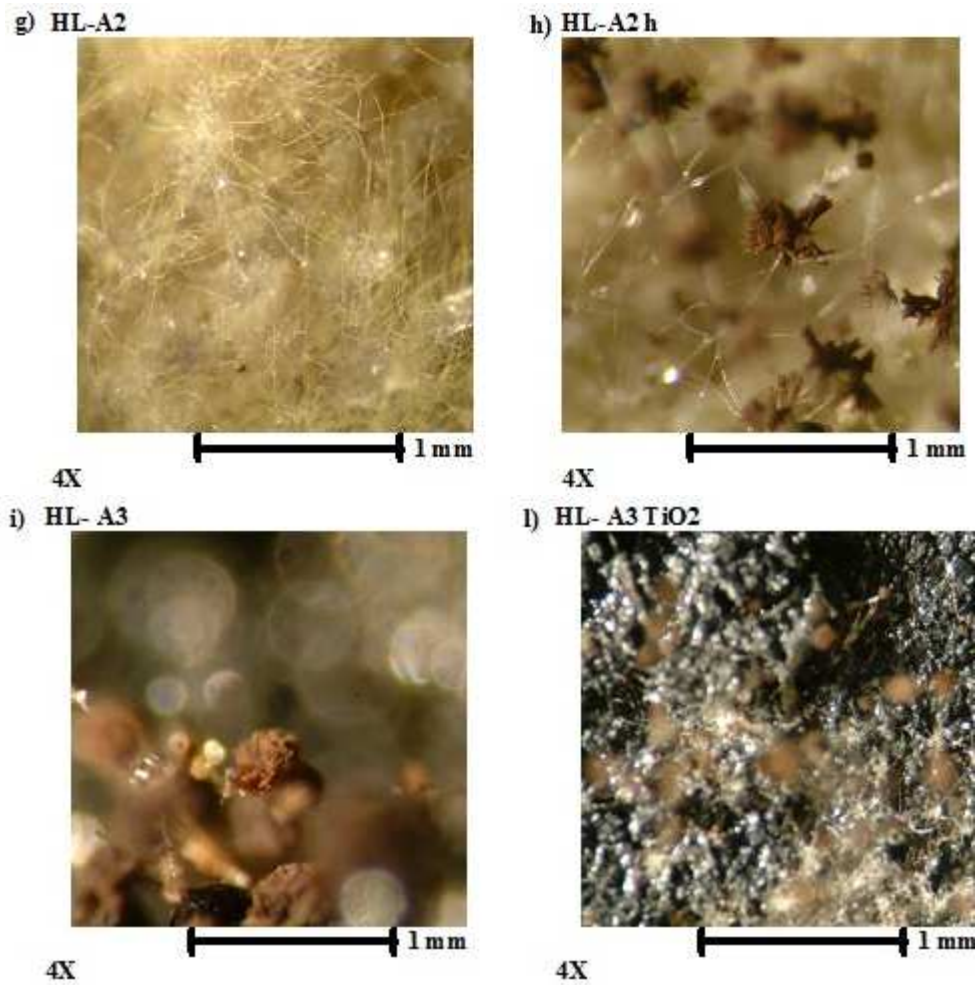
Figure 139 Stereomicroscope images of different mortars. The analyzed specimens are indicated on the pictures.

After 7 days from the inoculum, sand based mortars show a colonization only on the external part, due to the presence of cracks and conidia can grow in. Molds are not growing on mortars but on agar.

On the contrary, zeolite (A1) specimens are positive to molds growth. The colonization is well evident on all specimens a part from HL-A1 specimens.

Silica gel (A2) specimens with TiO_2 and hydrophobic admixture have low colonization.

Active carbon (A3) mortars show a visually observable colonization on the surface.

On sand based mortar, after 14 days from inoculum, molds are growing only on the cracks.

On zeolite and activated carbon based specimens the growth of hyphae and conidia is evident. Molds on zeolite based mortars are growing homogeneously on the surface; on active carbon mortars, molds come from the cracks and spread on all the surface of the specimens.

Silica gel specimens show a limited mold growth only where the inoculum is done.

126

Table 14 Average results from the elaboration photos. Z3 is the considered not colonized area

Mix	Day 21			Day 28		
HL-S	Z1:	1.94	%	Z1:	2.20	%
	Z2:	5.97	%	Z2:	4.54	%
	Z3:	92.14	%	Z3:	93.24	%
HL-S h	Z1:	2.50	%	Z1:	2.00	%
	Z2:	4.64	%	Z2:	6.37	%
	Z3:	92.84	%	Z3:	91.60	%
HL-S TiO2	Z1:	1.70	%	Z1:	0.90	%
	Z2:	10.94	%	Z2:	7.80	%
	Z3:	87.34	%	Z3:	91.30	%
HL-S TiO2 h	Z1:	1.80	%	Z1:	0.97	%
	Z2:	3.84	%	Z2:	8.80	%
	Z3:	94.37	%	Z3:	90.27	%
HL-A1	Z1:	6.97	%	Z1:	13.47	%
	Z2:	8.40	%	Z2:	12.77	%
	Z3:	84.64	%	Z3:	73.80	%
HL-A1 h	Z1:	12.94	%	Z1:	33.84	%
	Z2:	18.07	%	Z2:	25.90	%
	Z3:	68.97	%	Z3:	40.27	%
HL-A1 TiO2	Z1:	27.27	%	Z1:	39.57	%
	Z2:	33.24	%	Z2:	29.94	%
	Z3:	39.50	%	Z3:	30.54	%
HL-A1 TiO2 h	Z1:	9.37	%	Z1:	26.14	%
	Z2:	21.60	%	Z2:	23.27	%
	Z3:	69.10	%	Z3:	50.67	%
HL-A2	Z1:	1.40	%	Z1:	9.17	%
	Z2:	9.20	%	Z2:	24.97	%
	Z3:	89.37	%	Z3:	65.87	%
HL-A2 h	Z1:	0.64	%	Z1:	3.74	%
	Z2:	4.84	%	Z2:	11.87	%
	Z3:	94.54	%	Z3:	84.40	%
HL-A2 TiO2	Z1:	3.54	%	Z1:	7.70	%
	Z2:	5.10	%	Z2:	11.64	%
	Z3:	91.37	%	Z3:	80.67	%
HL-A2 TiO2 h	Z1:	1.14	%	Z1:	25.74	%
	Z2:	5.84	%	Z2:	36.90	%
	Z3:	93.04	%	Z3:	37.37	%
HL-A3	Z1:	62.34	%	Z1:	71.94	%
	Z2:	37.67	%	Z2:	28.07	%
	Z3:	NC	%	Z3:	NC	%
HL-A3 h	Z1:	81.30	%	Z1:	46.27	%
	Z2:	18.70	%	Z2:	53.74	%
	Z3:	NC	%	Z3:	NC	%
HL-A3 TiO2	Z1:	54.67	%	Z1:	67.47	%
	Z2:	45.34	%	Z2:	32.54	%
	Z3:	NC	%	Z3:	NC	%
HL-A3 TiO2 h	Z1:	68.44	%	Z1:	61.14	%
	Z2:	31.57	%	Z2:	38.87	%
	Z3:	NC	%	Z3:	NC	%
Blank	Z1:	51.95	%	Z1:	52.65	%
	Z2:	48.05	%	Z2:	47.35	%

: Not classifiable

Table 14 shows the average results from the elaboration of the pictures.

21 days after the inoculum, sand based mortars show a colonization only in correspondence of the cracks. This is confirmed also from the stereomicroscope images. Sand based mortars have the ability to inhibit the molds growth, which are growing only on the agar.

After 28 days from the inoculum in sand based mortars the percentage of not colonized area is lower than 10%. The presence of hydrophobic admixture and titanium dioxide (alone or together) are not influencing the molds growth. The higher presence of molds on hydrophobic mortars is depending on the concentrated drops of water. From stereomicroscope observations, it is possible to confirm that the growth is only on the drop of water and not on mortars. TiO_2 is not influencing the properties of mortars because it has not been activated before. It is well know that if TiO_2 is activated it has also antibacterial properties [24], [94].

Silica gel (A2) based mortars show a colonization only where the molds are inoculated. Molds have colonized only 10% of the specimen's surface. This percentage increases till 50% after 28 days. With hydrophobic admixture, this percentage is 20%. However, since mainly hyphae are detected but only few quantities of conides, which are strictly related to vitality of molds, in this case molds are also growing with high difficulty.

Zeolite (A1) based mortars specimens are colonized for about 30-40% at 21 days and more than 50% after 28 days. The surface of these specimens is a favorable environment for molds growth and proliferation. This can be due to elements such as potassium that provides additional feedings to molds.

Active carbon (A3) based mortars have the highest percentage of colonized area, more than 50%. In this case, microorganisms such as bacteria preferentially adhere to solid supports made of carbon materials, indicating high biocompatibility. Bacteria may multiply on the surface and activate carbon [95].

The addition of the hydrophobic admixture does not inhibit the capacity of mortars to growth mold. This admixture permits the formation of drops of water that are good surfaces for the growth of molds. Sometime these drops are well distributed and enhance the growth of molds.

Generally, the un-activated photocatalytic agent has no effects: in fact, the percentage areas of not colonized mortars with and without titanium dioxide are comparable. The differences detected in zeolite and silica gel based mortars in the presence of TiO_2 after 28 days are probably due only to agar rise in mortar porosity.

4.4.8. Depollution efficiency

Gas Chromatography (described in § 2.3.5.2) is the technique used to investigate depolluting properties of mortars. This test is conducted in 2 different conditions: dark condition and under UVA radiation (10 W/m^2) on the surface of the specimens). Specimens are cylinders with 8 cm diameter and 0.8 cm high.

The interest in this experimentation is not only to evaluate the adsorption and photocatalytic properties but also to investigate what happens in a saturation condition.

The first step is the calibration curve. It is possible to know the concentration of the tracer (MEK) inside the box of 16.65 l by the evaluation of areas of peaks due to a known MEK injection. Calibration is performed till 100 µl of MEK (Table 15).

Table 15 Concentration of MEK, values for calibration curve elaboration

Volume of MEK	Weight of MEK	Concentration of MEK
µl	g	mg/m³
10	0.008	480
25	0.020	1201
50	0.040	2402
100	0.080	4804

Two different curves are elaborated for both tests: under dark condition (NO UV) and under UVA radiation (UV). Figure 140 shows the measured data and the equations found.

Before testing, specimens are placed inside the box and then the box is sealed. For each specimen, the residual concentration of MEK inside the box is monitored in time.

a) plot of Concentration [mg/m³] versus Area [-] with equation $y = 0.0303x + 29.064$ and $R^2 = 0.9953$

b)
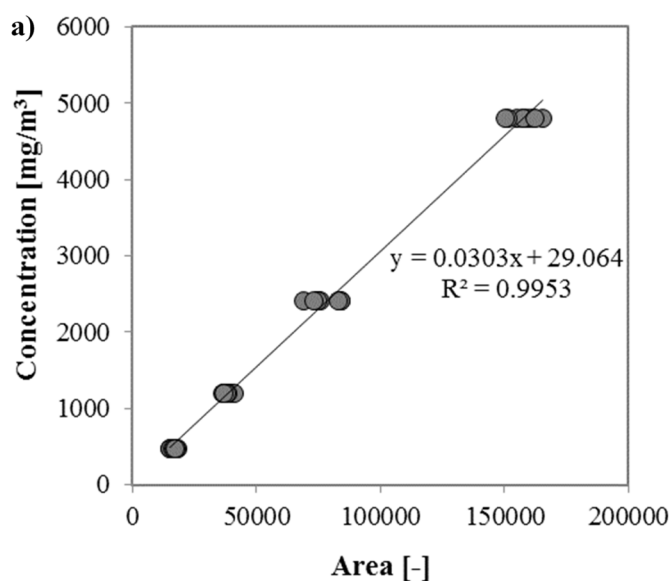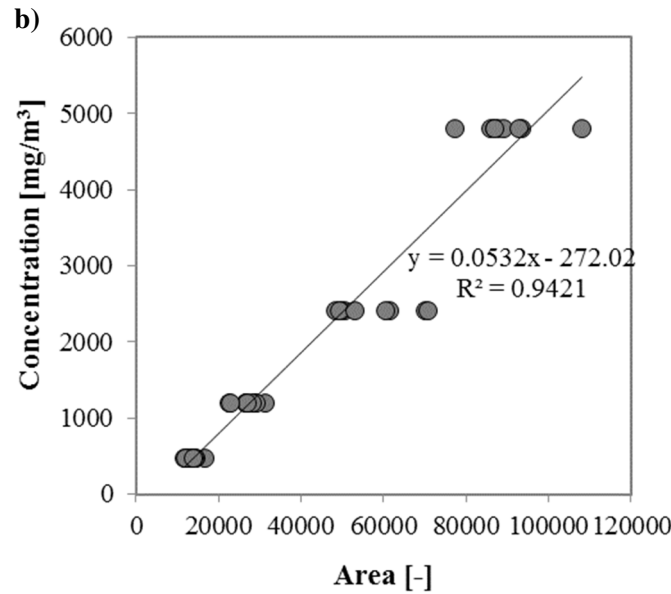
Figure 140 Calibration curves a) dark condition and b) UV radiation condition

The following figures (from Figure 141 to Figure 146) summarize the obtained results. The percentage is evaluated as C_i/C_0 where C_i is the concentration detected inside the box and C_0 is the theoretical initial concentration equal to 2402 mg/m^3 (the load of MEK is 50 µl) in this case.

To study the behavior of specimens under saturation conditions, MEK is injected more than one time. Re-load of MEK is done after 120 mins of test.

Only mortar containing TiO$_2$ are tested:

- injection of 50 µl of MEK and monitoring for 120 mins;
- injection of a re-load of 50 µl MEK after 120 min and successive monitoring.

Tests are repeated in dark condition and under UV radiation. The initial concentrations (C_0) of the successive loads are considered equal to the sum of the MEK residual concentration of the previous cycle and the new concentration inserted in the box.

The kinetics of the depolluting process (adsorption + photocatalysis) is monitored. In particular, the change in velocity in function of the gradual saturation of the active sites is monitored. So, in addition to defining the relationship between the residual concentration and the initial one inserted into the test cell, the logarithm of this ratio is calculated. The slope of the line is the value of the kinetic coefficient k.

$$-ln\left(\frac{C}{C_0}\right) = k_{app}t$$

Where:

C_0 is the initial MEK concentration and C is the concentration at time t;

k_{app} is the apparent first order reaction rate (min^{-1}) [96].

This parameter provides an objective indication of how much pollutants each mortar is able to remove in the same time range.

From previous results, it is decided to test only the most interesting specimens with TiO$_2$, excluding A3 (active carbon) based mortars that have the same behavior of A2 (silica gel) based mortars.
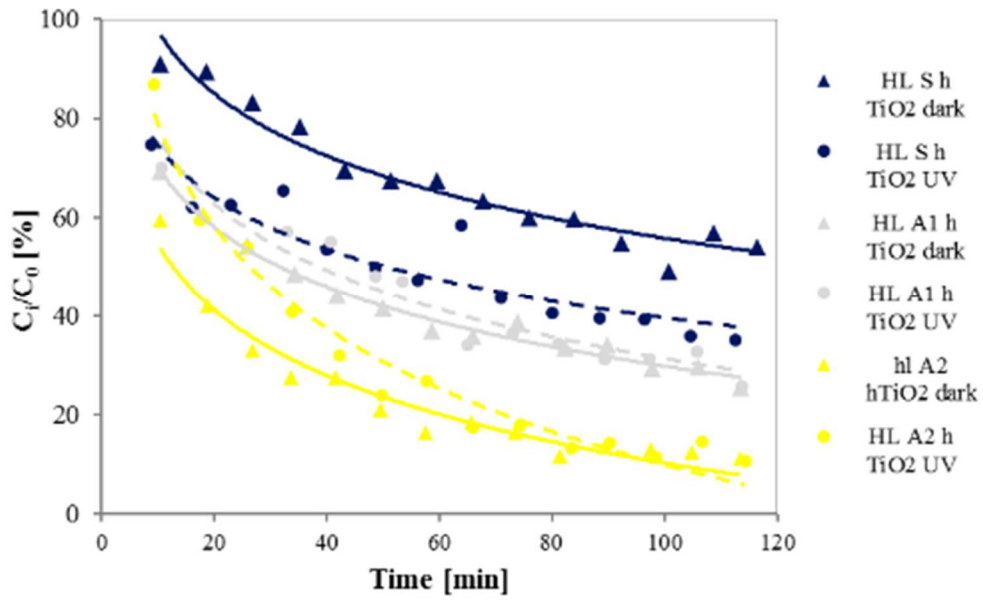
Figure 141 Depolluting activity of hydrophobic mortars for 120 mins
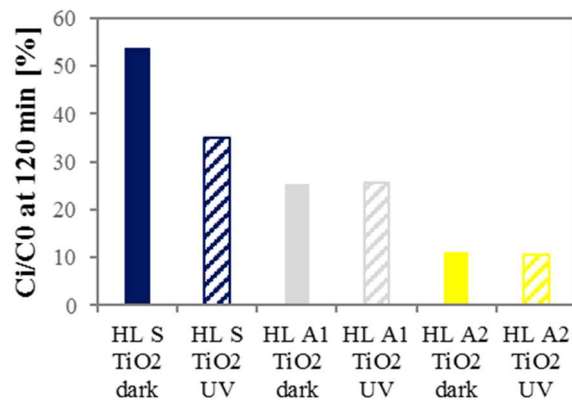
Figure 142 Depollution efficiency of hydrophobic mortars at 120 mins
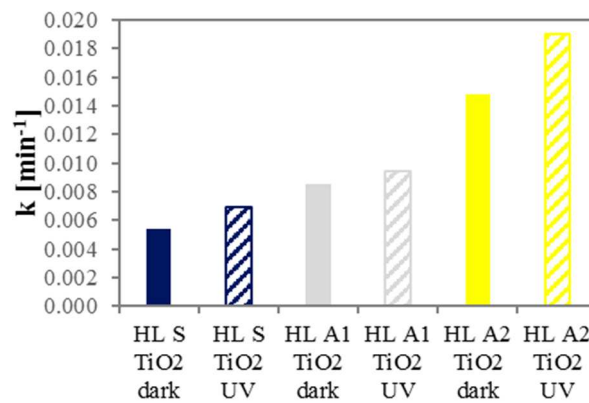
Figure 143 Kinetic coefficients of hydrophobic mortars at 120 mins
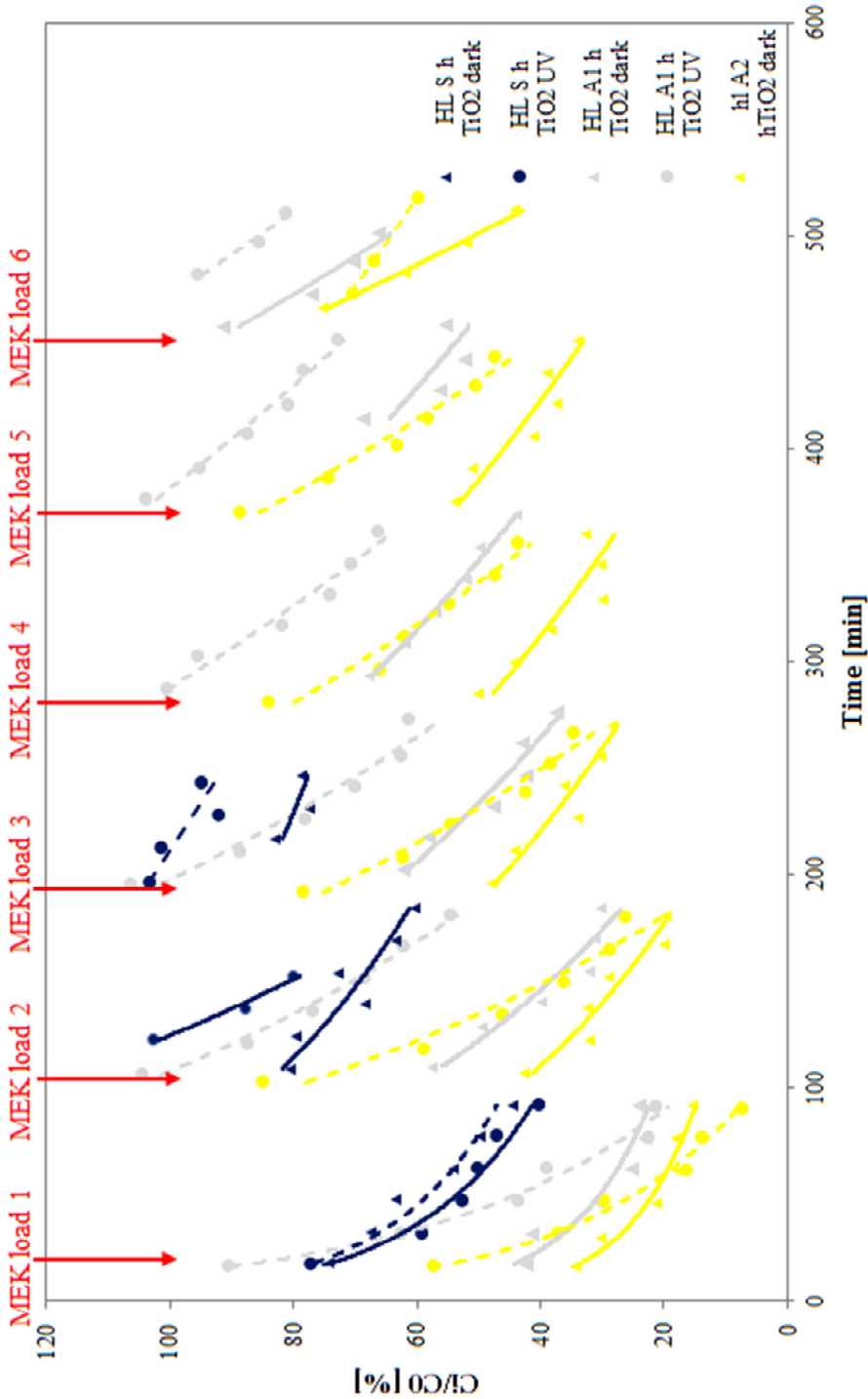
Figure 144 Depolluting activity of not hydrophobic mortars for 240 and 540 mins
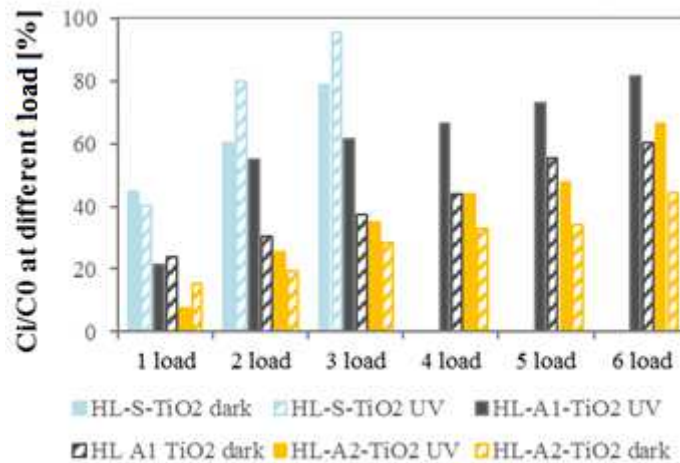
Figure 145 Depollution efficiency of not hydrophobic mortars at different MEK loads
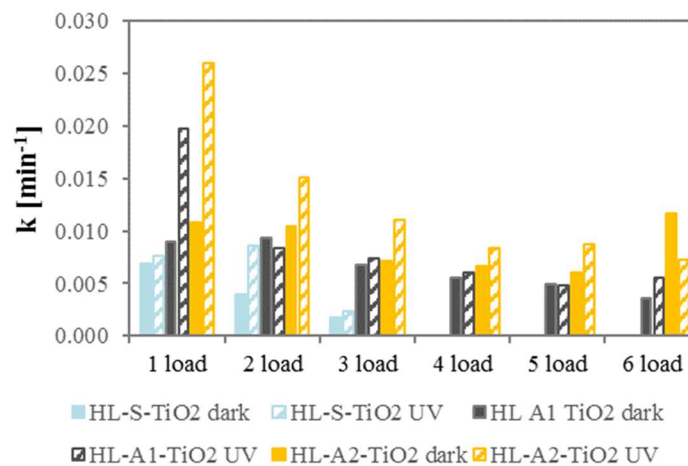
Figure 146 Kinetic coefficients of not hydrophobic mortars at different MEK loads

In dark condition, after the first MEK load, sand-based mortar removes 50%, zeolite mortar 65%, and silica gel mortar up to 80% of initial MEK at 120 min.
The depollution capacity decreases with the MEK loads.
Sand based mortars saturate after 3 MEK loads. After 6 MEK loads, the depollution efficiency of zeolite based mortars decrease from 65% to 20%, while in silica gel mortars decreases from 80 to 40% at 90 min. This behavior is justified by the progressive saturation of active sites on the surface of specimens as a result of further additions of MEK. The hydrophobic admixture does not affect the depolluting activity.

The system is generally not able to appreciate the single contribution of each process implied in the depolluting activity: adsorption and PCO.

Under UVA radiation, after the first MEK load, all sand based mortars remove 40% of MEK in 120 min of test. With the hydrophobic admixture, conventional mortar (HL S-h TiO2) removes 15% more MEK than the same mortars in dark condition. When

zeolite and silica gel are used at the first MEK load there is no increase in the depollution efficiency compared to dark condition, regardless of the hydrophobic admixture, probably because there are more active sites still available.

After the second MEK load, under UVA radiation, sand based mortars do not increase the removal efficiency. On the other hand, for zeolite and silica gel mortars it increases of about 10% and 20% respectively.

PCO increases, becoming the prevalent process, only when the specimen, due to the quantity of pollutant already adsorbed, is close to saturation. PCO is a process that occurs on the surface, therefore it cannot occur as long as pollutants are adsorbed by mortar pores. PCO results are hidden when at low MEK concentration the adsorption process is more influential. Only when the specimen is saturated, the pollutants stop at the surface and become available for PCO process.

In dark conditions, the kinetic coefficient k increases with the depollution efficiency.

Under UVA radiation, after the first MEK load, in sand based mortars k is 27% higher, in zeolite mortar is 100% higher, in silica gel mortar is 140% higher than the same value in dark condition. Silica gel mortars have in general the highest k, up to 3 times the value of sand mortars. Zeolite mortars have a double k value compared to the reference one. These differences decrease with the MEK loads.

4.5.   Conclusions

In conclusions, the results of this experimentation can be summarized as:
- Mortars have the same workability, that is stiff.
- Mortars with sand and active carbon have the highest compressive strength, 35% higher than sand based mortars. Mortars with silica gel have the lowest mechanical compressive strength, 90% lower than reference mortars. Zeolite based mortars have 5% higher mechanical resistance than sand based mortars. The values of mechanical properties could be considerate still acceptable.
- Mortars with silica gel and active carbon are classified as lightweight mortars.
- Mortars with sand have the lowest pore volume, followed by activated carbon mortars (with highest pores diameters) and zeolite (with smallest pores diameters).
- Mortars with hydraulic lime have 4 times higher water absorption coefficient than cementitious mortars. In case of unconventional aggregates based mortars, hydrophobic admixture reduces the water absorption capacity from 20% to 80%.
- Mortars with silica gel and active carbon have the highest permeability to water vapor, more than double of the value of sand based mortars.
- Mortars with zeolite have the highest moisture buffering value, 3 times higher than the value of conventional based mortars. Silica gel and active carbon

based mortars adsorb and desorb 1.5-2 times more water vapor then sand based mortars.

- Mortars with conventional sand show optimum inhibitory capacity against fungal growth. Silica gel mortars show a colonization 4 times higher than sand based mortar. Zeolite and active carbon gives to mortar an optimum substrate where mold can growth.
- Mortars with unconventional aggregates as silica gel remove more than 80% of MEK after 2 hours of test. After 90 mins, zeolite (A1) based mortars remove 65% of initial MEK concentration. The use of TiO_2 enhance depollution properties in terms of PCO improvement when, due to the quantity of pollutant already adsorbed, the specimen is close to saturation.

At this point, the main goals for the development of the optimal mortar should be the enhancement of mechanical properties of material, the use a more efficient photocatalytic agent, and the further increase of the sustainability of materials by using industrial by-products.

Chapter 5

5. Biomass waste materials as unconventional aggregates in multifunctional mortars for indoor application

5.1. Introduction

In this chapter, biomass waste materials are used to prepare unconventional mortars able to improve IAQ [38].

Reactive building materials offer an opportunity to provide indoor air cleaning with minimal energy use [13]. Hoang et al. [4] successfully used green building materials with depollution property toward ozone. The use of biomass materials can reduce the carbon impact of constructions, effectively improve the removal of Volatile Organic Compounds (VOCs) by adsorption and increase the sustainability of mortars [97].

The characterization of new mortars with biomass materials as unconventional aggregates becomes of great interest. In this study biomass wastes, are also considered in order to avoid the waste of resources and raw materials supply [98]. Hydraulic lime is used as binder [89].

In this chapter, the effect of using spruce sawdust shavings and biomass ashes as unconventional aggregates in hydraulic lime-based mortar for indoor application has been investigated and compared with calcareous sand in terms of developed mechanical strength, permeability, capillary water absorption, moisture buffering ability and VOCs adsorption. LCA is also performed (thanks to the collaboration with Department of Life and Environmental Sciences, Università Politecnica delle Marche, under the supervision of prof. Francesca Beolchini) in order to quantify the environmental implication related to the use of unconventional mortars.

Biomass waste materials (spruce sawdust, as it is and roasted, and biomass ashes) are provided by Department of Agricoltural, Food and Environmental Sciences, Università Politecnica delle Marche, by prof. Giuseppe Toscano.

5.2. Materials

The binder is hydraulic lime Plastocem, provided by Italcementi (L). This product is described in § 2.2.2.2.

Biomass wastes replace by volume calcareous conventional sand (SAN) used as reference. In particular, spruce sawdust shavings as it is (SPR N) and roasted spruce sawdust shavings (SPR R), obtained by torrefaction process (§ 2.2.4.6) are used. Furthermore, biomass bottom ash (BOT) and biomass fly ash (FLY) type A, described in § 2.2.4.5, are used always as aggregate replacement.

5.2.1. Mix design

Conventional mortars are manufactured with hydraulic lime and commercial sand; w/b ratio is volumetrically the same of previous mixtures (chapters 3 and 4).
From the traditional mortars, 100% sand volume is replaced by different unconventional aggregates. Table 15 reports the combinations, the codes and the colors used to recognize the different mortars.

Table 16 Mortars prepared. Summary of different combinations

Binder	Aggregate	Code ID	Code Color
Hydraulic lime	Calcareous sand	L SAN	
Hydraulic lime	Spruce sawdust shavings as it is	L SPR N	
Hydraulic lime	Roasted spruce sawdust shavings	L SPR R	
Hydraulic lime	Biomass fly ash type A	L BOT	
Hydraulic lime	Biomass bottom ash type A	L FLY	

The appropriate volume required for casting is evaluated according to the different tests that are performed. Aggregates are added in ssd conditions. Mix design proportions are shown in Table 17.

Table 17 Mix proportions (kg/m³) of mortars

Mix	Water	Hydr-aulic Lime	Sand SAN	SPR N	SPR R	BOT	FLY
L SAN	256	437	1536	-	-	-	-
L SPR N	256	437	-	579	-	-	-
L SPR R	256	437	-	-	370	-	-
L BOT	256	437	-	-	-	1135	-
L FLY	256	437	-	-	-	-	817

Mortars are casted in different moulds in order to obtain the suitable specimens for the determination of each property. During the cast mortars are vibrated manually to eliminate the excess of air. Vibration is carried out manually in order to avoid the segregation of light aggregates from lime paste.

5.3. Methods

Mortars are characterized in terms of fresh state properties. Workability is measured with a flow table, according to the current standards (§ 2.3.1).
After 28 days of curing, flexural and compressive strength are tested. Also, the specific strength is evaluated (§ 2.3.2.1).
After 28 days of curing, morphologies are investigated by Scanning Electron Microscope (SEM) and pore size distribution is evaluated by Mercury Intrusion Porosimetry (MIP), as described in § 2.3.2.2.
Free shrinkage and weight loss due to the water evaporation of mortars are monitored for about 50 days (§ 2.3.2.3).
Water is the medium where ions can be transported and can compromise the durability of building material. Water transport in mortars is evaluated with two different methodologies (§ 2.3.3.1 and 2.3.3.1.).
Transpirability of mortars for renders is a fundamental property, evaluated according to § 2.3.4.1.
The moisture buffering capacity of mortars is evaluated over dynamic variation of RH with a simplified procedure of the NORDTEST method (§ 2.3.4.2).
De-pollution properties of different mortars are evaluated by MEK adsorption (§ 2.3.5.2). LCA also is performed (§ 2.3.7).

5.4. Results and discussions

5.4.1. Workability

Table 18 shows workability of mortars in terms of slump flow and consistency values.

Table 18 Workability of different mortars: picture of mortar at fresh state after slump flow test, slump flow values and consistency.

Mix	L SAN
Slump (mm)	118
Consistency (%)	18

Mix	**L SPR N**	**L SPR R**
Slump (mm)	115	120
Consistency (%)	15	20
Mix	**L BOT**	**L FLY**
Slump (mm)	122	120
Consistency (%)	22	20

All mortars have the same consistency. The slump value is lower than 140 mm for all the mixes and, according to UNI EN 1015-6 [57], mortars are defined stiff.

5.4.2. Mechanical strength

Figure 147 shows the results in terms of maximum flexural strength.
Bottom ash based mortar has the best performance in terms of flexural strength that is at least twice of any other mortars.
Roasted spruce sawdust shavings mortar has slight higher flexural strength (10%) than sand-based mortar.
Others mortars register a decrease in flexural strength of about 50% for biomass fly ash mortar and 60% for spruce sawdust shavings as it is compared to traditional mortar.
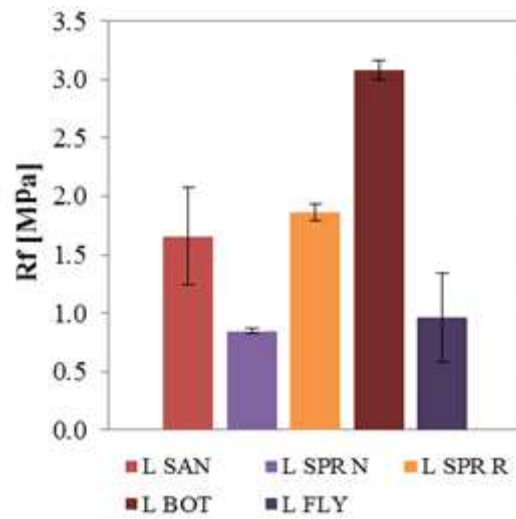
Figure 147 Flexural strength of biomass wastes and hydraulic lime-based mortars

Compressive strength is evaluated at 28 days and results are reported in Figure 148. In this case, bottom ash based mortar has also more than 50% higher compressive strength than reference L SAN mortar.

On the other hand, L SPR R, L FLY, L SPR N mortars reach the 80%, 50% and 20%, respectively, of the mechanical strength of reference L SAN mortar.

The enhancement of compressive strength is due to the pozzolanic reaction of ashes: despite the fact that bottom ash is a more porous material than calcareous sand (confirmed by the water absorption of bottom ash), the pozzolanicity of the ashes implies higher value of mechanical resistance [99].

During the torrefaction process the amount of organic compounds in biomass waste decreases [55] leading to an increase in compressive strength of the resulting mortar.
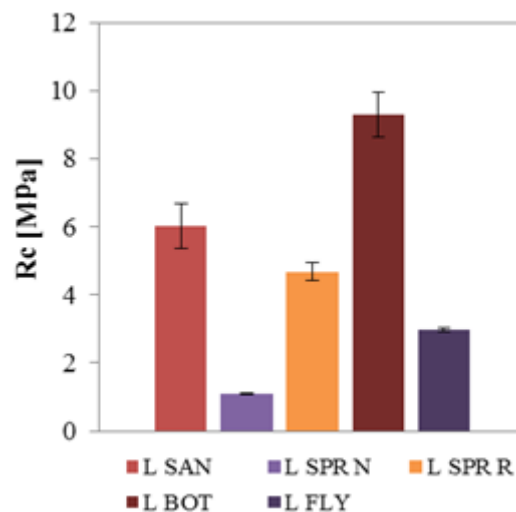
Figure 148 Compressive strength of biomass wastes and hydraulic lime-based mortars

According to the current standard UNI EN 998-1:2010 [80], the maximum value of density for indoor mortar to be classified as lightweight is 1300 kg/m^3. Figure 149 shows the results of density values for the different mortars.

Thanks to the total replacement of calcareous sand with biomass wastes, it is possible to obtain lightweight finishes, apart from biomass bottom ash based mortars that have a density higher than 1300 kg/m^3. As previously mentioned, this property is highly appreciated for non-structural material [81]. The use of ashes has already been demonstrated to enhance these properties in previous study [100]. In literature is shown that if the weight of the structures is decreased by using lightweight aggregate in concrete and mortars, both the structural stability and economic viability are assisted [101].

Mortars belong (according to [80]) to CS I (L SPR N), CS II (L FLY) CS III (L SPR R) and CS IV (L SAN and L BOT).
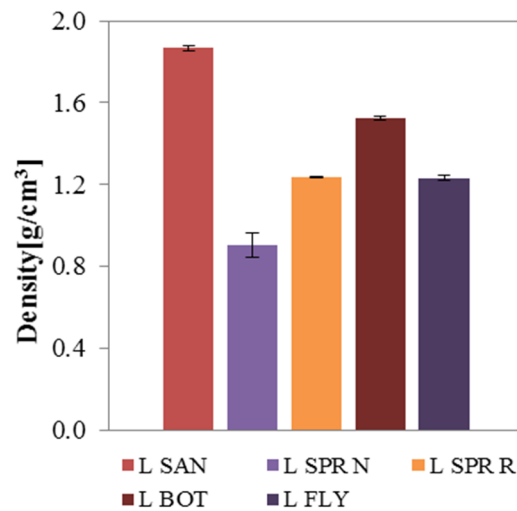
Figure 149 Hardened density (ρ) of biomass wastes and hydraulic lime-based mortars

Table 19 summarizes the average values of flexural, compressive strength, density and compression specific strength.

With regard to specific resistance Rcs, besides the low densities, biomass waste based mortars have comparable value of Rcs compared to calcareous sand based mortars. L BOT mortar has Rcs value 2 times higher than reference mortar. L SPR R mortar has the same value of calcareous sand mortars.

Table 19 Mechanical tests results: flexural strength (Rf), compressive strength (Rc) hardened density (ρ), and specific strength (Rsc) of. biomass wastes and hydraulic lime-based mortars

Mix	Rf [MPa]	Rc [MPa]	ρ [g/cm^3]	R$_{cs28}$ Pa/(kg/m^3)
L SAN	1.66	6.03	1.87	3.23
L SPR N	0.84	1.10	0.9	1.22
L SPR R	1.86	4.68	1.24	3.79
L BOT	3.08	9.29	1.52	6.09
L FLY	0.96	2.97	1.23	2.41

5.4.3. Microstructure of mortars: morphology and pore size distribution analysis

The mechanical results are explained with morphological observations obtained by SEM images.

The ITZ between calcareous sand and hydraulic lime is good, as previously demonstrated (Figure 75).

Even if natural spruce sawdust as unconventional aggregate significantly decreases the mechanical compressive strength of lime-based mortars, shows a good adhesion with lime paste. The elemental analysis is not performed because with the current equipment it is not possible to detect elemental carbon.

Roasted spruce sawdust shows a smoother surface than spruce sawdust as it is. This is due to the torrefaction process that induces a decrease in organic element.
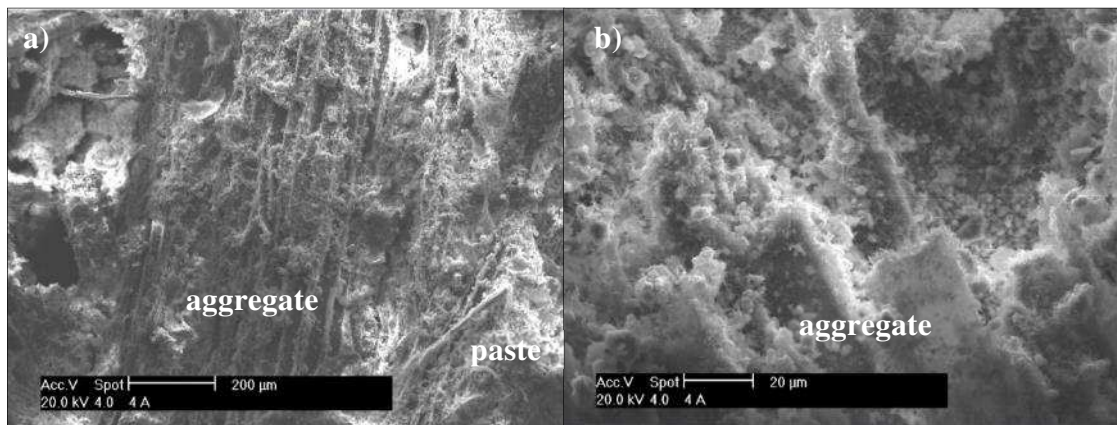
Figure 150 SEM images of L SPR N specimen
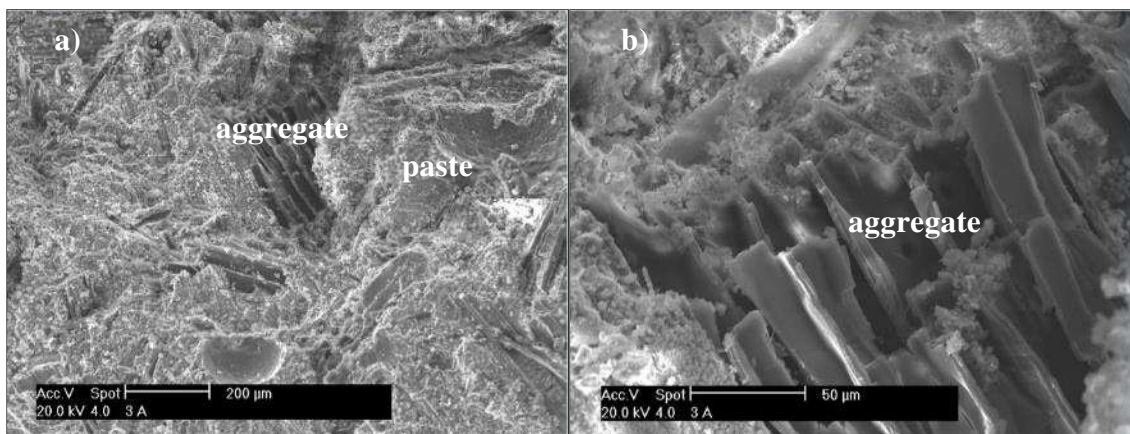
Figure 151 SEM images of L SPR R specimen

The ITZ between bottom ash and paste is optimum as shown in Figure 152, justifying the best mechanical behavior of this mortar in terms of compressive strength.

Additional hydration products are detected on the ITZ. These products are probably due to the pozzolanic reaction between ash and hydraulic lime [54]. This is also

possible because high amount of Si is detected with EDAX probe, as shown in Figure 153.
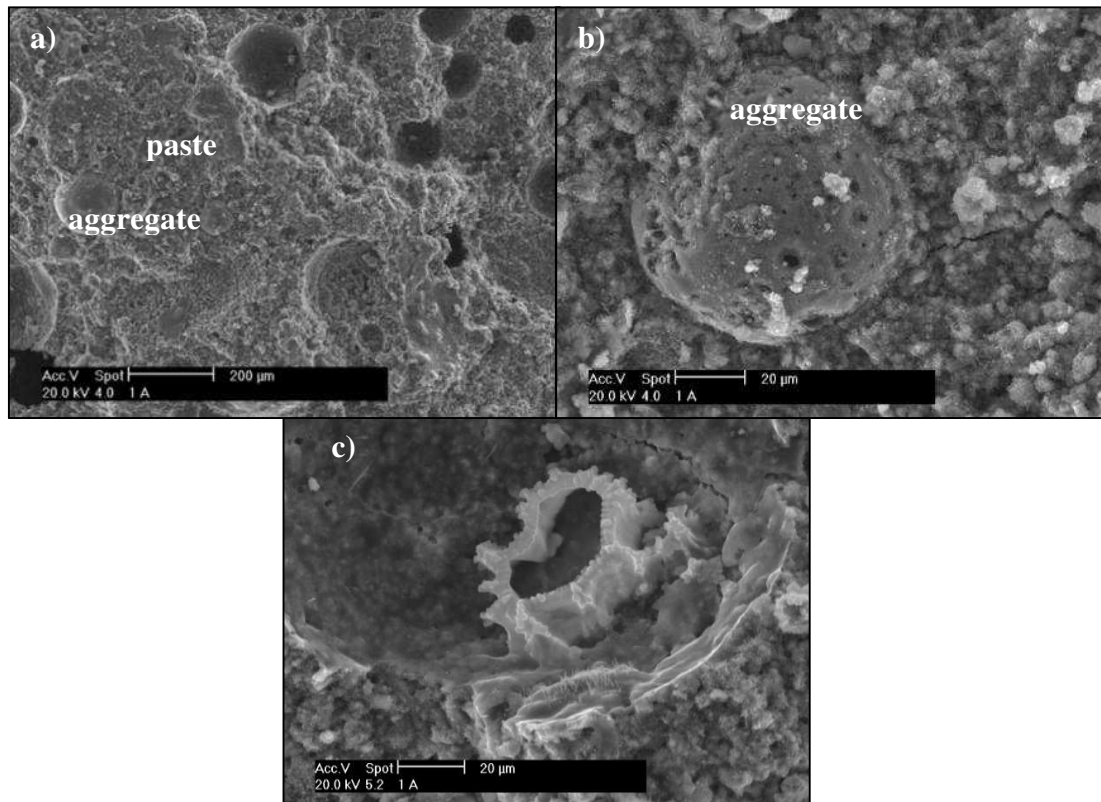
Figure 152 SEM images of L BOT specimen a) paste and aggregate, b) zoom on aggregate, c) additional hydration products
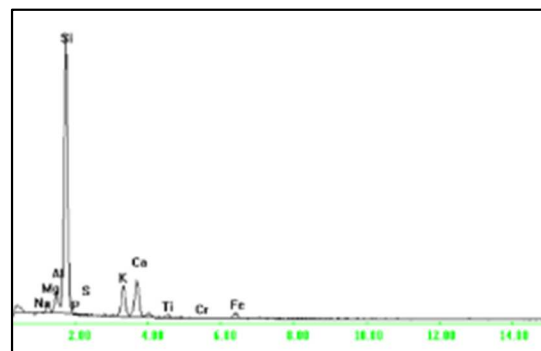
Figure 153 EDAX performed on L BOT (particles of aggregate)

Pore distribution curves are compared. All mortars have an unimodal distribution, except for bottom ash based mortar that have a bi-modal distribution (Figure 154) Hydraulic lime as binder introduces a porosity into the matrix with higher threshold pores diameter compared to cement, as already discussed (§ 3.4.3).

Hydraulic lime and calcareous sand mortar have a modal pore diameter of 1.199 µm and a threshold pore diameter of 2.545 µm.

Biomass waste materials as unconventional aggregates in multifunctional mortars for indoor application

Spruce sawdust shavings as it is based mortar has the highest pore diameter both for peak value (3.2708 µm) and threshold pore diameter, 8.89 µm.
Roast spruce sawdust shavings based mortar has the peak at 1.54 µm and threshold pore diameter is 1.51 µm.
Fly ash based mortar has peak at 0.9329 µm and the threshold pore diameter is 4.2036 µm.
Bottom ash based mortar has the same threshold pore diameter of fly ash based mortar. There are two pecks at 1.983 µm and 0.1254 µm.
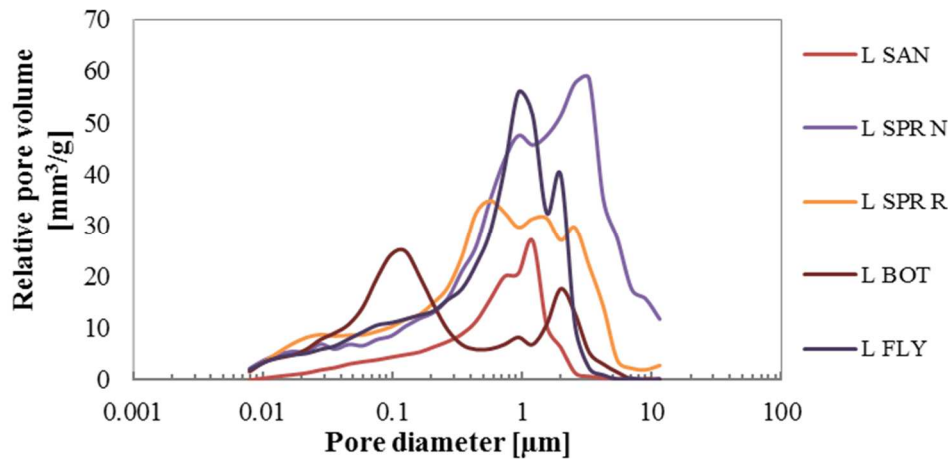
Figure 154 Relative pore volume distribution of different biomass wastes hydraulic lime based mortars

Total porosity can be evaluated both in the cumulative pore volume graph (Figure 155) and in the percentage volume of pores graph (Figure 156). Conventional aggregate (SAN) based mortars have the lowest percentage of void (about 30%).
Biomass waste materials introduce a higher quantity of porosity in the matrix compared to traditional mortars. Bottom ash mortars has 30% more pore volume than reference mortar, roast spruce sawdust shavings mortars about 55% more pore volume than reference mortar.
Fly ash and roasted spruce sawdust shavings based mortars have 60% and 65% more porosity, respectively, than reference mortars.
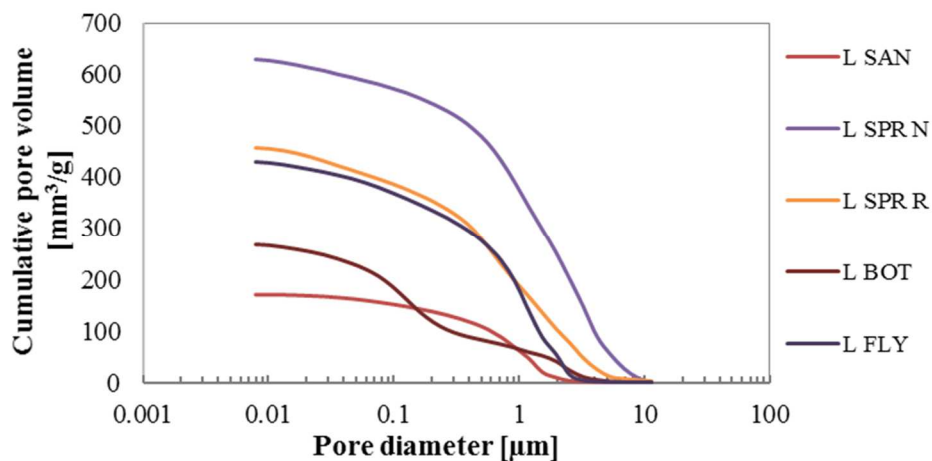
Figure 155 Cumulative pore volume distribution of different biomass wastes-based mortars:
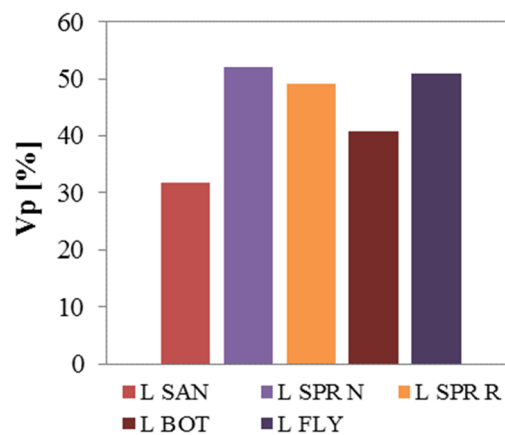
Figure 156 Total porosity of different biomass wastes mortars

5.4.4. Capillary water absorption

Before testing, mortars are dried completely in a ventilated oven at T = 80 °C.
Capillary water absorption coefficient of mortars is evaluated according to the Italian standard UNI EN 1015-18 [65]. Figure 157 shows the obtained data.
Spruce sawdust shavings as it is based mortar has the highest C value detected, 50% higher than reference mortar.
Fly ash based mortar has C value 25% higher than sand based mortar.
Roasted spruce sawdust shavings and bottom ash based mortars, despite having higher total percentage of porosity compared to reference mortar, show a 5% and a 50% lower value of capillary water absorption coefficient, respectively. Results can be due to the torrefaction process that makes the biomass increasingly hydrophobic [55].
In case of bottom biomass ash mortar, even if porosity is higher than reference one, the C value is the lowest. Coals are naturally hydrophobic [102] and a little amount of this coal is present in the biomass ash.
All mortars belong to W0 mortars, according to UNI EN 998-1:2010 [80].
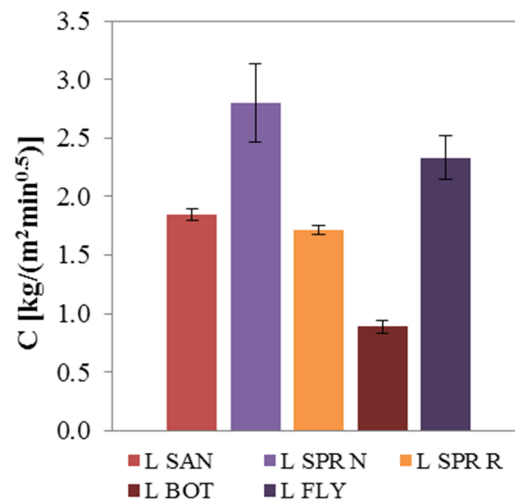
Figure 157 Capillary water absorption coefficient of different mortars according to UNI EN 1015-18.

Figure 158 shows the results from UNI EN 15801[66] test.

With this test methodology, fly-ash based mortar adsorbs the highest quantity of water. Spruce sawdust shavings as it is mortar adsorbs about 80% more water than reference mortar at 8 days, like roasted spruce sawdust shavings mortar. Hydrophobicity of roasted spruce sawdust shavings is evident during the first period of exposure to water, in fact this mortar absorbs slower than the spruce sawdust as it is. Another reason for the different lower absorption behavior of roast sawdust can be due to the smaller diameter of pores (peak of distribution for L SPR R is at 1.54 µm, for SPR N at 3.278 µm) [45].

In this case, bottom ash based mortar also absorbs the lower quantity of water, after 8 days it is the same quantity of calcareous sand based mortar, although the total volume of porosity of bottom ash based mortar is higher than that of sand based mortar. This can be due to the hydrophobicity of bottom ash.
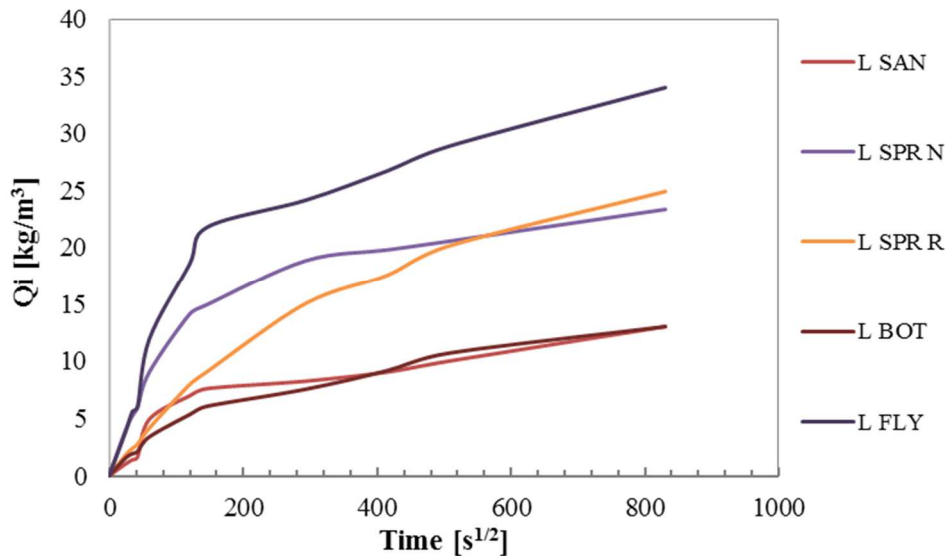
Figure 158 Capillary water absorption in time of hydraulic lime based mortars

5.4.5. Water vapor permeability

Water vapor permeability results, expressed in terms of µ factor, are shown in Figure 159. Lower value of µ factor indicates higher value of permeability.

Biomass bottom ash based mortar shows the highest value of water vapor resistance factor, about 20% higher than sand based mortars. All the other unconventional aggregated based mortar permits to have in mortar lower value of water vapor resistance factor than L SAN.

Fly ash based mortar has a µ value 35% less of sand mortars.

Roasted and as it is spruce sawdust shavings have µ values of 60% and 70% respectively less than sand based mortar.

For the analyzed mortars this value is very low, that means a very permeable material. The measured µ value for all unconventional based mortar, a part for L BOT, is less than the value measured in very permeable mortar, about 10 [85].

All mortars have a permeability to water vapor proportional to the porosity percentage (Figure 160), the more is the volume of pores, the less is the hygroscopic resistance factor.

Study [70] well explains the behavior of bottom ash based mortars: the lower the pore radius is, the lower is the transpirability [60].

The most permeable mortar corresponds to the mortar with the highest quantity of pores with highest pore diameter (L SPR N).
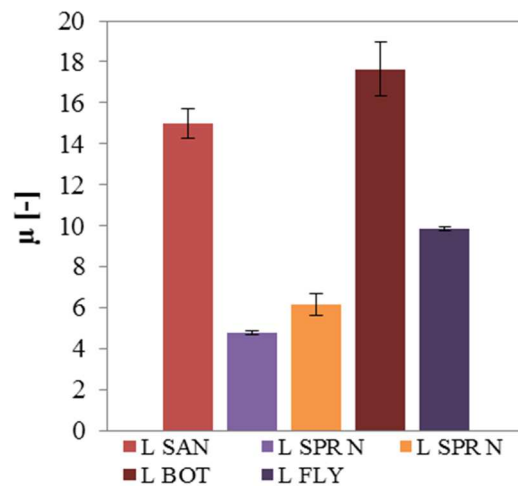
Figure 159 Water vapor resistance factor μ of biomass wastes mortars
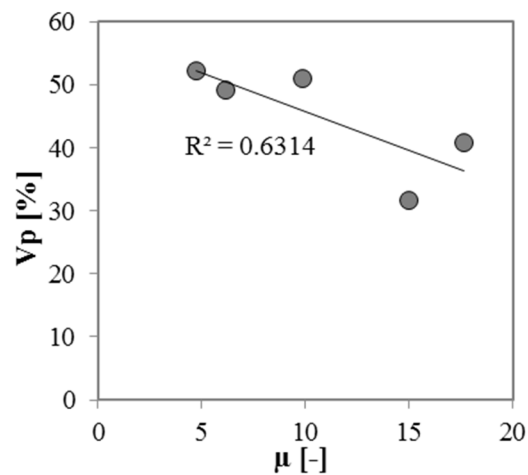
Figure 160 Correlation between porosity and water vapor resistance factor

5.4.6. Moisture Buffering Capacity

The interaction between mortars and the humidity of indoor environment is also studied through measuring the change in moisture content of specimens exposed at different RH. Figure 161 shows the change in water content (Δm) normalized on the surface of the specimens. MBV values are shown in Figure 162.

Sand based mortar has the smallest exchange of water vapor.

Bottom ash based mortar has 20% higher MBV exchange capacity than sand based mortar.

Fly ash based mortar has 60% higher MBV value than sand based mortar.

Spruce sawdust biomass based mortars have the highest capacity to exchange water vapor with the environment, more than three times than that of sand based mortar.

The average is made on the last three cycles.
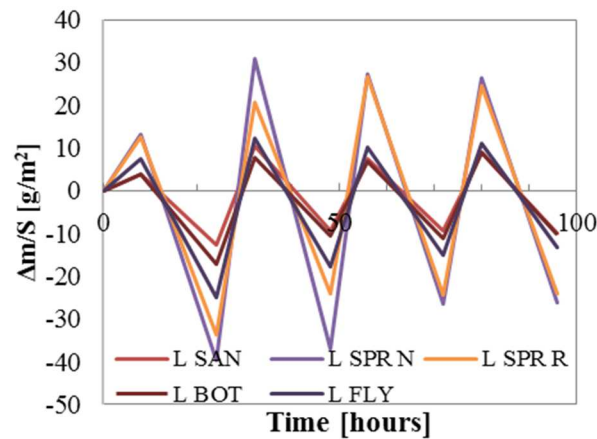
Figure 161 Changing of mass due to absorption/desorption phases, normalized on the specimens surface
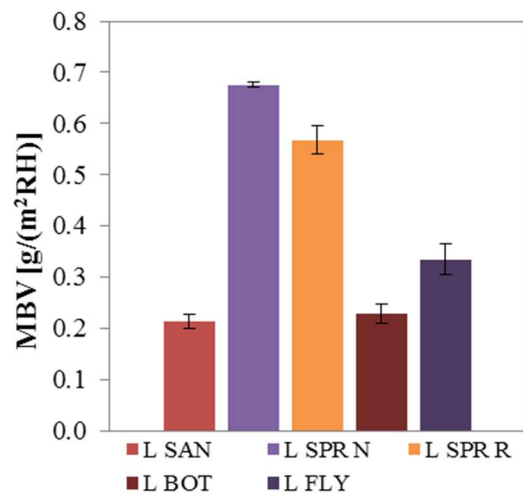
Figure 162 Moisture buffering value of hydraulic lime based mortars

Again, the differences in results are related to the pore size network of mortars. Figure 163 reports the correlation between MBV value and percentage of porosity (in this case linear relation is the best fitting). The higher the quantity of the pores is, the higher is the ability of the material to uptake/release water vapor.

Moreover, the higher the total volume of pores is and the higher is the available mortar surface with large pore volume that can provide enough space for adsorbate to be trapped in [86]. In fact, spruce sawdust based mortar is the mortar that shows the highest value of MBV and the highest pore diameter value. This is the same properties that also control permeability. By relating permeability with MBV, the higher the resistance of the permeability coefficient is, the lower the MBV value is. In this case the relation that best fits the data is logarithmic.
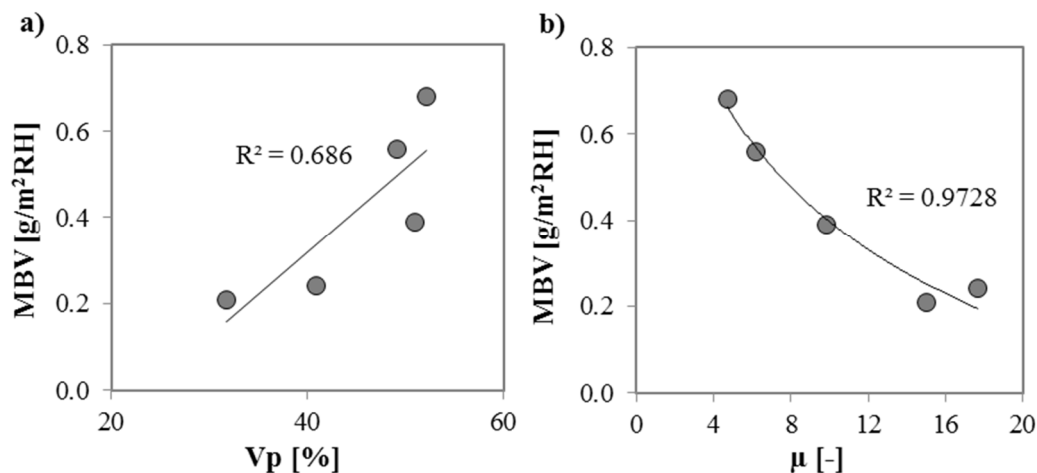
Figure 163 Correlation between a) MBV values and porosity and b) porosity and water vapor resistance factor

5.4.7. Adsorbent properties

Gas Chromatography is the technique (described in § 2.3.5.2) used to analyze depolluting properties of mortars with MEK as tracer. The test is conducted in order to investigate adsorbent properties of mortars. Specimens are cylinder with 3.6 cm base diameter and 4 cm high.

The first step is to carry out the calibration curve. It is possible to know the concentration of tracer (MEK) inside the box of 1 l by the evaluation of areas of peaks due to a known MEK injection. So, calibration is performed till 5 µl.

A known quantity of MEK is injected, then areas of chromatogram are detected and related in a graph with concentration. The concentration of the tracer is given in Table 20.

Table 20 Concentrations of MEK, values for calibration curve elaboration

Volume of MEK µl	Weight of MEK g	Concentration of MEK mg/m^3
2	0.002	1498
3	0.002	2248
4	0.003	2997
5	0.004	3746

Figure 164 shows the calibration curve.
Before the test the specimens are placed inside the box and then the box is sealed. For each specimen, the residual concentration of MEK inside the box is monitored in time.
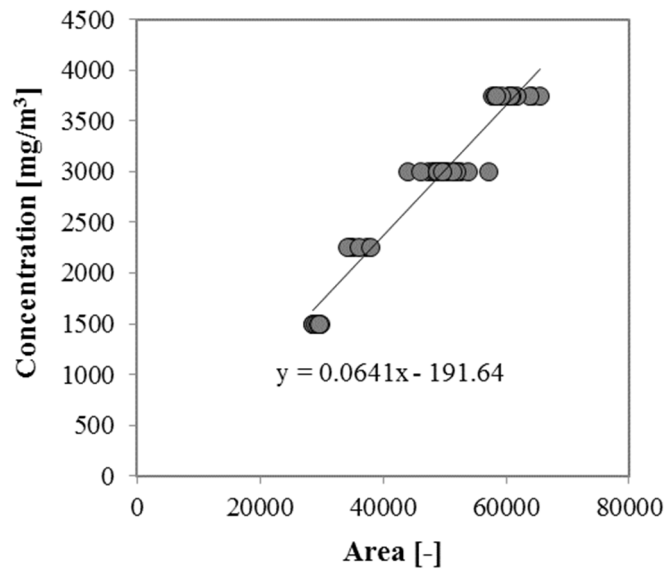
Figure 164 Calibration curves a) dark condition and b) UV light condition

Figure 165 summarizes the results obtained from the test showing the residual percentage of MEK inside the box. Percentage is evaluated as C_i/C_0 where C_i is the concentration of MEK detected inside the box and C_0 is the theoretical initial concentration of MEK. In this case the theoretical initial concentration is 2997 mg/m^3 (the MEK load is 4 µl).

In this case the evaluation of logarithmic trends is not necessary: the small volume enhance the different trend of mortar.
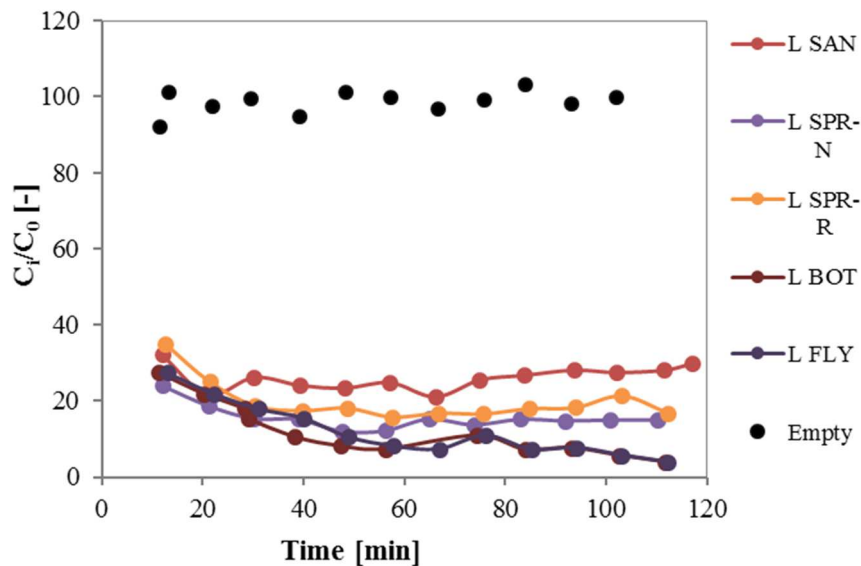
Figure 165 MEK adsorption in time for different mortars.

After 2 hours, sand based mortars adsorb about 60% of MEK. The use of different biomass wastes as unconventional aggregates always improves the depollution

properties of mortars. Both mortars with spruce sawdust shavings as it is and roasted adsorb the double of MEK adsorbed by sand based mortars.

The best performance is measured with biomass ashes where the reduction of MEK concentration is about 95% of the initial MEK injected, 55% higher than that of sand based mortars. All compared data are detected after 2 hours of test.

It is well known the action of some carbon-based materials such as active carbon. However, the cost of activated carbon and the loss of adsorption efficiency after regeneration of the exhausted activated carbon have limited its use in effluent waste water treatment. Studies report the suitability of some ashes (as rice husk ashes) in adsorption processes [103]. Ashes can represent an attractive low - cost alternative to remove heavy metals from industrial waste or for air purifying [104].

5.4.8. Life Cycle Assessment

The total CO_2 emission of traditional cementitious mortar (C-S), L-SAN and L-BOT is provided. During the evaluation of the LCA of the mortars, it has been considered (kg of CO_2 for each kg of product):

- Water: 0.0002 $kgCO_2/kg$;
- Cement 0.9 $kgCO_2/kg$;
- Calcareous sand/filler: 0.011 $kgCO_2/kg$;
- Hydraulic lime: 0.189 $kgCO_2/kg$ (considered as a mixture of cement and calcareous filler § 2.2.2.2).

Avoiding the landfilling of bottom ash there is an environmental gain of 0.543 $kgCO_2/kg$.

Taking into account the quantity of different materials necessary to prepare 1 m^3 of mortar (Table 5 and Table 17), it is possible to evaluate the impact.
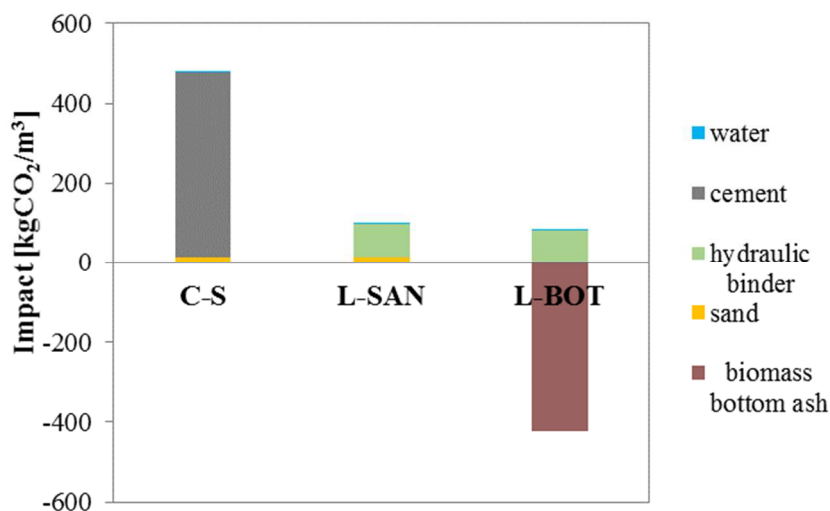
Figure 166 Potential impact of traditional mortars (C-S and L-SAN) and bottom biomass ash based mortar L-BOT.

System mass balance (Figure 166) of mortars shows that the use of hydraulic lime and the addition of aggregate from waste materials enhances the sustainability of mortar.

Indeed, L-BOT mortar not only does not imply CO_2 emissions in atmosphere, but has alsoa negative energy impact (of about 340 kg of CO_2 each m^3 of produced mortar).
In this perspective, the development of mortars with aggregates coming from biomasses is certainly interesting

5.5. Conclusions

The effects of replacing the volume of sand with unconventional aggregates based on different biomass wastes in lime based mortars for indoor applications implies:

- a decrease of density of mortars: spruce saw dust and fly ash mortars can be classified as lightweight mortars;
- a general decrease of compressive strength, but still acceptable for plastering/rendering applications. On the other hand, bottom biomass ashes increase the compressive strength of lime based mortars of about 50%;
- a general increase of capillary water absorption. However, bottom biomass ashes decrease the capillary water absorption of lime based of about 50%, while the torrefaction process permits to half the capillary water absorption of mortars manufactured with spruce sawdust shavings;
- an increase of water vapor permeability up to 65%;
- an enhancement of IAQ in terms of up to three times higher MBV and up to 55% increased capacity to adsorb VOCs.

Bio-based waste materials can be a valid alternative in terms of air-purifying sustainable materials. This property is still found if these materials are mixed in hydraulic lime based mortars.

Chapter 6

6. Optimized use of biomass wastes and adsorbent aggregate in photocatalytic hydraulic lime based mortars

6.1. Introduction

Recent studies are focusing on innovative finishes passively able to reduce ozone or Volatile Organic Compounds (VOC) [105]. Mortars able to increase indoor comfort of occupants through self-cleaning and depolluting properties and moisture buffering capacity [12] are studied and developed.
With the purpose of enhancing IAQ, TiO_2-enriched hydraulic binders [28] are tested in mortars where the volume of conventional sand is replaced by a combination of silica gel and biomass waste ashes, both fly and bottom.
By using hydraulic lime as a binder and biomass ashes the final product is more sustainable than conventional mortars.
This topic is of interest not only for scientists. Industries are paying more attention on IAQ enhancement. 'Biocover 3.5' by CIM Marcellina' or 'Biocalce' by Kerakoll are two examples of commercially available products used for indoor purposes publicized as passive air purifying materials.
In this chapter, these two commercial mortars are tested and compared to a new, multifunctional mortar. Also, a conventional mortar is considered as comparison.
Mortars have been compared in terms of mechanical strength, morphology and microstructure, capillary water absorption, shrinkage, permeability, moisture buffering ability, de-pollution properties and aesthetics features.

6.2. Materials

The binder is hydraulic lime Plastocem, provided by Italcementi (L). This product is described in § 2.2.2.2.
Calcareous sand (SAN) (described in §2.2.4.1) is used as a reference-conventional aggregate. Commercial pre-mixed mortars are 'Biocover 3.5' by CIM Marcellina (MAR) and 'Biocalce' by Kerakoll (KER), both described in § 2.2.5.

The unconventional aggregate is high adsorbent silica gel (S), described in § 2.2.4.3. In order to overcome the lack of silica gel in terms of mechanical strength in mortars, biomass (type B) ashes (2.2.4.5) bottom ash (B) and fly ash (F), are added to hydraulic lime.

Ashes are thermally treated to heighten silicates and to decrease the organic part that gives dark color to ashes. From TG analysis results, ashes are calcined 650 °C in an oven with a specific burning program.

Figure 167 Oven where the ashes are calcinated

Starting from a temperature of 20 °C, the biomass ashes are heated at T = 650 °C for 1.5 h. Temperature is kept constant for 2.5 h. At the conclusion of the cycle, biomasses are removed from the oven and cooled to room temperature in a desiccator.

Mass changes are monitored before and after the treatment Table 21.

Table 21 Mass monitored before and after the thermal treatment

	Mass before	Mass after	Mass loss
	g	g	%
Fly Ash	70.00	67.55	3.39
Bottom Ash	70.00	58.53	16.39
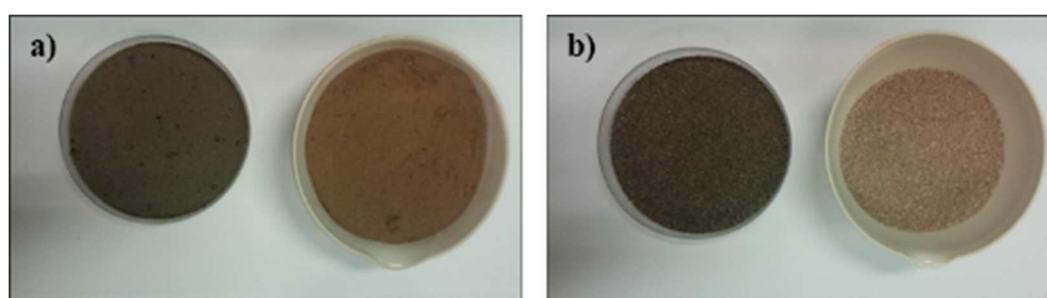
Figure 168 Ashes before and after the thermal treatment, a) fly ash and b) bottom ash

Two different types of titanium dioxide are added to give photocatalytic properties (§ 2.2.3.3): P-25 by Aeroxide (TiO2A) and KRONOClean 7000 (TiO2K), declared effective under visible light.

6.2.1. Mix design

Premixed mortars are prepared by adding water as indicated in technical data sheets. From the traditional mortars (w/b as previously indicated § 4.2.1), 100% sand volume is replaced by a combination of silica gel (50%), bottom ash (25%) and fly ash (25%). All percentages are expressed in volume. The same recipes are repeated with thermally treated fly and bottom ashes at same mass quantities. These two mortars are added with two different types of titanium dioxide: P-25 Aeroxide and KRONOClean 7000.

Table 22 Mortars prepared: summary of different combinations

Binder	Aggregates	Titanium dioxide	Code ID	Code Color
Hydraulic Lime	Calcareous sand		L-SAN	
	Premixed Kerakoll		KER	
	Premixed CIM Marcellina		MAR	
Hydraulic Lime	Silica Gel, Bottom Ash, Fly Ash		M1	
Hydraulic Lime	Silica Gel, Calcinated Bottom Ash, Calcinated Fly Ash		M1 tr	
Hydraulic Lime	Silica Gel, Bottom Ash, Fly Ash	P-25 Aeroxide	M1 TiO2A	
Hydraulic Lime	Silica Gel, Calcinated Bottom Ash, Calcinated Fly Ash	P-25 Aeroxide	M1 tr TiO2A	
Hydraulic Lime	Silica Gel, Bottom Ash, Fly Ash	KRONOClean 7000	M1 TiO2K	
Hydraulic Lime	Silica Gel, Calcinated Bottom Ash, Calcinated Fly Ash	KRONOClean 7000	M1 tr TiO2K	

The appropriate volume required for casting is evaluated according to the different tests that are performed Aggregates are added in ssd conditions. Mix design proportions are shown in Table 23.

Table 23 Mix proportions (kg/m^3) of mortars.

Mix	Water	Hy-lime	Sand	Silica gel	Bottom ash*	Fly ash*	TiO2A	TiO2K
L-SAN	256	437	1535	-	-	-	-	-
M1	256	437	-	379	281	204	-	-
M1 tr	256	437	-	379	281	204	-	-
M1 TiO2A	256	437	-	379	281	204	26	-

M1 tr TiO2A	256	437	-	379	281	204	26	-
M1 TiO2K	256	437	-	379	281	204	-	26
M1 tr TiO2K	256	437	-	379	281	204	-	26

*referred to both, as it is and calcined

Mortars are casted in different moulds in order to obtain the suitable specimens for the determination of each property. During the cast mortars are vibrated manually to eliminate the excess of air. It is used manually vibration because the mechanical vibration can induce a segregation of the lightweight aggregate with the cement paste.

6.3. Methods

Mortars are characterized in terms of fresh state properties. Workability is measured with a flow table, according to the current standards (§ 2.3.1).
After 28 days of curing, flexural and compressive strength are tested. The specific strength is also evaluated (§ 2.3.2.1).
After 28 days of curing morphologies are investigated by Scanning Electron Microscope (SEM) and pore size distribution is evaluated by Mercury Intrusion Porosimetry (MIP), as described in § 2.3.2.2.
Free shrinkage and weight loss due to the water evaporation of mortars are monitored for about 50 days (§ 2.3.2.3).
Water is the medium where ions can be transported and can compromise the durability of building material. Water transport in mortars is evaluated with two different methodologies (§ 2.3.3.1 and § 2.3.3.2).
Transpirability of mortars for renders is a fundamental property, evaluated according to § 2.3.4.1.
The moisture buffering capacity of mortars is evaluated over dynamic variation of RH with a simplified procedure of the NORDTEST method (§ 2.3.4.2).
De-pollution properties of different mortars are evaluated by two different experimental tests: in batch (§ 2.3.5.2), to explore adsorbent/photocatalytic properties, and in continuous flow test (§ 2.3.5.3).
The addition of ashes and wastes implies a darker coloration of mortar. The aesthetic properties are evaluated as described in § 2.3.6.

6.4. Results and discussions

6.4.1. Workability

Table 24 shows workability of mortars in terms of flow and consistency values.

Table 24 Workability of different mortars: picture of mortar at fresh state after slump flow test, slump flow values and consistency.

Mix	L-SAN
Slump (mm)	133
Consistency (%)	33

Mix	KER	MAR
Slump (mm)	105	135
Consistency (%)	5	35

Mix	M1	M1 tr
Slump (mm)	125	124
Consistency (%)	25	24

All mortars have the same consistency. The slump value is lower than 140 mm for all mixes and, according to UNI EN 1015-6 [57], mortars are defined stiff.

6.4.2. Mechanical strength

Figure 169 shows the results in terms of maximum flexural strength.
It is not possible to detect the flexural strength of KER because of too low mechanical resistance.
The highest value of mechanical strength is obtained with pre-mixed commercial product MAR, 75% higher than reference mortar.

Unconventional aggregates based mortars have the lowest value of flexural maximum strength, about 50% lower than sand-based mortars.

The addition of different types of titanium dioxide implies a decrease in flexural strength of 10%.

Thermal treatment of biomasses implies for M1 tr 10% more flexural strength in M1.
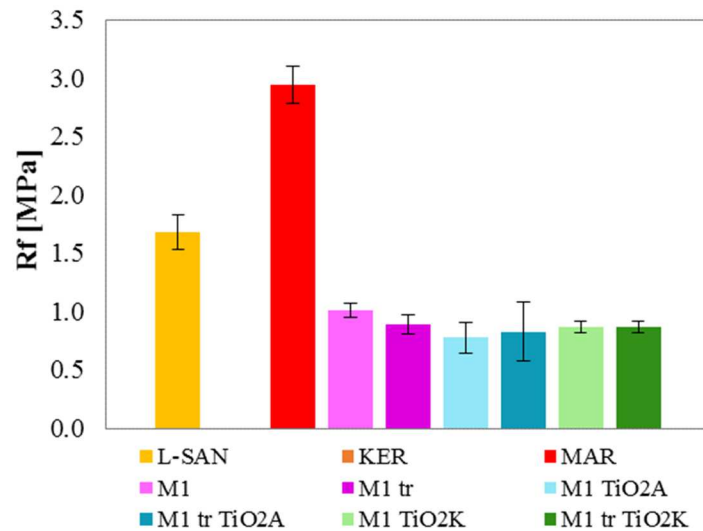
Figure 169 Flexural strength of mortars

Compressive strength is evaluated at 28 days and results are reported in Figure 170.

All mortars have lower value of compressive strength than conventional aggregate based mortar.

Commercial products MAR and KER have 5% and 55% respectively lower mechanical strength than reference mortars.

In general, the use of unconventional aggregates decreases compressive strength of about 25% compared to reference mortar, 20% compared to MAR, but all values are higher than KER mortar.

There is a reduction in terms of mechanical strength, but, if results from silica gel based mortars (§ 4.4.2.) are considered, it is evident that pozzolanicity of ashes positively influences mechanical resistance [99].

The thermal treatment of biomass in general implies 10% higher compressive strength than that of same mortar without the treatment. This can be due to the loss of organic materials during the burning process of biomass [106] that increases mechanical resistance.

The introduction of titanium dioxide does not change significantly the mechanical behavior, as previously shown in § 4.4.2.
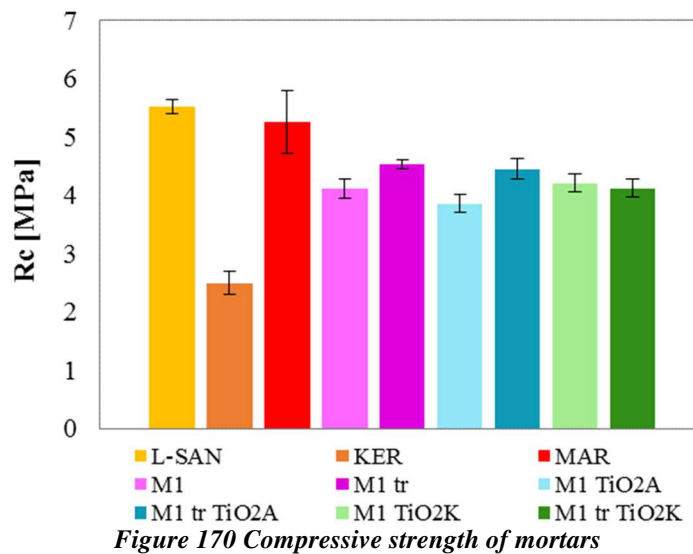
Figure 170 Compressive strength of mortars

According to the current standard UNI EN 998-1:2010 [80], the maximum value of density for indoor mortar to be classified as lightweight is 1300 kg/m^3. Figure 171 shows the results of density values for the different mortars.

Thanks to the total replacement of calcareous sand with silica gel and biomass ashes lightweight finishes are obtained.

Unconventional mortars have lower density than commercial products and traditional mortars of about 15% and 35%, respectively.

L-SAN and MAR belong (according to [80]) to CS III, KER belongs to CS II, all unconventional based mortars belong to CS II-CS III (according to [80])
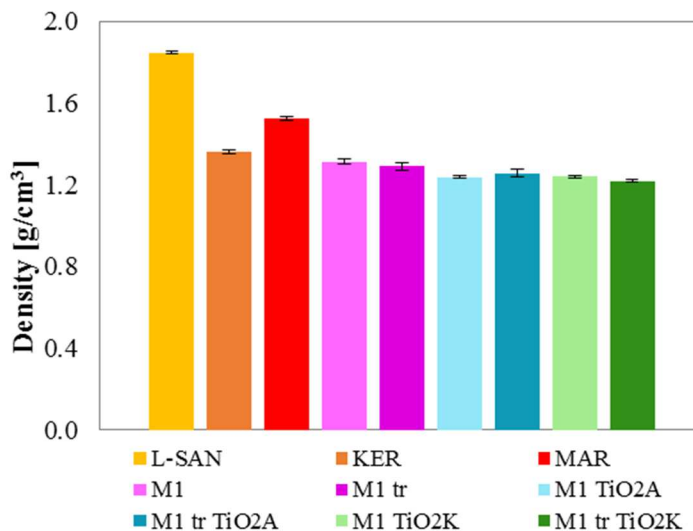
Figure 171 Hardened density (ρ) of mortars

The following table (Table 25) summarizes the average values of flexural, compressive strength, density and compression specific strength.

160

With regard to specific resistance Rcs it is evident that, besides the low densities, all unconventional multifunctional mortars have higher value (from 5% to 10%) than conventional mortar.

Commercial product MAR has the highest value, 15% higher than reference mortar and KER has the lowest value, 40% lower than reference mortar.

Table 25 Mechanical tests results: flexural strength (Rf), compressive strength (Rc) hardened density (ρ), and specific strength (Rsc) of biomass waste and hydraulic lime-based mortars

Mix	Rf [MPa]	Rc [MPa]	ρ [g/cm^3]	R_{cs28} Pa/(kg/m^3)
L-SAN	1.7	5.5	1.85	3.0
KER	0.0	2.5	1.36	1.8
MAR	2.9	5.3	1.52	3.5
M1	1.0	4.1	1.30	3.1
M1 tr	0.9	4.5	1.29	3.5
M1 TiO2A	0.8	3.9	1.24	3.1
M1 tr TiO2A	0.8	4.5	1.26	3.5
M1 TiO2K	0.9	4.2	1.24	3.4
M1 tr TiO2K	0.9	4.1	1.22	3.4

6.4.3. Microstructure of mortars: morphology and pore size distribution analysis

The mechanical results are explained by morphological observations obtained by SEM images. The following pictures focused on silica gel and biomass wastes interaction with hydraulic lime paste. Ti element is also mapped in order to confirm an adequate distribution of photocatalytic agent in the mortar.

The interface between calcareous sand and hydraulic lime is good, as previously demonstrated (Figure 75).

Morphology of M1 is investigated and related images and EDAX analysis are shown in Figure 172 and Figure 173.

ITZ is evident between silica gel and paste, while for bottom ash the interface is good and very difficult to recognize. The EDAX probes detect high amount of Ca (due to the binder), K and Al (due to the biomasses). Si is due to aggregates (principally silica gel but also ashes) and in small part to the binder.
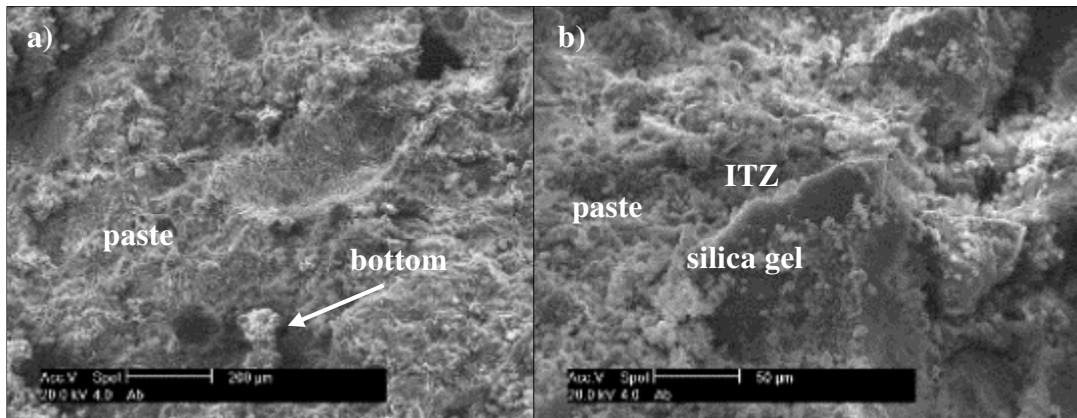
Figure 172 SEM images of M1 specimen
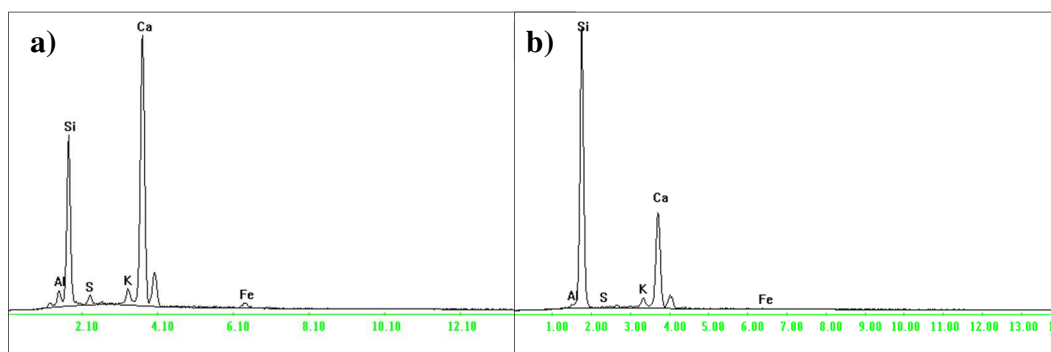
Figure 173 EDAX performed on the a) Figure 166 a) and on b) aggregate (silica gel)

Thermally treated ashes show the same ITZ with binder phase of not-thermally treated one (Figure 174).

Additional hydration products in the ITZ are detectable on M1 and M1 tr. These products are probably due to the pozzolanic reaction between ash and hydraulic lime [54], justifying the good mechanical behavior of these mortars in terms of compressive strength.
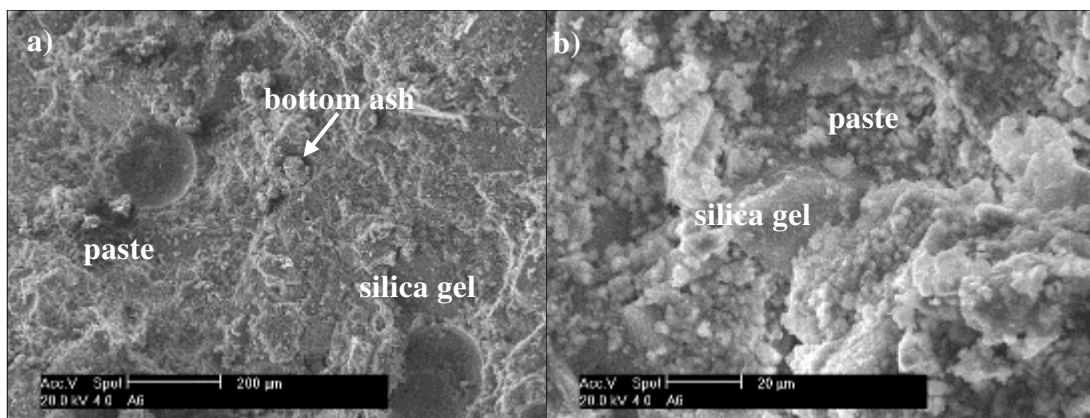
Figure 174 SEM images of M1 tr

No differences are detected with the addition of both TiO_2 agents (Figure 175). EDAX analysis confirms the presence of TiO_2 and, by element mapping its homogeneous distribution.
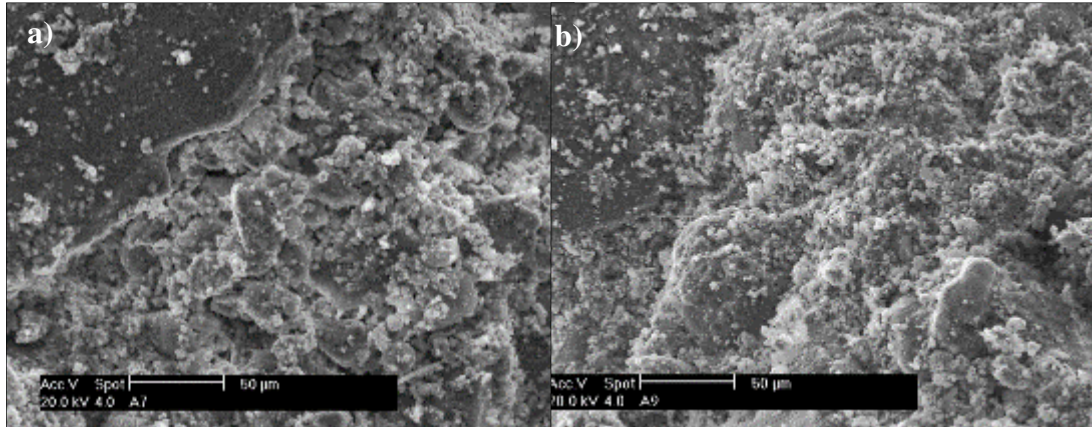
Figure 175 SEM images of a) M1 TiO2A mortar with P-25 and b) M1 TiO2K mortar with KRONOClean 7000
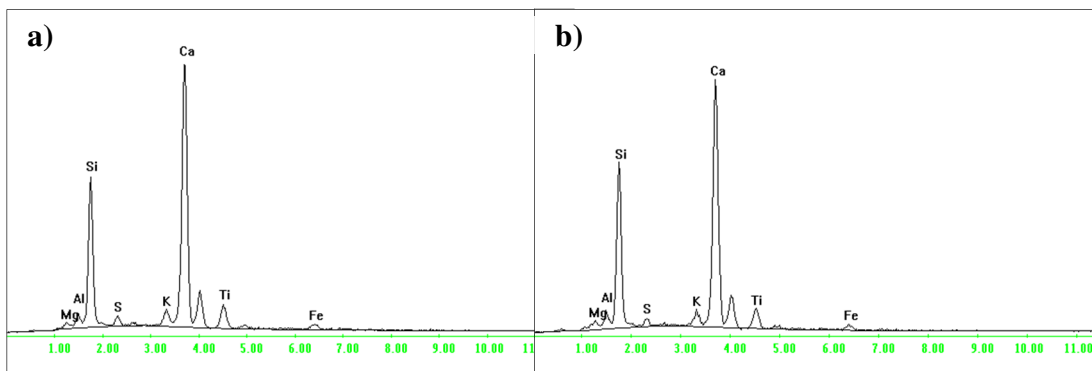
Figure 176 EDAX performed on a) M1 TiO2A mortar with P-25 and b) M1 TiO2K mortar with KRONOClean 7000
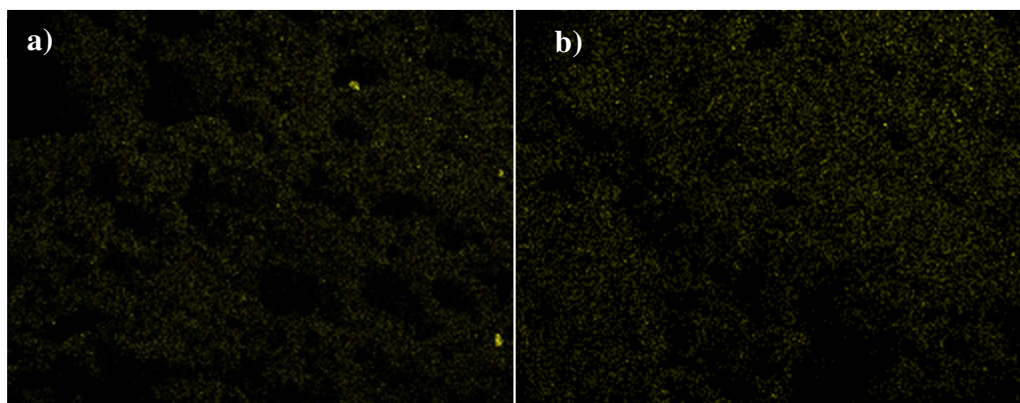
Figure 177 Mapping of the Ti element performed on a) M1 TiO2A mortar with P-25 and b) M1 TiO2K mortar with KRONOClean 7000

Optimized use of biomass wastes and adsorbent aggregate in photocatalytic hydraulic lime based mortars

Pore distribution curves of conventional, commercial and multifunctional mortars are compared.

Conventional and commercial mortars have a unimodal distribution, unconventional based mortars with and without thermal treatment of biomass ashes and with different types of TiO_2 have a bi-modal distribution. A tri-modal distribution is detected for M1 and M1 tr mortars.

Hydraulic lime introduces into the matrix a porosity with higher threshold pores diameter compared to cement mortar, as already discussed (§ 3.4.3).

Conventional mortar has a modal pore diameter of 0.929 µm and a threshold pore diameter of 1.5409 µm.

MAR has a modal diameter of 1.596 µm and a threshold pore diameter of 3.2708 µm. MAR has the highest threshold and modal pore diameter.

KER has a modal diameter of 0.901 µm and a threshold pore diameter of 1.199 µm.

All unconventional mortars have the first peak at 1.2 µm, except for M1 TiO2A that is at 0.932 µm. The second peak, at a lower pore diameter, is at 0.035 µm for M1 and M1 TiO2A, at 0.0358 µm for M1 tr and 0.0216 µm for the other mortars.

M1 and M1 tr mortars have additional peak at 0.0131 µm.
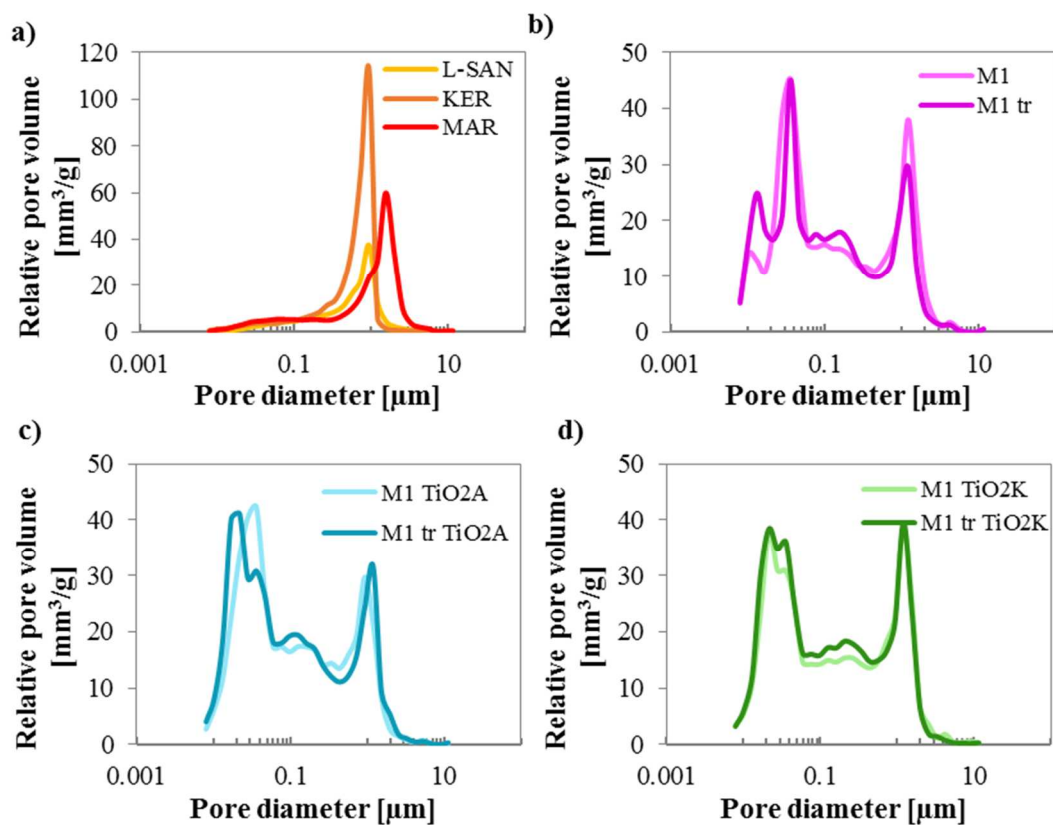
Figure 178 Relative pore volume distribution of different mortars a) sand based mortar and commercial products, b) unconventional aggregates based mortars with and without thermal treatment c) unconventional aggregates based mortars with and without thermal treatment with TiO2A-P-25 Aeroxide, d) unconventional aggregates based mortars with and without thermal treatment with TiO2K-KRONOCLEAN 7000
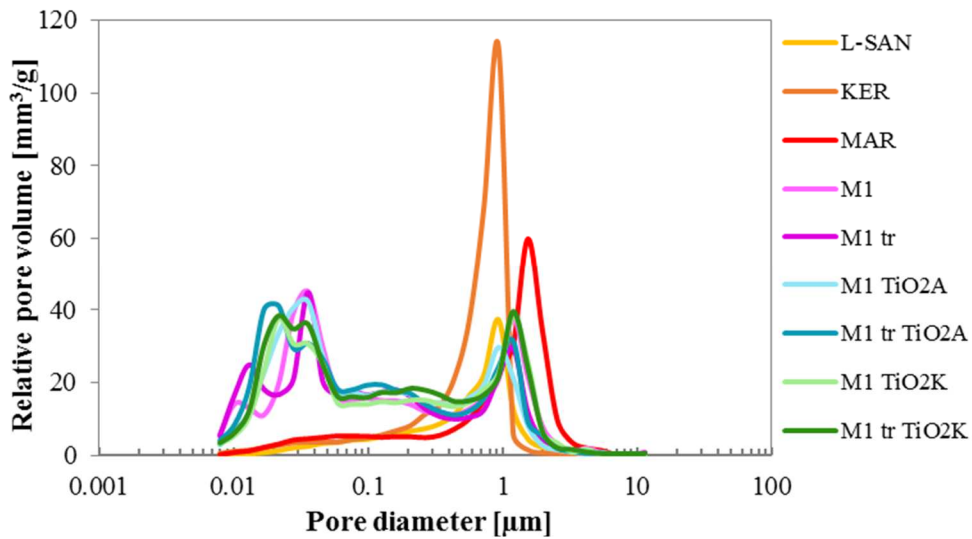
Figure 179 Relative pore volume distribution of different mortars

Total porosity can be evaluated both in the cumulative pores volume (Figure 180) and in the percentage pores volume graph (Figure 181).

Sand-based mortar has the lowest total porosity.

Commercial mortar MAR has 10% more total porosity and KER 15% more total porosity than L-SAN.

Unconventional based mortars have the highest value of total porosity. There are no significant differences in total porosity with the addition of TiO_2 or the thermal treatment of ashes.
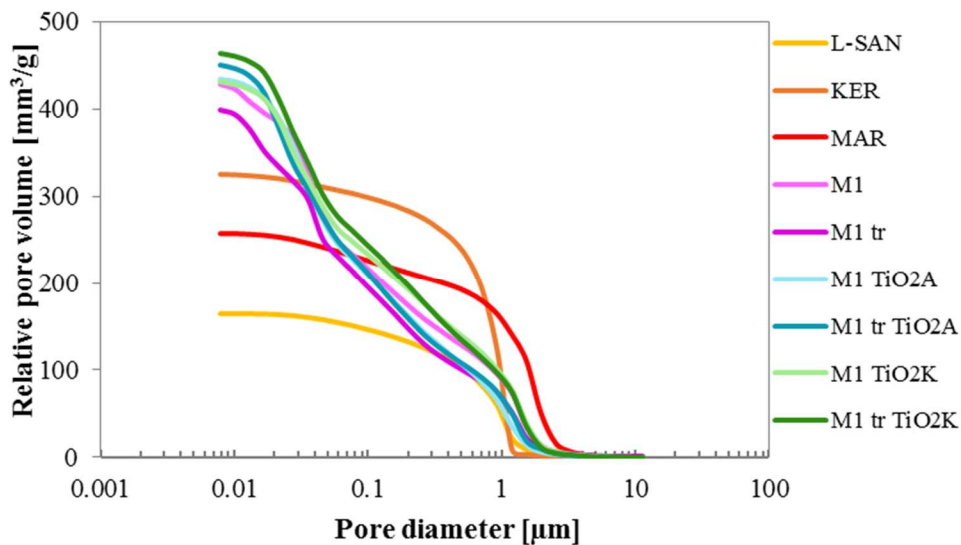
Figure 180 Cumulative pore volume distribution of different mortars
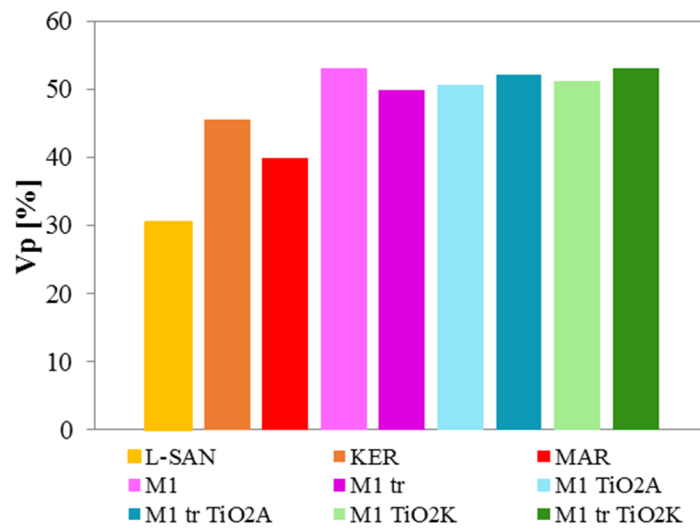
Figure 181 Total porosity of different mortars

6.4.4. Drying shrinkage and water loss measurement

Drying shrinkage is measured for 60 days.
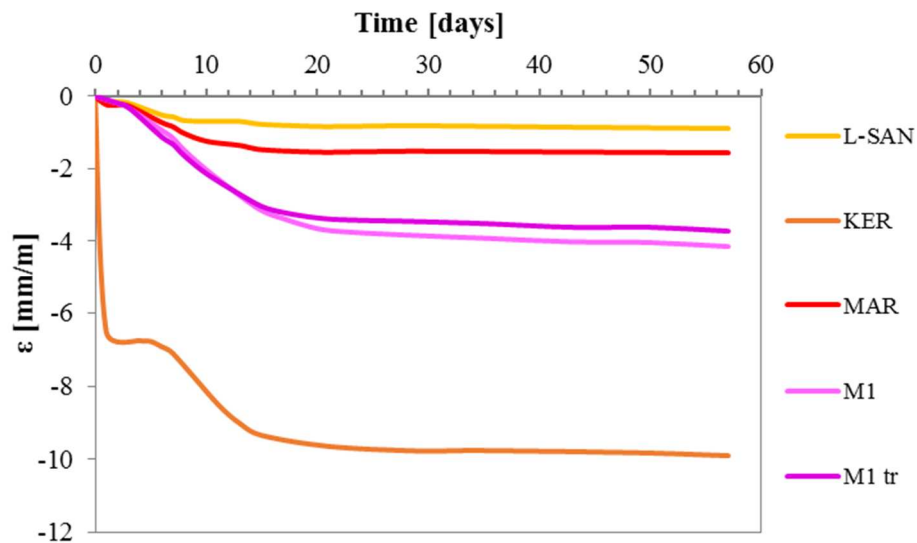
Figure 182 Monitoring of drying shrinkage of mortars at RH = 50% and T =20 °C
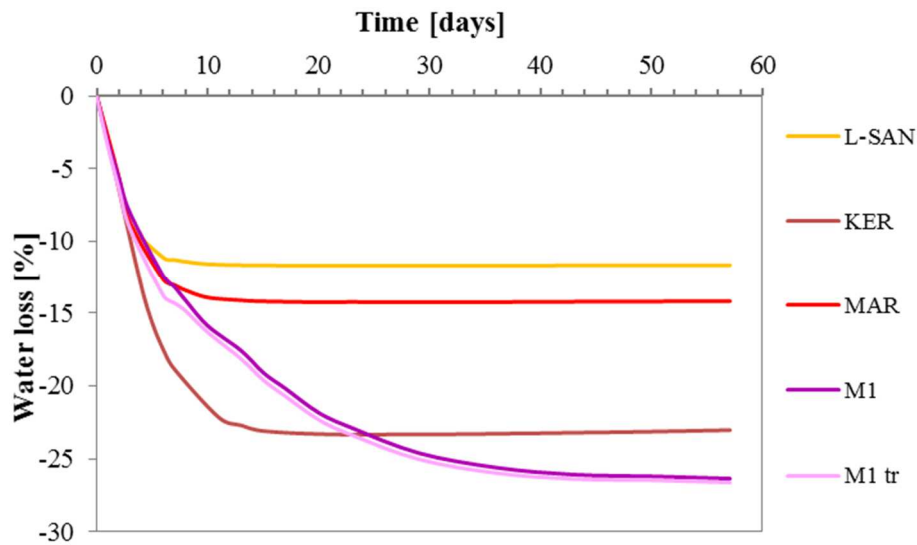
Figure 183 Monitoring of mass evaporation during drying shrinkage of mortars at RH = 50% and T =20 °C

The results are shown in Figure 182 and Figure 183. Values are obtained by monitoring the length of specimens placed in a climatic chamber at RH = 50% and T = 20 °C. The comparison of the results after 60 days of measurement is reported in Figure 184.

Sand based mortar has the lowest value of shrinkage and water loss. After one week of measurements, the specimens do not show significant variation in length. The replacement of sand with unconventional aggregate implies in mortars a high value of shrinkage (about 4 mm/m) and water loss (about 26%).

MAR has the same behavior of L-SAN but the values of shrinkage at 60 days are double than conventional mortar with a water loss 15% higher than conventional mortar.

KER has a deformation of -9.9 mm/m at 60 days but the water loss is 23% higher than unconventional mortar. Usually there is a linear correlation between shrinkage and water loss Figure 185. KER measurements are out of this relation (red dot on the graph).
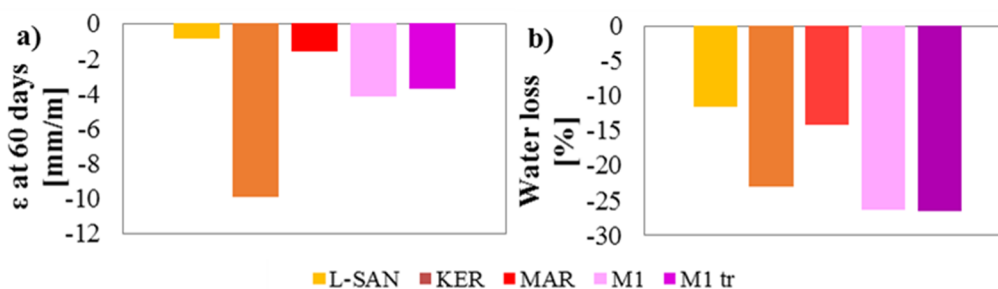
Figure 184 Drying shrinkage measurement at 60 days a) differences in length and water loss.
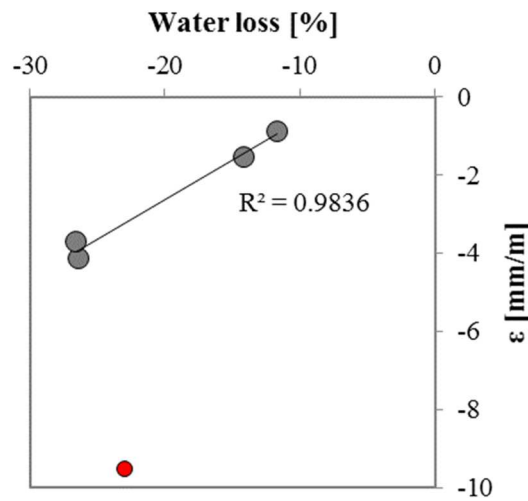
Figure 185 Water loss data plotted with ε

KER has aggregates with very small maximum diameter that implies higher quantity of water to maintain acceptable workability and, consequently, high water loss in unsaturated environments [107].

Mortars with silica gel and biomass have one peak on the pore size distribution at low diameter (around 0.03 µm) [108]. Shrinkage of mortars is related to the dimension of mortar pores: the lower the pore radius, the higher the induced stress [61].

Unconventional mortars have the highest amount of pores at the lowest diameter (and the highest total volume of pores) as reported in the cumulative pore distribution curve. Figure 186 shows that the higher the total volume of pores is, the lower is the elastic modulus (a part from KER, red dot on the graph) and the higher is the value of shrinkage at 60 days as previously showed § 2.3.2.3.
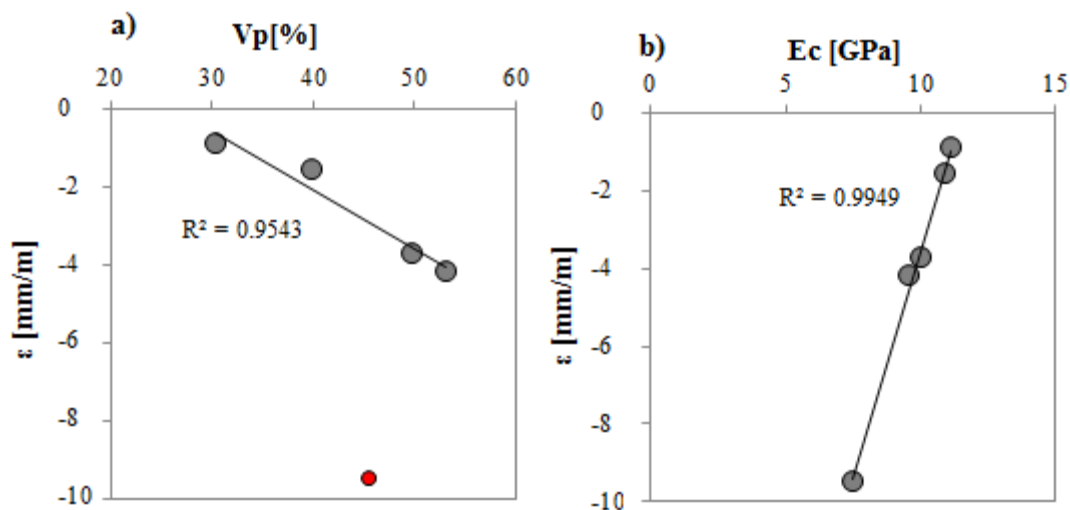
Figure 186 Correlations between shrinkage value at 40 days and a) total volume of porosity and b) elastic modulus

6.4.5. Capillary water absorption

Before testing, mortars are dried completely in a ventilated oven at 80 °C.

Capillary water absorption coefficient of mortars is evaluated according to the Italian standard UNI EN 1015-18 [65], data collected are shown in Figure 187.

All commercial products absorb less water than sand based mortar. C is about the 35% and 75% of C of reference mortar, for KER and MAR respectively. Commercial products are probably additivated with a hydrophobic admixture because data are consistent with those measured in our mortars with the hydrophobic admixtures (§4.4.4).

All unconventional mortars have higher C values than reference mortar. In particular: M1 has a value 25% higher than reference mortar. M1 with TiO_2 agents have a C value 10% higher than that of reference mortar.

Thermal treatment of ashes implies the same C for M1 tr and a slight increase of about 15%, for M1 tr TiO2A and M1 tr TiO2K.

Thermal treatment of ashes implies less organic unburnt content, and less porosity.

M1 absorbs 24% more water than M1 tr: M1 has the highest total porosity and the highest pore diameter. P-25 TiO_2 (TiO2A) treated biomass ashes mortar has a value of C 10% lower than the same without. In this case the total porosity is slightly lower. The same results are detected with KRONOClean 7000 TiO_2 (TiO2K) with differences of 5%. In case of as it is biomass ashes the addition of titanium dioxide implies lower value of C. If ashes are thermally treated C decrease of 10-20% compared to that of the same mortars without thermic treatment.

The high value of water absorption of the unconventional aggregates increases capillary water absorption of mortar. All mortars belong to W0 mortars, according to UNI EN 998-1:2010 [80].
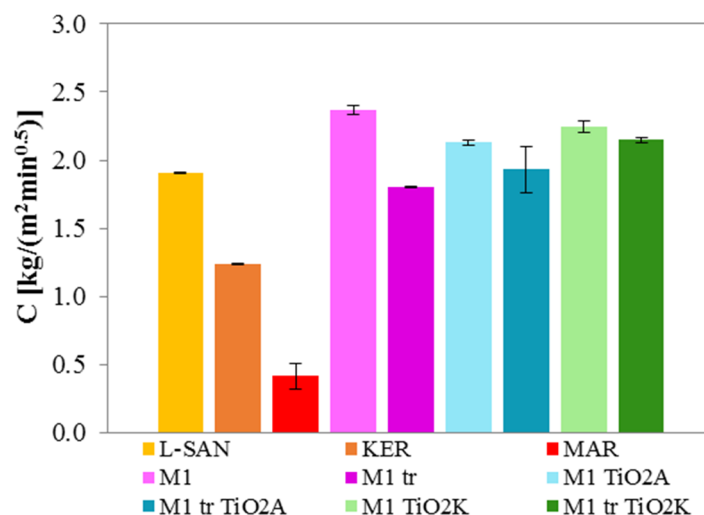
Figure 187 Capillary water absorption coefficient of different mortars according to UNI EN 1015-18.

UNI EN 15801[66] test result are shown in Figure 225.

In this case, commercial mortar MAR also absorbs the smallest amount of water during the test, 35% less than sand based mortar, despite the fact that the total porosity of MAR is higher than L SAN. This is probably due to the presence of a hydrophobic admixture. KER adsorbs about 30% higher quantities of water than sand based mortar.

Unconventional aggregates based mortars absorb the highest quantities of water, with double values compared to sand based mortar.

With this test procedure, the effect of thermal treatment of biomass ashes is less evident, only 5%.

In case of P-25 TiO_2 addition (TiO2A), the mortar absorbs 30% more water than that with unburnt biomasses. In case of KRONOClean TiO_2 (TiO2K) there are no differences with the thermal treatment of biomasses.

The use of different TiO_2 agents implies 10% increase of absorbed water.

Water first fills capillary pores of larger size and then gradually the smaller ones. In the second phase of the test, after 24h, the water absorption of unconventional mortars dramatically increases due to their high amount.
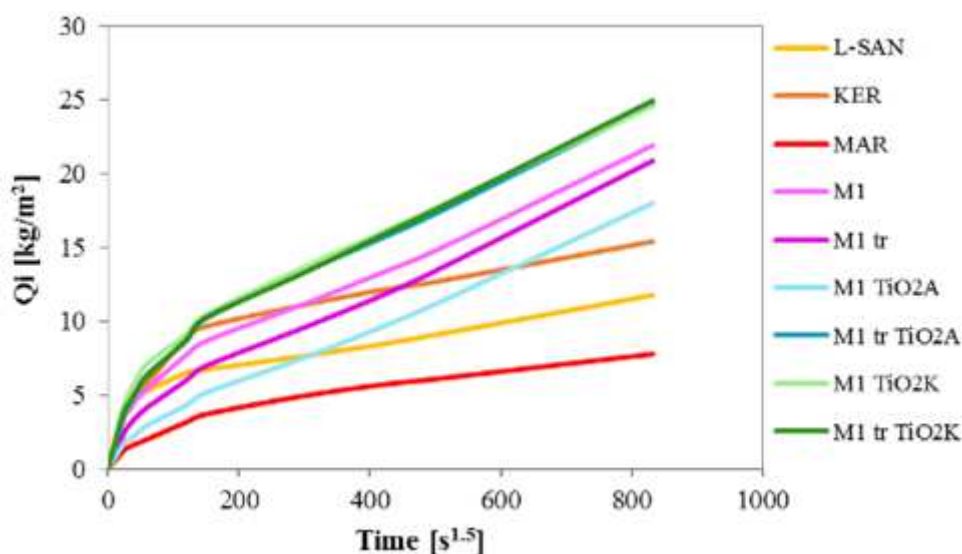
Figure 188 Capillary water absorption in time of hydraulic lime based mortars

6.4.6. Water vapor permeability

Water vapor permeability results, expressed in terms of μ factor, are shown in Figure 189. Lower values of μ factor indicates higher value of permeability.

During this test the influence of TiO_2 is negligible, so mortars without TiO_2 agents are tested.

Sand based mortar shows the highest value of water vapor resistance factor.

Commercial mortars have μ value lower than SAN L mortar, of about 30% for KER and 20% for MER. M1 has the lowest value of μ, 40% lower than SAN L mortar.

These differences are due to the porosity induced by the different aggregates. For KER, as an example the results follow [70]: the higher the pore radius is, the higher is the transpirability [60].

In the case of unconventional aggregates mortars, the total amount of porosity is more influent. All mortars have a permeability to water vapor proportional to the porosity percentage (Figure 190), the higher the volume of pores is, the lower is the hygroscopic resistance factor.
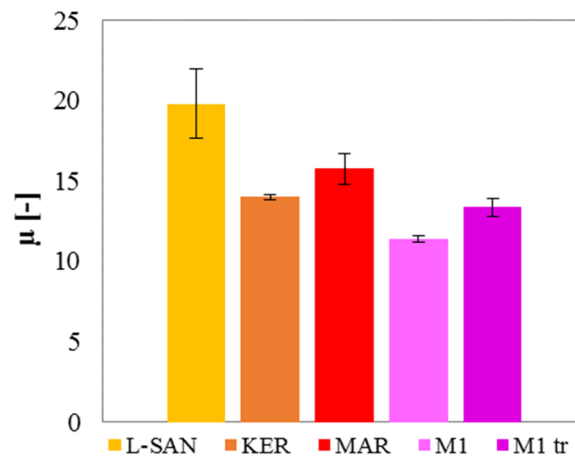
Figure 189 Water vapor resistance factor μ of different mortars
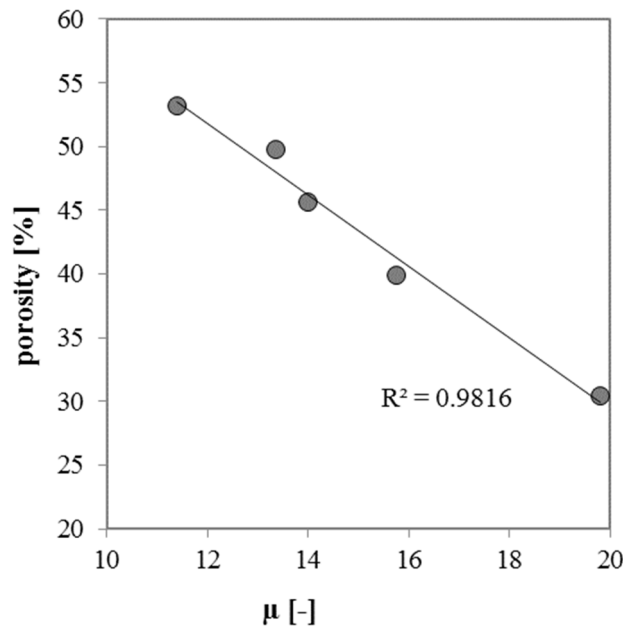
Figure 190 Linear correlation between porosity and water vapor resistance factor

6.4.7. Moisture Buffering Capacity

The interaction between mortars and the humidity of indoor environment is also studied by measuring the change in moisture content of specimens exposed at different RH. Figure 191 shows the change in water content (Δm) normalized on the surface of the specimens. MBV values are shown in Figure 192 and Table 49. During this test the influence of TiO_2 is negligible, so mortars without TiO_2 agents are tested.

Reference mortar has the lowest ability to exchange water vapor and consequently the lowest MBV.

Commercial mortars have a higher capacity to exchange water vapor than sand based mortar of about 5% for KER and 30% for MAR.

Unconventional mortars have up to 3 times higher MBV compared to reference mortars.

Optimized use of biomass wastes and adsorbent aggregate in photocatalytic hydraulic lime based mortars

If biomasses are thermally treated (M1 tr) MBV is at least 2 times higher than reference mortars
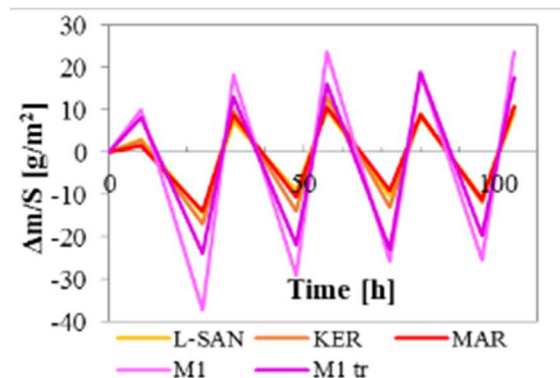
Figure 191 Changing of mass due to absorption/desorption phases, normalized on the specimens surface
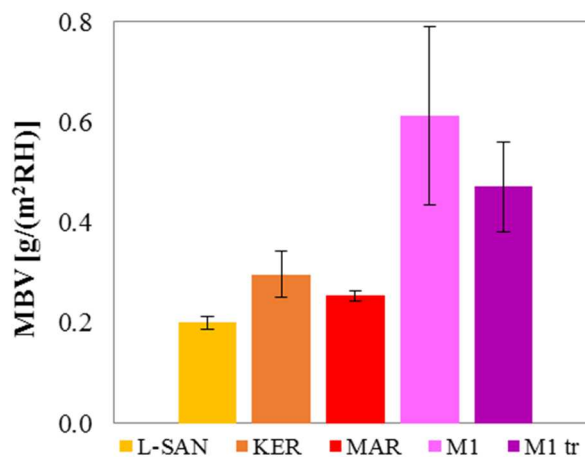
Figure 192 Moisture buffering value of hydraulic lime based mortars

Again, the differences in results are related to the different pore size networks of the mortars. Higher permeability usually indicates higher water vapor exchanging ability [73].

Moreover, the higher the total volume of pores is and the higher is the available mortar surface with large pore volume that can provide enough space for adsorbate to be trapped in [86].

Unconventional mortars have the highest value of total porosity and the highest values of MBV. These behaviors are confirmed in Figure 193. Figure shows the correlation between MBV and permeability and transpirability. The trend lines chosen best represent the behavior of data.
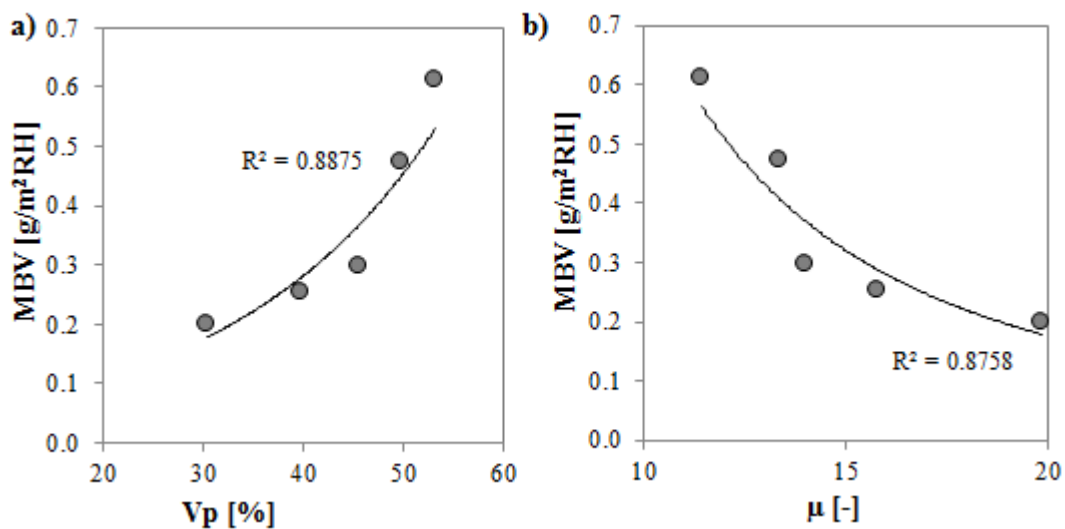
Figure 193 Correlation between a) MBV values and porosity and b) porosity and water vapor resistance factor

6.4.8. Depollution efficiency

Gas Chromatography is the technique (described in § 2.3.5.2) used to analyze depolluting properties of mortars with MEK as tracer. Tests are conducted in three different conditions: dark condition, visible (VIS) radiation and UVA radiation (UV): 10 W/m^2 of UVA and VIS radiation is guarantee on the surface of the specimens. Specimens are cylinders of 8 cm in diameter and for 0.8 cm high.
The first step is to carry out the calibration curves.
A known quantity of MEK is injected inside the box of 16.65 l, areas of chromatogram are detected and related with concentration in a graph. The concentrations of the tracer are given in Table 26.

Table 26 Concentrations of MEK, values for calibration curve

Volume of MEK	Weight of MEK	Concentration of MEK
µl	g	mg/m^3
5	0.004	240
10	0.008	480
25	0.020	1201
50	0.040	2402
75	0.060	3604

Three different curves are elaborated: under dark condition (dark), under UVA radiation (UV) and under visible radiation (VIS). Figure 194 shows the detected data. The found equations are necessary to convert the detected area in MEK concentration inside the box.

Optimized use of biomass wastes and adsorbent aggregate in photocatalytic hydraulic lime based mortars

Before the test, the specimen is placed inside the box and the box is sealed. For each specimen, the residual concentration of MEK inside the box is monitored during the time.

a)

$y = 0.0305x + 47.608$
$R^2 = 0.9934$

b)

$y = 0.0328x + 83.118$
$R^2 = 0.9845$
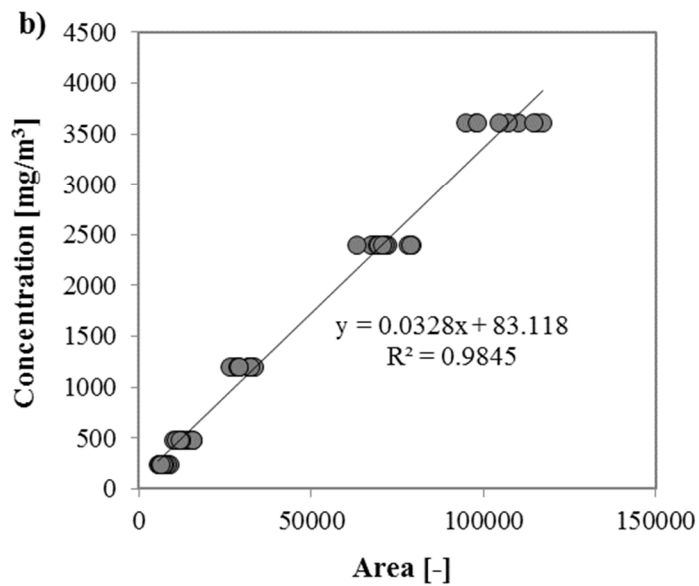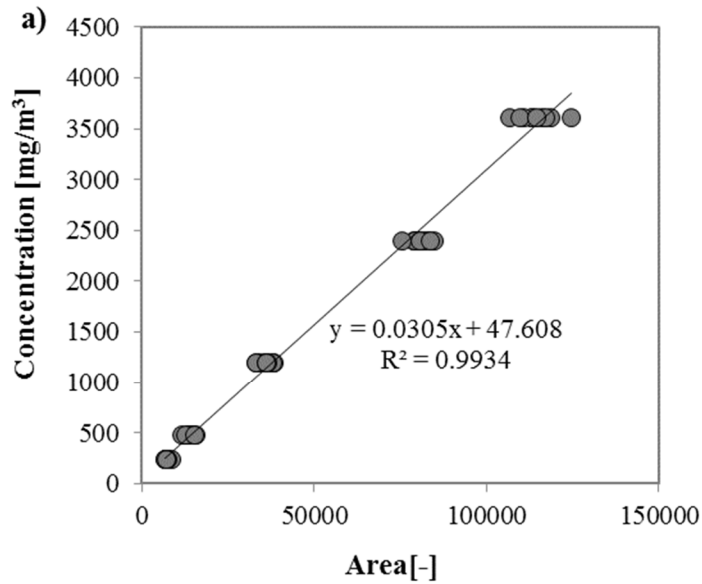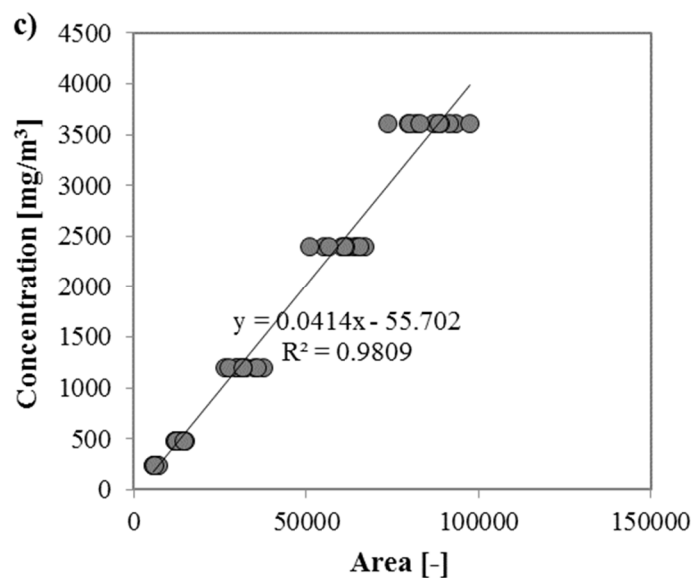
Figure 194 Calibration curves for a) dark conditions, b) VIS light radiation, c) UV light radiation

The following figures (from Figure 195 to Figure 203) summarize the obtained results. They show the residual percentage of MEK inside the box. Percentage is evaluated as C_i/C_0 where C_i is the MEK concentration detected inside the box and C_0 is the MEK theoretical initial concentration. In this case the theoretical initial concentration is 2402 mg/m^3 (the MEK load is 50 µl).
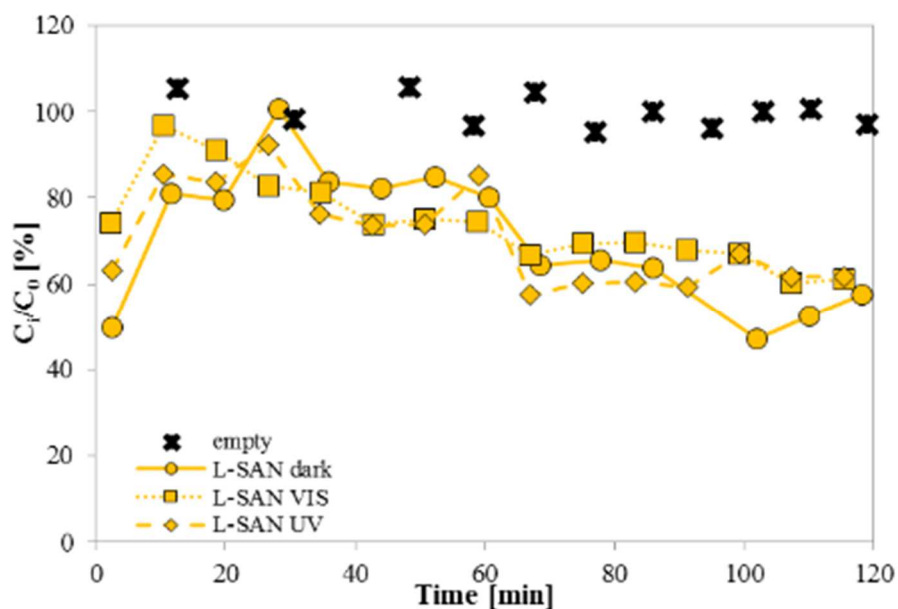
Figure 195 Depollution capacity at different test condition of L-SAN
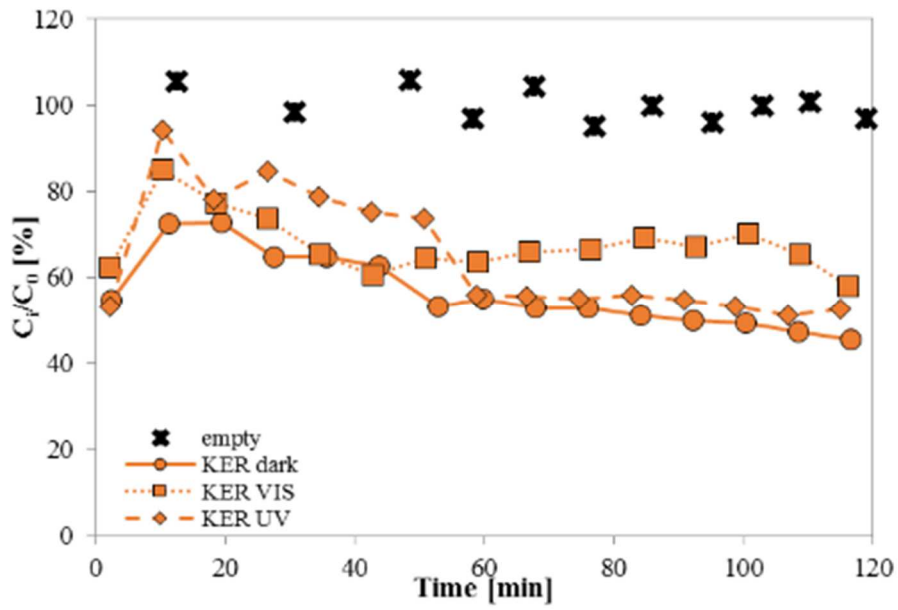
Figure 196 Depollution capacity at different test condition of KER
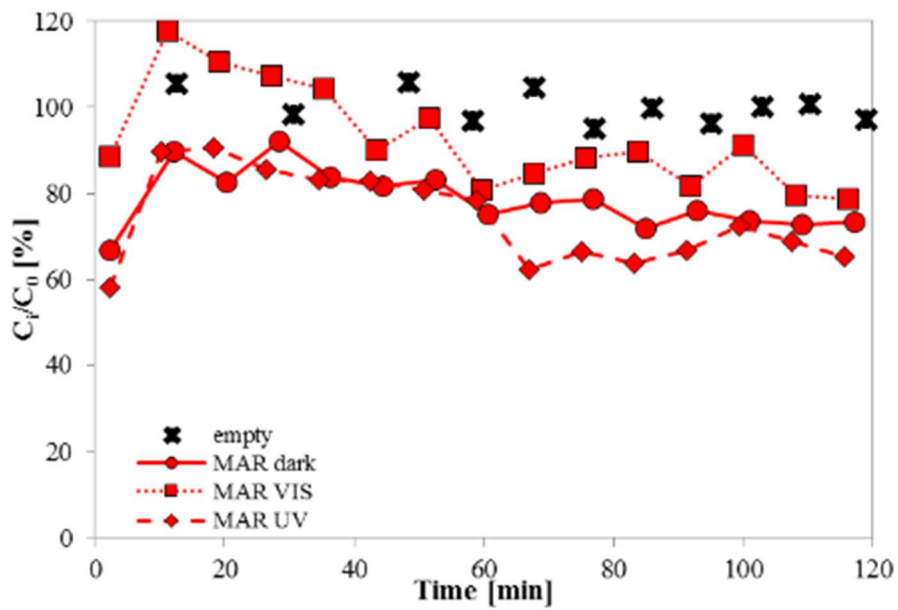
Figure 197 Depollution capacity at different test condition of MAR
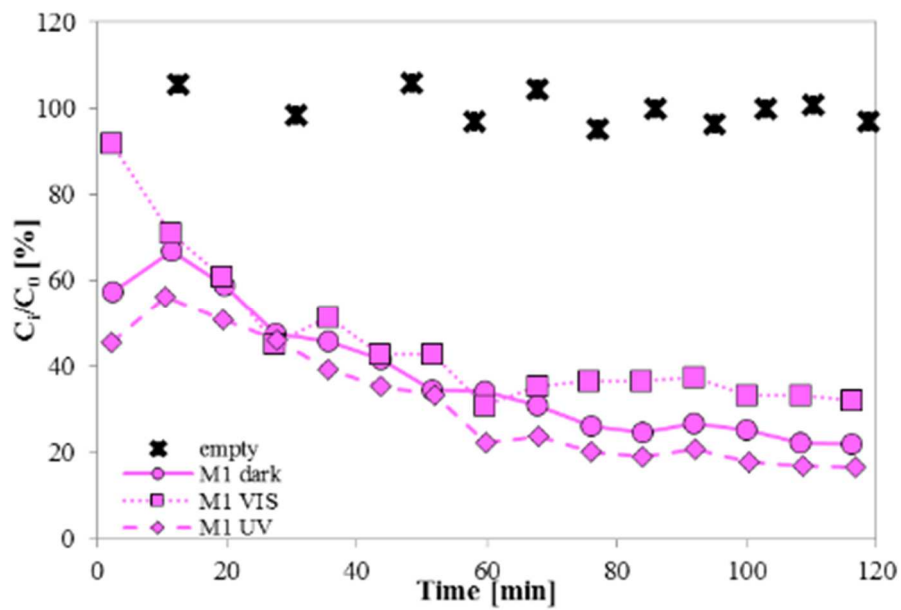
Figure 198 Depollution capacity at different test condition of M1
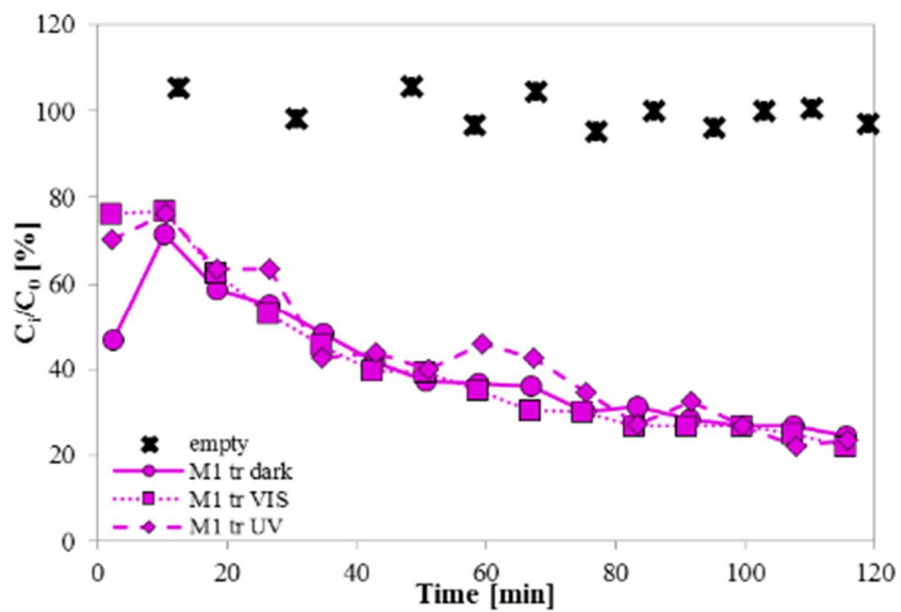
Figure 199 Depollution capacity at different test condition of M1 tr
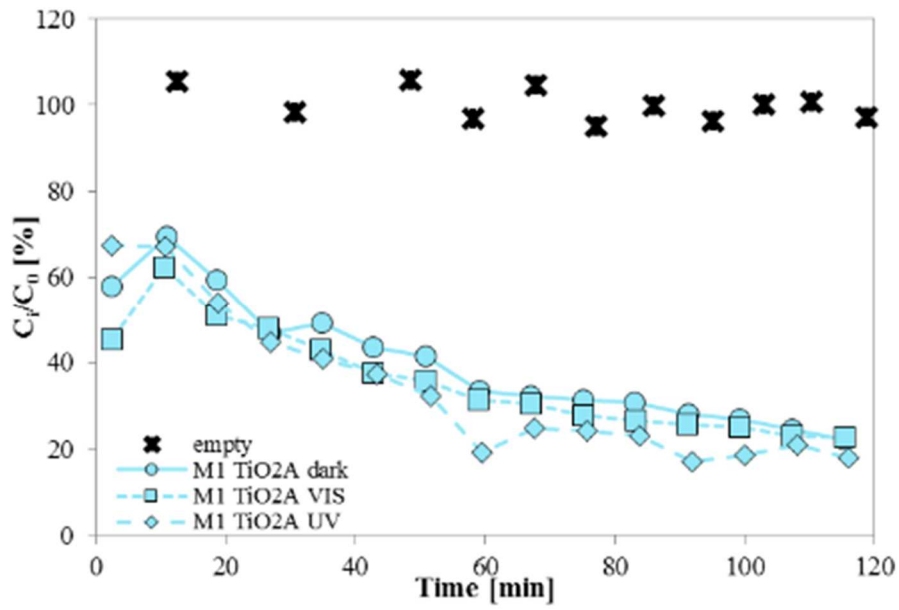
Figure 200 Depollution capacity at different test condition of M1 TiO2A
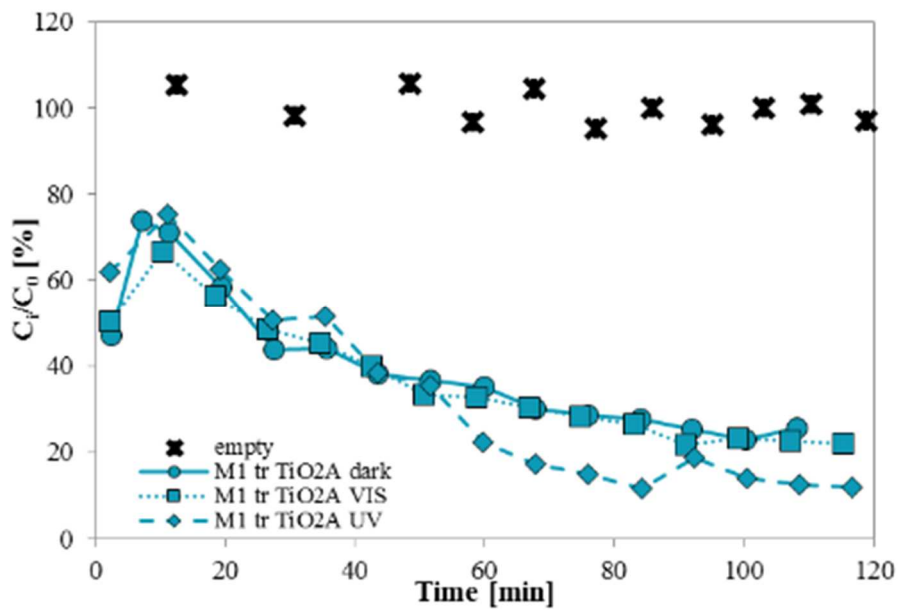
Figure 201 Depollution capacity at different test condition of M1 tr TiO2A
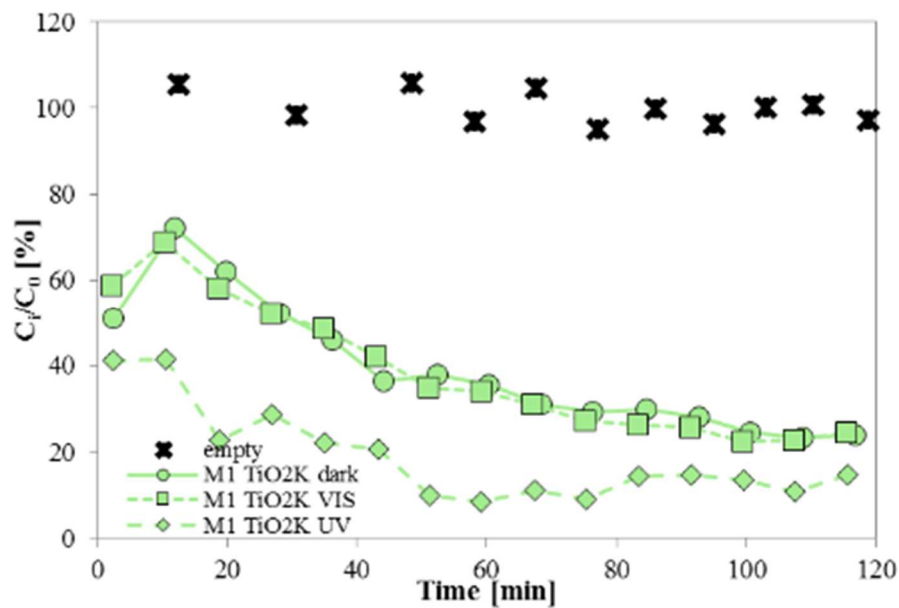
Figure 202 Depollution capacity at different test condition of M1 TiO2K
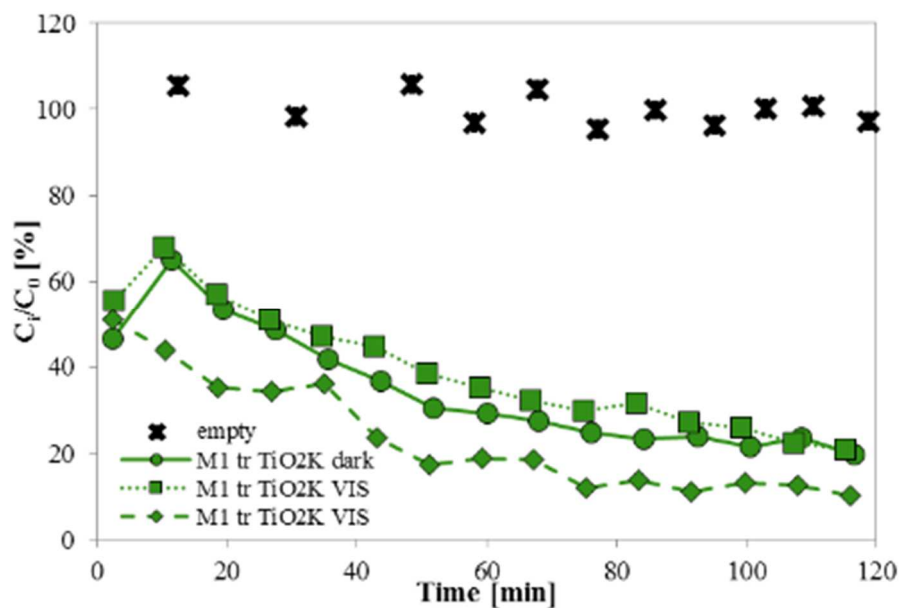
Figure 203 Depollution capacity at different test condition of M1 tr TiO2K

Commercial product KER and MAR have 20% higher and 20% lower depolluting properties than reference mortars, respectively.

Unconventional mortars show a depolluting ability about 40% higher than those of reference mortars. After 2 hours of test, with these materials the residual MEK in the box is only 20% [26].

The addition of TiO_2 does not influence the depolluting capacity in dark condition. Under visible light the positive influence of TiO_2 KRONOClean (which is commercialized as having depolluting properties under visible light) is not detected. P-25 TiO_2 seems to give a slight (of about 4%) enhancement of depolluting capacity under visible light. Depolluting capacity is increased of about 40% and the residual

concentration passes from 20 - 22% to 14 - 7% in case of M1 TiO2A and M1 tr TiO2A and 21 - 19% to 8 - 9% in case of M1 TiO2K and M1 tr TiO2K.

UVA radiation increases depolluting capacity thanks to the activation of both TiO_2 agents which give to mortars photocatalytic activity.

Depolluting property is higher in unconventional mortars than conventional ones thanks to the combination of the adsorbent process and the PCO. PCO is enhanced by the distribution of the pores, according to [109] the activity of photocatalyst is enhanced by a high presence of nano-pores, and the high porosity of these specimens allow the absorption of the pollutants in the internal structure of the mortar [34]. In literature is reported that the larger the volume of pores with diameter higher than 80 nm is, the higher the PCO efficiency [35].

During the test, standard and commercial mortars seem to reach saturation conditions, while the unconventional mortars continue to adsorb-decompose the tracer also after many MEK loads as shown in § 4.4.8.
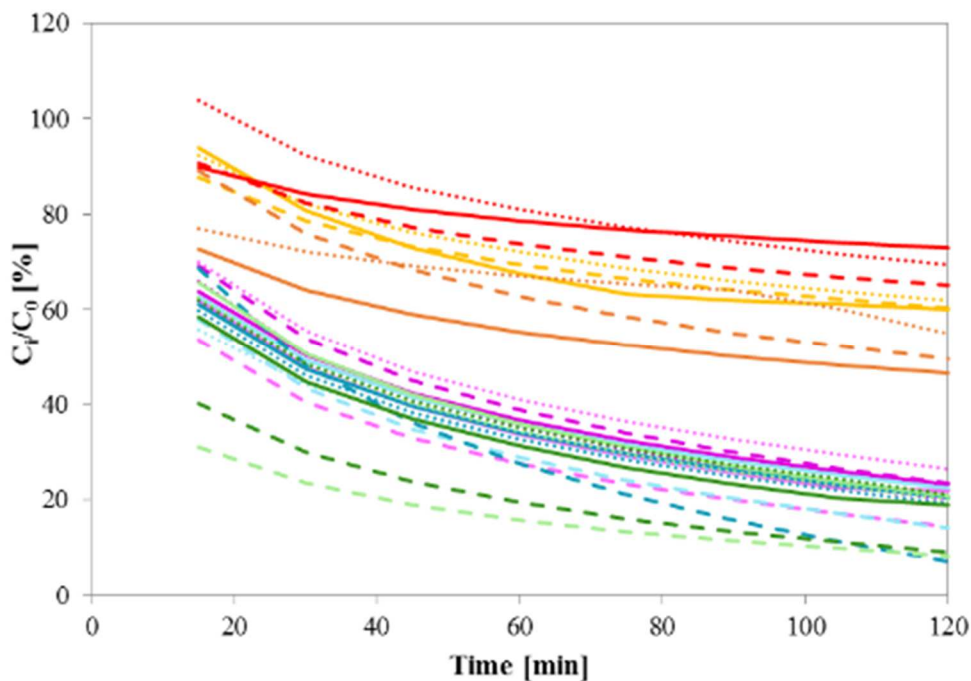
Figure 204 Trend line, legend is in Figure 200
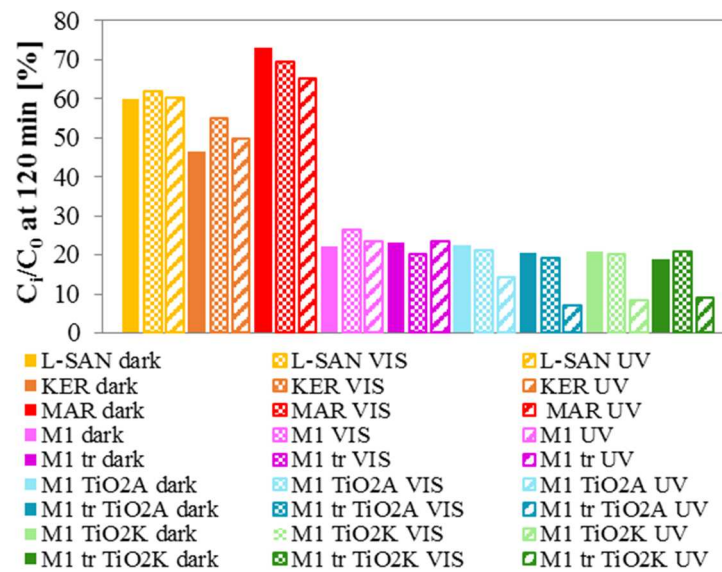
Figure 205 Residual concentration of MEK inside the test box after 120 mins of test

6.4.9. Aesthetic evaluation

Table 27 shows the results obtained from the colorimetric evaluation of mortars. The lightest mortar is reference mortar based on calcareous sand and hydraulic lime. Thermal treatment of biomass permits the removal of darker particles; in fact the mortars with thermal treated biomasses are lighter than that the mortar prepared with as it is biomass ashes.

Commercial products are darker than M1 tr TiO2K. The addition of both TiO_2 permits to obtain lighter mortar.

Table 27 Colorimetric evaluation of different mortars. Results are listed from darker to lighter mortar

Mix		RGB coordinates detected						Color average	Picture example
		1	2	3	4	5	average		
M1	R	193	185	185	184	184	186		
	G	186	178	178	177	178	179		
	B	167	159	159	158	152	159		
M1-TiO2A	R	197	206	187	192	184	193		
	G	193	198	181	186	177	187		
	B	174	178	161	165	158	167		
M1 TiO2K	R	190	198	203	188	198	195		
	G	188	191	196	179	188	188		
	B	164	170	170	162	165	166		
MAR	R	203	204	212	203	203	205		
	G	182	182	186	183	181	183		
	B	150	145	148	146	147	147		
M1 tr	R	205	209	210	206	205	207		
	G	199	196	193	195	198	196		
	B	174	168	162	169	171	169		
M1 tr TiO2A	R	205	212	203	209	199	206		
	G	197	206	192	201	184	196		
	B	187	178	172	175	152	173		

KER	R	210	212	217	216	209	213	
	G	193	196	200	204	187	196	
	B	164	170	165	169	161	166	
M1 tr TiO2K	R	211	214	215	209	222	214	
	G	205	202	205	204	206	204	
	B	187	176	176	179	181	180	
L-SAN	R	225	222	221	215	224	221	
	G	218	218	212	208	220	215	
	B	201	193	190	184	202	194	

6.5. Conclusions

In conclusions, the results of this experimentation can be summarized as:

- Unconventional, traditional and commercial mortars have the same stiff workability.
- Unconventional mortars have 5% lower mechanical resistance than traditional one. In general, thermal treated biomasses improve the mortars mechanical due to a lower content in organic matter. However, the values of mechanical properties are still acceptable. Mortar with sand has the highest value of compressive strength. Commercial products show a decrease in mechanical strength of about 5% and 55% for MAR and KER respectively.
- Unconventional mortars, regardless of thermal treatment and TiO_2 agents, are classified as lightweight mortars while density is lower than 1.3 g/m^3. Density is decreased of about 30% compared to reference mortar.
- Unconventional mortars, regardless of thermal treatment and TiO_2 agents, have the highest value of porosity, 20% higher than sand based mortars. The distribution is bi-tri modal with an increase of low diameter pores.
- Unconventional mortars have shrinkage values around 4 mm/m after 60 days of test, 4 times higher than the reference. Mortars with conventional aggregates have the lowest value of shrinkage. KER has 8 times higher value of shrinkage than reference mortar and MAR has double value of free shrinkage than reference mortar
- Unconventional mortars have at least 20% higher water absorption compared to reference mortar. Commercially available mortars have the lowest absorption capacity, probably due to a hydrophobic admixture;
- Unconventional mortars, with and without thermal treatment, have the lowest value of water vapor resistance factor, around 10, 40% lower than that of reference mortars.
- Unconventional mortars have at least double MBVs than reference mortar. MBVs for reference mortar and commercial ones are very close between them.
- Unconventional mortars increase the depolluting capacity of reference mortar of about 40%, and of commercial products of more than 40% than reference mortar.

It is important to point out that the effectiveness of TiO_2 under visible light, even if the product is commercialized as active under visible light, has not been detected.

In conclusion, the unconventional based mortars characterized in this chapter fulfill all requirements for indoor application mortar. There is an improvement in terms of IAQ, regulation of humidity and airborne pollutants removal.

They potentially have high sustainability, thanks to the use of hydraulic lime and biomasses waste instead of conventional aggregates, despite the use of titanium dioxide that have high impact on environment [110]. Moreover, the additional functionalities of finishes could decrease the environmental impact of construction materials [111].

The thermal treatment of ashes does not imply significant differences in terms of enhancement of properties so, due to the high energy involved, it is decided to develop un-treated ashes based mortars.

Lightweight characteristics are an optimum feature for non-structural materials and high permeability gives to the mortars high transpirability.

As a future development, it is essential to find a titanium dioxide agent able to be active in the mortar mixes not only under UVA radiation but also under visible light. The study of long term performances such as saturation behaviour are also important in order to complete the study of these mortars. The influence of mold growth on mortars can be studied also considering the influence of a biocide. Those complementary developments would be explored in further studies and researches.

Chapter 7

7. Lightweight photocatalytic mortars for indoor air quality enhancement

7.1. Introduction

For researchers and industries, it is becoming mandatory to pay attention on comfort and health of indoor environment occupants. PCO can represent an optimum option to provide healthier indoor environments. The application of nanotechnology in construction materials can play an important role in the quality of the building itself [15]. It is of interest the study of alternative binders as the partial substitution of Ordinary Portland Cement (OPC) with by-products, in order to obtain more sustainable materials for indoor applications, that can be used not only for new buildings but also for rehabilitation purpose of old constructions [34] (only few studies are about lime based mortars).

In this chapter the aim of the research is to develop a new material, with different binders and lightweight aggregates, able to fulfill the conventional requirements of mortars for finishes and also to improve IAQ and comfort of occupants. This performance-based design takes into account an accurate selection of raw materials, under a sustainability point of view. Mortars are studied in terms of fresh state properties, mechanical properties, microstructure, durability in terms of capillary water absorption and PCO ability.

This experimental part has been developed at Eindhoven University of Technology, Eindhoven, Netherlands, under the supervision of prof.dr.ir. H.J.H. Brouwers and dr. Q. Yu.

7.2. Materials

The binders are cement by ENCI, CEM I 42.5 N as described in § 2.2.2.1 and natural hydraulic lime NHL 3.5 (NHL) provided by KIEM (described in § 2.2.2.2). 50% volume of these binders is substituted with class F fly ash (FA) as pozzolanic addition (§ 2.2.3.1).

Two different types of lightweight aggregates are used at the same volumetric content: expanded glass (EG) and natural expanded silicates (ES) (described in § 2.2.4.7).

The PCO is permitted by the addition of TiO_2 in form of slurry during the mortar preparation, KRONOClean 7404 (§ 2.2.3.3). It is added to 70% of the mixing water in

184

order to guarantee the best TiO_2 dispersion in mortars. Zeolite powder replaces 1% of volume of binder to improve the PCO reaction enhancing the absorption phase [112]. BET specific surface of zeolite powder is measured and the value is 28.56 m²/g

7.2.1. Mix design and proportions

7.2.1.1. Proportioning methodology

A good balance between properties that can guarantee IAQ and mechanical behavior [113] is one of the targets required in this experimentation. In order to reach this objective, the maximum packaging theory is adopted. Powders (cement or natural hydraulic lime and fly ash) are combined with aggregates in order to obtain the best granulometric size distribution from the original method developed by Andreasen and Andersen [114]. The following equation represents this modified model [115]:

$$P(D) = \frac{D^q - D^q_{min}}{D^q_{max} - D^q_{min}} \, [\%]$$

Where:
P(D) is the fraction of total solid (binders, powders and aggregates) for the mixture;
D_{min} and D_{max} are respectively the minimum and the maximum diameter of the distribution.
For this experimentation, D_{max} is chosen at 1 mm, suitable for mortars for indoor applications.
The optimized curve is based on Least Square Method (LSM) [116], [117]:

$$RSS = \sum_{i=1}^{n} \left[P_{mix}\left(D_i^{i+1}\right) - P_{tar}\left(D_i^{i+1}\right) \right]^2 \, [\text{-}]$$

Where:
P_{mix} is the composed mixture, %;
P_{tar} (D_i^{i+1}) is the calculated target curve, %.
Variables in equation of P(D) are the respective proportion of the solid material:

$$\varphi_{solid,k} = \frac{V_{solid,k}}{\sum_{k=1}^{m} V_{solid,k}} \, [\text{-}]$$

Where:
$\varphi_{solid,k}$ is the individual volumetric proportion;
$V_{solid,k}$ is the volume of each solid material, in m³.
The total volume of the mixture (1 m³) is the sum of the volume of all the components:

$$V_{tot} = V_{water} + V_{air} + V_{binder} + V_{aggrerates} \, [\text{m}^3]$$

Where:
V_{water} is the total volume of air, calculated from w/b, in m³;

V_{air} is the total volume of air, evaluated as 4%.

V_{binder} is the total volume of the binder powders, in m^3;

$V_{aggregates}$ is the total volume of aggregates, in m^3

The volume of binder is for half composed by cement or natural hydraulic lime and the other half by fly ash.

7.2.1.2.   Mixes

For the preparation of different mixes the w/b and the maximum cement content are fixed. The amount of water is kept constant for all the mixes. Maximum diameter of aggregates (D_{max}) is 1000 µm. The distribution modulus q is very variable, previous results [118] suggested a q value of 0.5. From these conditions, it is possible to evaluate the different fractions of materials.

Binder, in 1 m^3 volume of mortar, is 0.191 m^3, where:

- Cement: (CEM I 42.5 N) = 270 kg/m^3;
- Fly Ash: $270*(\rho_{FA}/\rho_{cem})$ = 201 kg/m^3;
- Natural Hydraulic Lime: $270*(\rho_{NHL}/\rho_{cem})$ = 219 kg/m^3.

w/b = 0.55 by weight for a reference mortar where binder is considered 50% of volume of cement and 50% of volume of limestone. For 1 m^3 the water volume is 0.275 m^3, w = 275 kg/m^3.

Taking into account previous consideration, lightweight aggregates are 0.513 m^3 in 1 m^3 of mortar. The volume of aggregates has to be divided in three different fractions. Following figure and table report the mixes (Table 28, Table 29 and Figure 206).

Table 28 Mortars prepared. Summary of different combinations

Binder	Aggregate	Code ID	Code Color
Ordinary Portland Cement and Fly Ash	Expanded silicates	CEM-ES	
Ordinary Portland Cement and Fly Ash	Expanded glass	CEM-EG	
Natural Hydraulic Lime and Fly Ash	Expanded silicates	NHL-ES	
Natural Hydraulic Lime and Fly Ash	Expanded glass	NHL-EG	

a) Cem-FA and expanded silicates

A&A q 0.5 — Optimized mix
CEM I 42.5R — Fly Ash
Rotocel 0.90-0.30 — Rotocel 0.25-0.5
Rotocel 0.5-1

b) Cem-FA and expanded glass

A&A q 0.5 — Optimized mix
CEM I 42.5R — Fly Ash
Liaver 0.1-0.3 — Liaver 0.25-0.5
Liaver 0.5-1

c) **NHL-FA and expanded silicates**

d) **NHL-FA and expanded glass**
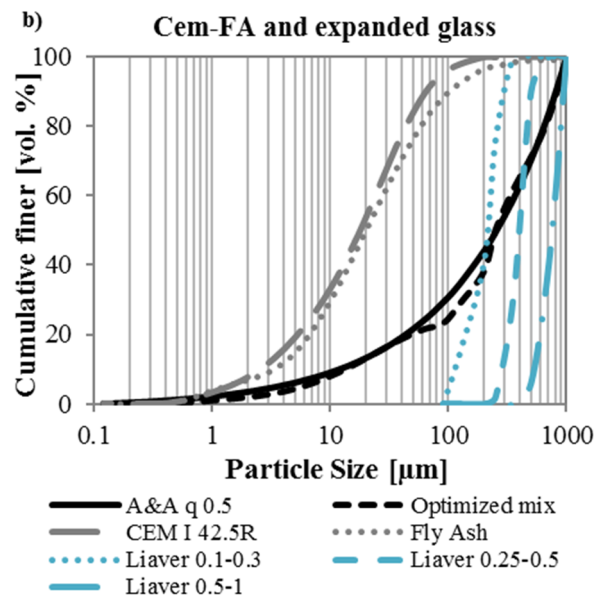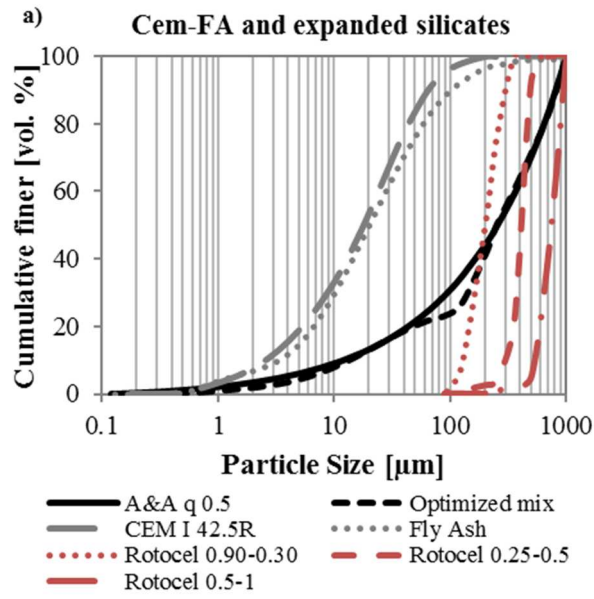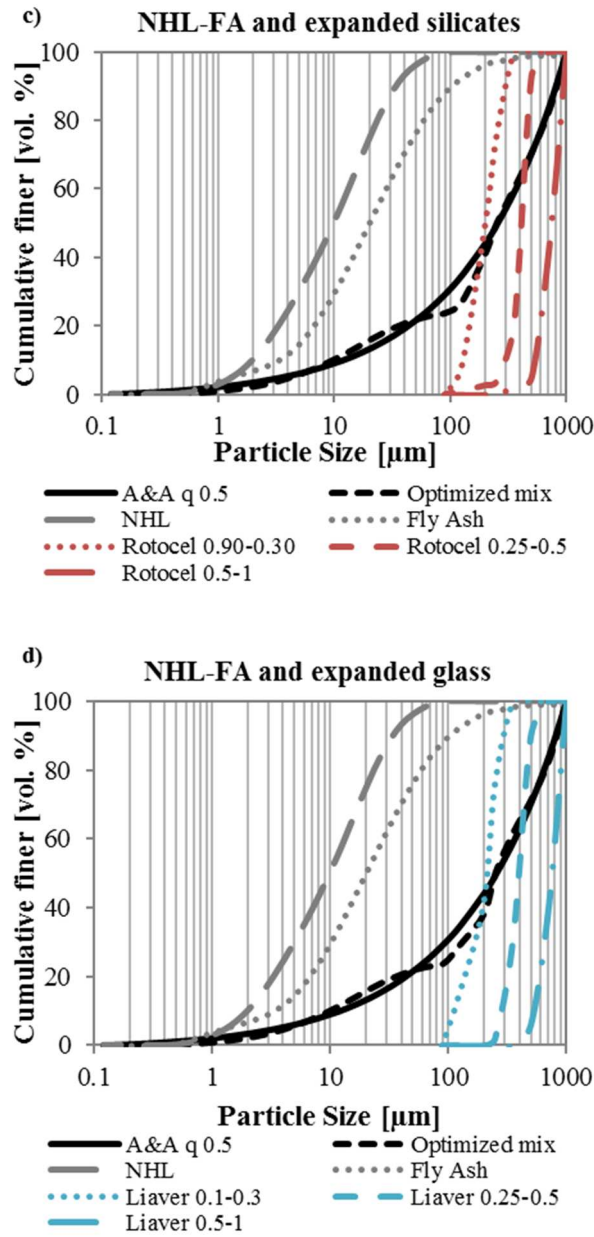
Figure 206 PSDs of the involved ingredients, the target A&A curves and the resulting optimized mix for each mortar mix a) CEM-ES, b) CEM-EG, c) NHL-ES, d) NHL-EG

Table 29 Composition of mixes designed applying mix design concept.
Quantities of materials in kg/m³

	CEM-ES	CEM-EG	NHL-ES	NHL-EG
q	0.5	0.5	0.5	0.5
w/b (by weight)	0.58	0.58	0.64	0.64
w/b (by volume)	1.60	1.60	1.60	1.60
Cement	270.0	270.0	-	-
Fly Ash	201.0	201.0	201.0	201.0

Natural Hydraulic Lime	-	-	219.0	219.0
Water	275.0	275.0	275.0	275.0
Rotocel® 0.09-0.3	154.3	-	154.3	-
Rotocel® 0.25-0.5	64.6	-	64.6	-
Rotocel® 0.5-1	120.0	-	120.0	-
Liaver® 0.1-0.3	-	180.5	-	180.5
Liaver® 0.25-0.5	-	47.1	-	47.1
Liaver® 0.5-1	-	90.0	-	90.0

Reference mortars are usually prepared with normal sand with grain size d_{max} of 2 or 4 mm. The purpose of this research is finding mortars suitable to be the finish layer for indoor applications. For this reason, it is decided to use aggregates with maximum diameter less than 1 mm.

Figure 207 compares the grain size distribution of normal sand and the curves of Rotocel® and Liaver® (the used lightweight aggregates). The normal sand grain size distribution curve presents higher slope compared to that of lightweight aggregates, due to the higher d_{max} of normal sand. As regards the distributions of two lightweight aggregates, it is important to note that they are very close: percentages of the different fractions result be the same.
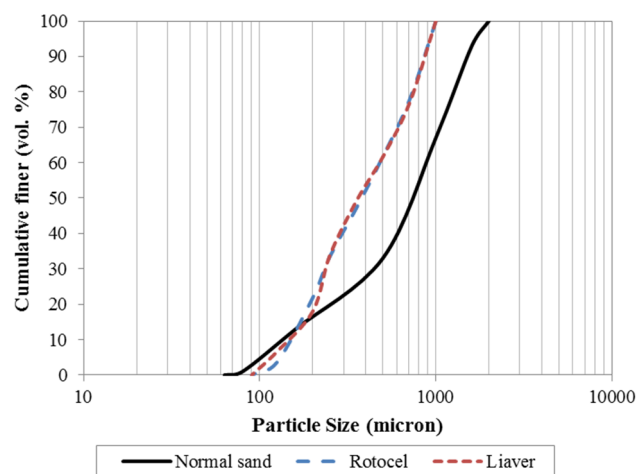
Figure 207 Comparison between PSDs of sand with 2 mm maximum diameter and lightweight aggregate.

The appropriate volume required for casting is evaluated according to the different tests that are performed. Aggregates are added in dry conditions to maintain the same water content.

To test PCO efficiency, TiO_2 photocatalyst is added as slurry during the mortar preparation. TiO_2 is substituted in 2 different quantities, 2% and 4% of binder volume. Zeolite is substituted during the preparation of mortars as 1% of binder volume to improve the PCO reaction enhancing the absorption phase. Mix design quantities are reported in Table 30.

	CEM-ES-2	CEM-ES-4	CEM-EG-2	CEM-EG-4	NHL-ES-2	NHL-ES-4	NHL-EG-2	NHL-EG-4
q	0.5	0.5	0.5	0.5	0.5	0.5	0.5	0.5
w/b (by weight)	0.60	0.61	0.60	0.61	0.68	0.69	0.68	0.69
w/b (by volume)	1.6	1.6	1.6	1.6	1.6	1.6	1.6	1.6
Cement	262.1	256.7	262.1	256.7	0	0	0	0
Fly Ash	195.3	191.3	195.3	191.3	195.3	191.3	195.3	191.3
Natural Hydraulic Lime	0	0	0	0	212.0	207.6	212.0	207.6
Water	256.9	238.8	256.9	238.8	256.9	238.8	256.9	238.8
Rotocel® 0.09-0.3	154.3	154.3	0	0	154.3	154.3	0	0
Rotocel® 0.25-0.5	64.6	64.6	0	0	64.6	64.6	0	0
Rotocel® 0.5-1	120	120	0	0	120	120	0	0
Liaver® 0.1-0.3	0	0	180.5	180.5	0	0	180.5	180.5
Liaver® 0.25-0.5	0	0	47.1	47.1	0	0	47.1	47.1
Liaver® 0.5-1	0	0	90	90	0	0	90	90
Slurry TiO2	30.153	60.305	30.153	60.305	30.153	60.305	30.153	60.305
Zeolite	4.056	4.056	4.056	4.056	4.056	4.056	4.056	4.056

Table 30 Mixes

7.3. Methods

Mortars are characterized in terms of fresh state properties. Workability is measured with a flow table, according to the current standards (§ 2.3.1).
After 28 days of curing, flexural and compressive strength are tested. Also, the specific strength is evaluated (§ 2.3.2.1).
Pore size distribution is evaluated by Mercury Intrusion Porosimetry (MIP) and Brunauer-Emmett-Teller (BET) as described in § 2.3.2.2.
Free shrinkage and weight loss due to the water evaporation of mortars are monitored for about 35 days (§ 2.3.2.3).
Water is the medium where ions can be transported and can compromise the durability of building material. Water transport in mortars is evaluated with two different methodologies (§ 2.3.3.1 and §2.2.3.1).
The influence of the mortar on the indoor comfort is considered by measuring the thermal conductivity of mortars as suggested in § 2.3.4.3.
PCO capacity test is performed measuring the degradation of NOx, through plug-flow equipment as described in § 2.3.5.3, according to the current standard ISO 22197.

7.4. Results and discussions

7.4.1. Workability

Table 31 shows workability of mortars in terms of slump flow and consistency values.

Table 31 Workability of different mortars: picture of mortar at fresh state after slump flow test, slump flow values and consistency.

Mix	CEM-ES	CEM-EG
Slump (mm)	115	151
Consistency (%)	15	51
Mix	**NHL-ES**	**NHL-EG**
Slump (mm)	111	143
Consistency (%)	11	43
Mix	**CEM-ES-2**	**CEM-ES-4**
Slump (mm)	111	105
Consistency (%)	11	5
Mix	**CEM-EG-2**	**CEM-EG-4**
Slump (mm)	150	133
Consistency (%)	50	33

Mix	**NHL-ES-2**	**NHL-ES-4**
Slump (mm)	109	102
Consistency (%)	9	2
Mix	**NHL-EG-2**	**NHL-EG-4**
Slump (mm)	151	140
Consistency (%)	51	40

All mortars are prepared with the same amount of water and the same volumetric w/b, so fresh properties are influenced only by aggregates and powders contents. In spite of different binders, when expended silicates are used the mortars have the same workability class: stiff with natural expanded silicates, and plastic with expanded glass (classes according to UNI EN 1015-6 [57]). Different values are due to the different shapes of aggregates: the spherical shape of expanded glass allows less friction forces between the aggregates that can flow better. Liaver has round and more regular spheres than Rotocel, which has natural origins and irregular granules shape. This means a higher surface that needs to be wetted by water for the cast.

When NHL is replacing cement, the slump values decrease. This is due to the finer particles present in NHL as shown in Figure 6.
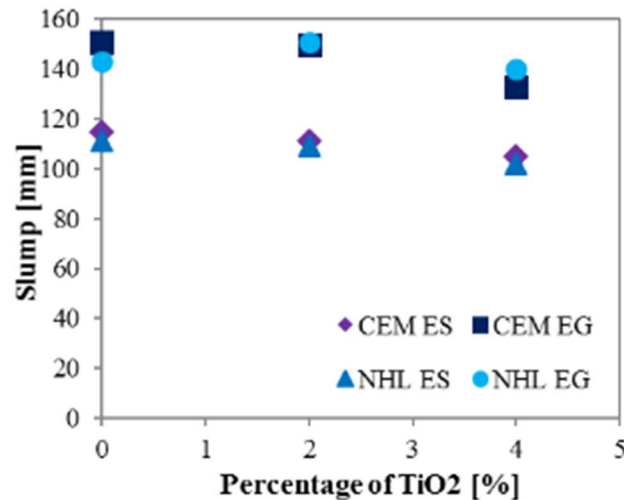
Figure 208 Influence of TiO₂ percentage of on slump flow values of mortars.

As regards to mixes prepared for PCO analysis, same recipes with TiO_2 additions have the same class of workability a part from CEM-EG-4 that passes from plastic to stiff. Generally, the presence of TiO_2 implies loss of workability as previously indicate in literature [15], [119].

Higher percentage of substitution of TiO_2 implies, obviously, higher loss of slump flow value and lower consistency value on TiO_2 mortar. However, mortars generally belong to the same class than that without TiO_2, a part for CEM-EG-4.

In general, 2% of TiO_2 addition does not change the values (or only for negligible values) of slump.

One of the main problems in lightweight mortar or concrete is gravity: the differences in the densities of the binder paste and lightweight aggregates is high and can induce segregation. However, in this experimentation segregation problems are not detected.

7.4.2. Mechanical strength

Figure 208 and Figure 209 show the results in terms of development of flexural and compressive strength during curing time.

As expected, cement based mortars have higher resistance, both flexural and compressive, about three times higher. NHL based mortars need more time to reach acceptable value of mechanical resistance. During time, an increment of mechanical performance, thanks to the beneficial action of fly ash, is expected. However, for indoor finishes the compressive strength should be higher than 3 MPa and this goal is reached for all the different mixes.
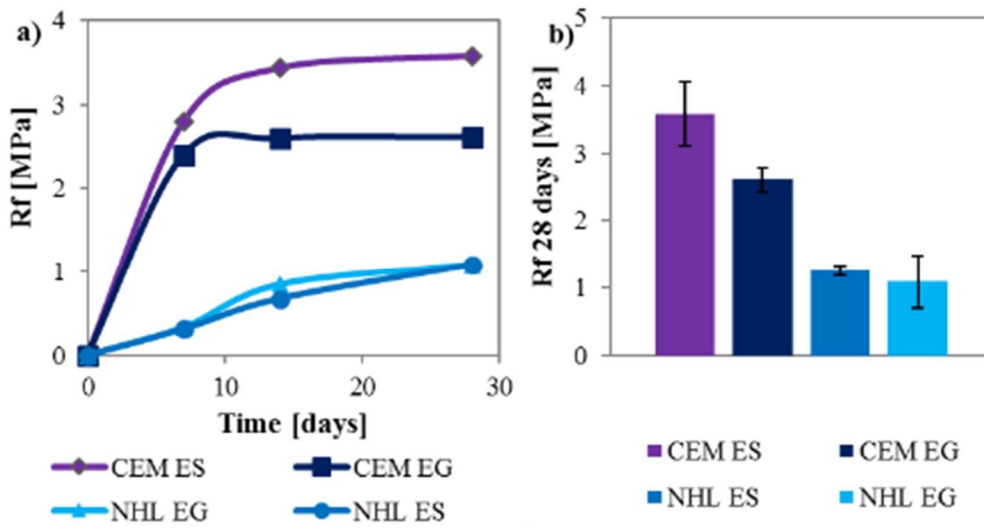
Figure 209 Flexural strength of lightweight mortars. a) development in time b) value at 28 days
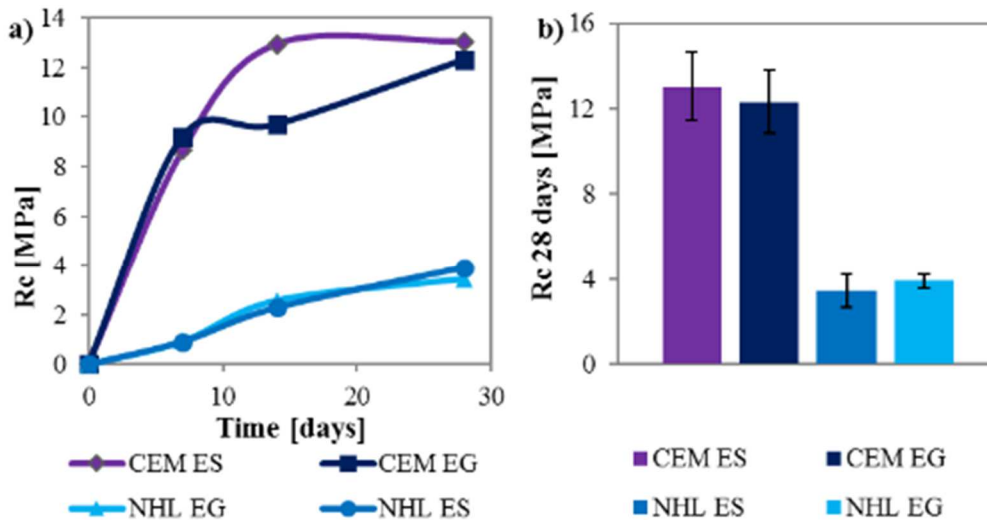
Figure 210 Compressive strength of lightweight mortars. a) development in time b) value at 28 days

According to the current standard UNI EN 998-1:2010 [80], the maximum value of density for indoor mortar to be classified as lightweight is 1300 kg/m^3. Figure 212 shows the results of density values for the different mortars.

Density is evaluated both in fresh and hardened states. All mortars can be classified as lightweight mortars due to low density. This property is influenced by both binders and aggregates.

With the same binder, the expanded glass mortars show less density of natural expanded silicates mortars. With the same aggregate, NHL mortars have less density than cement based mortar.

In case of cement based mortar, water loss is about 24% with expanded silicate and 20% with expanded glass. In case of NHL the percentage of water loss is around 30% for both. This means obviously, that, in case of cement based mortar, water is more reactive to participate in the formation of hydration products as C-S-H gel, after curing cement based mortars have less free water.
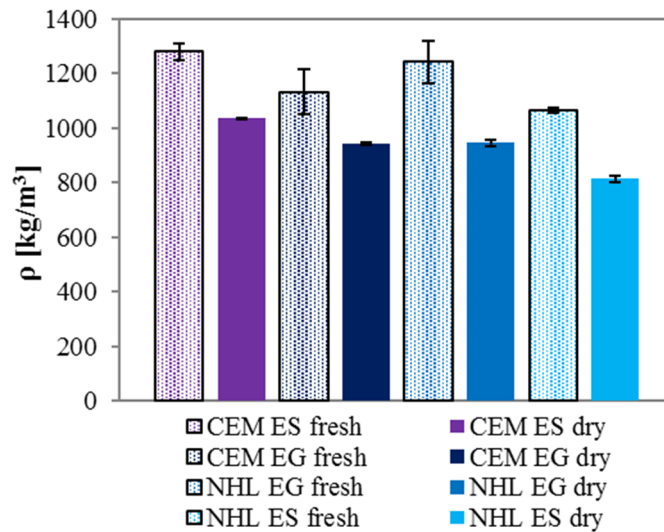
Figure 211 Fresh and hardened density (ρ) of lightweight based mortars

In Figure 212 compressive strength data of cement based mortar are plotted with density. Analogous correlations found in the literature are also reported as comparison [120], [121].
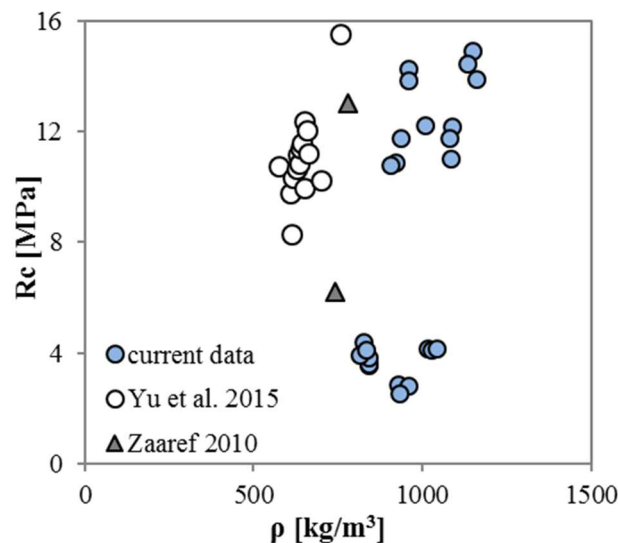
Figure 212 Correlation between mechanical resistance and density. Current data and data from literature [120]*,* [121]

7.4.3. Microstructure of mortars: morphology and pore size distribution analysis

Figure 213 shows the aspect of the different mortars. Mortars have high macro-porosity (diameter of pores of about 1-2 mm). Lime-based mortars have more pores than cementitious mortar.
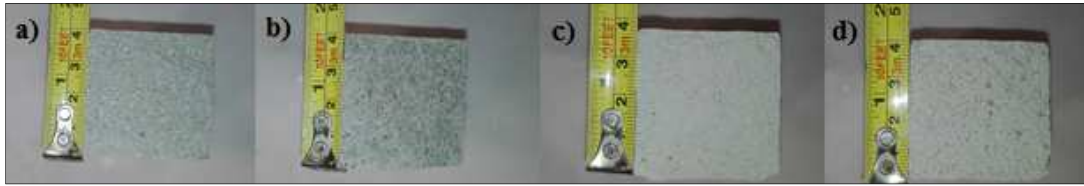
Figure 213 Visive aspect of mortars: a) CEM-ES, b) CEM-EG, c) NHL-ES and d) NHL-EG

Pore distribution curves of lightweight mortars are compared. The pore distributions of mortars are different and influenced by the type of aggregate: natural expanded silicates Rotocel® implies a bimodal distribution and expanded glass, Liaver® a unimodal distribution. Probably this is due to the more regular round shape of Liaver®. Figure 214 shows the results from MIP analysis.

The diameter of modal pore is less than 1 µm for cement-based, CEM ES has 0.0915 µm, CEM EG has 0.3026 µm, and more than 1 µm for NHL based, NHL ES has 1.7058 µm and NHL EG has 1.042 µm.
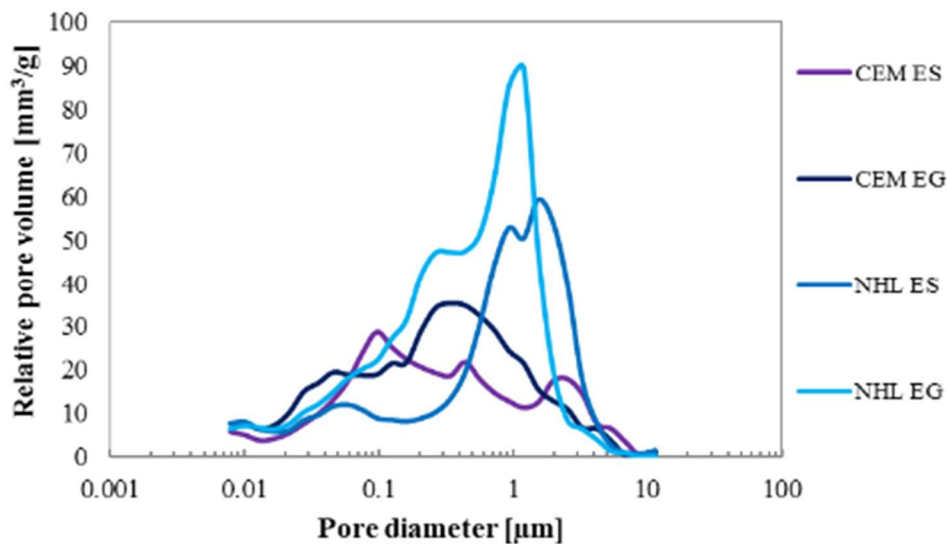
Figure 214 Relative pore volume distribution of different mortars

From the MIP analysis, it is possible to quantify the total amount of open porosity. Results are shown in Figure 215 and Figure 216.

Obviously, lightweight based mortars show a higher total volume pores than cement based mortars, as already discussed (§ 3.4.3) and as found in literature [122].

This is due to the intrinsic porosity of the aggregates and the high w/b ratio. The use of NHL instead of cement as a binder introduces a 10% of total porosity. With the same binder, the use of expanded glass introduces a porosity 5% more than expanded silicates.
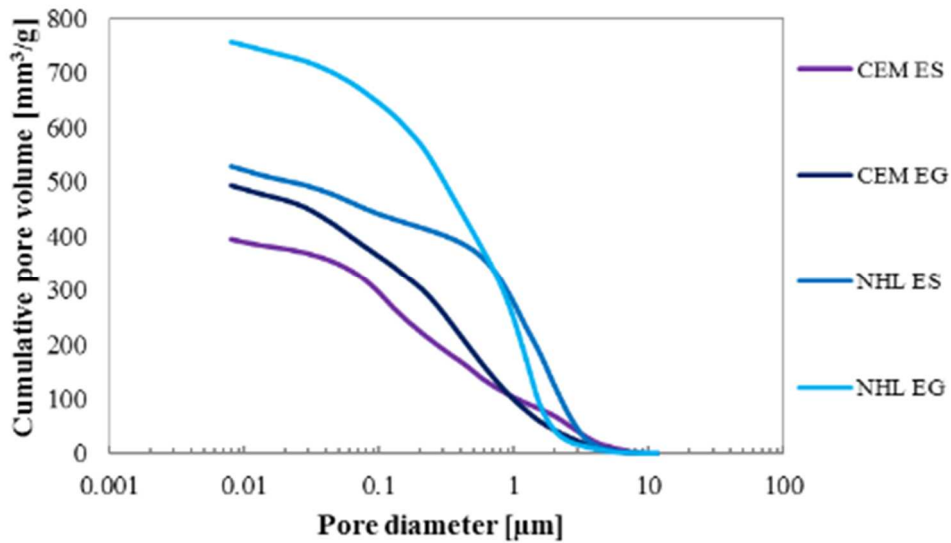
Figure 215 Cumulative pore volume distribution of different lightweight mortar
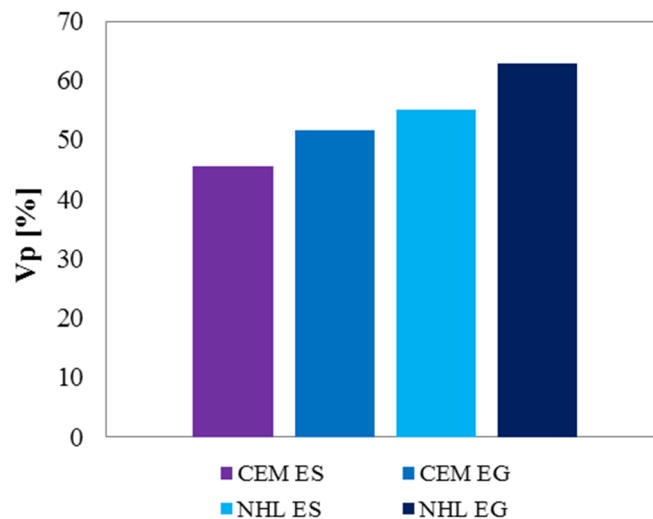
Figure 216 Total porosity of different lightweight mortars

Due to the presence of porosity with small pore diameters in mortars, it is decided to investigate pore size distribution also with BET analysis performed on small pieces of mortars after 28 days of curing. Results are shown in Figure 217.

The pores of cement based mortars are more concentrated in smaller diameters assimilated to gel porosity. For NHL based mortars the peaks are around 100 nm.
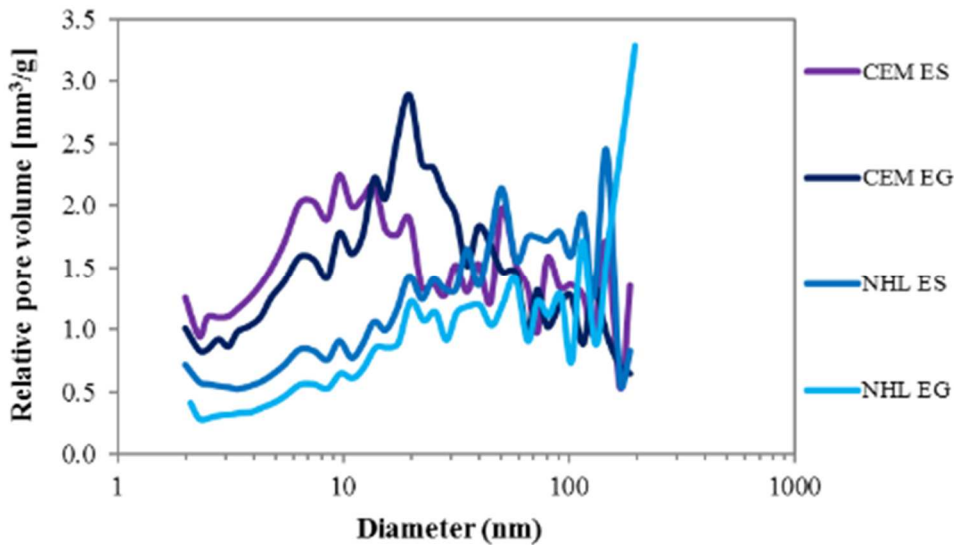
Figure 217 Pore distribution of mortars from BET analysis

7.4.4. Shrinkage measurement

Drying shrinkage is measured for 35 days at 60% RH at T 20 °C.
Data of shrinkage are shown in Figure 218 and Figure 219. At 35 days values of shrinkage are: 0.83 mm/m for CEM EG, 1.01 mm/m for CEM ES, 3.43 mm/m for NHL EG and 3.03 mm/m for NHL ES.
Natural hydraulic lime based mortars show higher value of shrinkage than that detected in cement based mortars. This is related to the low mechanical resistance of lime mortars after 24 hours from the cast. Moreover, the loss of mass due to water evaporation is higher in lime than in cement based mortars. The correlation between mass loss and shrinkage value is present, as confirmed in Figure 221.
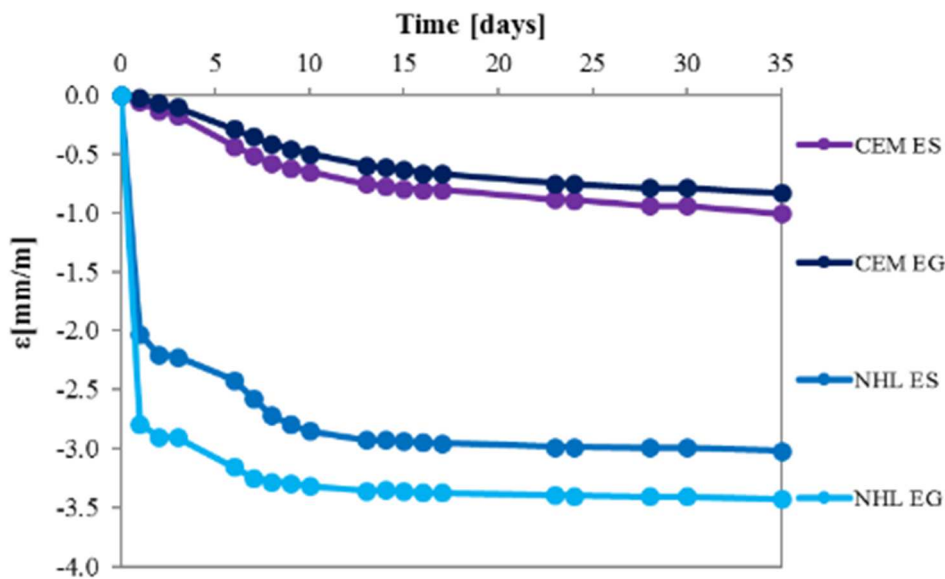
Figure 218 Drying shrinkage of mortars at RH = 60% and T =20 °C
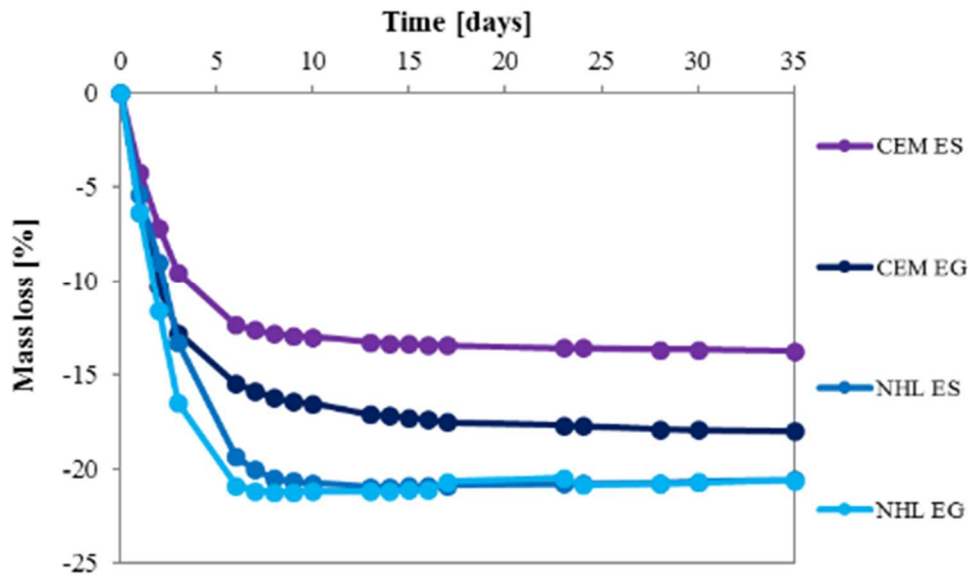
Figure 219 Water evaporation during drying shrinkage of mortars at RH = 60% and T =20 °C
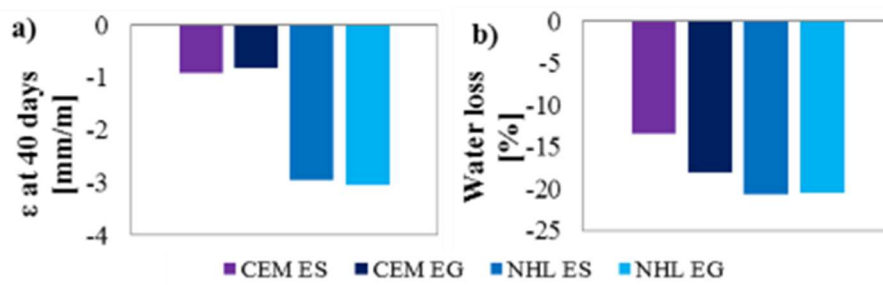
Figure 220 Drying shrinkage of mortars at 35 days a) differences in length and b) water loss.
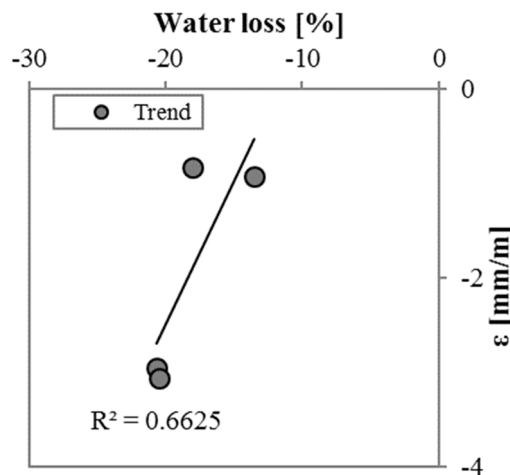
Figure 221 Correlation between shrinkage values and water loss of the mortars

Shrinkage of mortars is related to the dimension of mortar pores: the lower the pore radius, the higher the induced stress [61] following Laplace equation (§ 2.3.2.3). Figure 222 shows the relation between the shrinkage values and the total volume of

pores, the higher is porosity and the higher is the shrinkage of mortars. In fact, shrinkage is also depending on the elastic modulus (Ec) of mortars, the higher is Ec and the lower is the shrinkage.
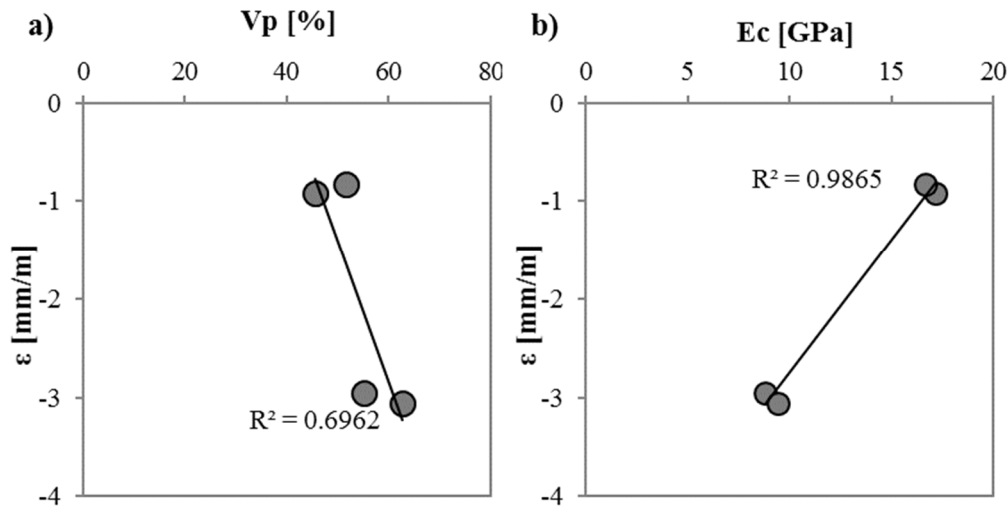
Figure 222 Correlations between shrinkage value at 35 days and a) total volume of porosity and b) elastic modulus

7.4.5. Capillary water absorption

Before testing, mortars are dried completely in a ventilated oven at 80 °C.
Capillary water absorption follows due to Washburn equation [45]. This property is highly influenced by the binder [26].
Capillary water absorption coefficient of mortars is evaluated according to the Italian standard UNI EN 1015-18 [65]. Figure 223 shows the results.
Water is absorbed at first in bigger pores and then in capillary pores.
NHL mortar present pores with higher diameter than cement based mortar and this explains the three and four times higher values of C in case of NHL based mortar. Another reason is the percentage of accessible porosity, the higher is the porosity and the higher is the value of the coefficient (Figure 224).
As regards the aggregates, expanded glass based mortar has higher values of absorption coefficient compared to natural silicate.
In presence of cement, the coefficient is higher for about 20%, with NHL is up to 35% higher (percentages are referred to expanded silica and expanded glass based mortar). All mortars belong to W0 mortars, according to UNI EN 998-1:2010 [80] a part from CEM ES that belongs to W1.
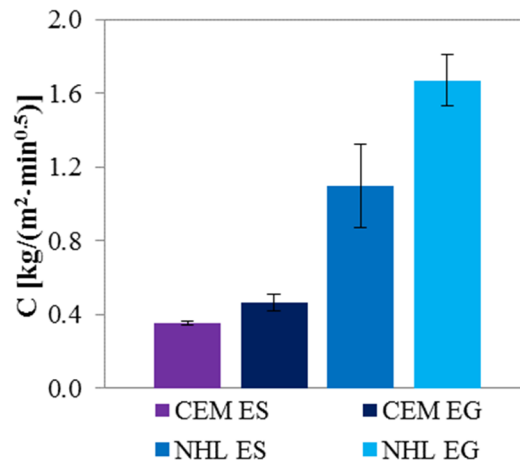
Figure 223 Capillary water absorption coefficient of lightweight mortars according to UNI EN 1015-18.
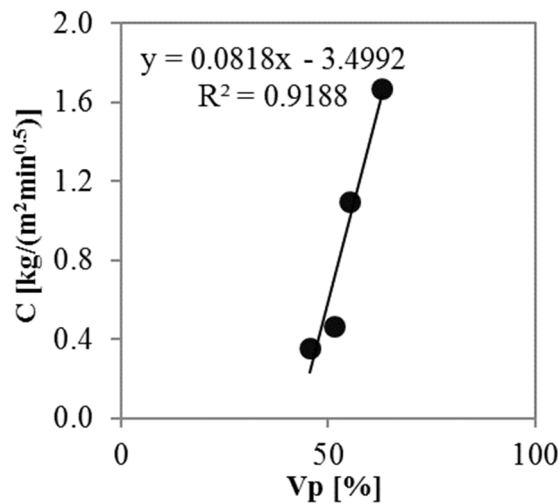
Figure 224 Linear correlation between capillary water absorption coefficient and porosity

UNI EN 15801[66] test results are shown in Figure 225.

In this case, the total amount of porosity is also more influential than the dimension of pores itself. In fact, the results obtained with longer exposure to water confirm the results obtained with the shorter contact.

NHL EG has the highest amount of porosity, 60% higher than CEM ES and has consequently the highest amount of water trapped in. In case of cement, the water absorption is 15% higher in Liaver® than in Rotocel® lightweight aggregate. The different response with the same aggregate can be due to the shape: Liaver® is round shape and Rotocel® is more irregular and this implies a high tortuosity for the water path [123].
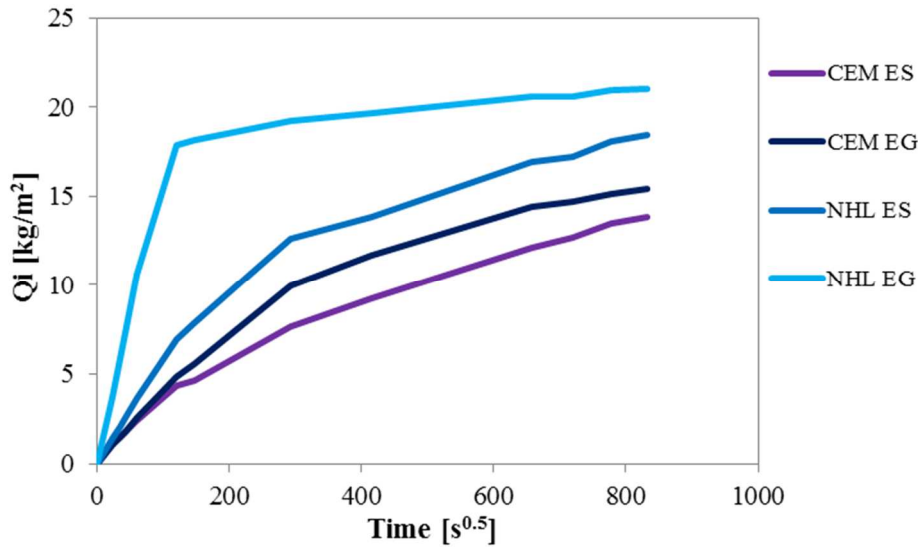
Figure 225 Capillary water absorption in time of lightweight mortars

7.4.6. Thermal properties

Thermal properties are studied in terms of thermal conductivity. In order to evaluate the influence of RH on thermal insulation properties of mortars, measurements are carry out at dry condition and at 60% RH. Results are shown in Table 31. However, there are no great changes in thermal transmittance measured in different RH values. Due to the small difference in data, it is decided to compare only thermal conductivity at dry conditions. CEM ES has the highest value of thermal conductivity, 0.22 W/mK. CEM EG has a value 15% less. If NHL based mortars are considered, NHL ES and NHL EG have 30% and 40% less thermal conductivity values compared to the same aggregate but with different binder respectively, with corresponding values of 0.18 and 0.15 W/mK.

Table 32 Thermal properties of analyzed mortar (at T=20 °C)

	Dry condition		60% RH condition		moisture uptake
	W	cp	W	cp	
	W/(mK)	J/(m^{3}K)10^6	W/(mK)	J/(m^{3}K)10^6	%
Mix C	0.25	1.25	0.25	1.33	2.0
Mix D	0.22	1.14	0.22	1.18	1.1
Mix I	0.18	1.06	0.18	1.05	1.8
Mix J	0.15	0.88	0.15	0.92	2.0

As expected, when density increases, thermal conductivity increases. There is a linear correlation between dry density and thermal conductivity as shown in Figure 226, as already found in another study [124].

Thermal conductivity is proportional to the total porosity [125] as shown in Figure 226. In this case the behavior is related to the porosity of the aggregate Liaver®. The porosity is not connected, and with the selection of appropriate construction materials [126] it is possible to obtain an increase in terms of thermal insulation properties
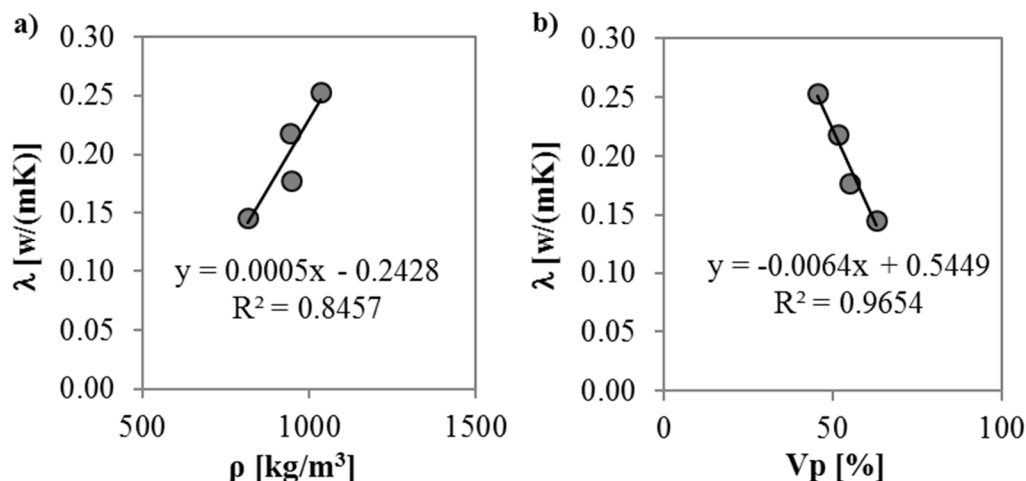
Figure 226 Correlation between a) thermal conductivity and density and b) thermal conductivity and percentage of volume of pores

7.4.7. NOx removal

The addition of TiO_2 gives to mortar photocatalytic properties. The Langmuir Hinshelwood model is used to interpret the data. Flow can be assimilated as a laminar flow. Results and test conditions are reported in Table 33.

Table 33 Tests conditions and NOx conversion rate

	Light source	E	Q	RH	NOx in	Conversion rate
	-	w/m^2	L/min	%	ppm	%
CEM ES 2%	VIS	10	3	50	1	2.8
CEM ES 2%	UVA	10	3	50	1	33.5
CEM ES 2%	VIS	10	1.5	50	0.5	11.6
CEM ES 4%	VIS	10	3	50	1	4.4
CEM ES 4%	UVA	10	3	50	1	42.1
CEM ES 4%	VIS	10	1.5	50	0.5	13.8
CEM EG 2%	VIS	10	3	50	1	3.2
CEM EG 2%	UVA	10	3	50	1	28.6
CEM EG 2%	VIS	10	1.5	50	0.5	10.9
CEM EG 4%	VIS	10	3	50	1	3.9
CEM EG 4%	UVA	10	3	50	1	35.0
CEM EG 4%	VIS	10	1.5	50	0.5	17.7
NHL ES 2%	VIS	10	1.5	50	0.5	27.6
NHL ES 4%	VIS	10	1.5	50	0.5	14.3

| **NHL EG 2%** | VIS | 10 | 1.5 | 50 | 0.5 | 25.6 |
| **NHL EG 4%** | VIS | 10 | 1.5 | 50 | 0.5 | 45.9 |

Figure 227 shows the content of TiO_2 in cement based mortars and the efficiency under UVA radiation. The flux is 3 l/min and with the concentration of 1 ppm of NO_x in, it is evident how higher amount of TiO_2 means higher PCO properties. The increase of efficiency from 2% to 4% TiO_2 content is 20% for both aggregates. In general, the use or Rotocel® instead of Liaver® permits an increase in performances of about 15%.
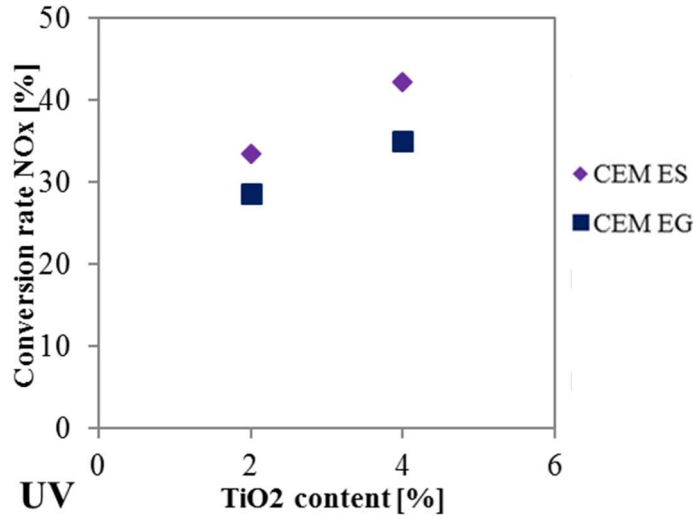
Figure 227 Test results performed under UVA radiation

Results obtained with visible light- VIS (flux of 1.5 l/min and concentration of 0.5 ppm in NO_x in) for cementitious mortars show (Figure 228) an obviously decrease, but still acceptable, depollution properties, of about 65% for Rotocel® based mortar. The decrease is less for Liaver® cement mortar: in case of 2% TiO_2 is about 60% and in case of 4% TiO_2 is 50% less compared to that under UVA radiation. With a double amount of TiO_2, there is an increase in PCO conversion rate in cement mortar of about 15% and 30% for Liaver® with visible or UVA radiation.

In this case Liaver® mortar has three times higher PCO efficiency than Rotocel® based mortar.

Liaver® mortar shows higher workability than Rotocel® mortar: TiO_2 could result more dispersed in the mixes and consequently on the surface of the mortar.

Cement based mortars finishes result less efficient for PCO properties. NHL-EG based mortar has a 60% higher PCO efficiency than CEM-ES based mortar with the same content of TiO_2 (4%). This can be due to the higher presence of hydration products (gel) that can cover the active sites of titanium dioxide [88].

The most effective depolluting mix results are those with NHL, Liaver® and 4% of TiO_2.

The best behavior of NHL EG with 4% TiO_2 could be related to the porosity of mortar: this mortar has the highest amount of porosity and the highest number of pores around 100 µm (from BET-MIP). This pore size distribution and total porosity that favors the pollutant access into the internal structure of the mortar [34].

Literature also reports the optimum influence of recycled glass cullet that could have the same effect of expanded recycled glass [40].
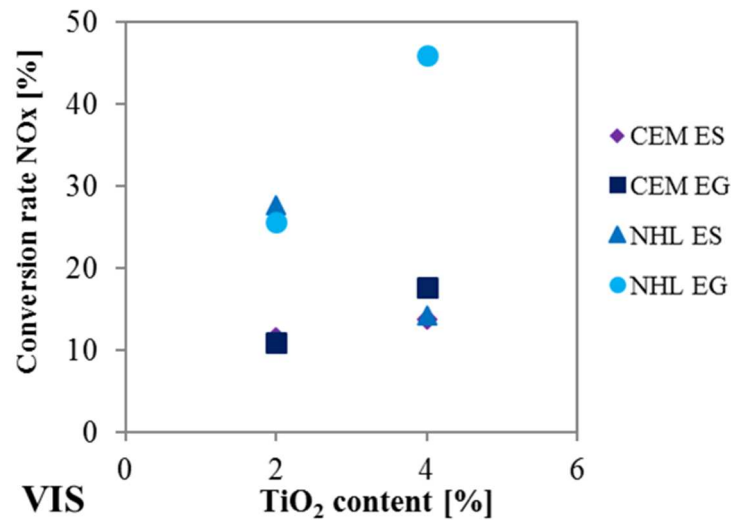
Figure 228 Test results performed under visible radiation

7.5. Conclusions

This chapter assesses the enhancement of IAQ through the use of lightweight building materials.

The research is conducted comparing two different binders, cement and fly ash and natural hydraulic lime and fly ash combined with two different siliceous lightweight aggregates, one natural and the other coming from glass waste. The addition of a carbon-doped TiO_2 catalyst (to be effective in indoor environments) and zeolite add to mortars PCO properties.

Natural hydraulic lime and expanded glass waste mortars represent a good alternative to the traditional one. This mortar implies:

- A decrease of mechanical performances, if compared to cement-based mortars, but still acceptable.
- An increase of thermal properties (not affected by indoor RH levels) with $\lambda = 0.15$ W/mK.
- An increase on the depolluting efficiency with the addition of 4% of TiO_2. Efficiency of mortars is 45%, which is 60% higher than that of cement based mortars at the same percentage of TiO_2.

Chapter 8

8. Conclusions

The current work is aimed to develop innovative multifunctional mortars for finishes able to passively improve IAQ, for the health and comfort of occupants, in terms of permeability, moisture buffering value, depolluting activity and molds growth, besides fulfilling the ordinary requirements.

For this purpose, in new mortars, inorganic binders are used with and without photocatalytic agents. Moreover, conventional sand has been replaced by volume with unconventional aggregates, characterized by high adsorption properties and currently used not in the building sector but in chromatography or filters for water and air depollution.

In case of photocatalytic cement mortars, the substitution of sand with unconventional aggregates implies:
- a decrease up to 80% in mechanical strength;
- an increase up to 50% in lightness;
- an increase up to 200% in capillary water absorption. This can be easily counteracted with a hydrophobic admixture;
- an increase up to 200% in permeability to water vapor;
- an increase up to 60% in moisture buffering capacity;
- an increase up to 80% in depolluting properties (MEK removal).

The substitution of cement with hydraulic lime as binder, with the addition of a TiO_2 photocatalytic powder, implies:
- an increase up to 15% in lightness;
- an increase up to 70% in capillary water absorption;
- an increase up to 65% in water vapor permeability;
- an increase up to 15% in depollution properties.

In order to obtain more sustainable materials, the effect of using biomass wastes in the innovative mortars has also been tested. In hydraulic based mortars, it implies:
- an increase up to 50% in lightness;
- an increase up to 50% of mechanical performance;
- an increase up to 65% in permeability to water vapor;
- an increase up to 200% in moisture buffering ability;

- an increase up to 55% in depolluting properties (MEK removal).

From all the results, the optimized recipe for the innovative multifunctional mortar is based on hydraulic lime as binder, silica gel as unconventional aggregate, and bottom and fly biomass ashes.
This optimized mortar has:

- low density of 1200 kg/m^3, which allows the classification as lightweight;
- satisfactory mechanical strength of 4.5 MPa;
- low water vapor permeability resistance factor of 10;
- high moisture buffering value of 0.6 gr/(m^{2}RH);
- high depolluting capacity: after 120 minutes 80% of MEK removal.

It was expected an increase in depolluting ability under visible light by adding in the innovative mortars TiO$_2$ agents commercialized as active under visible light. On the contrary, this increase has been detected only under UVA radiation, meaning that the adopted TiO$_2$ powders were not activated by visible light, as reported in the data sheets.

Therefore, the optimal mixture shall be further improved by using another photocatalytic agent active under visible light to be introduced in the mixture or applied superficially.

Then, the innovative multifunctional product could be tested on pilot/real scale.

References

[1]   S. Wang, C. Yan, and F. Xiao, "Quantitative energy performance assessment methods for existing buildings," *Energy Build.*, vol. 55, pp. 873–888, 2012.

[2]   A. P. Jones, "Indoor air quality and health," *Atmos. Environ.*, vol. 33, no. 28, pp. 4535–4564, 1999.

[3]   P. Wolkoff, "Indoor air pollutants in office environments: Assessment of comfort, health, and performance," *Int. J. Hyg. Environ. Health*, vol. 216, no. 4, pp. 371–394, 2013.

[4]   C. P. Hoang, K. A. Kinney, and R. L. Corsi, "Ozone removal by green building materials," *Build. Environ.*, vol. 44, no. 8, pp. 1627–1633, 2009.

[5]   S. E. Frey, H. Destaillats, S. Cohn, S. Ahrentzen, and M. P. Fraser, "The effects of an energy efficiency retrofit on indoor air quality," *Indoor Air*, vol. 25, no. 2, pp. 210–219, 2015.

[6]   WHO, "Development of WHO Guidelines for Indoor Air Quality - Report on a Working Group Meeting," *World Heal. Organ. Reg. Off. Eur.*, pp. 1–27, 2006.

[7]   Y. Sekine and A. Nishimura, "Removal of formaldehyde from indoor air by passive type air-cleaning materials," *Atmos. Environ.*, vol. 35, no. 11, pp. 2001–2007, 2001.

[8]   O. F. Osanyintola and C. J. Simonson, "Moisture buffering capacity of hygroscopic building materials: Experimental facilities and energy impact," *Energy Build.*, vol. 38, no. 10, pp. 1270–1282, 2006.

[9]   A. V. Arundel, E. M. Sterling, J. H. Biggin, and T. D. Sterling, "Indirect health effects of relative humidity in indoor environments," *Environ. Health Perspect.*, vol. VOL. 65, no. 3, pp. 351–361, 1986.

[10]   T. Verdier, M. Coutand, A. Bertron, and C. Roques, "A review of indoor microbial growth across building materials and sampling and analysis methods," *Build. Environ.*, vol. 80, pp. 136–149, 2014.

[11]   H. Matsumoto, M. Shimizu, and H. Sato, "The contaminant removal efficiency of an air cleaner using the adsorption/desorption effect," *Build. Environ.*, vol. 44, no. 7, pp. 1371–1377, 2009.

[12]   J. Vieira, L. Senff, H. Gonçalves, L. Silva, V. M. Ferreira, and J. A. Labrincha, "Functionalization of mortars for controlling the indoor ambient of buildings," *Energy Build.*, vol. 70, pp. 224–236, 2014.

[13]   Kunkel D., E. Gall, J. A. Siegel, A. Novoselac, G. C. Morrison, and R. L. Corsi, "Passive reduction of human exposure to indoor ozone," *Build. Environ.*, vol. 45, no. 2, pp. 445–452, 2010.

[14]   R. Meininghaus, L. Gunnarsen, and H. N. Knudsen, "Diffusion and Sorption of Volatile Organic Compounds in Building Materials−Impact on Indoor Air Quality," *Environ. Sci. Technol.*, vol. 34, no. 15, pp. 3101–3108, 2000.

[15]   L. Senff, D. M. Tobaldi, S. Lucas, D. Hotza, V. M. Ferreira, and J. A. Labrincha, "Formulation of mortars with nano-SiO2 and nano-TiO2 for

degradation of pollutants in buildings," *Compos. Part B*, vol. 44, pp. 40–47, 2013.

[16] A. Folli, C. Pade, T. B. Hansen, T. De Marco, and D. E. MacPhee, "TiO2 photocatalysis in cementitious systems: Insights into self-cleaning and depollution chemistry," *Cem. Concr. Res.*, vol. 42, no. 3, pp. 539–548, 2012.

[17] M. M. Ballari, Q. L. Yu, and H. J. H. Brouwers, "Experimental study of the NO and NO2 degradation by photocatalytically active concrete," *Catal. Today*, vol. 161, no. 1, pp. 175–180, 2011.

[18] A. Fujishima, X. Zhang, and D. A. Tryk, "TiO2 photocatalysis and related surface phenomena," *Surf. Sci. Rep.*, vol. 63, no. 12, pp. 515–582, 2008.

[19] Q. L. Yu, M. M. Ballari, and H. J. H. Brouwers, "Indoor air purification using heterogeneous photocatalytic oxidation. Part II: Kinetic study," *Appl. Catal. B Environ.*, vol. 99, no. 1–2, pp. 58–65, 2010.

[20] S. Lorencik, Q. L. Yu, and H. J. H. Brouwers, "Design and performance evaluation of the functional coating for air purification under indoor conditions," *Appl. Catal. B Environ.*, vol. 168–169, pp. 77–86, 2015.

[21] H. J. Kim, S. S. Kim, Y. G. Lee, and K. D. Song, "The hygric performances of moisture adsorbing/desorbing building materials," *Aerosol Air Qual. Res.*, vol. 10, no. 6, pp. 625–634, 2010.

[22] S. Cerolini, M. D'Orazio, C. Di Perna, and A. Stazi, "Moisture buffering capacity of highly absorbing materials," *Energy Build.*, vol. 41, no. 2, pp. 164–168, 2009.

[23] C. Rode, R. Peuhkuri, B. Time, K. Svennberg, T. Ojanen, P. Mukhopadhyaya, M. Kumaran, and S. W. Dean, "Moisture Buffer Value of Materials in Building," *J. ASTM Int.*, vol. 4, no. 5, pp. 1–12, 2007.

[24] M. Z. Guo, T. C. Ling, and C. S. Poon, "Nano-TiO2-based architectural mortar for NO removal and bacteria inactivation: Influence of coating and weathering conditions," *Cem. Concr. Compos.*, vol. 36, no. 1, pp. 101–108, 2013.

[25] S. Wei, Z. Jiang, H. Liu, D. Zhou, and M. Sanchez-Silva, "Microbiologically induced deterioration of concrete - A review," *Brazilian J. Microbiol.*, vol. 44, no. 4, pp. 1001–1007, 2013.

[26] F. Tittarelli, C. Giosuè, A. Mobili, and M. L. Ruello, "Influence of binders and aggregates on VOCs adsorption and moisture buffering activity of mortars for indoor applications," *Cem. Concr. Compos.*, vol. 57, 2015.

[27] F. Wang, L. Yang, G. Sun, L. Guan, and S. Hu, "The hierarchical porous structure of substrate enhanced photocatalytic activity of TiO2/cementitious materials," *Constr. Build. Mater.*, vol. 64, pp. 488–495, 2014.

[28] A. H. Aïssa, E. Puzenat, A. Plassais, J.-M. Herrmann, C. Haehnel, and C. Guillard, "Characterization and photocatalytic performance in air of cementitious materials containing TiO2. Case study of formaldehyde removal," *Appl. Catal. B Environ.*, vol. 107, no. 1–2, pp. 1–8, 2011.

[29] M. V. Diamanti, F. Lollini, M. P. Pedeferri, and L. Bertolini, "Mutual interactions between carbonation and titanium dioxide photoactivity in concrete," *Build. Environ.*, vol. 62, pp. 174–181, 2013.

[30] M. Faraldos, R. Kropp, M. A. Anderson, and K. Sobolev, "Photocatalytic

References

hydrophobic concrete coatings to combat air pollution," *Catal. Today*, vol. 259, pp. 228–236, 2016.

[31] C. Urzì and F. De Leo, "Evaluation of the efficiency of water-repellent and biocide compounds against microbial colonization of mortars," *Int. Biodeterior. Biodegrad.*, vol. 60, no. 1, pp. 25–34, 2007.

[32] M. Horgnies, I. Dubois-Brugger, and E. M. Gartner, "NO x de-pollution by hardened concrete and the influence of activated charcoal additions," *Cem. Concr. Res.*, vol. 42, no. 10, pp. 1348–1355, 2012.

[33] L. Barcelo, J. Kline, G. Walenta, and E. Gartner, "Cement and carbon emissions," *Mater. Struct.*, vol. 47, no. 6, pp. 1055–1065, 2013.

[34] S. S. Lucas, V. M. Ferreira, and J. L. B. De Aguiar, "Incorporation of titanium dioxide nanoparticles in mortars — Influence of microstructure in the hardened state properties and photocatalytic activity," *Cem. Concr. Res.*, vol. 43, pp. 112–120, 2013.

[35] R. Sugrañez, J. I. Álvarez, M. Cruz-yusta, I. Mármol, J. Morales, J. Vila, and L. Sánchez, "Enhanced photocatalytic degradation of NOx gases by regulating the microstructure of mortar cement modified with titanium dioxide," *Build. Environ.*, vol. 69, no. x, pp. 55–63, 2013.

[36] I. Karatasios, M. S. Katsiotis, V. Likodimos, A. I. Kontos, G. Papavassiliou, P. Falaras, and V. Kilikoglou, "Photo-induced carbonation of lime-TiO2 mortars," *Appl. Catal. B Environ.*, vol. 95, no. 1–2, pp. 78–86, 2010.

[37] J. Torkaman, A. Ashori, and A. Sadr Momtazi, "Using wood fiber waste, rice husk ash, and limestone powder waste as cement replacement materials for lightweight concrete blocks," *Constr. Build. Mater.*, vol. 50, pp. 432–436, 2014.

[38] C. Giosuè, A. Mobili, G. Toscano, M. L. Ruello, and F. Tittarelli, "Effect of Biomass Waste Materials as Unconventional Aggregates in Multifunctional Mortars for Indoor Application," *Procedia Eng.*, vol. 161, pp. 655–659, 2016.

[39] N. Todorova, T. Giannakopoulou, S. Karapati, D. Petridis, T. Vaimakis, and C. Trapalis, "Composite TiO2/clays materials for photocatalytic NOx oxidation," *Appl. Surf. Sci.*, vol. 319, no. 1, pp. 113–120, 2014.

[40] J. Chen and C. S. Poon, "Photocatalytic activity of titanium dioxide modified concrete materials – Influence of utilizing recycled glass cullets as aggregates," *J. Environ. Manage.*, vol. 90, no. 20 09, pp. 3436–3442, 2009.

[41] J. Ângelo, L. Andrade, L. M. Madeira, and A. Mendes, "An overview of photocatalysis phenomena applied to NOx abatement," *J. Environ. Manage.*, vol. 129, no. x, pp. 522–539, 2013.

[42] S. Guo, Z. Wu, and W. Zhao, "TiO2-based building materials: Above and beyond traditional applications," *Chinese Sci. Bull.*, vol. 54, no. 7, pp. 1137–1142, 2009.

[43] M. Arandigoyen and J. I. Alvarez, "Pore structure and mechanical properties of cement – lime mortars," *Cem. Concr. Res.*, vol. 37, no. February, pp. 767–775, 2007.

[44] X. Gao, Q. L. Yu, and H. J. H. Brouwers, "Reaction kinetics, gel character and strength of ambient temperature cured alkali activated slag-fly ash blends," *Constr. Build. Mater.*, vol. 80, pp. 105–115, 2015.

[45] E. W. Washburn, "Note on a method of determining the distribution of pore sizes in a porous material," *Proc. Natl. Acad. Sci. U. S. A.*, vol. 7, no. 4, pp. 115–116, 1921.

[46] F. Tittarelli and G. Moriconi, "The effect of silane-based hydrophobic admixture on corrosion of galvanized reinforcing steel in concrete," *Corros. Sci.*, vol. 52, no. 9, pp. 2958–2963, 2010.

[47] J. Weitkamp, "Zeolites and catalysis," *Solid State Ionics*, vol. 131, no. 1, pp. 175–188, 2000.

[48] S. W. Baek, J. R. Kim, and S. K. Ihm, "Design of dual functional adsorbent/catalyst system for the control of VOC's by using metal-loaded hydrophobic Y-zeolites," *Catal. Today*, vol. 93–95, pp. 575–581, 2004.

[49] D. Caputo, B. Liguori, and C. Colella, "Some advances in understanding the pozzolanic activity of zeolites: The effect of zeolite structure," *Cem. Concr. Compos.*, vol. 30, no. 5, pp. 455–462, 2008.

[50] G. M. Roy, *Activated Carbon Applications in the Food and Pharmaceutical Industries*. Technomic Publishing Company, 1995.

[51] E. R. Teixeira, R. Mateus, A. F. Camõesa, L. Bragança, and F. G. Branco, "Comparative environmental life-cycle analysis of concretes using biomass and coal fly ashes as partial cement replacement material," *J. Clean. Prod.*, vol. 112, pp. 2221–2230, 2016.

[52] J. Yliniemi, H. Nugteren, M. Illikainen, M. Tiainen, R. Weststrate, and J. Niinim??ki, "Lightweight aggregates produced by granulation of peat-wood fly ash with alkali activator," *Int. J. Miner. Process.*, vol. 149, pp. 42–49, 2016.

[53] S. Maschio, G. Tonello, L. Piani, and E. Furlani, "Fly and bottom ashes from biomass combustion as cement replacing components in mortars production: Rheological behaviour of the pastes and materials compression strength," *Chemosphere*, vol. 85, no. 4, pp. 666–671, 2011.

[54] R. Barbosa, N. Lapa, D. Dias, and B. Mendes, "Concretes containing biomass ashes: Mechanical, chemical, and ecotoxic performances," *Constr. Build. Mater.*, vol. 48, pp. 457–463, 2013.

[55] G. Toscano, A. Pizzi, E. Foppa Pedretti, G. Rossini, G. Ciceri, G. Martignon, and D. Duca, "Torrefaction of tomato industry residues," *Fuel*, vol. 143, pp. 89–97, 2015.

[56] Ente Nazionale Italiano di Unificazione, "UNI EN 1015-3 Metodi di prova per malte per opere murarie. Parte 6 : Determinazione della massa volumica apparente della malta fresca (mediante tavola a scosse)," 2007.

[57] Ente Nazionale Italiano di Unificazione, "UNI EN 1015-6 Metodi di prova per malte per opere murarie Parte 6: Determinazione della massa volumica apparente della malta fresca," 2007.

[58] M. Collepardi, *The new concrete*. Treviso: Grafiche Tintoretto, 2006.

[59] Ente Nazionale Italiano di Unificazione, "UNI EN 1015-11 Metodi di prova per malte per opere murarie Parte 11: Determinazione della resistenza a flessione e a compressione della malta indurita," 2007.

[60] A. Mobili, A. Belli, C. Giosuè, T. Bellezze, and F. Tittarelli, "Metakaolin and fly ash alkali-activated mortars compared with cementitious mortars at the

References

same strength class," *Cem. Concr. Res.*, vol. 88, 2016.

[61] R. Kumar and B. Bhattacharjee, "Porosity, Pore Size Distribution and In-situ Strength of Concrete," *Cem. Concr. Res.*, vol. 33, no. 1, pp. 155–164, 2003.

[62] T. Fen-Chong, K. Li, P. Dangla, and Q. Zeng, "Pore structure of cement pastes through NAD and MIP analysis," *Adv. Cem. Res.*, vol. 28, no. 1, pp. 23–32, 2015.

[63] Ente Nazionale Italiano di Unificazione, "UNI 6687 Malta normale. Determinazione del ritiro idraulico. Prova di laboratorio.," 1973.

[64] F. Demir, "A new way of prediction elastic modulus of normal and high strength concrete-fuzzy logic," *Cem. Concr. Res.*, vol. 35, no. 8, pp. 1531–1538, 2005.

[65] Ente Nazionale Italiano di Unificazione, "UNI EN 1015-18 Metodi di prova per malte per opere murarie Parte 18 Determinazione del coefficiente di assorbimento d'acqua per capillarità della malta indurita," 2004.

[66] Ente Nazionale Italiano di Unificazione, "UNI EN 15801 Conservazione dei beni culturali Metodi di prova Determinazione dell'assorbimento dell'acqua per capillarità," 2010.

[67] R. V Silva, J. de Brito, and R. K. Dhir, "Performance of cementitious renderings and masonry mortars containing recycled aggregates from construction and demolition wastes," *Constr. Build. Mater.*, vol. 105, pp. 400–415, 2016.

[68] Ente Nazionale Italiano di Unificazione, "UNI EN 1015-19 Metodi di prova per malte per opere murarie Parte 19 Determinazione della permeabilità al vapore d'acqua delle malte da intonaco indurite," 2008.

[69] Ente Nazionale Italiano di Unificazione, "UNI EN 12572 Prestazione igrotermica dei materiali e dei prodotti per edilizia Determinazione delle proprietà di trasmissione del vapore," 2006.

[70] A. J. Katz and A. H. Thompson, "Quantitative prediction of permeability in porous rock," *Phys. Rev. B*, vol. 34, no. 11, pp. 8179–8181, 1986.

[71] M. O. Abadie and K. C. Mendonça, "Moisture performance of building materials: From material characterization to building simulation using the Moisture Buffer Value concept," *Build. Environ.*, vol. 44, no. 2, pp. 388–401, 2009.

[72] C. Rode, R. Peuhkuri, L. H. Mortensen, K. K. Hansen, B. Time, A. Gustavsen, T. Ojanen, J. Ahonen, K. Svennberg, and J. Arfvidsson, *Moisture buffering of building materials, BYG DTU Report*. Technical University of Denmark, 2005.

[73] E. Latif, M. Lawrence, A. Shea, and P. Walker, "Moisture buffer potential of experimental wall assemblies incorporating formulated hemp-lime," *Build. Environ.*, vol. 93, no. P2, pp. 199–209, 2015.

[74] Ente Nazionale Italiano di Unificazione, "UNI EN 15457 Pitture e vernici Metodo di laboratorio per valutare l'efficacia dei preservanti del film impiegati nei prodotti vernicianti contro la crescita fungina Laboratory method for testing the efficacy of film preservatives in a coating against fung," 2008.

[75] J. Mensah-Attipoe, T. Reponen, A. Salmela, A. M. Veijalainen, and P. Pasanen, "Susceptibility of green and conventional building materials to

microbial growth," *Indoor Air*, vol. 25, no. 3, pp. 273–284, 2015.

[76] A. Amato, L. Rocchetti, V. Fonti, M. L. Ruello, and F. Beolchini, "Secondary indium production from end-of-life liquid crystal displays," *Phys. Status Solidi Curr. Top. Solid State Phys.*, vol. 5, pp. 1–5, 2016.

[77] European Commission - Joint Research Centre - Institute for Environment and Sustainability, *General guide for Life Cycle Assessment - Detailed guidance.* 2010.

[78] G. Hüsken, M. Hunger, and H. J. H. Brouwers, "Experimental study of photocatalytic concrete products for air purification," *Build. Environ.*, vol. 44, no. 12, pp. 2463–2474, 2009.

[79] F. Tittarelli, "Effect of low dosages of waste GRP dust on fresh and hardened properties of mortars: Part 2," *Constr. Build. Mater.*, vol. 47, pp. 1539–1543, 2013.

[80] Ente Nazionale Italiano di Unificazione, "UNI EN 998-1 Specifiche per malte per opere murarie Parte 1 Malte per intonaci interni ed esterni," 2010.

[81] F. G. Branco and L. Godinho, "On the use of lightweight mortars for the minimization of impact sound transmission," *Constr. Build. Mater.*, vol. 45, pp. 184–191, 2013.

[82] B. Uzal, L. Turanli, H. Yücel, M. C. Göncüoğlu, and A. Çulfaz, "Pozzolanic activity of clinoptilolite: A comparative study with silica fume, fly ash and a non-zeolitic natural pozzolan," *Cem. Concr. Res.*, vol. 40, no. 3, pp. 398–404, 2010.

[83] R. Zhang, X. Cheng, P. Hou, and Z. Ye, "Influences of nano-TiO 2 on the properties of cement-based materials : Hydration and drying shrinkage," *Constr. Build. Mater.*, vol. 81, pp. 35–41, 2015.

[84] S. Banerjee, D. D. Dionysiou, and S. C. Pillai, "Self-cleaning applications of TiO 2 by photo-induced hydrophilicity and photocatalysis," *"Applied Catal. B, Environ.*, vol. 176–177, pp. 396–428, 2015.

[85] M. Rahim, O. Douzane, A. D. Tran Le, G. Promis, B. Laidoudi, A. Crigny, B. Dupre, and T. Langlet, "Characterization of flax lime and hemp lime concretes: Hygric properties and moisture buffer capacity," *Energy Build.*, vol. 88, pp. 91–99, 2015.

[86] Y. Wu, G. Gong, C. W. Yu, and Z. Huang, "Proposing ultimate moisture buffering value (UMBV) for characterization of composite porous mortars," *Constr. Build. Mater.*, vol. 82, pp. 81–88, 2015.

[87] V. Pavlík and M. Uzáková, "Effect of curing conditions on the properties of lime , lime – metakaolin and lime – zeolite mortars," *Constr. Build. Mater.*, vol. 102, pp. 14–25, 2016.

[88] J. Chen, S. C. Kou, and C. S. Poon, "Photocatalytic cement-based materials: Comparison of nitrogen oxides and toluene removal potentials and evaluation of self-cleaning performance," *Build. Environ.*, vol. 46, no. 9, pp. 1827–1833, 2011.

[89] R. Walker and S. Pavía, "Moisture transfer and thermal properties of hemp-lime concretes," *Constr. Build. Mater.*, vol. 64, pp. 270–276, 2014.

[90] P. Maravelaki-kalaitzaki, Z. Agioutantis, E. Lionakis, M. Stavroulaki, and V. Perdikatsis, "Physico-chemical and mechanical characterization of hydraulic

References

mortars containing nano-titania for restoration applications," *Cem. Concr. Compos.*, vol. 36, pp. 33–41, 2013.

[91] R. Demirboğa, "Influence of mineral admixtures on thermal conductivity and compressive strength of mortar," *Energy Build.*, vol. 35, no. 2, pp. 189–192, 2003.

[92] S. Diamond, "Mercury porosimetry An inappropriate method for the measurement of pore size distributions in cement-based materials," *Cem. Concr. Res.*, vol. 30, pp. 1517–1525, 2000.

[93] J. Kurnitski, T. Kalamees, J. Palonen, L. Eskola, and O. Seppänen, "Potential effects of permeable and hygroscopic lightweight structures on thermal comfort and perceived IAQ in a cold climate," *Indoor Air*, vol. 17, no. 1, pp. 37–49, 2007.

[94] T. Verdier, M. Coutand, A. Bertron, and C. Roques, "Antibacterial Activity of TiO2 Photocatalyst Alone or in Coatings on E. coli: The Influence of Methodological Aspects," *Coatings*, pp. 670–686, 2014.

[95] K. I. Y. Yoon, J. H. Byeon, C. W. O. O. Park, and J. Hwang, "Antimicrobial Effect of Silver Particles on Bacterial Contamination of Activated Carbon Fibers," pp. 1251–1255, 2008.

[96] S. N. Hosseini, S. M. Borghei, M. Vossoughi, and N. Taghavinia, "Immobilization of TiO2 on perlite granules for photocatalytic degradation of phenol," *Appl. Catal. B Environ.*, vol. 74, no. 1–2, pp. 53–62, 2007.

[97] P. Feng, "Brief discussion of green buildings," *Procedia Eng.*, vol. 21, pp. 939–942, 2011.

[98] R. C. E. Modolo, V. Ferreira, L. A. Tarelho, J. A. Labrincha, L. Senff, and L. Silva, "Mortar formulations with bottom ash from biomass combustion," *Constr. Build. Mater.*, vol. 45, pp. 275–281, 2013.

[99] V. Sata, J. Tangpagasit, C. Jaturapitakkul, and P. Chindaprasirt, "Effect of W/B ratios on pozzolanic reaction of biomass ashes in Portland cement matrix," *Cem. Concr. Compos.*, vol. 34, no. 1, pp. 94–100, 2012.

[100] B. Carrasco, N. Cruz, J. Terrados, F. A. Corpas, and L. Pérez, "An evaluation of bottom ash from plant biomass as a replacement for cement in building blocks," *Fuel*, vol. 118, pp. 272–280, 2014.

[101] J. K. Prusty and S. K. Patro, "Properties of fresh and hardened concrete using agro-waste as partial replacement of coarse aggregate - A review," *Constr. Build. Mater.*, vol. 82, pp. 101–113, 2015.

[102] U. Demir, Y. A., S. Kelebek, B. Oteyaka, A. Ucar, and O. Sahbaz, "Characterization and column flotation of bottom ashes from Tuncbilek power plant," *Fuel*, vol. 87, pp. 666–672, 2008.

[103] K. Y. Foo and B. H. Hameed, "Utilization of rice husk ash as novel adsorbent: A judicious recycling of the colloidal agricultural waste," *Adv. Colloid Interface Sci.*, vol. 152, no. 1–2, pp. 39–47, 2009.

[104] N. Soltani, A. Bahrami, M. I. Pech-Canul, and L. A. González, "Review on the physicochemical treatments of rice husk for production of advanced materials," *Chem. Eng. J.*, vol. 264, pp. 899–935, 2015.

[105] E. K. Darling, C. J. Cros, P. Wargocki, J. Kolarik, G. C. Morrison, and R. L. Corsi, "Impacts of a clay plaster on indoor air quality assessed using chemical

and sensory measurements," *Build. Environ.*, vol. 57, pp. 370–376, 2012.

[106] M. G. Beltrán, A. Barbudo, F. Agrela, J. R. Jiménez, and J. De Brito, "Mechanical performance of bedding mortars made with olive biomass bottom ash," *Constr. Build. Mater.*, vol. 112, pp. 699–707, 2016.

[107] T. Bilir, O. Gencel, and I. Bekir, "Properties of mortars with fly ash as fine aggregate," *Constr. Build. Mater.*, vol. 93, pp. 782–789, 2015.

[108] Y. Ma and G. Ye, "The shrinkage of alkali activated fly ash," *Cem. Concr. Res.*, vol. 68, pp. 75–82, 2015.

[109] S. Care and F. Derkx, "Determination of relevant parameters influencing gas permeability of mortars," *Constr. Build. Mater.*, vol. 25, no. 3, pp. 1248–1256, 2011.

[110] S. Middlemas, Z. Z. Fang, and P. Fan, "Life cycle assessment comparison of emerging and traditional Titanium dioxide manufacturing processes," *J. Clean. Prod.*, vol. 89, pp. 137–147, 2015.

[111] A. R. Jayapalan, B. Y. Lee, and K. E. Kurtis, "Can nanotechnology be 'green'? Comparing efficacy of nano and microparticles in cementitious materials," *Cem. Concr. Compos.*, vol. 36, no. 1, pp. 16–24, 2013.

[112] K. Hashimoto, K. Wasada, M. Osaki, E. Shono, K. Adachi, N. Toukai, H. Kominami, and Y. Kera, "Photocatalytic oxidation of nitrogen oxide over titania – zeolite composite catalyst to remove nitrogen oxides in the atmosphere," *Appl. Catal. B Environ.*, vol. 30, pp. 429–436, 2001.

[113] Q. L. Yu, P. Spiesz, and H. J. H. Brouwers, "Development of cement-based lightweight composites – Part 1 : Mix design methodology and hardened properties," *Cem. Concr. Compos.*, vol. 44, pp. 17–29, 2013.

[114] A. H. M. Andreasen and A. J., "Ueber die Beziehung zwischen Kornabstufung und Zwischenraum in Produkten aus losen Kornern (mit einigen Experimenten)," *Kolloid-Zeitschrift*, vol. 50, no. 3, pp. 217–228, 1930.

[115] J. E. Funk and D. R. Dinger, *Predictive process control of crowded particulate suspensions: applied to ceramic manufacturing*. USA: Kluwer Academic, 1994.

[116] G. Hüsken, *A multifunctional design approach for sustainable concrete with application to concrete mass products, PhD thesis*. Eindhoven, Netherlands: Eindhoven University of Technology., 2010.

[117] Q. L. Yu, *Design of environmentally friendly calcium sulfate-based building materials. Towards and improved indoor air quality. PhD thesis*. Eindhoven, Netherlands: Eindhoven University of Technology., 2012.

[118] G. Quercia, G. Hüsken, and H. J. H. Brouwers, "Water demand of amorphous nano silica and its impact on the workability of cement paste," *Cem. Concr. Res.*, vol. 42, no. 2, pp. 344–357, 2012.

[119] I. Papayianni and M. Stefanidou, "Strength – porosity relationships in lime – pozzolan mortars," *Constr. Build. Mater.*, vol. 20, pp. 700–705, 2006.

[120] Q. L. Yu, P. Spiesz, and H. J. H. Brouwers, "Ultra-lightweight concrete: Conceptual design and performance evaluation," *Cem. Concr. Compos.*, vol. 61, pp. 18–28, 2015.

[121] M. E. Zareef, *Conceptual and structural design of buildings made of lightweight and infra- lightweight concrete. PhD Tesis*. Berlin, German:

References

Techn. Univ, 2010.

[122] P. Chindaprasirt and S. Rukzon, "Strength , porosity and corrosion resistance of ternary blend Portland cement , rice husk ash and fly ash mortar," *Constr. Build. Mater.*, vol. 22, pp. 1601–1606, 2008.

[123] F. Tittarelli and S. P. Shah, "Effect of low dosages of waste GRP dust on fresh and hardened properties of mortars: Part 1," *Constr. Build. Mater.*, vol. 47, pp. 1532–1538, 2013.

[124] M. M. Barbero-Barrera, A. García-Santos, and F. J. Neila-González, "Thermal conductivity of lime mortars and calcined diatoms . Parameters influencing their performance and comparison with the traditional lime and mortars containing crushed marble used as renders," *Energy Build.*, vol. 76, pp. 422–428, 2014.

[125] H. K. Kim, J. H. Jeon, and H. K. Lee, "Workability, and mechanical, acoustic and thermal properties of lightweight aggregate concrete with a high volume of entrained air," *Constr. Build. Mater.*, vol. 29, pp. 193–200, 2012.

[126] N. U. Kockal, "Investigation about the effect of different fine aggregates on physical, mechanical and thermal properties of mortars," *Constr. Build. Mater.*, vol. 124, pp. 816–825, 2016.

Appendix A

A.1. Cement based mortars:

Table 34 Capillary water absorption coefficient of different mortars according to UNI EN 1015-18

Mix	C [kg/m²min^{0.5}]
C-S	0.63
C-S h	0.08
PC-S	0.58
PC-S h	0.05
C-A1	0.62
C-A1 h	0.19
PC-A1	0.74
PC-A1 h	0.16
C-A2	1.43
C-A2 h	0.50
PC-A2	2.07
PC-A2 h	0.44
C-A3	1.26
C-A3 h	0.73
PC-A3	1.28
PC-A3 h	0.45

Table 35 Capillary water absorption: Qi

time s^{0.5}	0	24.49	34.64	42.43	60.00	120.00	146.97	293.94	415.69	509.12	831.38
Mix	Q_0	Q_{10}	Q_{20}	Q_{30}	Q_{60}	Q_{4h}	Q_{6h}	Q_{24h}	Q_{48h}	Q_{72h}	Q_{192h}
	kg/m²	kg/m²	kg/m²	kg/m²	kg/m²	kg/m²	kg/m²	kg/m²	kg/m²	kg/m²	kg/m²
C-S	0.00	1.15	1.67	2.04	2.77	5.23	5.98	10.13	11.78	12.78	15.86
C-S h	0.00	0.43	0.59	0.70	0.94	1.74	1.99	3.28	4.01	4.59	6.40
PC-S	0.00	1.18	1.75	2.16	2.98	5.77	6.76	11.28	13.33	14.29	16.57
PC-S h	0.00	0.24	0.34	0.42	0.58	1.10	1.28	2.19	2.83	3.35	5.02
C-A1	0.00	1.75	2.17	2.51	2.98	5.00	5.59	10.17	11.22	12.16	15.83
C-A1 h	0.00	1.01	1.29	1.47	1.78	3.03	3.47	5.72	7.06	7.90	10.16
PC-A1	0.00	1.84	2.60	3.03	3.74	5.67	6.35	10.07	11.22	11.97	16.81
PC-A1 h	0.00	1.03	1.38	1.58	1.98	3.30	3.75	6.08	7.22	8.05	10.45
C-A2	0.00	3.04	4.00	4.55	5.46	9.05	9.59	14.19	17.04	21.00	38.01
C-A2 h	0.00	1.62	2.07	2.35	2.98	5.25	5.93	10.88	14.14	16.94	27.86

PC-A2	0.00	3.03	4.35	5.06	5.81	11.41	13.38	16.31	18.98	21.16	29.38
PC-A2 h	0.00	0.92	1.07	1.27	1.66	3.11	3.73	6.52	9.38	11.79	18.98
C-A3	0.00	0.35	0.60	0.77	1.15	2.69	3.36	6.05	7.89	9.07	12.45
C-A3 h	0.00	0.30	0.47	0.60	0.90	2.13	2.73	5.18	7.21	8.56	12.45
PC-A3	0.00	0.32	0.68	0.84	1.20	2.77	3.84	7.18	10.36	12.06	16.34
PC-A3 h	0.00	0.46	0.69	0.88	1.28	3.13	3.87	6.62	9.38	11.00	15.29

Table 36 Water vapor resistance factor μ of cement-based mortars

Mix	μ [-]
C-S	41.2
C-S h	45.6
PC-S	37.1
PC-S h	38.3
C-A1	32
C-A1 h	31.3
PC-A1	35.0
PC-A1 h	35.7
C-A2	12.3
C-A2 h	9.7
PC-A2	11.9
PC-A2 h	11.9
C-A3	11.2
C-A3 h	15.2
PC-A3	14.3
PC-A3 h	14.4

Table 37 Moisture buffering value of cementitious mortars

Mix	MBV g/(m²RH)
C-S	0.3
C-S h	0.3
PC-S	0.3
PC-S h	0.3
C-A1	0.4
C-A1 h	0.4
PC-A1	0.5
PC-A1 h	0.4
C-A2	0.5
C-A2 h	0.5
PC-A2	0.5
PC-A2 h	0.3

C-A3	0.3
C-A3 h	0.2
PC-A3	0.3
PC-A3 h	0.3

A.2. Hydraulic lime based mortars:

Table 38 Capillary water absorption coefficient of different mortars according to UNI EN 1015-18

Mix	C [kg/m²min$^{0.5}$]
HL-S	1.92
HL-S-h	0.07
HL-S TiO2	1.38
HL-S TiO2 h	0.08
HL-A1	1.99
HL-A1 h	0.50
HL-A1 TiO2	1.36
HL-A1 TiO2 h	0.54
HL-A2	4.13
HL-A2-h	0.24
HL-A2 TiO2	3.64
HL-A2 TiO2 h	0.19
HL-A3	1.48
HL-A3-h	1.41
HL-A3 TiO2	1.60
HL-A3 TiO2 h	1.45

Table 39 Capillary water absorption: Qi

time s$^{0.5}$	0	24.49	34.64	42.43	120.00	146.97	293.94	415.69	509.12	831.38
Mix	Q_0 kg/m²	Q_{10} kg/m²	Q_{20} kg/m²	Q_{30} kg/m²	Q_{4h} kg/m²	Q_{6h} kg/m²	Q_{24h} kg/m²	Q_{48h} kg/m²	Q_{72h} kg/m²	Q_{192h} kg/m²
HL-S	0.00	1.21	1.67	1.96	9.05	17.60	20.20	20.35	20.43	20.48
HL-S-h	0.00	0.15	0.20	0.23	0.78	0.94	1.87	2.52	2.90	4.12
HL-S TiO2	0.00	1.74	2.16	2.48	8.73	13.16	21.30	21.45	21.51	21.63
HL-S TiO2 h	0.00	0.55	0.64	0.71	1.49	1.66	2.63	3.28	3.64	4.74
HL-A1	0.00	2.11	2.73	3.13	8.41	11.40	18.68	21.10	26.70	32.62
HL-A1 h	0.00	2.06	2.57	2.91	6.39	7.81	12.76	15.42	18.51	24.53
HL-A1 TiO2	0.00	1.96	2.69	3.12	8.72	12.05	19.93	23.27	29.93	36.14
HL-A1 TiO2 h	0.00	2.15	2.66	2.93	6.32	7.92	12.50	14.99	17.85	23.05
HL-A2	0.00	0.83	1.12	1.39	15.27	20.97	29.55	36.07	39.31	43.56
HL-A2-h	0.00	0.14	0.23	0.30	1.78	2.41	5.88	9.11	11.65	20.14

HL-A2 TiO2	0.00	0.26	0.40	0.52	11.28	14.19	22.14	27.06	29.04	33.63
HL-A2 TiO2 h	0.00	0.13	0.21	0.27	1.52	2.04	4.95	7.50	9.43	16.29
HL-A3	0.00	0.88	1.18	1.43	6.23	7.98	13.01	17.35	18.74	26.43
HL-A3-h	0.00	0.39	0.57	0.71	6.15	8.52	15.18	20.11	21.42	28.61
HL-A3 TiO2	0.00	1.25	1.62	1.98	9.15	11.97	18.18	24.16	26.37	30.69
HL-A3 TiO2 h	0.00	1.47	1.87	2.11	8.28	10.05	15.72	20.88	22.27	30.35

Table 40 Water vapor resistance factor μ of different mortars

Mix	μ [-]
HL-S	15.2
HL-S-h	16.5
HL-S TiO2	14.2
HL-S TiO2 h	14.9
HL-A1	11.4
HL-A1 h	11.9
HL-A1 TiO2	11.1
HL-A1 TiO2 h	12.1
HL-A2	5.5
HL-A2-h	6.1
HL-A2 TiO2	5.6
HL-A2 TiO2 h	6.0
HL-A3	6.5
HL-A3-h	6.4
HL-A3 TiO2	5.5
HL-A3 TiO2 h	6.1

Table 41 Moisture buffering value of hydraulic lime based mortars

Mix	MBV g/(m^{2}RH)
HL-S	0.1
HL-S-h	0.2
HL-S TiO2	0.1
HL-S TiO2 h	0.1
HL-A1	0.4
HL-A1 h	0.5
HL-A1 TiO2	0.7
HL-A1 TiO2 h	0.5
HL-A2	0.5
HL-A2-h	0.3
HL-A2 TiO2	0.6
HL-A2 TiO2 h	0.3

HL-A3	0.3
HL-A3-h	0.2
HL-A3 TiO2	0.4
HL-A3 TiO2 h	0.3

A.3. Biomass waste materials and hydraulic lime based mortars:

Table 42 Capillary water absorption coefficient of different mortars according to UNI EN 1015-18

Mix	C [kg/(m^{2}min$^{0.5}$)]
L SAN	1.85
L SPR N	2.80
L SPR R	1.71
L BOT	0.89
L FLY	2.33

Table 43 Capillary water absorption: Qi

time s$^{0.5}$	0	24.49	34.64	42.43	60.00	120.00	146.97	293.94	415.69	509.12	831.38
Mix	Q_0	Q_{10}	Q_{20}	Q_{30}	Q_{60}	Q_{4h}	Q_{6h}	Q_{24h}	Q_{48h}	Q_{72h}	Q_{192h}
	kg/m^2	kg/m^2	kg/m^2	kg/m^2	kg/m^2	kg/m^2	kg/m^2	kg/m^2	kg/m^2	kg/m^2	kg/m^2
L SAN	0.00	1.04	1.40	1.63	4.94	6.97	7.61	8.26	9.05	10.02	13.02
L SPR N	0.00	3.97	5.24	5.99	9.06	14.11	14.98	18.87	19.82	20.60	23.38
L SPR R	0.00	1.82	2.39	2.76	4.17	7.96	9.13	15.08	17.58	20.19	24.95
L BOT	0.00	1.55	1.93	2.12	3.39	5.33	6.07	7.55	9.17	10.70	13.10
L FLY	0.00	3.84	5.62	6.02	11.95	18.54	21.83	24.20	26.76	28.95	34.06

Table 44 Water vapor resistance factor μ of different mortars

Mix	μ [-]
L SAN	15.0
L SPR N	4.8
L SPR R	6.2
BOT	17.6
L FLY	9.8

Table 45 Moisture buffering value of hydraulic lime-based mortars

Mix	MBV g/(m^{2}RH)
L SAN	0.2
L SPR N	0.7
L SPR R	0.6

Appendix A

BOT	0.2
L FLY	0.3

A.3. Unconventional innovative based mortars:

Table 46 Capillary water absorption coefficient of different mortars according to UNI EN 1015-18

Mix	C [kg/(m²min^{0.5})]
L-SAN	1.91
KER	1.24
MAR	0.40
M1	2.37
M1 tr	1.81
M1 TiO2A	2.13
M1 tr TiO2A	1.93
M1 TiO2K	2.25
M1 tr TiO2K	2.15

Table 47 Capillary water absorption: Qi

time s^{0.5}	0	24.49	34.64	42.43	60.00	120.00	146.97	293.94	415.69	509.12	831.38
Mix	Q_0	Q_{10}	Q_{20}	Q_{30}	Q_{60}	Q_{4h}	Q_{6h}	Q_{24h}	Q_{48h}	Q_{72h}	Q_{192h}
	kg/m²	kg/m²	kg/m²	kg/m²	kg/m²	kg/m²	kg/m²	kg/m²	kg/m²	kg/m²	kg/m²
L-SAN	0.00	4.21	4.58	4.85	5.31	6.49	6.71	7.60	8.41	9.14	11.73
KER	0.00	3.52	4.12	4.71	5.84	8.90	9.65	11.09	12.13	12.78	15.44
MAR	0.00	1.28	1.54	1.71	2.03	3.19	3.69	4.92	5.70	6.15	7.78
M1	0.00	3.63	4.17	4.65	5.45	7.75	8.64	11.10	13.26	15.00	21.93
M1 tr	0.00	2.46	3.10	3.49	4.19	6.03	6.95	9.50	11.72	13.64	20.89
M1 TiO2A	0.00	1.76	2.07	2.32	2.98	4.33	5.12	7.44	9.57	11.34	17.97
M1 tr TiO2A	0.00	3.65	4.55	5.14	6.41	8.69	10.14	13.25	15.59	17.49	24.67
M1 TiO2K	0.00	4.37	5.36	5.98	7.15	9.15	10.38	13.57	15.98	17.90	24.61
M1 tr TiO2K	0.00	3.91	4.63	5.25	6.34	8.79	10.23	13.22	15.82	17.80	24.99

Table 48 Water vapor resistance factor μ of different mortars

Mix	μ [-]
L-SAN	19.8
KER	14.0
MAR	15.8
M1	11.4

M1 tr	13.4

Table 49 Moisture buffering value of hydraulic lime-based mortars

Mix	MBV g/(m^{2}RH)
L-SAN	0.2
KER	0.3
MAR	0.2
M1	0.6
M1 tr	0.5

A.5. Lightweight aggregates based mortars:

Table 50 Capillary water absorption coefficient of lightweight mortars according to UNI EN 1015-18

Mix	C [kg/(m^{2}min$^{0.5}$)]
CEM ES	0.36
CEM EG	0.47
NHL ES	1.10
NHL EG	1.67

Table 51 Capillary water absorption: Qi

time s$^{0.5}$	0	24.49	34.64	42.43	60.00	120.00	146.97	293.94	415.69	509.12	831.38
Mix	Q_0	Q_{10}	Q_{20}	Q_{30}	Q_{60}	Q_{4h}	Q_{6h}	Q_{24h}	Q_{48h}	Q_{72h}	Q_{192h}
	kg/m^2	kg/m^2	kg/m^2	kg/m^2	kg/m^2	kg/m^2	kg/m^2	kg/m^2	kg/m^2	kg/m^2	kg/m^2
CEM ES	0.00	1.13	1.49	1.78	2.40	4.38	4.63	7.65	9.22	12.12	12.68
CEM EG	0.00	1.04	1.47	1.80	2.56	4.86	5.60	9.98	11.67	14.43	14.73
NHL ES	0.00	1.40	2.07	2.56	3.63	6.95	7.90	12.63	13.85	16.90	17.25
NHL EG	0.00	3.73	5.83	7.29	10.62	17.84	18.16	19.25	19.64	20.56	20.58